POLYTECHNIQUE MONTRÉAL

affiliée à l'Université de Montréal

Systematic assessment of microbial risks associated with hydrometeorological events for drinking water safety management

ÉMILE SYLVESTRE

Département des génies civil, géologique et des mines

Thèse présentée en vue de l'obtention du diplôme de *Philosophiæ Doctor*

Génie Civil

Septembre 2020

POLYTECHNIQUE MONTRÉAL

affiliée à l'Université de Montréal

Cette thèse intitulée:

Systematic assessment of microbial risks associated with hydrometeorological events for drinking water safety management

Présentée par **Émile SYLVESTRE**

en vue de l'obtention du diplôme de *Philosophiæ Doctor*

a été dûment acceptée par le jury d'examen constitué de :

Benoit BARBEAU, président

Sarah DORNER, membre et directrice de recherche

Michèle PRÉVOST, membre et codirectrice de recherche

Charles HAAS, membre externe

Stephanie MCFAYDEN, membre externe

ACKNOWLEDGEMENTS

RÉSUMÉ

Les fortes pluies et le traitement inadéquat des sources d'eau de surface sont des facteurs causaux à l'origine de plusieurs épidémies de maladies d'origine hydrique. Alors que les changements climatiques intensifient le cycle hydrologique, une attention accrue sur la gestion des risques sanitaires liés aux évènements météorologiques est recommandée dans plusieurs guides sur la gestion de la qualité de l'eau potable. Cependant, les jeux de données disponibles permettant de caractériser les concentrations microbiennes à l'eau brute des usines de production d'eau potable et la performance de leurs procédés de traitement sont limités. Conséquemment, les variations à court terme da la qualité microbiologique de l'eau sont hautement incertaines. Le développement de méthodes permettant de quantifier ces variations à court terme et d'évaluer leurs risques est donc nécessaire afin de favoriser le développement des approches d'analyse de risque.

L'objectif principal de ce projet de recherche est de développer et de mettre en œuvre une méthodologie permettant d'évaluer systématiquement les risques microbiens associés aux événements hydrométéorologiques se produisant aux usines de production d'eau potable. Les objectifs spécifiques de ce projet sont les suivants: (1) présenter un catalogue de distributions de probabilités pouvant potentiellement décrire les variations temporelles des microbiennes à l'eau brute des usines, et fournir une approche statistique permettant d'estimer leurs paramètres et de comparer leur ajustement relatif; (2) évaluer le potentiel d'une technologie de mesure en ligne de l'activité de la β-D-glucuronidase (GLUC) pour évaluer les pointes de micro-organismes pathogènes et d'indicateurs fécaux à l'eau brute durant des événements hydrométéorologiques et évaluer leur réduction à grande échelle par des procédés de traitement conventionnels; (3) déterminer quelles distributions de probabilités permet de prédire adéquatement les concentrations microbiennes à l'eau brute durant des évènement hydrométéorologique; (4) évaluer l'impact des variations à court terme des concentrations microbiennes à l'eau brute sur les risques microbiologiques liés à la consommation d'eau potable.

Dans la première partie de cette thèse, des distributions de probabilités ont été sélectionnées pour évaluer les variations temporelles des concentrations microbiennes à l'eau brute. Le premier article présente une analyse statistique de données de suivi règlementaire d'*E. coli* collectées à six usines. Le deuxième article présente une analyse statistique de données de suivi mensuel de

Cryptosporidium et de *Giardia* collectées à 30 usines. Ces analyses statistiques montrent que l'identification adéquate des distributions est nécessaire pour modéliser les variations temporelles de *Cryptosporidium* à l'eau brute lorsque les jeux de données sont petits ($n < 30$ échantillons par usine). La sélection d'une distribution log-normales plutôt qu'une distribution gamma peut considérablement augmenter (>0,5-log) la limite supérieure de l'intervalle de crédibilité à 95% sur la concentration moyenne. L'application de méthodes permettant de favoriser le choix d'un modèle est donc nécéssaire pour assurer la sélection de distributions convenablement conservatices. Toutefois, les différences entre les valeurs données par le critère marginal d'information sur la déviance (mDIC) sont géréalement trop faibles pour justifier le choix d'une distribution. En conséquence, différentes distributions ajustées de la même manière sur un jeu de données peuvent prédire différents niveaux de risque.

Une approche permettant de résoudre ce problème est de comparer les prédictions des queues supérieures de différentes distributions à des données d'échantillonnage collectées lors de périodes critiques de contamination à la source. Dans le troisième article, une stratégie d'échantillonnage déclenchée par des mesures en ligne de l'activité de la β-D-glucuronidase (GLUC) est proposée afin de caractériser les concentrations microbiennes de pointes durant quatre évènements hydrométéorologiques à trois usines. Les résultats de cette étude montrent que la capacité du suivi de l'activité GLUC à caractériser des évènements de fréquence faible est variable selon le type de source. Selon des données de suivi de routine, les probabilités de dépassement de la concentration moyenne journalière d'*E. coli*, de *Cryptosporidium* et de *Giardia* évaluées durant les évènements visés sont généralement faibles ($< 5\%$) à deux usines and modérées (10-35%) à une usine. La distribution log-normale ajustée sur des données de suivi de routine prédit de manière conservatrice les concentrations moyennes journalières d'*E. coli*, de *Cryptosporidium* et de *Giardia* évaluées durant chacun des évènements. La distribution gamma permet de prédire les concentrations moyennes journalières de *Cryptosporidium* durant ces évènements mais ne permet pas de prédire convenablement les concentrations moyennes journalières d'*E. coli* et de *Giardia*. La queue supérieure de la distribution gamma pourrait donc être trop petite pour prédire adéquatement les concentrations microbiennes à la source durant des évènements hydrométéorologiques.

L'étude de la performance à grande échelle des procédés de traitement de ces mêmes trois usines en périodes normales et lors d'événement hydrométéorologiques est ensuite présentée dans deux articles. Durant les trois événements de fonte des neiges, l'enlèvement par les procédés de décantation (lamellaire à floc lesté ou lit de boues pulsé) a augmenté proportionnellement aux concentrations de *Giardia*, d'adénovirus, de rotavirus, d'*E. coli* et de *C. perfringens* à l'eau brute. Durant l'événement de pluie, l'enlèvement d'*E. coli* et de *C. perfringens* par le décanteur à lit de boues pulsé n'a pas augmenté mais la réduction par filtration rapide sur sable a augmenté proportionnellement aux concentrations d'*E. coli* et de *C. perfringens* à l'eau brute. Les concentrations de *Cryptosporidium* à l'eau brute et les taux de réduction de *C. perfringens* mesurés durant ces évènements ont été utilisées dans un modèle d'évaluation quantitative du risque microbien (ÉQRM) pour estimer les risques journaliers d'infection par *Cryptosporidium* à l'eau potable. Les résultats de cette modélisation ÉQRM indiquent que les risques journaliers d'infection durant ces évènements hydrométéorologiques ne sont pas plus élevés que les risques journaliers en périodes normales. Par conséquent, à ces usines, le risque annuel d'infection n'est probablement pas dominé par les variations à court terme des concentrations microbiennes à la source. Les résultats de ces campagnes d'échantillonnage indiquent également que le taux d'inactivation d'*E. coli* et d'adénovirus par les procédés d'ozonation est inférieure à ceux obtenues lors d'études d'inactivation en laboratoire, potentiellement en raison de mauvaises conditions hydrauliques et conditions de mélange. De plus, des adénovirus infectieux ont été détectés à l'eau traitée par une filière de traitement incluant une décantation lamellaire à floc lesté, une inter-ozonation, une filtration sur charbon actif granulaire, et une désinfection UV à une dose d'opération de 40 mJ cm^{-2}.

Il est anticipé que les méthodologies proposées pour caractériser la contamination à la source et la performance à grande échelle des procédés de traitement va aider les responsables gouvernementaux de réglementation, les ingénieurs et les gestionnaires des ressources en eau, et les chercheurs dans ce domaine à évaluer les exigences de suivi règlementaire et déterminer si les cibles de risque sanitaires sont atteintes.

ABSTRACT

Heavy rainfall and inadequate treatment of surface water sources are common causative factors of waterborne disease outbreaks. As climate change intensifies the hydrological cycle, an enhanced focus on the risk management of weather events has been recommended in future revisions of guidance documents for drinking water quality. However, real-world data sets describing concentrations of microbial pathogens in water sources and their full-scale reduction by water treatment processes are typically small. Consequently, short-term changes in microbial water quality are highly uncertain. The development of methods to quantify these short-term fluctuations and evaluate their health risks is needed to enhance the applicability and usefulness of risk assessment approaches.

The general objective of this research project is to develop and implement a methodology to systematically assess microbial risks associated with hydrometeorological events at drinking water treatment plants (DWTPs). The specific objectives of this research project are: (1) to present a catalogue of candidate probability distributions to describe temporal variations in source water microbial concentrations, and provide a statistical approach to estimate their parameters from monitoring data and compare their relative fit; (2) to evaluate the potential of online measurements of β-D-glucuronidase (GLUC) activity to assess short-term variations in source water microbial concentrations.; (3) to determine which probability distributions adequately predict source water microbial concentrations during hydrometeorological events, and (4) to assess the impact of short-term variations in source water microbial concentrations on microbial risks associated with drinking water consumption.

In the first part of this work, candidate probability distributions were selected to evaluate temporal variations in source water microbial concentrations at various DWTPs. The first article presents the statistical analysis of regulatory monitoring *E. coli* data sets from six DWTPs. The second article presents the statistical analysis of routine monitoring *Cryptosporidium* and *Giardia* data sets from 30 DWTPs. These statistical analyses demonstrated that correct identification of the candidate distribution is needed to model temporal variations in source water *Cryptosporidium* concentrations when available data sets are small ($n < 30$ samples per site). The selection of a log-normal distribution rather than the gamma distribution can considerably increase (>0.5-log) the

upper bound of the 95% credibility interval on the mean concentration. The application of methods to assist model selection is therefore needed to ensure that appropriately conservative distributions are selected for source water characterization. However, differences in marginal deviance information criterion (mDIC) values were generally too small for discrimination between candidate distributions. Consequently, candidate distributions fit the data equally well but may predict different risk estimates when they are used as input distributions in risk assessment.

A possible approach to address this issue is to compare the upper tail predictions of candidate distributions to event-based monitoring data collected during critical periods of source water contamination. In the third article, an event-based sampling strategy triggered by online β-D-glucuronidase (GLUC) activity measurements was thus developed and implemented to capture microbial peaks during four hydrometeorological events at three DWTPs. Our results indicated that the potential of GLUC activity for characterizing low-frequency events was site-specific. Based on routine monitoring data, the exceedance probabilities of daily mean *E. coli*, *Cryptosporidium* and *Giardia* concentrations evaluated during targeted events were generally low (< 5%) at two sites and moderate (10-35%) at one site. The log-normal distribution fitted to routine monitoring data conservatively predicted daily mean concentrations of *E. coli, Cryptosporidium* and *Giardia* evaluated during all targeted events. The gamma distribution did predict daily mean *Cryptosporidium* concentrations during these events but did not reasonably predict daily mean *E. coli* and *Giardia* concentrations. The upper tail of the gamma distribution may therefore be too thin to predict source water microbial concentrations during hydrometeorological events adequately.

The investigation of the microbial reduction performance of full-scale treatment processes during hydrometeorological events is presented in two articles. It was found, during three snowmelt events, that the reduction performance of high-rate clarifiers (ballasted or floc blanket) increased proportionally to source water concentrations of *Giardia*, adenovirus, rotavirus, *E. coli* and *C. perfringens*. During the rainfall event, the reduction performance of *E. coli* and *C. perfringens* by floc blanket clarifier did not increase; however, the reduction performance of *E. coli* and *C. perfringens* by rapid sand filtration did increase proportionally to their source water concentrations. Site-specific source water *Cryptosporidium* data and *C. perfringens* reduction data were entered into a QMRA model to estimate daily infection risks by *Cryptosporidium* via the consumption of drinking water. The daily infection risks during snowmelt and rainfall episodes were not higher

than the daily risks during baseline conditions. Hence, the annual infection risk is not likely to be dominated by variations in source water pathogen concentrations at these sites. Additionally, these sampling campaigns demonstrated that the full-scale inactivation performances of *E. coli* and adenovirus by ozonation systems were lower than those obtained in lab-scale inactivation studies, potentially because of poor mixing and hydraulic conditions. Limited effectiveness of UV disinfection against naturally occurring adenovirus was also found at operative doses of 40 mJ cm^{-2} after a combination of ballasted clarification, ozonation, granular activated carbon filtration.

It is anticipated that the proposed methodologies for source water characterization and full-scale performance demonstration will help regulators, water supply engineers and managers, and researchers in this field to evaluate monitoring requirements and determine whether microbial health-based targets are achieved.

TABLE OF CONTENTS

LIST OF TABLES

LIST OF FIGURES

LIST OF ABBREVIATIONS

AIC   Akaike information criterion

APHA   American Public Health Association

BIC   bayesian information criterion

BGM   buffalo green monkey kidney cells

CCDF   complementary cumulative distribution function

CDF   cumulative distribution function

CEAEQ   Centre d'expertise en analyse environnementale du Québec

CFU   colony-forming unit

CPAM   cationic polyacrylamide

CPE   cytopathic effect

CSO   combined sewer overflow

DALY   disability-adjusted life year

DAPI   4',6-diamidino-2-phenylindole

DIC   deviance information criterion

DNA   deoxyribonucleic acid

DWTP   drinking water treatment plant

ÉQRM   évaluation quantitative du risque microbien

FIB   faecal indicator bacteria

GAC   granular activated carbon

GLUC   β-D-glucuronidase

HACCP   hazard analysis and critical control points

ICC-qPCR integrated cell culture quantitative polymerase chain reaction

IID   independent and identically distributed

LOD   limit of detection

LT2ESWTR Long Term 2 Enhanced Surface Water Treatment Rule

MAD   mean absolute deviation

MCMC   Markov chain Monte Carlo

mDIC   marginal deviance information criterion

MFU   mean fluorescence unit

MPN   most probable number

NOM   natural organic matter

NTU   nephelometric turbidity units

pppy   per person per year

QMRA   quantitative microbial risk assessment

qPCR   quantitative polymerase chain reaction

RNA   ribonucleic acid

RSD   relative standard deviation

RT-PCR   reverse transcription polymerase chain reaction

SD   standard deviation

SSRC   spores of sulphite-reducing clostridia

TNTC   Too numerous to count

VBNC   viable but non-culturable

USEPA   United States Environmental Protection Agency

UV   ultraviolet

WHO   World Health Organization

WSP   water safety plan

WWTP   wastewater treatment plant

LIST OF SYMBOLS

a	particle radii
C	concentration of the disinfectant
$\bar{C}_{Event}$	daily mean concentration during an event
C_{in}	Influent concentration
C_{out}	Effluent concentration
C_{raw}	Concentration in raw water
ct	concentration x time
D	deviance
D	dose
G	mean velocity gradient
J	Joule
k	number of microorganisms
LR	$\log_{10}$ reduction
$LR_{effective}$	effective $\log_{10}$ reduction
m_x	measurement scale correction
n	sample size
n	particle concentration
n	coefficient of dilution
N	number of microorganisms surviving
n_0	initial particle concentration
N_p	number of viral genome copies
r	analytical recovery

S	Shannon entropy
Se	sensitivity
Sp	specificity
t	detention time
T_f	scaling factor
V	volume
V_P	volume of a pellet
V_{PCR}	volume of a PCR reaction
x	number of microorganisms
$\sigma_{\overline{LR}}$	standard error on the mean $\log_{10}$ reduction
α	collision efficiency coefficient
β	collision rate coefficient
μ	mean value
ν	virus concentration
λ	wavelength

LIST OF APPENDICES

CHAPTER 1.   INTRODUCTION

1.1 Background

The 1993 Milwaukee cryptosporidiosis outbreak, the largest documented North American water supply waterborne outbreak, was described as being caused by a high concentration of *Cryptosporidium* oocysts in source water inadequately removed by conventional treatment processes after a coagulant change-over (Mac Kenzie et al. 1994, Hrudey and Hrudey 2004). Concerns with the occurrence of this outbreak and others during this period led researchers to develop performance-based standards for the control of bacteria, viruses, and protozoa in drinking water (Regli et al. 1991, Haas et al. 1993, Haas et al. 1996). During the same period, several studies showed that low- and medium-pressure UV systems were very effective against *Cryptosporidium* oocysts (Clancy et al. 1998, Clancy et al. 2000, Craik et al. 2001, Shin et al. 2001). The implementation of performance-based standards and the installation of UV treatment technologies in many drinking water treatment plants may have played a significant role in reducing the waterborne disease burden over the three last decades.

Drinking waterborne outbreaks occurring in affluent nations since 2000 were recently compiled in literature reviews (Moreira and Bondelind 2017, Hrudey and Hrudey 2019). According to Hrudey & Hrudey (2019), most of these outbreaks could have been avoided if drinking water suppliers had recognized rather basic lessons: 1) faecal contaminants can be present in all water sources, and 2) some microorganisms shed by livestock and wildlife can be infectious to humans. Many of the cases reviewed also outlined a relationship between waterborne outbreaks and meteorological conditions (Moreira & Bondelind, 2017; Hrudey & Hrudey, 2019). Heavy rain and inadequate treatment of surface water sources were potential causative factors for outbreaks caused by *Cryptosporidium* (Stirling et al. 2001, Jennings and Rhatigan 2002, Pelly et al. 2007, DeSilva et al. 2015), *Giardia* (Nygard et al. 2006), norovirus (Larsson et al. 2014), and *Shigella sonnei* (Arias et al. 2006).

Comparing causative factors of waterborne outbreaks is limited by the fact that compliance and enforcement of drinking water regulations can vary regionally. However, taken together, these outbreak investigations suggest that weaknesses in treatment performances can lie dormant for weeks, months, or years until the occurrence of a transient peak in raw water contamination

overwhelmed treatment barriers. Hrudey & Hrudey (2019) concluded that the occurrence of waterborne outbreaks after heavy rainfall events is certainly common enough to justify increased vigilance for such events. Furthermore, as the frequency of extreme rainfall events is expected to increase in many countries around the world (IPCC 2014), enhanced focus on the management of weather events has been recommended in future revisions of guidance documents for drinking water quality (Khan et al. 2015, Howard et al. 2016). The current framework for drinking water quality management allows, to some extent, to assess microbial risk related to variations in raw water contamination. A brief overview of this framework is presented next.

Since the turn of the millennium, quality assurance of drinking water is shifting from a reactive approach focused on the examination of faecal indicator bacteria in finished water toward a preventive, risk-based approach to water quality management (Fewtrell and Bartram 2001). This framework involves the definition of a quantitative tolerable health-based target and the systematic assessment of risks to determine the magnitude of treatment and operation control required to achieve this target. The water safety plan (WSP), analogous to the *hazard analysis and critical control points* (HACCP) system in the food industry, has been promoted by the World Health Organization (WHO) as an instrument to make the risk-based approach operational (Bartram 2009). Water safety planning is now widely practiced globally (WHO 2017c). One of the key elements of a WSP is the identification of hazardous events (i.e., a situation or an incident that can affect the safety of the water supply (WHO 2009b). Heavy rainfall events are typically considered as potentially hazardous events because surface runoff can increase the loading of microorganisms into the water source (Signor et al. 2005). Moreover, WHO recently recommended to specifically consider hazardous events associated with climate variability and change in the WSP process (WHO 2017a).

Different risk assessment methods (qualitative, semiquantitative, quantitative) have been proposed to evaluate the likelihood and the consequences of hazardous events (WHO 2016b). Quantitative microbial risk assessment (QMRA), the quantitative characterization and estimation of potential health effects associated with exposure of human to microbial agents (Haas et al. 1999), can be used to quantify health risks associated with hazardous events (Medema and Ashbolt 2006, Medema and Smeets 2009, Smeets et al. 2010, Petterson and Ashbolt 2016). The WHO recently published a guidance document to promote and standardize the application of QMRA for water safety management (WHO 2016b). The QMRA process has been used in various regions of the

world to support the development of drinking water guidelines (Government of New Zealand 2007, WHO 2017b, Health Canada 2019) and regulations (VROM-Inspectorate 2005, USEPA 2006).

There are, however, limitations in the available data and models for expanding the application of QMRA. Microbial pathogens cannot be directly measured in drinking water because concentrations are too low for detection; therefore, a bottom-up approach must be adopted to quantify the exposure. However, real-world data sets describing concentrations of microbial pathogens in water sources and their full-scale reduction by water treatment processes are typically very small. Consequently, short-term changes in microbial water quality are highly uncertain. The development of methods to systematically quantify these short-term fluctuations will significantly enhance the usefulness of the QMRA approach. More specifically, the characterization of short-term changes in source water quality will be increasingly necessary to evaluate how drinking water treatment plants cope with current and future hydrometeorological events.

1.2 Structure of the thesis

Introduction (Chapter 1): Chapter 1 provides background on the role of the water safety plan and the quantitative microbial risk assessment processes in supporting the management of infectious microorganisms in drinking water.

Literature review (**Chapter 2**)**:** This chapter reviews mathematical approaches for the evaluation of temporal variations in source water microbial concentrations and microbial reduction across treatment processes.

Research objectives, hypothesis and methodology (**Chapter 3**)**:** In Chapter 3, the research objectives, hypothesis, and the methodology of the thesis are presented.

Chapters 4–8 present the content of this research project in the form of four submitted, accepted, or published scientific publications, and one scientific publication to submit.

1. **Article 1 (Chapter 4):** Can routine monitoring of *E. coli* fully account for peak event concentrations at drinking water intakes in agricultural and urban rivers? Published in *Water Research*.

2. **Article 2 (Chapter 5):** Importance of distributional forms for the assessment of protozoan pathogens concentrations in drinking water sources. Accepted in *Risk Analysis*.

3. **Article 3 (Chapter 6):** Impact of hydrometeorological events for the selection of parametric models for protozoan pathogens in drinking water sources. Accepted in *Risk Analysis*.

4. **Article 4 (Chapter 7):** Demonstrating the reduction of enteric viruses by drinking water treatment during snowmelt episodes in an urban watershed. Submitted to *Water Research*.

5. **Chapter 8:** Using surrogate data to assess microbial risks associated with hydrometeorological events for drinking water safety.

The general findings and implications of this work are discussed in **Chapter 9**.

The main conclusions and recommendations of this research project are presented in **Chapter 10**.

CHAPTER 2. LITERATURE REVIEW

Abstract: This chapter investigates fundamental issues related to the assessment of microbial risks associated with hydrometeorological events at drinking water treatment plants. Mathematical approaches for evaluating temporal variations in microbial concentrations in source water and pathogen reduction across treatment processes are presented. A special focus is on the consideration of low-probability contamination events in risk assessment. Candidate probability distributions describing simple statements about underlying processes are proposed for the assessment of temporal variations in source water microbial concentrations. Rate laws governing the removal and inactivation of pathogens in drinking water treatment processes are presented, and their potential deviations under dynamic conditions are discussed.

2.1 Introduction

One of the main tasks in drinking water safety management involves the prediction and mitigation of hazardous events (WHO 2017b). Accurate knowledge of the frequency, amplitude, and duration of microbial contamination peaks in drinking water sources is of paramount importance for risk assessment and management (Teunis et al. 2004). Rainfall events are known to promote the rapid transport of microbial contaminants in surface water, which may lead to transient raw water contamination peaks at drinking water intakes (Atherholt et al. 1998, Kistemann et al. 2002, Signor et al. 2005). Snowmelt events have also been recently identified as critical periods of source water microbial contamination in urbanized catchments (Jalliffier-Verne et al. 2016, Madoux-Humery et al. 2016). Accounting for the impact of such hazardous events in the quantification of microbial treatment requirements has been frequently recommended in the scientific literature (Medema and Ashbolt 2006, Signor and Ashbolt 2009, Schijven et al. 2011, Petterson et al. 2015) and in guidance documents (WHO 2009b, 2016b). However, reasonable methods to address this issue have not yet been extensively explored. The aim of this Chapter is, therefore, to present a mathematical framework to account for microbial risks associated with hydrometeorological events in microbial risk assessment for drinking water safety.

2.2 Exposure assessment framework for water safety management

The starting point in any QMRA is to consider the dose–response framework for infectious microorganisms. The probability of response (infection, acute illness) resulting from any single

inoculated pathogen acting independently to cause infection typically follows an exponential or a beta Poisson dose–response model (Haas 1983, Teunis and Havelaar 2000). For these dose–response models, the number of microorganisms in the dose is Poisson distributed. Thus, the exposure is usually characterized in terms of the arithmetic mean number of organisms in the dose (Haas 1996)[1]. The exposure assessment can therefore be viewed as an attempt to quantify the mean dose of a pathogen ingested by a person via the consumption of contaminated drinking water.

Concentrations of pathogens in treated drinking water are usually too low to be accurately detected by current detection methods. Due to this limitation, the exposure is generally predicted by quantifying the concentration of the pathogen in raw water and its reduction by water treatment processes. A generic model for the exposure assessment can be formulated as follows (Teunis and Schijven 2019):

$$D = C_{raw} \times \frac{1}{Se} \times Sp \times Z_{1,...,n} \times V_{ing} \tag{2.1}$$

where D is the dose of a pathogen ingested via drinking water; C_{raw} is the pathogen concentration in raw water; Se is the sensitivity of the enumeration method; Sp is the specificity of the enumeration method; Z is the fraction of pathogen that passes n consecutive water treatment processes; and V_{ing} is the volume ingested. Input probability distributions can be used to characterize these variables over time. Mathematical approaches to describe the temporal variations in microbial concentrations in raw water and pathogen reduction across treatment processes are presented in sections 2.3 and 2.4, respectively.

---

[1] The number of organisms in the dose may be overdispersed relative to the Poisson distribution; however, for a given mean dose, the risk predicted with a mixed Poisson model (e.g., negative binomial distribution) is always less than the risk predicted with a Poisson distribution (Haas 2002, Nilsen and Wyller 2016). The Poisson distribution represents a conservative upper bound estimate of the risk.

2.3 Framework for assessing source water concentrations

2.3.1 Statistical model for microbial count data

The simplest model to describe the distribution of microbial counts per unit volume in a suspension is the Poisson distribution. The probability of finding k organisms in a homogenous sample x of volume V collected from a suspension of mean concentration μ is given by the Poisson distribution:

$$P(x = k) = \frac{\bar{\mu}V^k}{k!} \exp{(-\bar{\mu}V)} \tag{2.2}$$

At the same location, the mean concentration $\bar{\mu}$ is a single sample will vary per unit time because of the effect of hydrometeorological conditions on the transport of microorganisms, the presence/absence of sources of microbial contamination in the catchment, etc. To describe temporal variations in the mean concentration μ, a "mixing" continuous probability distribution can be combined with the Poisson distribution to yield a discrete mixed Poisson distribution (Haas et al. 1999). A mixed Poisson distribution can be written as Equation (2.2) integrated with a mixing distribution as follows:

$$P(x; V, \beta) = \int_0^\infty P_p(x; \bar{\mu}V)\, h(\mu; \beta) d\mu \tag{2.2}$$

where h is the mixing distribution of parameters β describing the temporal variations in the mean concentration $\bar{\mu}$. The negative-binomial distribution (gamma-Poisson mixture) is generally considered as an input distribution to characterize pathogen data (Teunis et al. 1997, Schijven et al. 2011, Petterson et al. 2015, WHO 2016b), in part because the negative binomial distribution can be written in closed form (Teunis and Schijven 2019). Other continuous distributions can be used as mixing distributions to describe different underlying processes generating temporal variations in microbial concentrations (Haas et al. 1999). The selection of an adequately conservative mixing distribution may be key to predict the frequency and the magnitude of microbial peak events in source water. A catalogue of candidate mixture distributions is therefore proposed in the next section.

2.3.2 Candidate mixture distributions

One possible approach to select candidate distribution is to read their distributional forms as statements about processes (Frank 2014). It can be demonstrated using information theory and the notion of maximum entropy that probability distributions typically arise as simple combinations of linear scaling (additive processes) and logarithmic scaling (multiplicative processes or additive processes on the log scale). In statistical mechanics, a continuous probability distribution can be determined by maximizing the Shannon entropy S under a constraint on the average value and a constraint on total probability[2]. The method of Lagrange multipliers can be used to maximize S subject to these two constraints[3]. The solution takes the simple form (Frank 2014):

$$p_x \propto e^{-\lambda x} \tag{2.5}$$

The probability distribution p_x is therefore directly proportional to an exponential distribution $e^{-\lambda x}$ with $\lambda = 1/\mu$. To generalize the solution of Eq. (2.5) into a single framework, the measurement scale may be constrained, yielding

$$p_x \propto e^{-\lambda T_f} \tag{2.6}$$

where T_f is a scaling measure (Frank and Smith 2010). Many distributional forms can be expressed by choosing an expression for T_f. The base scale becomes purely linear if $T_f = x$ (exponential distribution) or purely logarithmic if $T_f = \log(x)$ (Pareto type I distribution).

The transition from a logarithmic scale to a linear scale with the magnitude of observations can be expressed if $T_f = \log(x) - bx$ (gamma distribution). The logarithmic scale $T_f \approx \log(x)$ dominates when x is small, whereas the linear scale $T_f \approx -bx$ dominates when x is large. Inversely, a transition from a linear scale to a logarithmic can be expressed if $T_f = \log(1 + x/\alpha)$ (Pareto type

---

[2] The Shannon entropy is given by $S = -\int p_x \log(p_x) dx$ and is maximized under a constraint on the average value $G_1(p_x) = \int p_x x dx - \mu = 0$ and a constraint on total probability $G_2(p_x) = \int p_x dx - 1 = 0$

[3] This method consists in constructing a new function $F' = -S - \kappa G_1(p_x) - \lambda G_2(p_x)$ and maximizing it by writing the partial derivates of F' with respect to p_x's equal to zero.

II/Lomax distribution). The scale is linear $T_f \approx x/\alpha$ for small values of x whereas the scale is logarithmic $T_f \approx \log(x/\alpha)$ for large values of x.

It can also be useful to apply a change of variable to express the probability distribution on a different scale. In these cases, a measurement scale correction m_x needs to be added to the generalized form presented in Eq. (2.6)

$$p_x \propto m_x e^{-\lambda T_f} \tag{2.7}$$

in which $m_x = |g'(x)|$, where g' is the derivative of the scale correction function g (Frank, 2014). For example, for a change of variable $y = \log(x)$, the scale y can be changed to the scale x, by using $g(x) = \log(x)$, which yield $m_x = g'(x) = x^{-1}$. If the Gaussian distribution is expressed using $T_f = (x - \mu)^2$ [4], then the log-normal distribution can be expressed by a change of scale with $T_f = (\log(x) - \mu)^2$ and $m_x = x^{-1}$.

$$p_x \propto x^{-1} e^{-\lambda (\log(x) - \mu)^2} \tag{2.8}$$

Table 2-1 lists the base form of commonly observed distributions arising from combinations of linear scaling and logarithmic scaling. The advantage of these candidate distributions is that they can be read in terms of underlying processes. In practice, determining in which context tail events scale linearly or logarithmically may be useful to guide the risk assessment. The consideration of other distributions, such as extreme value distributions, could be valuable to extend this list.

---

[4] By applying a constraint on the variance rather than a constraint on the mean, the solution of Eq. (2.5) takes the form $p_x \propto e^{-\lambda(x-\mu)^2}$ where $\lambda = 1/2\sigma^2$, which is the normal (Gaussian) distribution.

Table 2-1: Common probability distribution as statements about processes. Adapted from Frank (2014).

Distribution	Base form	Base scale
Exponential	$e^{-\lambda x}$	Linear
Normal (Gaussian)	$e^{-\lambda x^2}$	Linear
Log-normal	$x^{-1}e^{-\lambda(\log x)^2}$	Linear (on the log-scale)
Gamma	$x^{-\lambda}e^{-c_1\lambda x}$	Log-linear
Pareto type I	$x^{-\lambda}$	Log
Pareto type II/Lomax	$(c_1 + x)^{-\lambda}$	Linear-log

Complementary cumulative distribution function (CCDF) graphs are commonly used in risk assessment to visually compare candidate distributions with different upper tail behaviors (Haas 1997, Smeets et al. 2008). A CCDF graph is simply a distribution of the exceedance probability versus the consequence (in our case, the concentration of the microorganism) represented on a log-log scale. Figure 2-1 illustrates theoretical CCDF distributions for candidate probability distributions presented earlier. This CCDF graph shows that, at low exceedance probabilities, the Gamma and normal distributions decay exponentially with tail probabilities (linear scaling). In contrast, the Lomax distribution has a power-law tail (logarithmic scaling). In this example, the log-normal and Lomax tails have disproportional roles in defining the mean of these distributions (Figure 2-1). Correct identification of the tail behavior can therefore be of importance when the variability in microbial concentrations is high. However, in practice, characterizing tail behaviors with time series data can be particularly difficult because only small sample sizes are typically available. The next section will look more closely into this issue.
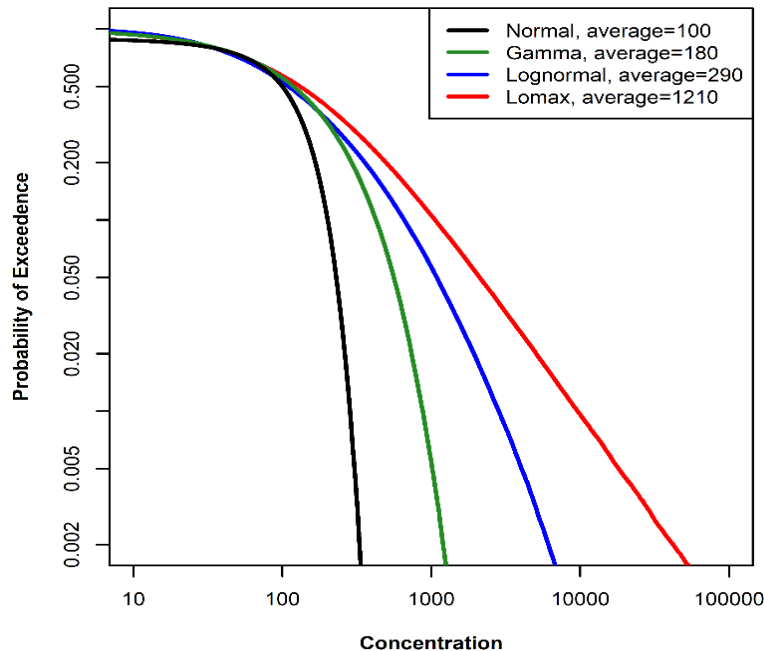
Figure 2-1: Complementary cumulative distribution function (CCDF) curves for four candidate distributions, including normal (μ=100, σ=80), gamma (α=0.9, β=0.005), log-normal (μ=4.7, σ=1.4), and Lomax (α=1.1, λ=150)

2.3.3 Time series concepts ─Stationarity and ergodicity

Continuous probability distributions can be used for the analysis of time series data if random fluctuations exhibit both *ergodicity* and *stationarity*. The concept of ergodicity implies that the parameter values of these distributions can be adequately deduced from a sufficiently large sample of the random process. Stationarity signifies that the parameter values will not vary over time. These two assumptions are not commonly validated in practice, but their implications need to be considered when a real system is intended to be represented.

The ergodic assumption will be violated if multiple underlying processes with their own statistical properties are superposed. Figure 2-1 shows that the normal, gamma, log-normal, and Lomax distributions have similar behaviors from exceedance probabilities of 1.0 to 0.2 but have distinct behaviors at lower exceedance probabilities. Therefore, the underlying process can only be validated if the sample size is large enough to characterize the upper tail. In Figure 2-2, the sample mean of randomly generated samples from these distributions is tracked for various sample sizes.

The sample means stabilize rapidly for thin tail distributions (normal, gamma), but not for heavy tail distributions (log-normal, Lomax).
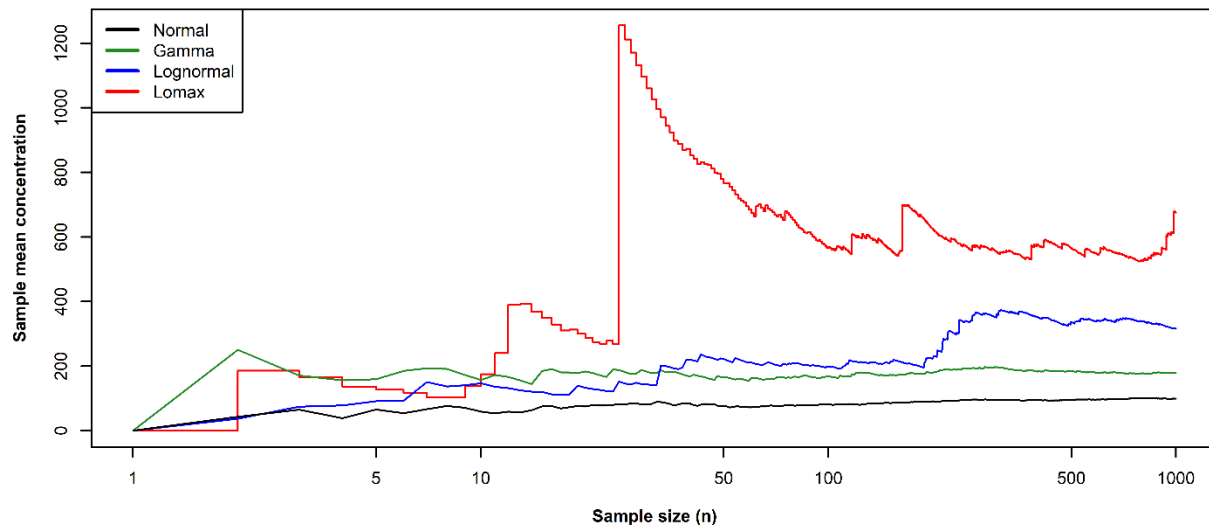
Figure 2-2: Sample mean concentration from randomly generated samples for four candidate distributions, including normal ($\mu=100$, $\sigma=80$), gamma ($\alpha=0.9$, $\beta=0.005$), log-normal ($\mu=4.7$, $\sigma=1.4$), and Lomax ($\alpha=1.1$, $\lambda=150$)

In drinking water safety management, sample numbers are often small ($n<30$ samples per site) because of the high costs of pathogen analysis. Therefore, pathogen concentrations cannot be characterized at low exceedance probabilities, and the tail of the distribution can only be extrapolated. A potential solution to validate these extrapolations may be to identify critical periods of raw water contamination with a surrogate and monitor pathogen concentrations during these periods (Teunis and Schijven 2019). The probability that these observations fall in the upper tail of a candidate distribution may then be evaluated to inform model selection. Stationarity is a more difficult assumption to validate in a water quality assessment. Nonstationarity may arise from the combination of the effects of climate change and human disturbances on a river catchment (Milly et al. 2008). Large faecal indicator data sets collected over multiple years might be useful to evaluate stochastic trends and distributional shifts. Pathogen/surrogate indicator data are frequently collected in rounds of source water monitoring (e.g., every 5 years), which may implicitly address the problem of nonstationarity. Nevertheless, probability distributions are conditional on historical data; thus, a distribution may not accurately predict concentrations during an accident or an extreme

weather event. The identification of early signals and precursors is needed to manage these types of event.

2.4 Framework for assessing pathogen reduction across treatment processes

2.4.1 First-order process

A commonly used model to describe the degree to which a treatment process reduces an influent microorganism concentration is the log-reduction (LR). This quantification method assumes that the reduction is a first-order process with respect to the influent concentration of the microorganism. If the reduction of an organism by a treatment process is first-order with respect to the influent concentration C_{in}, then the effluent concentration C_{out} can be calculated as follows:

$$C_{out} = C_{in}\exp\left(-kt\right) \tag{2.9}$$

where t is the detention or retention time in the treatment process, and k is a first-order rate constant (Haas et al. 1999). By assuming that the treatment process is operating under steady-state conditions (kt is a constant), the log-reduction can be obtained empirically by taking the common logarithm of the ratio of the concentration before and the concentration after the process. A point estimate of the log-removal (LR) across a treatment unit can be calculated as follows:

$$\mathrm{LR} = \log_{10}\left(\frac{C_{in}}{C_{out}}\right) \tag{2.10}$$

The first-order model considerably simplifies the exposure assessment because the same fraction of microorganisms is expected to be removed regardless of the influent concentration C_{in}. Furthermore, if all treatment processes of a treatment train are first-order and independent, then the total average reduction performance of the treatment train can be calculated by multiplying the average rate of passage (10^{-LR}) of each process (Haas and Trussell 1998, Teunis et al. 2009, Schmidt et al. 2020). The concept of log-reduction is widely used in the water industry to characterize the reduction performance of treatment processes (USEPA 2006, Ministry of Health 2008, Health Canada 2019). However, under real-world dynamic conditions, the first-order rate constant k may vary in time. In this case, a deviation from the first-order process would occur.

2.4.2 Potential deviations from the first-order process

2.4.2.1 Coagulation/flocculation processes

The first-order rate model presented in Equation (2.10) neglects the mechanism of particle aggregation during flocculation. However, this mechanism may have a significant influence on the removal of a microorganism. Increases in the removal of protozoan parasites by conventional treatment have often been associated with increases in turbidity/particle concentrations in raw water (LeChevallier et al. 1991, LeChevallier and Norton 1992, Nieminski and Ongerth 1995, McTigue et al. 1998, Dugan et al. 2001).

The Smoluchowski coagulation theory of particles may help understanding how microorganisms are aggregated during flocculation. The prediction of flocculation rates can be viewed as a two-step process (Gregory 2005). First, a mathematical expression (size distribution function) is derived to keep particle count as a function of their size. Second, a collision rate coefficient based on a physical model (Brownian motion, fluid shear, differential sedimentation) is introduced into the expression that keeps counts of collisions. The relative contribution of these mechanisms during flocculation will primarily depend on the size of the particles in the system (Han and Lawler 1992, Youn and Lawler 2019). According to Smoluchowski, the collision between particles of sizes i and j in a suspension can be treated as a second-order rate process given by

$$J_{ij} = \alpha_{ij}\beta_{ij}n_i n_j \tag{2.11}$$

where α_{ij} is a collision efficiency coefficient; β_{ij} is a collision rate coefficient; and n_i and n_j are the particle concentrations (Gregory and O'Melia 1989). Concentrations of microorganisms in natural aquatic environments are typically much lower than concentrations of abiotic particles. Thus, the removal of microorganisms during conventional flocculation should be governed by heteroaggregation between microorganisms and abiotic particles. If the initial concentration of a i-sized microorganism $n_{i,0}$ is assumed to be much smaller than the initial concentration of a j-sized abiotic particle $n_{j,0}$, then the rate of loss of the concentration of a i-sized microorganism n_i can be approximated by a pseudo-first-order process given by:

$$\frac{dn_i}{dt} \approx -\alpha_{ij}\beta_{ij}n_{j,0}n_i \tag{2.12}$$

where α_{ij} is a collision efficiency coefficient; β_{ij} is a collision rate coefficient; and t is the detention time in the flocculator. Integrating Equation (2.12) once yields:

$$n_i = n_{i,0} \exp(-n_{j,0}\alpha_{ij}\beta_{ij}t) \tag{2.13}$$

Therefore, even without knowing any details of α_{ij} and β_{ij}, it can be anticipated that the particle concentration in raw water is influencing the aggregation rate of microorganisms during flocculation.

2.4.2.2 Disinfection processes

In the context of microbial decay promoted by disinfection, the first-order rate constant k from Equation (2.9) is conventionally replaced by kC^n to form the Chick–Watson model (Haas et al. 1999). This model is expressed by the differential rate law:

$$\frac{dN}{dt} = -kC^nN \tag{2.14}$$

where dN/dt is the rate of inactivation, N is the number of survivors at contact time t, k is the Chick–Watson coefficient for a specific microorganism and set of conditions, C is the concentration of the disinfectant, n is the coefficient of dilution (i.e., the average number of molecules of disinfectant necessary to inactivate a microorganism). Equation (2.14) can be generalized for nonlinear behaviors by the following differential rate law (Gyürék and Finch 1998):

$$\frac{dN}{dt} = -kmN^x t^{m-1}C^n \tag{2.15}$$

which integrated once yields

$$\ln\left(\frac{N}{N_0}\right) = -\left(\frac{1}{x-1}\right)\ln[1 + N_0^{x-1}(x-1)kC^n t^m] \tag{2.16}$$

where m and x are empirical constants. Equation (2.16) indicates that if x is different than 1, then the inactivation efficiency depends on N_0. This dependency has been observed in experimental disinfection studies of *Giardia muris* by ozone (Haas and Kaymak 2003) and of *E. coli* by monochloramine (Kaymak and Haas 2008). Haas and Kaymak (2003) hypothesized that quorum sensing (i.e., cell-cell communication mechanism) could alter the response of organisms at higher

concentrations or that higher concentrations of organisms could form a more significant amount of disinfection by-product which could be inactivation agents themselves.

2.4.3 Implications for risk assessment

Deviations from the first-order process for coagulation/flocculation and disinfection suggest that these treatment processes are operated under dynamic conditions instead of steady-state conditions. Mechanistic models may be more useful to predict treatment performance under dynamic conditions (WHO 2016b). The development of mechanistic models would require site-specific data sets representing a wide range of operational conditions. The incorporation of correlations among exposure variables in a quantitative risk assessment may have a substantial effect on risk estimates (Smith et al. 1992, Haas 1999, Wu and Tsang 2004). Further work is needed to evaluate how these correlations could be assessed and incorporated in QMRA.

2.5 Conclusions

The importance of considering the impact of hydrometeorological events in drinking water safety management has been frequently recommended in the scientific literature and guidance documents. A systematic assessment of microbial risks posed by such events is needed to inform risk management strategies. Identifying critical periods of source water contamination and evaluating the full-scale performance of treatment processes during these periods could substantially improve the assessment of these risks. High-resolution data on full-scale performances by physicochemical and disinfection processes are needed to evaluate whether deviations from the first-order process are significant in practice.

CHAPTER 3. RESEARCH OBJECTIVES, HYPOTHESIS AND METHODOLOGY

3.1 Research objectives and hypothesis

The general objective of this research project is to present a method to systematically assess microbial risks associated with hydrometeorological events at drinking water treatment plants. The specific objectives are:

Objective 1: To present a catalogue of candidate probability distributions to describe temporal variations in source water microbial concentrations, provide a statistical approach to estimate their parameters from data and compare their relative fit.

Objective 2: To evaluate the potential of autonomous online measurements of β-D-glucuronidase (GLUC) activity to assess short-term variations in source water microbial concentrations.

Objective 3: To determine which probability distributions adequately predict source water microbial concentrations during hydrometeorological events.

Objective 4: To assess the impact of short-term fluctuations in source water microbial concentrations on microbial risks associated with drinking water consumption.

The interdependencies between these objectives are presented with a flowchart in Figure 3-1.

Achieving these objectives should address specific questions, such as:

- Can online GLUC activity monitoring facilitates the identification of microbial peaks in surface water, and if so, which candidate probability distribution adequately predict them?

- Do microbial reduction performances of full-scale treatment processes deviate from the first-order rate during hydrometeorological events?

- What is the magnitude of the short-term infection risks during hydrometeorological events? Do these short-term risks drive the aggregate risk over the long-term?

The research hypotheses and their validation criteria are listed in Table 3-1

General objective
To present a method to systematically assess microbial risks associated with hydrometeorological events at surface drinking water treatment plants

Stochastic modeling of source water data	**Event-based monitoring of source & treatment**
1. Catalogue of candidate probability distributions as statements about process 2. Bayesian model to estimate distribution parameters using routine monitoring data 3. Model comparison and selection using information criteria and predictive checks	4. Monitoring strategy using autonomous online measurement of β-D-glucuronidase activity and meteorological indices to trigger sampling 5. Assessment of short-term variations in microbial pathogens/indicators concentrations 6. Assessment of short-term variations in microbial reduction by full-scale treatment

QMRA framework

7. Evaluation of the impact of distribution selection on the mean concentration of the microorganism and its uncertainty
8. Validation of probability distributions for short-term variations in microbial pathogens/indicators concentrations
9. Demonstration of the capacity of full-scale treatment processes to cope with increases in microbial contamination at the source
10. Quantification of short-term microbial risks in baseline & event conditions

Figure 3-1: Flowchart representing the objectives of the thesis

Table 3-1: Research hypotheses, criteria for their validation, and corresponding articles

	Statement	Hypothesis	Validation	Article
1	A precise estimate of the mean source water microbial concentration and its uncertainty is required for defining site-specific drinking water treatment requirements.	Correct identification of the tail behavior of a probability distribution fitted to monitoring data is necessary to estimate the mean source water microbial concentration and its uncertainty.	The upper bound of the 95% uncertainty interval on the mean source water microbial concentration varies from >0.5-log among distributions fitted to the same data.	1,2,3
2	The characterization of low-frequency events of source water microbial contamination is needed to validate the tail behavior of a probability distribution fitted to small monitoring data sets.	Online β-D-glucuronidase monitoring captures events necessary for characterizing low-frequency events in source water microbial concentrations.	The exceedance probability of the daily mean microbial concentration during captured events is < 5% based on a gamma distribution fitted to historical monitoring data.	1,3,5
3	Transient peaks in source water microbial contamination should be explicitly considered in source water characterization.	The gamma distribution does not reasonably predict source water microbial concentrations during snowmelt and rainfall events.	The gamma distribution predicts daily mean concentrations at an exceedance probability < 0.1% during snowmelt and rainfall events.	1,3
4	The reduction of microorganisms by each treatment process is assumed to be a first-order process with respect to their influent concentration.	The concentration of microorganisms in treated drinking water increases proportionally to its source water concentration.	An increase in the daily mean microbial concentration >1.0-log is measured in settled water or filtered water during a source water event.	3,4,5

3.2 Methodology

The selection of sites for case studies, the design and implementation of baseline and event-based monitoring campaigns, and the development of methods for the statistical analysis of microbial datasets are presented in this section. The selection of reference pathogens and surrogate microorganisms and the specific procedures required for their concentration and enumeration will be presented in Chapters 4–8.

3.2.1 Site selection

In Quebec, Canada, weekly or monthly sampling of raw water for the enumeration of *Escherichia coli* (*E. coli*) is required at surface drinking water treatment plants (DWTPs) by the *Regulation respecting the quality of drinking water* (Chapter Q-2, r.40) since 2012. Also, for research purposes, *Cryptosporidium* and *Giardia* were monitored by the Government of Quebec at 30 DWTPs for two years between 2011 and 2019. *E. coli*, *Cryptosporidium*, and *Giardia* data from these 30 DWTPs were available for site selection. The statistical analysis of six *E. coli* data sets will be presented in Chapter 4. These sites were selected to investigate temporal variations in *E. coli* concentrations at DWTPs highly vulnerable to (un)treated municipal wastewater discharges and agricultural runoff. Three of the six sites evaluated in Chapter 4 were selected for detailed investigations of short-term fluctuations in source water quality during hydrometeorological events (snowmelt and rainfall episodes). Figure 3-2 shows aerial photographs of the location of these DWTPs and lists primary sources of microbial contamination identified in their catchments. Unit processes involved in the treatment train of these DWTPs are shown schematically in Figure 3-3. The DWTPs selected for each article and their general catchment characteristics are listed in Table 3-2.
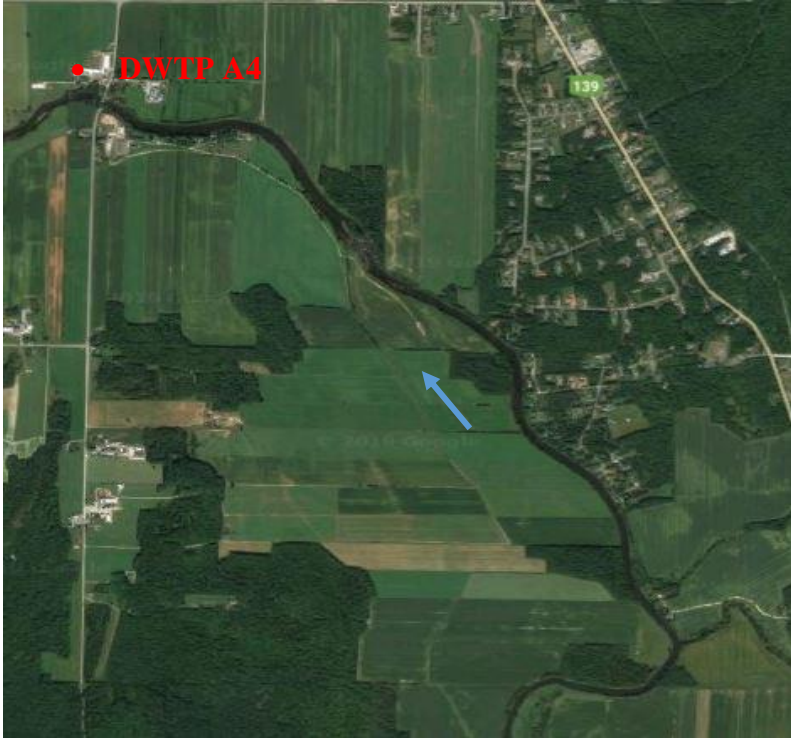
DWTPs C6 and C7: Snowmelt events (spring 2017-18)	DWTP A4: Rainfall event (autumn 2017)
Map data © 2020, Google Canada	Map data © 2020, Google Canada
River flow rate (spring): 400 m^3/s Primary sources of microbial contamination • Five wastewater treatment plants • >200 combined sewer overflows	Average river flow rate (autumn): 15 m^3/s Primary sources of microbial contamination • Agricultural spraying: April to October • One wastewater treatment plant (aerated pond, 10 km upstream, 1000 m^3/d) • Four combined sewer overflows

Figure 3-2: Maps and catchment characteristics of selected sites
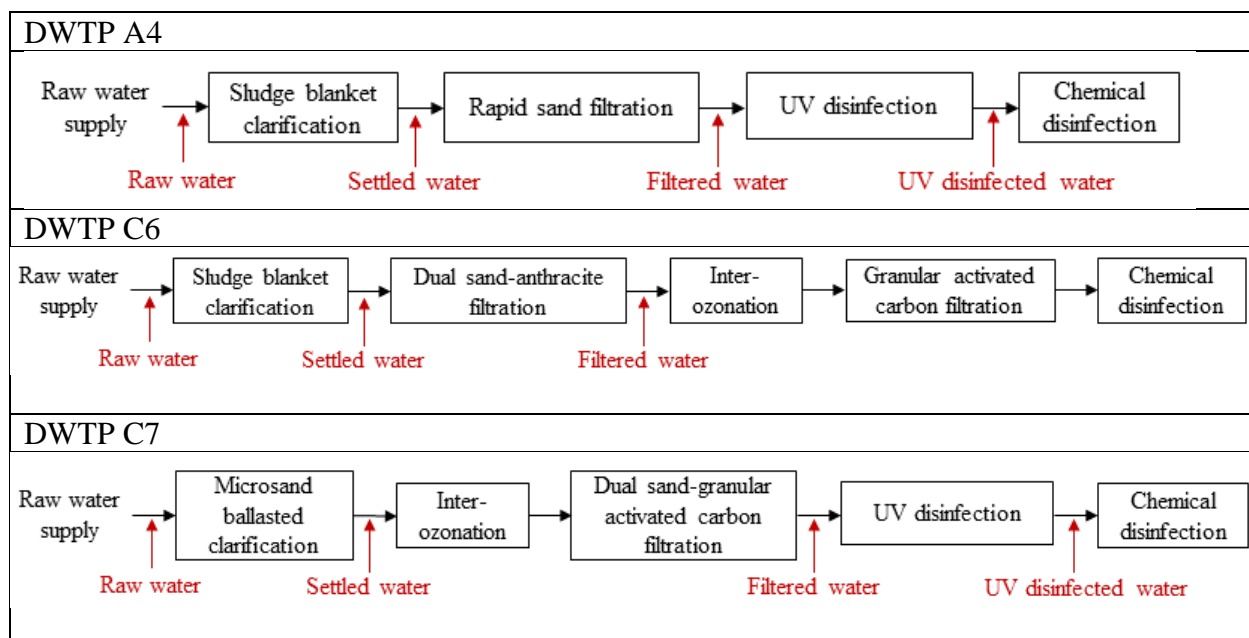
Figure 3-3: Unit processes involved in the treatment train of drinking water treatment plants studied in this thesis and location of sampling points

Table 3-2: Drinking water treatment plants studied in this thesis and their catchment characteristics

Article 1 (Source)	Article 2 (Source)	Article 3 (Source, treatment)	Article 4 (Source, treatment)	Chapter 8 (Source, treatment)	Main land cover	Catchment size (km^2)	Mean discharge of river (m^3/s)
-	DWTP A01	-	-	-	Agricultural	100	<20
-	DWTP A02	-	-	-	Agricultural	200	<20
-	DWTP A1	-	-	-	Forested	100	<20
-	DWTP A2	-	-	-	Mixed	<100	<20
-	DWTP A3	-	-	-	Mixed	500	<20
DWTP B	DWTP A4	DWTP A4	-	DWTP A	Agricultural	<100	<20
-	DWTP B1	-	-	-	Mixed	2500	23
-	DWTP B2	-	-	-	Forested	4000	26
-	DWTP B3	-	-	-	Mixed	2500	26
-	DWTP B4	-	-	-	Mixed	4200	27
-	DWTP B5	-	-	-	Mixed	1100	36
-	DWTP B6	-	-	-	Mixed	2500	70
-	DWTP B7	-	-	-	Agricultural	3400	74
-	DWTP C1	-	-	-	Mixed	10 000	114
-	DWTP C2	-	-	-	Agricultural	10 000	114
-	DWTP C3	-	-	-	Mixed	7 000	114
-	DWTP C4	-	-	-	Mixed	10 000	190
-	DWTP C5	-	-	-	Agricultural	10 000	190
DWTP C1	DWTP C6	DWTP C6	DWTP A	-	Urban	>50000	286
DWTP C2	DWTP C7	-	DWTP B	DWTP B	Urban	>50000	286
-	DWTP C8	-	-	-	Mixed	23000	330
-	DWTP C9	-	-	-	Mixed	23000	330
-	DWTP C10	-	-	-	Urban	>50000	1,365
DWTP D	DWTP C11	-	-	-	Urban	>50000	1,365
-	DWTP C12	-	-	-	Urban	>50000	16000
-	DWTP C13	-	-	-	Mixed	>50000	16000
-	DWTP C14	-	-	-	Mixed	>50000	16000
DWTP A	DWTP D1	-	-	-	Agricultural	200	Reservoir
-	DWTP E1	-	-	-	Forested	100	Lake
-	DWTP E2	-	-	-	Forested	3000	Lake

3.2.2 Event-based monitoring campaigns

3.2.2.1 Rationale for event-based monitoring

In the context of this research, event-based monitoring consists of sampling a microbial contaminant under conditions (hazardous event) when microbial concentrations are expected to be high (rainfall/snowmelt episodes, sewer bypass event). Data from event-based monitoring were used to: 1) validate the prediction of parametric models describing temporal variations in source water microbial concentrations, and 2) demonstrate the full-scale performance of treatment processes during critical periods of source water contamination.

3.2.2.2   Identification of critical periods of microbial contamination

Fully automated measurement systems (ColiMinder™ VWM GmbH, Vienna, Austria) were installed at the selected DWTPs to measure β-D-glucuronidase (GLUC) activity in raw water at high-frequency (every ~15-30 minutes). Detailed technical information about the technology can be found in Koschelnik et al. (2015). Short-term variations in GLUC activity were measured for about one month before event-based monitoring campaigns to estimate the baseline GLUC activity level. Event-based monitoring campaigns were triggered by site-specific changes in GLUC activity levels and meteorological indices (24-hour cumulative rainfall, air temperature). Figure 3-4 shows results from GLUC activity measurements at an urban DWTP.
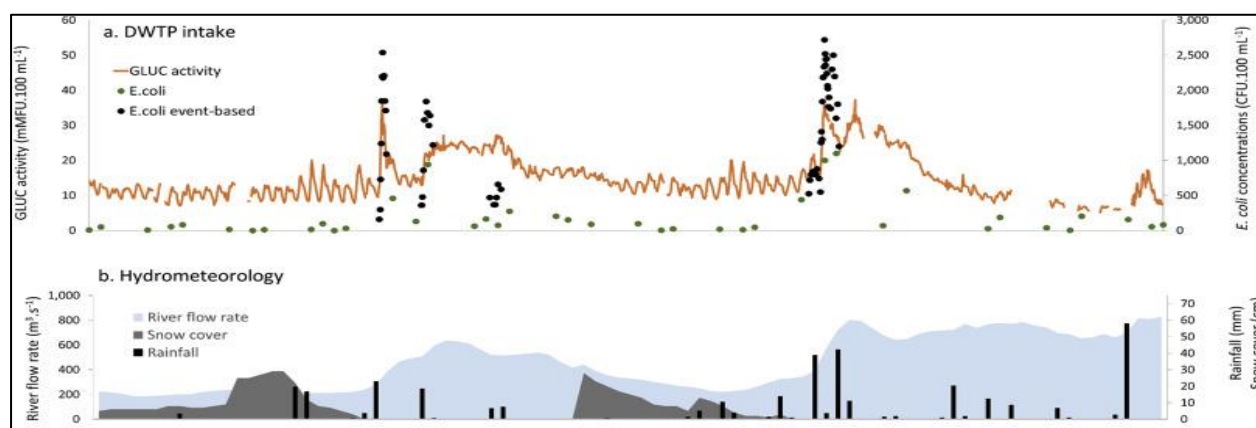
Figure 3-4: Near real-time GLUC activity measurements combined with routine and event-based monitoring of *E. coli* at the intake of a drinking water treatment plant during combined snowmelt/rainfall-induced runoff events. Adapted from Burnet et al. (2019b).

3.2.2.3   Monitoring the reduction performance of full-scale treatment processes

Monitoring the removal or inactivation of microorganisms by full-scale treatment processes is challenging because it requires the concentration of large volumes of water. Measuring short-term fluctuations in the removal performance of a treatment process requires a concentration method rapid enough to concentrate multiple large volumes in a relatively short amount of time. The Hemoflow method was used to simultaneously concentrate *E. coli* and *C. perfringens* spores in raw, settled, filtered and UV-disinfected water samples (Veenendaal and Brouwer-Hanzens 2007). A Hemoflow HF80S filter (Fresenius, Ontario, Canada) can only concentrate water at a rate of approximately 1 L/min. Therefore, installations with four Hemoflow-filters in parallel were built to concentrate large water volumes (1000-1500 L) in about 6 hours. Viruses were concentrated

from water samples using electropositive filters NanoCeram VS2.5-5 (Argonide Corp, Sanford, FL, USA). Large volume samples were filtered on-site at high-frequency under a constant flow rate of 5-15 L min^{-1}. Schematic overviews of the Hemoflow and NanoCeram concentration systems are presented in Figure 3-5.

Hemoflow ultrafiltration filter	NanoCeram electropositive filter
Adapted from: media.springernature.com/lw785/springer-static/	
Schematic overview of the Hemoflow system	Schematic overview of the NanoCeram system
A picture (A) and a schematic overview (B) of the Hemoflow-system 1, sample-collection point; 2, water meter; 3, water tank with float; 4, pump; 5, Hemoflow-filter; 6, filtrate; 7, pressure meter; 8, returning tube; 9, tube clamp; a, c en d connection points for tubes Adapted from: Veenendall & Brouwer-Hanzens (2007)	Adapted from Fout *et al.* (2016)
On-site Hemoflow concentration	On-site NanoCeram concentration

Figure 3-5: Simultaneous concentration of multiple microbial indicators using Hemoflow ultrafiltration filters and virus concentration using NanoCeram cartridge filters

3.2.3 Statistical analysis of microbial data sets

Hierarchical Bayesian models were developed for the statistical analysis of microbial data sets using the software JAGS (Plummer 2013). Bayesian methods were selected because Bayesian

statistics can produce reasonable results when only small data sets are available (van de Schoot and Miocević 2020). The fundamentals of Bayesian analysis will be briefly discussed in this section. The application of hierarchical Bayesian models for the analysis of pathogen data will be detailed in Chapters 5 and 7.

3.2.3.1   Bayesian computation

In microbial risk assessment, statistical inference is preferably undertaken using original observations (microorganism counts, analyzed volume) rather than reported concentrations (Haas et al. 1999). The modeling of original observations is advantageous because it allows incorporating different sources of uncertainties into the statistical analysis. In Bayesian inference, the distribution of values of a parameter θ given the observed data D is evaluated with the Bayes' theorem:

$$P(\theta|x) = \frac{P(D|\theta)P(\theta)}{\int_{\theta} P(D|\theta)P(\theta)\, d\theta} \tag{3.1}$$

where $P(\theta|D)$ is the posterior; $P(D|\theta)$ is the likelihood; $P(\theta)$ is the prior; and the denominator is the marginal likelihood, i.e., the overall probability of the data D according to the model. The marginal likelihood is calculated by averaging across all θ values weighted by the strength of belief in those values (Kruschke 2014). The computation of the marginal likelihood in hierarchical models may require the calculation of intractable integrals. In such cases, Markov chain Monte Carlo (MCMC) methods can be used to generate parameter values from the posterior distribution of the model without computing the integral in the marginal likelihood.

A popular MCMC method is the Metropolis algorithm. The Metropolis algorithm works by generating sample values of a parameter θ by taking a random walk through the parameter space as follows:

1. The random walk starts at an arbitrary point specified by a proposal distribution (e.g., a normal distribution centred at the current position in the parameter space).

2. For each time step t, the random walk progress by proposing a new position in the parameter space. An acceptance ratio r is computed to decide whether the proposed location is accepted.

$$r(\theta_{\text{new}}, \theta_{t-1}) = \frac{P(D|\theta_{\text{new}})P(\theta_{\text{new}})}{P(D|\theta_{t-1})P(\theta_{t-1})} \qquad (3.2)$$

If $r > 1$, then θ_{new} is accepted. If the $r \leq 1$, then a random number from uniform [0,1] is generated. If the random number is $\leq r$, θ_{new} is accepted, if not, θ_{new} is rejected and a new value of the parameter θ is randomly generated from the proposal distribution.

The process is repeated thousands of times, and, in the long run, the positions visited by the random walk approximate the posterior distribution. The influence of the selection of an arbitrary starting value can be reduced by discarding the first part of the sample (the burn-in period). The posterior estimates can be summarized using a measure of central tendency (e.g., mean) of the posterior distribution and a credibility interval.

A limitation of the Metropolis algorithm is that the proposal distribution needs to be adequately tuned to estimate the posterior accurately. This procedure may be inconvenient when the inference of multiple unknown parameters is required (as in hierarchical models). Gibbs sampling is a more practical alternative for sample generation from distributions of at least two dimensions. This algorithm is the basis of the popular software JAGS (Just Another Gibbs Sampler). The basic insight of Gibbs sampling is to leverage the structure of the proposal distribution by repeatedly sampling from the conditional distribution when one of the variables is fixed. For example, for a model with two variables (x_1, x_2), for each iteration, x_1 is sampled from the conditional distribution $P(x_1|x_2)$ with x_2 fixed, then x_2 is sampled from the conditional distribution $P(x_2|x_1)$ using the new value of x_1. See Bolstad (2009) and Kruschke (2014) for accessible mathematical tutorials on the Metropolis algorithm and Gibbs sampling.

3.2.3.2 MCMC diagnostics

The interpretation and validation of MCMC estimates within the Bayesian framework are essential steps to ensure that results can be trusted. The main issues to check to validate MCMC results will be presented in this section.

First, the stability of the MCMC chains must be checked visually and numerically for all parameters to ensure that the chains are representative of the posterior. Visual checks of trace plots and density plots are illustrated in the upper-left and the lower-right panels of Figure 3-6, respectively. The regularity of the trace plot and the smoothness of the density plot can be checked to ensure that the

posterior distribution is computed adequately. A popular numerical check is the shrink factor: the ratio of the variance within the individual chains to the variance between the chains (Gelman and Shirley 2011). The evolution of the shrink factor is illustrated in the lower-left panel of Figure 3-6. The convergence of the chains can be verified by evaluating if the shrink factor is close to 1 for all parameters.

Second, the level of autocorrelation in the Markov chains must be evaluated to ensure that the entire posterior distribution has been explored. Autocorrelation can be defined as the serial correlation of the chain values with the chain values at a given number of steps ahead (lag). The evolution of the autocorrelation for lags of 1 to 35 is illustrated in the upper-right panel of Figure 3-6. In this panel, the effective sample size (ESS) is a numerical indicator evaluated by calculating the ratio of the sample size to the amount of autocorrelation (Kass et al. 1998). An ESS of 10,000 has been recommended to obtain reasonably accurate estimates of the 95% credibility interval of a posterior distribution (Kruschke, 2014). The program JAGS in R can be used to automatically builds MCMC chains and returns a sample from the posterior distribution (Plummer 2013).

Third, the choice of prior distribution may significantly influence the posterior, especially when the sample size is small. The model may underfit the data if the prior is too diffuse, but overfit the data if the prior is too informative. It is recommended to conduct a sensitivity analysis using different specifications of a prior for estimating their influence on the posterior (van de Schoot and Miocević 2020). A sensitivity analysis of the impact of the specification of a prior on the variance parameter of the log-normal distribution will be presented in Chapter 6.
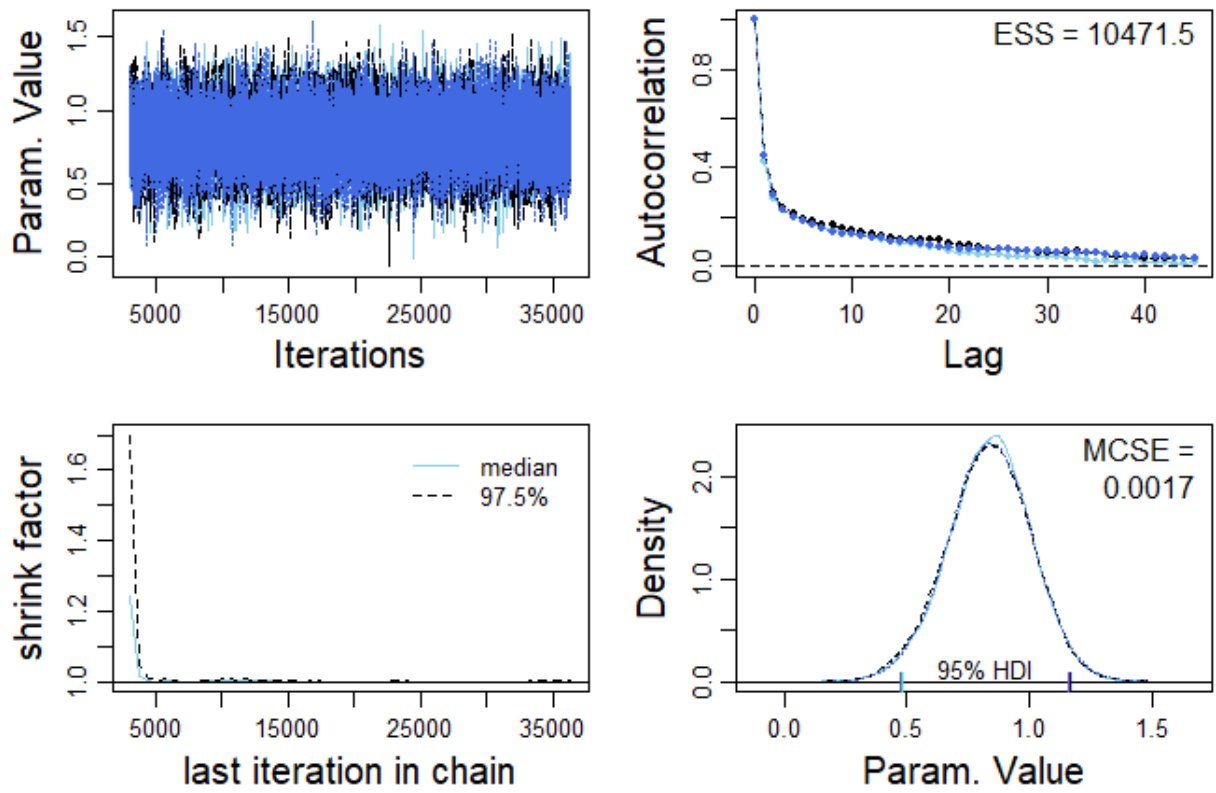
Figure 3-6: Illustration from MCMC diagnostics for a specified parameter. *Upper-left:* Evolution of parameter values of three chains as the number of iterations increases (trace plot). A burn-in period of 2000 steps was applied. *Upper-right:* Autocorrelation diagnostic for lags from 1 to 35. *Lower-left:* Evolution of Gelman and Rubin's shrink factor as the number of iterations increases. *Lower-right:* Density plots of the parameter values sampled in three MCMC chains. Generated in R using the diagMCMC function from Kruschke (2014).

3.2.3.3 Model comparison

Information criteria can be used to measure the relative goodness of fit of Bayesian models for a given data set. These criteria rank models by balancing goodness-of-fit and complexity using deviance and a penalty term weighted by the number of parameters to reduce the risk of overfitting. The deviance information criterion (DIC) was used for model comparison in Chapters 4 and 5. The DIC is given by:

$$\text{DIC} = \bar{D} - (\bar{D} - \hat{D}) = \bar{D} + p_D \tag{3.3}$$

where $\overline{D}$ is the mean of D, the deviance for each set of sampled parameter values in the posterior distribution, and $\widehat{D}$ is the deviance calculated at the posterior mean. The difference $\overline{D} - \widehat{D} = p_D$ can be interpreted as the penalty term. The DIC assumes that the sample size is much larger than the number of parameters of the model and that the posterior is a multivariate normal distribution (Spiegelhalter et al. 2002). For Bayesian hierarchical models, the DIC can be expressed either as conditional upon latent variables (cDIC) or after marginalizing over latent variables (mDIC) (Spiegelhalter et al. 2002, Celeux et al. 2006). For a mixed Poisson model, the conditional-level likelihood is the Poisson distribution, and the marginal-level likelihood is the mixture distribution. A method for the calculation of the mDIC will be presented in Chapter 5.

Finally, each model should be check by simulating replicated data under the predictive distribution and then comparing these predictions to the observed data (Gelman and Hill 2006). This model checking approach is known as graphical posterior predictive checks. Complementary cumulative distribution function (CCDF) graphs can be useful tools to visualize the upper tail behavior of a distribution (see Section 2.3.2).

CHAPTER 4. ARTICLE 1 - CAN ROUTINE MONITORING OF *E. COLI* FULLY ACCOUNT FOR PEAK EVENT CONCENTRATIONS AT DRINKING WATER INTAKES IN AGRICULTURAL AND URBAN RIVERS?

This chapter proposes the use of four probability distributions (gamma, log-normal, Lomax, bimodal log-normal) to model temporal variations in *E. coli* concentrations using large data sets from regulatory monitoring at six drinking water treatment plants located in urban and agricultural catchments. Data collection and model validation methods are presented to verify whether selected parametric distributions predicted peak *E. coli* concentrations. This article is published in *Water Research*. Supplementary information is presented in Appendix A.

Can routine monitoring of *E. coli* fully account for peak event concentrations at drinking water intakes in agricultural and urban rivers?

Émile Sylvestre [a,b], Jean-Baptiste Burnet [a,b], Patrick Smeets [c], Gertjan Medema [c,d], Michèle Prévost [a], Sarah Dorner [b]

[a] NSERC Industrial Chair on Drinking Water, Department of Civil, Geological, and Mining Engineering, Polytechnique Montreal, Montreal, Quebec, H3C 3A7, Canada

[b] Canada Research Chair in Source Water Protection, Department of Civil, Geological, and Mining Engineering, Polytechnique Montreal, Montreal, Quebec, H3C 3A7, Canada

[c] KWR Watercycle Research Institute, Groningenhaven 7, 3433 PE Nieuwegein, The Netherlands

[d] Sanitary Engineering, Department of Water Management, Faculty of Civil Engineering and Geosciences, Delft University of Technology, P.O. Box 5048, 2600GA, Delft, The Netherlands

* Corresponding author e-mail: emile.sylvestre@polymtl.ca

Abstract In several jurisdictions, the arithmetic mean of *Escherichia coli* concentrations in raw water serves as the metric to set minimal treatment requirements by drinking water treatment plants (DWTPs). An accurate and precise estimation of this mean is therefore critical to define adequate requirements. Distributions of *E. coli* concentrations in surface water can be heavily skewed and require statistical methods capable of characterizing uncertainty. We present four simple parametric models with different upper tail behaviors (gamma, log-normal, Lomax, mixture of two log-normal distributions) to explicitly account for the influence of peak events on the mean concentration. The performance of these models was tested using large *E. coli* data sets (200 to 1800 samples) from raw water regulatory monitoring at six DWTPs located in urban and agricultural catchments. Critical seasons of contamination and hydrometeorological factors leading to peak events were identified. Event-based samples were collected at an urban DWTP intake during two hydrometeorological events using online β-D-glucuronidase activity monitoring as a trigger. Results from event-based sampling were used to verify whether selected parametric distributions predicted targeted peak events. We found that the upper tail of the log-normal and the Lomax distributions better predicted large concentrations than the upper tail of the gamma distribution. Weekly sampling for three years in urban catchments and for four years in agricultural catchments generated reasonable estimates of the average raw water *E. coli* concentrations. The proposed methodology can be easily used to inform the development of sampling strategies and statistical indices to set site-specific treatment requirements.

4.1 Introduction

The World Health Organization's (WHO) water quality guidelines recommend a preventive and risk-based approach for drinking water quality management. For this purpose, a spectrum of microbial risk assessment approaches is available, from simple sanitary inspections and risk matrices to more complex ones such as quantitative microbial risk assessment (QMRA) (WHO 2016b).The QMRA approach can provide relative estimates of microbial risks at drinking water treatment plants (DWTPs), which may be particularly useful to prioritize investments in improving water treatment or in implementing source water protection measures. However, in many situations, data on pathogen occurrence and concentrations in raw water are not available at DWTPs, and only faecal indicator bacteria (FIB) are measured to characterize source water quality. Therefore, to support the implementation of a source-to-tap approach, simplified classification methods, known as "bin classification" were developed to determine minimum treatment

requirements according to a specific level of FIB concentrations in raw water. Different summary statistics (e.g., mean concentration, maximum concentration) and sampling strategies (weekly sampling, monthly sampling, event-based sampling) are specified in regulatory requirements worldwide for bin classification (Supplementary Table 4-1).

The arithmetic mean is a valid metric for characterizing microbial concentrations in order to characterize the risk of multiple exposures to low doses of pathogens (Haas, 1996). The annual mean is usually considered in QMRA because annual health-based targets are recommended in guidelines and regulations (Sinclair et al. 2015). Precise estimation of the mean is challenging for surface water because microbial concentrations can vary over several orders of magnitude within hours or days (Burnet et al. 2019b). This metric relies on the law of large numbers; as the sample size grows, its sample mean gets closer to the true mean. However, the meaning of "large" depends on the distribution of the data. The convergence is much faster for normal or thin-tailed distribution than for heavy-tailed distributions. If the variance is very large, any new observation can be large enough to overwhelm all previous observations, regardless of the number of accumulated observations.

Numerous studies have shown that heavy rainfall can rapidly increase microbial contamination loads in water (Atherholt et al. 1998, Kistemann et al. 2002, Signor et al. 2005). In urban areas, combined sewer overflow (CSO) discharges induced by heavy rainfall or snowmelt events can cause recurring microbial peaks in raw water at DWTPs (Jalliffier-Verne et al., 2016, Madoux-Humery et al., 2016). In agricultural areas, similar heavy rainfall episodes can increase microbial contamination of surface waters as a result of overland transport, tile drainage systems and resuspension from stream sediments (Dorner et al. 2006). A statistical approach was proposed to incorporate such peak events in the risk assessment for a hypothetical frequency of occurrence (Petterson et al. 2006). However, methods for the estimation of peak event frequency have not been proposed yet. Stochastic models are used in other fields to evaluate the frequency of extreme precipitation events, streamflow peaks (Katz et al. 2002), and extreme pollution from runoff (Harremoës 1988). These models have implications for quantifying the frequency of extreme events at DWTPs but have not been utilized in the context of microbial safety of drinking water.

In Quebec, Canada, raw water *E. coli* concentrations are measured since 2013 at least weekly for large DWTPs (>10,000 inhabitants). These extensive datasets provide a unique opportunity to study temporal variations in different catchments. The objective of the study was to first develop a methodology to correctly estimate the mean *E. coli* concentrations in surface drinking water sources by considering peak events. Large routine monitoring datasets from six DWTPs were fitted with parametric distributions having different upper tail behaviors. For the best-fit distributions, we then evaluated the required minimum sample size to estimate the mean concentration for different ranges of uncertainty. Secondly, key contributors to the mean concentration level were identified by examining the influence of seasonality and hydrometeorological factors on temporal variations. Finally, we conducted event-based sampling during two hydrometeorological events at an urban DWTP to evaluate whether the selected parametric distributions predicted these targeted peak events. Implications for the development of sampling strategies and probabilistic models are discussed for setting health-based drinking water treatment requirements.

4.2 Material and methods

4.2.1 Study sites

Six DWTPs fed by rivers located in urban and agricultural catchments were selected and classified by the mean annual river flow rate in ascending order from A to D (Table 4-1). DWTPs C2 and D2 were located downstream DWTPs C1 and D1, respectively. Wastewater treatment plants, CSO discharge points, and the dominant land cover type were identified for areas 15 km upstream of the drinking water intakes. In Quebec, CSOs are equipped with recording devices to measure the frequency and the daily cumulative duration of discharges (Gouvernement du Québec 2015). CSO discharges are forbidden during dry periods but are permitted with restrictions during rainfall and snowmelt episodes (CCME 2009, Gouvernement du Québec 2015). In agricultural areas, manure must be spread on unfrozen soils between April and October (Gouverment du Québec 2018).

Table 4-1: Sampling strategies for *E. coli* in raw water and characterization of the catchment of six surface drinking water treatment plants in Quebec, Canada

DWTP	Sampling period	Sampling frequency	Mean flow rate of the river (m^3/s) [min-max]	Main land cover type in the intake protection zone [A]	WRRFs/CSOs in the intake protection zone [A]
A	2009-2017	Weekly	10 [0.1-100]	Agricultural	0/8
B	2013-2017	Weekly	15 [3-100]	Agricultural	1/4
C1	2009-2017	Daily M-T	300 [20-1000]	Urban	4/26
C2	2013-2017	Weekly	300 [20-1000]	Urban	3/25
D	2009-2017	Daily M-T	1000 [500-3000]	Urban	0/44
E	2010-2015	Daily	9000 [7000-10,000]	Urban	1/0

[A] 15 km upstream and 100 m downstream from the withdrawal site. The distances include surface water, portions of tributaries and a 120 m strip of land measured from the high-water mark.

4.2.2 Hydrometeorological data

The impact of hydrometeorology on the variations in raw water *E. coli* concentrations at DWTP C1 were investigated to identify critical periods of contamination for event-based sampling. Daily river flow rate, snow cover, and total precipitation were obtained from online databases. River flow rate was measured at a provincial gauging station five kilometers downstream of DWTP C1. The other parameters were obtained from the Montreal Pierre Elliott Trudeau international airport weather station located 17 kilometers south of the DWTP.

4.2.3 Regulatory *E. coli* monitoring

Escherichia coli was chosen as an indicator of microbial water quality because of its widespread use in drinking water regulations and because it provides evidence of recent faecal pollution (WHO 2011). Depending on the DWTP, we obtained routine *E. coli* monitoring results for five to nine years between 2009 and 2017. Raw water samples were collected daily from Monday to Thursday (daily M-T) or once a week between Monday and Thursday (weekly). All samples were collected during regular working hours (from 9:00 to 18:00). E. coli was enumerated with plate counts on EC-MUG medium (APHA 2012) by membrane filtration using modified membrane-thermotolerant *E. coli* agar (modified mTEC) (EPA method 1603) or by the defined substrate technology using the IDEXX Quanti-Tray/2000 System with Colilert reagent (APHA 2012). *E. coli* concentrations were reported either in most probable number (MPN) or colony-forming unit

(CFU) per 100 milliliters. Two ten-fold serial dilutions (0.1, 0.01) were carried out for the modified mTEC method to obtain countable ranges of 20-80 CFUs per plate, and no dilution with countable ranges of 1-2,419 MPN/100 mL was applied with Colilert. Hence, the upper limit of detection with this modified mTEC and the Colilert methods were 8,000 CFU/100 mL and 2,420 MPN/100 mL, respectively. For event-based monitoring, one ten-fold serial dilution (0.1) was applied for the Colilert assay to increase the upper limit of detection to 24,196 MPN/100 mL. Non-detect values were replaced with a limit of detection of 1 *E. coli*/100 mL for statistical analyses. This simple approach for handling non-detects has a negligible impact on statistical inference because, at these DWTPs, the proportions of non-detects are small (<5%). Poisson mixture distributions could be used to handle non-detects in cases in which their proportion would be higher. Burnet et al. (2019a) observed a strong correlation ($r = 0.94$) between membrane filtration and the Colilert assay at DWTP C1. For ease of interpretation, all *E. coli* results were presented as *E. coli*/100 mL.

4.2.4 Indices for the identification of heavy tails

Two simple measures were considered to evaluate the statistical dispersion of each empirical distribution of *E. coli* concentrations. The kurtosis was selected to evaluate if infrequent extreme deviations were captured in historical data. A high kurtosis can indicate that tail events are not properly characterized and that the true mean could be higher than the sample mean. The ratio of the standard deviation to the mean absolute deviation (MAD) was further examined as it increases with the heavy-tailedness of the distribution (Taleb 2015).

4.2.5 Statistical inference of *E. coli* concentrations

Statistical inference was undertaken based on reported *E. coli* concentrations to draw conclusions on the mean concentration and its uncertainty. Continuous distributions were selected to describe the variation in *E. coli* concentrations without taking into account the random (Poisson) distribution of counts because only data in the form of concentration measurements were available. The variations in faecal indicator concentrations in water are often described using log-normal distributions (Thomas 1955, Ott 1994). Here, we evaluated how the gamma, log-normal and Lomax distributions described the variations in raw water *E. coli* concentrations at each DWTP. Those distributions were selected because they have different simple underlying generative processes (Frank 2014) and embrace a spectrum of tail behaviors (Haas 1997). The Lomax distribution, also known as Pareto type II, has not previously been selected to describe the variability of microbial contamination in water but has many applications in natural sciences (Newman 2005, Sornette

2006). This distribution can be interpreted as an exponential distribution with a power-law tail. The power-law tail is characterized by a much slower decay as compared to an exponential distribution.

Two different approaches were adopted for statistical inference. First, a Bayesian approach was applied for the inference of the three candidate distributions. Distributions were parametrized by shape k and scale θ (gamma); mean μ and standard deviation σ (log-normal); or shape α and scale λ (Lomax) (Table 4-2). The parameters were provided with broad, noncommittal prior distributions so that the prior had a minimal influence on the posterior (Kruschke 2014).

Table 4-2: Likelihood and priors selected for Bayesian inference

Distribution of density	Likelihood function	Prior probability distribution	Average	Variance
Gamma	$\dfrac{1}{\Gamma(k)\theta^k}x^{k-1}e^{-\frac{x}{\theta}}$	$k \sim \mathcal{U}\,(0,10)$ $\theta \sim \mathcal{U}\,(0,10000)$	$k\theta$	$k\theta^2$
Lomax	$\dfrac{\alpha}{\lambda}\left[1+\dfrac{x}{\lambda}\right]^{-(\alpha+1)}$	$\alpha \sim \mathcal{U}\,(0,10)$ $\lambda \sim \mathcal{U}\,(0,10000)$	$\dfrac{\lambda}{\alpha-1}$ for $\alpha>1$ Otherwise undefined	$\dfrac{\lambda^2\alpha}{(\alpha-1)^2(\alpha-2)}$ for $\alpha>2$ ∞ for $1<\alpha\leq2$ Otherwise undefined
Log-normal	$\dfrac{1}{x\sigma\sqrt{2\pi}}e^{-\frac{(\ln x-\mu)^2}{2\sigma^2}}$	$\sigma \sim \mathcal{U}(10^{-3}sd(y),,10^3 sd(y))$ $\mu \sim \mathcal{N}(mean(y),\frac{1}{10sd(y)^2})$ where $y=\ln(x)$	$\exp\left(\mu+\dfrac{\sigma^2}{2}\right)$	$[\exp(\sigma^2)-1]\exp(2\mu+\sigma^2)$

A sample of posterior parameter pairs was constructed using a Markov chain Monte Carlo procedure using Gibbs sampling. The models were specified and run in JAGS (v4.2.0) (Plummer 2013) from R (v3.4.1). Markov Chain Monte Carlo methods were performed using rjags (v4-6) (Plummer 2013). Four Markov chains were implemented for each parameter. The model was run for 10^4 iterations after a burn-in phase of 10^3 iterations. The Brooks-Gelman-Rubin scale reduction factor indicated that convergence was obtained for each of these four chains (Gelman and Shirley 2011). The uncertainty on the parameter values of the Bayesian models and the predicted mean concentration was then evaluated. The goodness of fit of each Bayesian model was measured with the deviance information criterion (DIC) (Spiegelhalter et al. 2002) as follows:

$$DIC = -2(L - P) \tag{4.1}$$

where L is the log-likelihood of the data given the posterior means of the parameters and P is an estimate of the effective number of the parameter in the model (Gelman et al. 2013). A lower DIC indicates a better model fit.

A second method was applied for statistical inference because bimodality was observed at DWTP B and only normal mixture models were available in JAGS. Maximum likelihood estimation was computed for a mixture of two gamma distributions and for a mixture of two log-normal distributions via expectation-maximization algorithms with the R package 'mixR' (Yu 2018). The goodness of fit of these two distribution models was measured with the deviance, the Akaike information criterion (AIC) and the Bayesian information criterion (BIC). AIC and BIC also reward goodness of fit and includes a penalty that is a function of the number of estimated parameters. The uncertainty on the parameter values of the mixture models and the predicted mean concentrations was not evaluated. Source codes are provided in the Supplementary Material, Section B.

4.2.6 Minimum sample size determination

The minimum sample size required to accurately estimate the true mean of a log-normal distribution for different confidence intervals was determined by iterations with the Cox method (Olsson 2005). The confidence interval for a log-normal distribution with a mean µ and the standard deviation σ is:

$$\mu + \sigma^2 \pm z \sqrt{\frac{\sigma^2}{n} + \frac{\sigma^4}{2(n-1)}} \tag{4.2}$$

where the value of z to evaluate the 95% confidence interval is 1.96, and n is the sample size.

4.2.7 Identification of critical contamination periods

Lorenz curves (Cowell, 2000) were used to summarize the quantile share information contained in empirical *E. coli* distributions. To produce these graphs, *E. coli* samples were ordered by their concentration, starting with the lowest and then plotted against the cumulative proportion of the ordered samples (running from zero to one along the horizontal axis). Ordinary Lorenz curve values were multiplied by the mean concentration to evaluate the distributions of *E. coli* concentrations in terms of long-term mean concentrations. This curve is known as a *generalized* Lorenz curve

(Shorrocks 1983). The generalized Lorenz curves were computed with the R package 'ineq' (Zeileis and Kleiber 2014). Long-term and seasonal variations were assessed. The seasons were defined as winter (Dec-Feb), spring (Mar-May), summer (June-Aug), and fall (Sept-Nov).

The short-term variability in *E. coli* concentrations was examined at DWTP C1 from January to April (snowmelt period) between 2013 and 2017. The observed variables were: *E. coli* concentrations, the flow rate of the river, the snow cover, and the daily precipitation. An online instrument measuring β-D-glucuronidase (GLUC) activity (ColiMinder[TM] VWM GmbH, Vienna, Austria) was installed at the DWTP intake to characterize periods of high variability in microbial contamination during the 2017 snowmelt period. The technology was used to track *E. coli* at near real-time frequency following field and laboratory validation completed by Burnet et al. (2019a). Detailed technical information about the technology can be found in Koschelnik et al. (2015). The instrument was installed at the intake of the DWTP in November 2016 and measured GLUC activity every two hours. GLUC activity measurements obtained during the first month after the installation allowed to differentiate baseline from peak levels of contamination during and following autumn and winter rainfall episodes. During periods of high fluctuations of the GLUC activity level, we adjusted the measurements to hourly frequency. Based on the short-term dynamics of the GLUC activity, two snowmelt events were identified. Grab samples were collected every three to five hours for 20 hours during a first GLUC activity peak in February 2017, and for 60 hours during a second GLUC activity peak in April 2017.

4.3 Results

4.3.1 Descriptive statistics

The sample mean of *E. coli* concentrations in raw water varied between DWTPs, from 22 to 507 *E. coli*/100 mL (Table 4-3). Overall, the mean and the mean absolute deviation (MAD) decreased with the mean flow rate of the river. A 0.2 $\log_{10}$ increase in the mean and MAD was observed between DWTP C1 and C2. DWTPs B, C2, and E displayed the highest SD to MAD ratio. The kurtosis was greater than 155 at DWTPs C2 and E, but was only 25 at DWTP B, indicating potential bimodality of the empirical distribution.

Table 4-3: Statistical characterization of empirical distributions of raw water *E. coli* concentrations in *E. coli*/100 mL at six drinking water treatment plants

DWTP	n	Sample average	Standard deviation (SD)	Mean absolute deviation (MAD)	Ratio SD/MAD	Skewness	Excess kurtosis
A	434	507	967	563	1.72	3.89	19.42
B	245	386	1168	523	2.23	4.89	25.56
C1	1584	202	271	165	1.64	4.08	22.39
C2	437	318	668	272	2.46	10.70	155.88
D	1043	88	150	83	1.81	5.12	36.78
E	1807	22	58	23	2.44	10.48	162.52

4.3.2 Distribution selection

Best-fit parameters of the gamma, Lomax, and log-normal distributions at DWTPs A and B predicted differences up to 0.5 $\log_{10}$ between the lowest estimated mean concentrations and the highest estimated mean concentrations (Table 4-4). For DWTPs A and B, the predicted means of the Lomax distribution were higher than for the gamma and log-normal distributions. The uncertainty on the predicted mean of the Lomax distribution was not stable at DWTPs A and B since the mean concentration was not defined when the value of the shape parameter α was less than 1.0 (the tail had infinite area). The differences among the predicted mean of the three models at DWTPs C1, C2, D and E was less than 0.1 $\log_{10}$. The influence of the behavior of the tail of a distribution on the predicted mean is discussed in section 3.1. To define what is an important difference in DIC for the selection of a model, Spiegelhalter et al. (2002) suggested to apply the same rules of thumb as was proposed by Burnham and Anderson (2004) for the Akaike Information Criterion (AIC): differences in AIC within 1-2 of the "best" model (minimum AIC value) deserve consideration, and differences within 3-7 have considerably less support. Therefore, the log-normal or the Lomax distribution better fitted the observed data than the gamma distribution at all DWTPs (Table 4-4). At DWTP B, the difference in DIC was small between the log-normal distribution and the Lomax distribution. Gamma mixture and log-normal mixture distributions were also considered for DWTP B (Table 4-5). The deviance of the mixture of two log-normal distributions was much lower than the deviance of the Lomax distribution (deviance of 3,057). With the mixture models, a distribution was fitted to the tail of the observations at a probability of exceedance of 14% for the gamma model and 6% for the log-normal model. The difference between the sample mean and the combined predicted mean of the mixture models was lower than 0.1 $\log_{10}$.

Table 4-4: Maximum a posteriori probability (MAP) of the parameters of gamma, Lomax, and log-normal distributions of raw water *E. coli* concentrations at six drinking water treatment plants. The arithmetic mean estimated by each model in *E. coli*/100 mL are presented with their 95% credibility interval (CI). The performance of each fit is quantified with the deviance information criterion (DIC). Boldfaced cells indicate the best-fit model for each dataset.

	Gamma distribution				Lomax distribution				Log-normal distribution			
DWTP	k	θ	Mean[A] (95 CI)	DIC	α	λ	Mean[A] (95 CI)	DIC	μ	σ	Mean[A] (95 CI)	DIC
A	0.53	935	500 (446, 580)	6130	1.27	219	811	6040	5.04	1.62	563 (454, 730)	**6034**
B[B]	0.42	924	387 (317, 475)	3225	1.10	88	880	3059	4.39	1.56	261 (199, 358)	3061
C1	0.85	237	202 (192, 213)	19973	4.77	753	200 (188, 214)	**19904**	4.62	1.30	236 (217, 259)	19987
C2	0.81	384	320 (285, 352)	5905	3.66	756	302 (265, 348)	**5830**	5.04	1.26	340 (290, 400)	5848
D	0.79	111	88 (82, 95)	11381	2.48	131	88 (79, 99)	11204	3.72	1.21	85 (77, 93)	**11111**
E	0.62	35	22 (21, 23)	14515	1.70	16	22 (22, 27)	13895	2.13	1.29	19 (17, 20)	**13755**

[A] *E. coli* concentration in *E. coli*/100 mL

[B] Best-fit model presented in Table 4-5

Table 4-5: Maximum likelihood estimation of the parameters of gamma mixture and log-normal mixture distributions of raw water *E. coli* concentrations at drinking water treatment plant B. The performance of the fit is quantified with the deviance, the Akaike information criterion (AIC) and the Bayesian information criterion (BIC). Boldfaced values indicate the best fit model.

	DWTP B			
	Gamma Mixture		Log-normal mixture	
	Part 1	Part 2	Part 1	Part 2
Proportion	0.86	0.14	0.94	0.06
k / μ	1.06	0.70	4.14	8.29
θ / σ	87	3137	1.23	0.50
Average (MPN/100 mL)	92	2201	136	4529
Combined average (MPN/100 mL)	387		399	
Deviance	3041		**3023**	
AIC	3050		**3032**	
BIC	3068		**3050**	

4.3.3 Posterior predictive checks

Cumulative distribution function (CDF) and complementary CDF (CCDF) plots were produced to illustrate the fit of the gamma, log-normal and Lomax distributions to routine monitoring data. Overall, the gamma distribution accurately estimated the sample mean (Table 4-4) but overestimated low concentrations (Figure 4-1) and underestimated large concentrations (Figure 4-2). The power-law tail of the Lomax distribution (straight-line on the CCDF plot) predicted higher concentrations than the tail of the log-normal distribution when the value of the scale parameter λ was lower than the sample mean. At DWTP E, the DIC of the Lomax distribution was higher than the DIC of the log-normal distribution, even if the Lomax distribution was a better fit for the tail events. The bulk of the distribution, in which most of the samples were located, was therefore log-normally distributed, but not the tail. Figure 4-3 shows that the mixture of two log-normal distributions provided a better fit to the empirical tail than the unimodal distributions at DWTP B. The log-normal distribution fit on the highest values only describes the variability of around 5% of the data, suggesting that specific conditions, such as hydrometeorological events, could generate a different probability pattern than baseline conditions in this agricultural catchment.
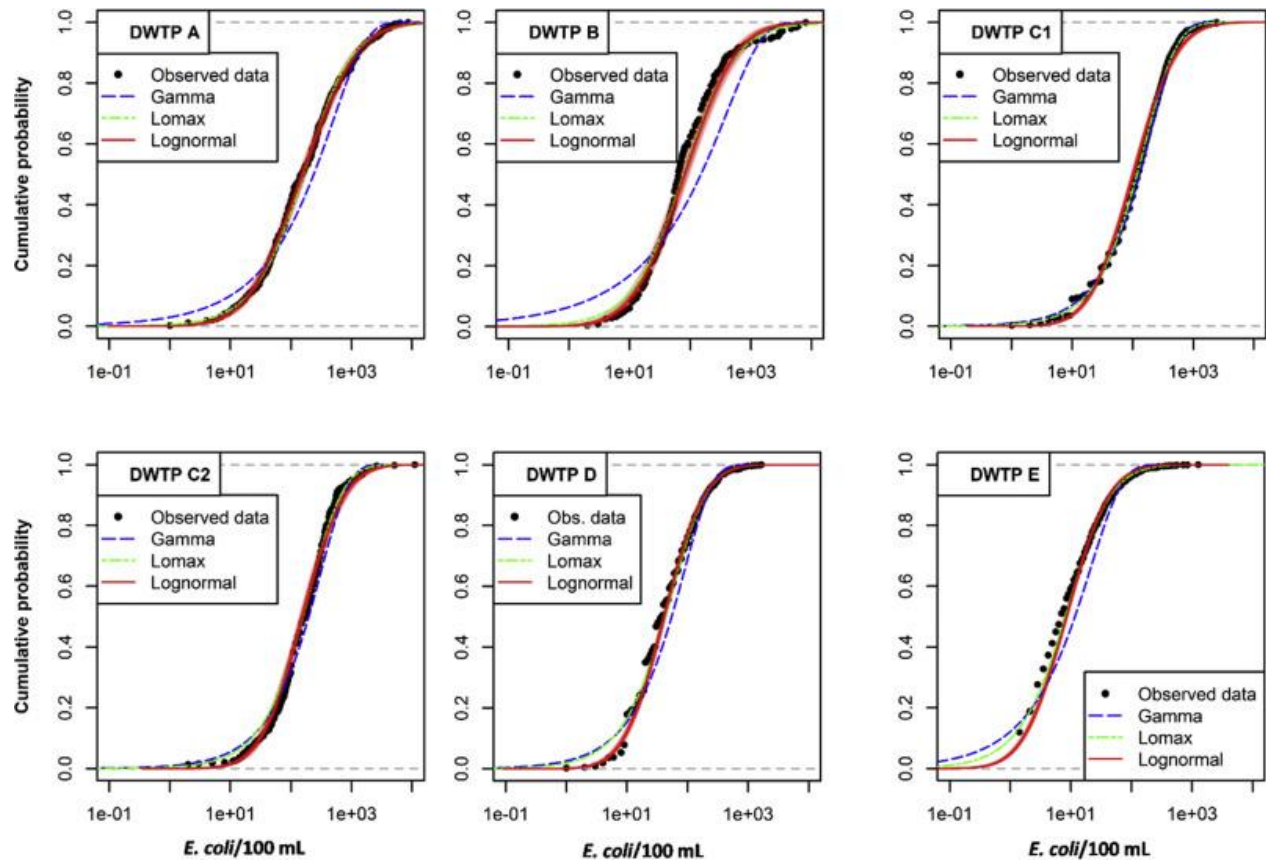
Figure 4-1: Cumulative distribution function plots of gamma, Lomax, and log-normal distributions of raw water *E. coli* concentrations at six drinking water treatment plants. The 95% uncertainty interval is shown for the log-normal distribution.
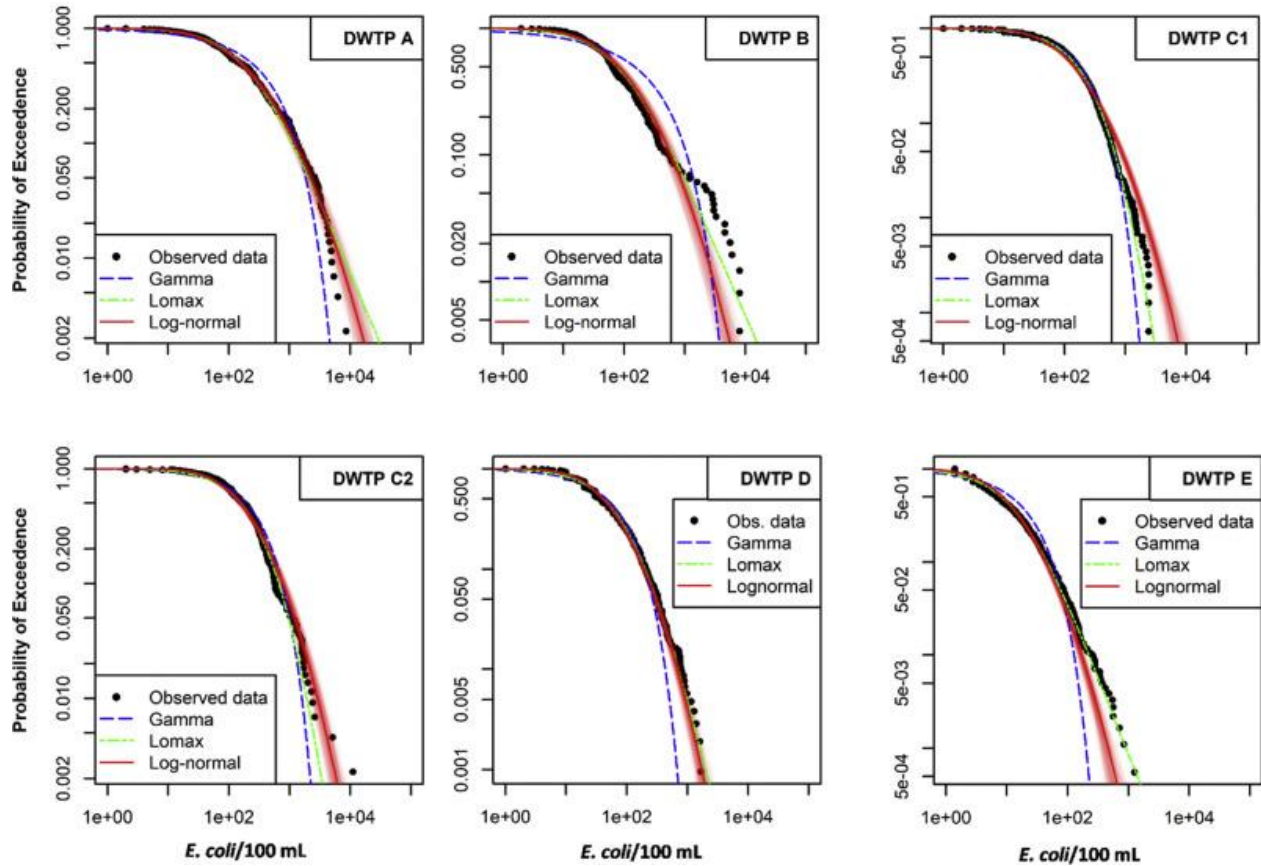
Figure 4-2: Complementary cumulative distribution function plots of gamma, Lomax, and log-normal distributions of raw water *E. coli* concentrations at six drinking water treatment plants. The 95% uncertainty interval is shown for the log-normal distribution.
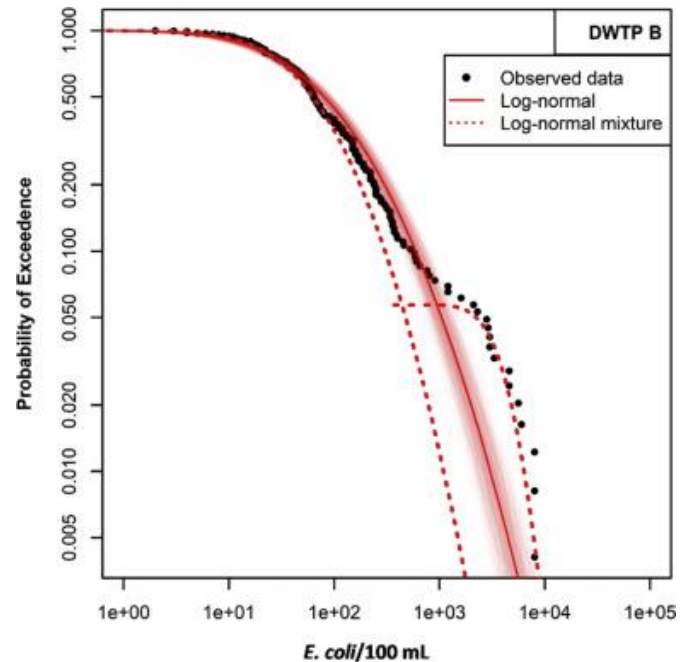
Figure 4-3: Complementary cumulative distribution function plot of the log-normal distribution and the mixture of two log-normal distributions of raw water *E. coli* concentrations at drinking water treatment plant B. The 95% uncertainty interval is shown for the unimodal log-normal distribution.

4.3.4 Sample size determination

The value of the parameter sigma of the log-normal distribution had an important influence on the minimum sample size at DWTPs A, C1, C2, and D (Table 4-6). A sigma increase of 0.4 doubled the minimum sample size from DWTP D to DWTP A. For all DWTPs, a three-fold increase in minimum sample size was required to reduce the range of the confidence interval from 0.5 $\log_{10}$ to 0.3 $\log_{10}$. A ten-fold increase was needed to reduce that range from 0.3 $\log_{10}$ to 0.1 $\log_{10}$.

Table 4-6: Minimum sample sizes for estimating the arithmetic mean in a given confidence interval for log-normally distributed *E. coli* concentrations.

	Best-fit parameter		Confidence interval on the arithmetic mean				
DWTP	μ	σ	0.5 $\log_{10}$	0.4 $\log_{10}$	0.3 $\log_{10}$	0.2 $\log_{10}$	0.1 $\log_{10}$
A	5.04	1.62	71	111	196	441	1760
C1	4.62	1.30	37	57	101	227	905
C2	5.04	1.26	34	53	93	207	826
D	3.72	1.21	30	47	83	185	736

4.3.5 Seasonal variations of *E. coli* concentrations

The generalized Lorenz curves show that a small proportion of samples contributes highly to the long-term mean (Figure 4-4). In each graph, the black diagonal line represents perfect equality where each sample would have the same contribution to the mean concentration. Therefore, the more the empirical curve deviates from the diagonal, the more the tail of the distribution contributes to the mean. For example, at DWTP B, the long-term mean illustrated with the black curve breaks at a mean concentration of approximately 100 *E. coli*/100 mL. The bimodality of the empirical distribution causes that break. From this point, around 10% of the total number of samples (also 10% of the total period at the DWTP) increases the long-term mean from 100 *E. coli*/100 mL to 387 *E. coli*/100 mL: an increase of 0.6 $\log_{10}$. These curves can also describe the seasonality of the contamination. Seasonal and annual means are illustrated by the maximum value of their generalized Lorenz curve. A seasonal distribution has more influence on the annual mean when the maximum value of a seasonal curve is higher than the maximum value of the annual curve. Thus, the annual mean was mostly influenced by summer and fall conditions in the agricultural catchments (DWTPs A, B) and by winter or spring conditions in the urban catchments (DWTPs C1, C2, E). Smaller differences between seasons were observed at DWTP D.
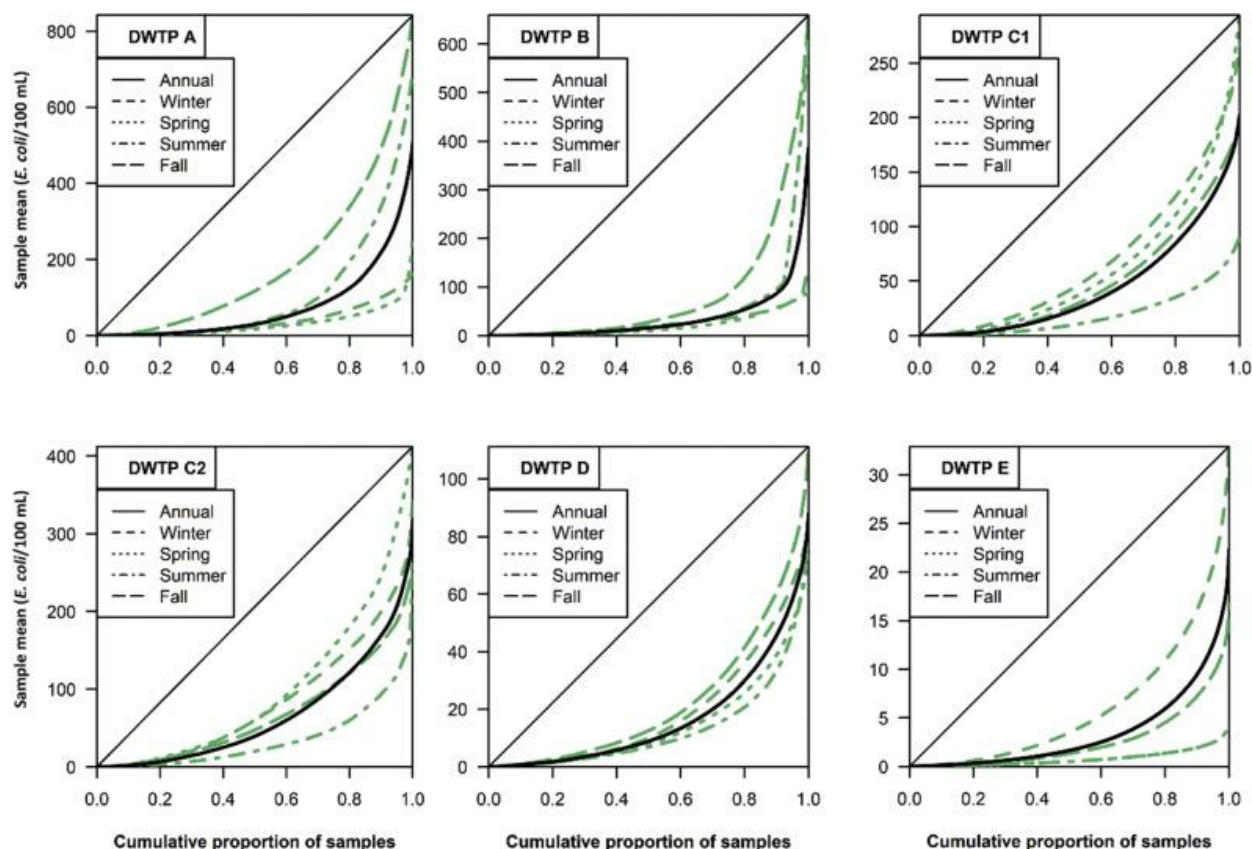
Figure 4-4: Generalized Lorenz curves of the distribution of raw water *E. coli* concentrations at six drinking water treatment plants. On each graph, the black curve shows the distribution of all the samples and the green curves show seasonal distributions.

4.3.6 Short-term variations of *E. coli* concentrations

Time series analysis of hydrometeorological factors and raw water *E. coli* concentrations were used to identify periods of high contamination at DWTP C1 from January 2013 to April 2016 (Figure 4-5). Peak concentrations (over 1,000 *E. coli*/100 mL) were frequently detected during the snowmelt period, usually occurring from March to April. However, these peak events were not always detected during the rapid decline of the snow cover (e.g. March-April 2013). In 2016, precipitation in winter was dominated by rainfall rather than snow, and no peaks were observed. These different hydrometeorological conditions had a noticeable impact on the annual distribution of *E. coli* concentrations at DWTP C1. The annual mean was 341 *E. coli* /100 mL for 2014 and 146 *E. coli*/100 mL for 2016, a difference of 0.4 $\log_{10}$.
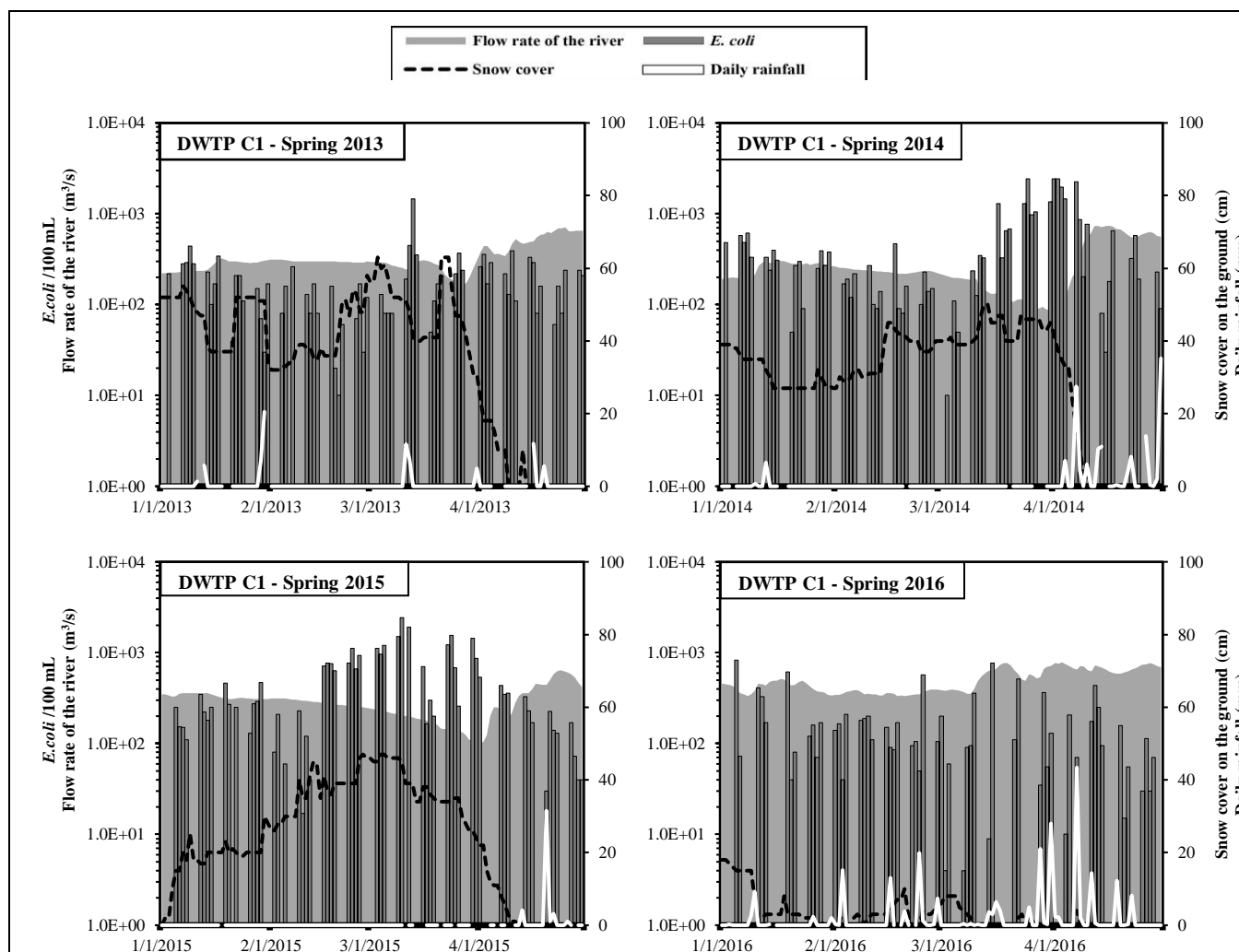
Figure 4-5: Raw water *E. coli* concentrations in samples collected each week from Monday to Thursday at DWTP C1 during the snowmelt periods from 2013 to 2016 (dark-grey column). The grey area is the daily flow rate of the river, the black dotted line is the daily snow cover on the ground, and the solid white line is the daily cumulated rainfall.

In 2017, event-based sampling revealed the influence of hydrometeorological factors on the short-term dynamics of *E. coli* concentrations (Figure 4-6). For the February event, *E. coli* concentrations varied from 161 to 2,247 *E. coli*/100 mL within 7 hours and reached a maximum concentration of 2,420 *E. coli*/100 mL. Concentrations higher than 1,000 *E. coli*/100 mL were observed for 21 hours. No routine samples were collected because the event happened over the weekend. The April peak occurred during the week and was also sampled during routine monitoring. *E. coli* concentrations varied from 440 to 3684 *E. coli*/100 mL, and concentrations higher than 1,000 *E. coli*/100 mL were observed for 66 hours. The maximum daily mean concentrations during the February and April

peaks were 1,588 *E. coli*/100 mL and 2,567 *E. coli*/100 mL, respectively. Both daily mean concentrations were higher than the 97th percentile (8 years of data) of daily M-T sampling. The maximum concentrations sampled during the April peak was higher than the maximum concentration sampled in 8 years of routine monitoring data.
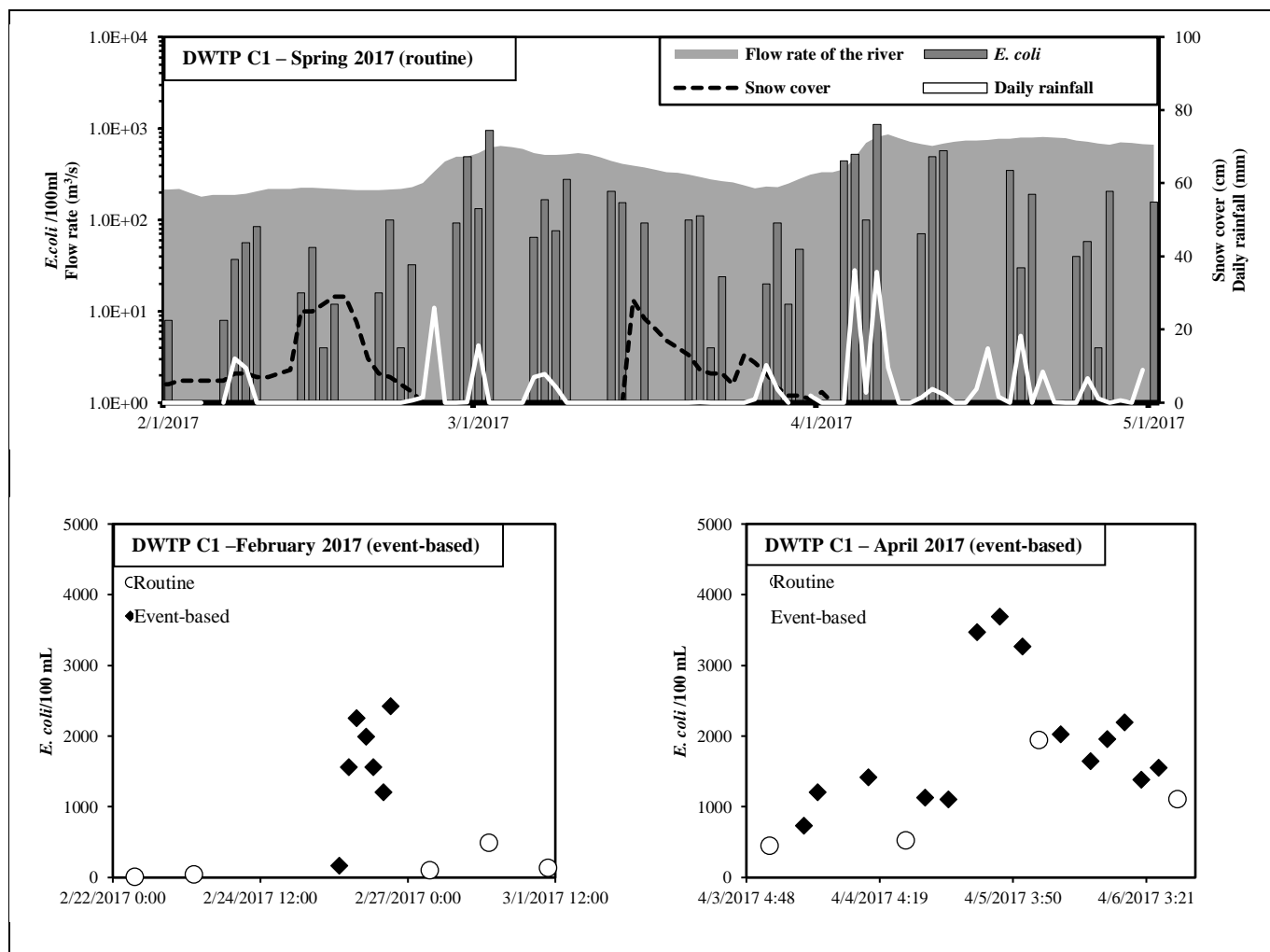
Figure 4-6: Top: Raw water *E. coli* concentrations in samples collected each week from Monday to Thursday at DWTP C1 from January to May 2017 (dark-grey column). The grey area is the daily flow rate of the river, the black dotted line is the daily snow cover on the ground, and the solid white line is the daily cumulated rainfall. Bottom-left: Short-term *E. coli* concentration variations during the event of February 25-26. Bottom-right: Short-term *E. coli* concentration variations during the event of April 3-6. White points are routine samples, and black diamonds are event-based samples.

Maximum daily mean concentrations from event-based sampling are represented with vertical lines on the CCDF plot (Figure 4-7). Both lines crossed the tails of the modeled distributions; thus, tail events were captured with the event-based sampling strategy. The probability of occurrence of the event was back calculated for each distribution. The gamma distribution did not predict the maximum daily mean during the April peak. The log-normal distribution predicted a frequency of occurrence of these daily peaks between two to twenty days per year. The Lomax distribution predicted these events at a lower frequency varying between two days a year and one day every five years.
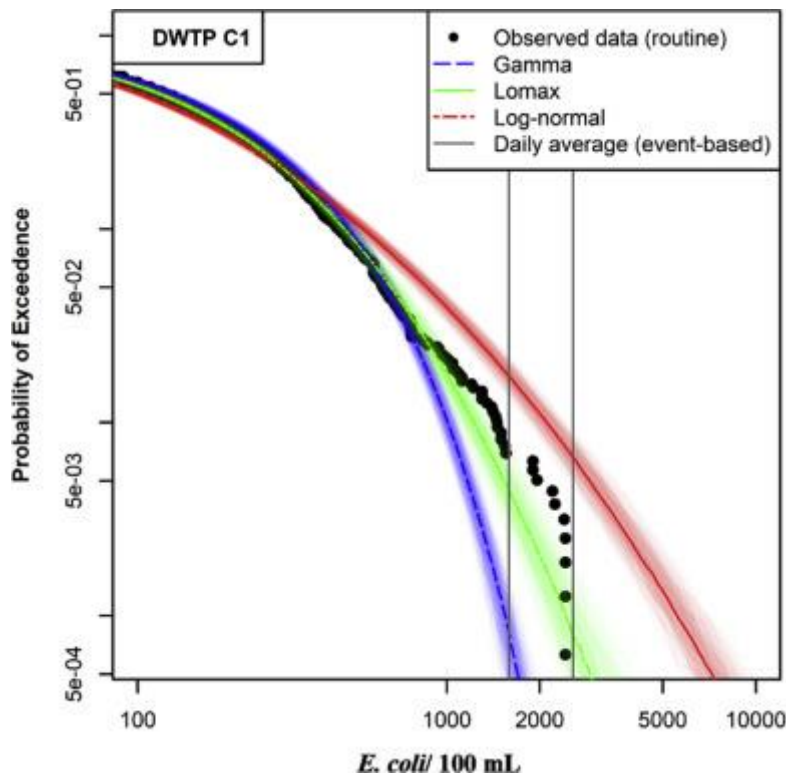
Figure 4-7: Complementary cumulative distribution function plot of the tail of gamma, Lomax, and log-normal distribution fitted to raw water *E. coli* concentrations at drinking water treatment plant C1.The 95% uncertainty interval is shown for each distribution. The vertical grey lines illustrate the daily mean concentration of the two event-based campaigns in February and April 2017 for all probabilities of exceedance.

4.4 Discussion

4.4.1 Optimizing distribution selection to describe *E. coli* variations in source water

Candidate parametric distributions were selected to fit raw water *E. coli* measurements. Underlying generative processes of distributions were considered for the selection. The combination of small-scale processes at a higher aggregate scale tends to yield a common probability distribution consistent with given constraints that maximize the entropy (Frank 2009). A maximization of entropy with a constraint on the arithmetic mean results in an exponential distribution. If the constraint is on the mean logarithm, then observations follow a power-law distribution. The scaling often changes between linear and logarithmic as magnitude changes. The gamma distribution is a product of a power-law x^{k-1} and an exponential function $e^{-\frac{x}{\theta}}$ (Table 4-2). At small magnitudes, the scaling is logarithmic because the power-law component dominates, and at large magnitudes, the scaling is linear because the exponential function dominates. The value of $(k-1)/\theta$ determines the magnitude at which those scales dominate. Thus, only the linear scaling of the gamma distribution dominated at all DWTPs because k was less than 1.0 (Table 4-3).

The Lomax distribution has the inverse scale: a linear-log scaling. Thus, it can be understood as an exponential distribution with a power-law tail. The scale parameter λ indicates the level at which the distribution changes from a linear scaling to a logarithmic scaling (this parameter can be viewed as a power-law tail threshold). Therefore, the logarithm scaling starts at a concentration below the sample mean at DWTPs A, B, and E, and above the sample mean at DWTPs C1, C2, D (Table 4-3). A disadvantage of the Lomax distribution is that the predicted mean is not finite when the value of the shape parameter α is below 1.0. Truncated Lévy distributions can be considered in these cases (Koponen 1995, Mantegna and Stanley 1995, Mariani and Liu 2007). These distributions still have a power-law form, but with infinite tail truncated or exponential cut-offs. The log-normal distribution follows a Gaussian distribution on the log-scale; therefore, the information dissipates on the additive log-scale, and the generative process is multiplicative.

At all DWTPs, the tail of the log-normal and the Lomax distributions predicted the observed concentrations better than the tail of the gamma distribution (Figure 4-2). Log-normal and power-law distributions have similar multiplicative processes. The argument as to whether one is more

accurate than the other has arisen across a variety of fields (Mitzenmacher 2004). Under general conditions, the power-law tail can be obtained with the inclusion of an additive term to the basic multiplicative process. This additive term is added only when the system crosses a lower threshold, acting as a barrier preventing collapse to zero (Sornette and Cont 1997). Hence, hydrometeorological events could be generating this lower threshold and produce power-law behavior in the distributions as it was observed at DWTP E.

The kurtosis and the SD to MAD ratio are proposed as indices to identify the behavior of the tail of the distribution. The log-normal distribution produced only a conservative bound for tail observations when the SD to MAD ratio was less than 2.0 (DWTPs A, C1, D). At a higher ratio (DWTPs B, C2, E), the log-normal distributions could not conservatively estimate all observations (Figure 4-2). The sample kurtosis was much smaller at DWTP B than at DWTPs C2 and E (Table 4-3). At DWTP B, the measure of the deviance (Table 4-5) and the posterior predictive check (Figure 4-3) indicated that the mixture of two log-normal distributions better fitted *E. coli* concentrations than the Lomax distribution. The hypothesis of a bimodal behavior in the distribution of environmental contaminants was previously suggested (Pollard et al. 2002). The evaluation of a bimodal behavior at DWTP B was necessary because the Lomax distribution predicted a much higher mean concentration than the sample mean. DWTPs C2 and E had sample kurtosis greater than 155. The power-law tail of the Lomax distribution predicted observed data at DWTP E. The value of the shape parameter α of 1.7 was large enough to calculate a finite credibility interval on the mean (Table 4-3). At DWTP C2, only one sample with a concentration of 11,000 *E. coli*/100 mL increased the SD to MAD ratio from 1.80 to 2.46 and the kurtosis from 40 to 155.

Differences between the sample and predicted mean of the best-fit model were lower than 0.1 $\log_{10}$ at all DWTPs. Therefore, the sample mean was a reliable index to estimate the true mean raw water *E. coli* concentration at these DWTPs. In other words, the evaluated sample sizes were large enough to converge to the true mean of the log-normal distribution (DWTPs A, C1, C2, D), the mixture of two log-normal distributions (DWTP B), and the Lomax distribution (DWTP E). However, upper limits of detection of 8,000 CFU/100 mL at DWTP B and of 2,419 MPN/100 mL at DWTP C1 may underestimate the size of the upper tail. Hence, the number of dilutions should always be

carefully selected to avoid dealing with an upper limit of detection when data are collected for statistical inference.

4.4.2 Evaluation of the sample size to estimate mean of *E. coli* concentrations at DWTP intakes

Required confidence or credibility intervals on mean estimates are usually not indicated in guidelines and regulations (Supplementary Table 4-1). The estimates of the mean concentrations are used to determine minimum treatment targets, usually quantified in $\log_{10}$ reduction values. A large uncertainty on the mean will increase the probability of misclassification of a treatment bin category. Health-based targets will not be met if treatment requirements are underestimated, while unnecessary costly treatment processes will be added if treatment requirements are overestimated. To reduce the uncertainty to an appropriate level, we are proposing the use of the Cox method to determine the minimum sample size when the best-fit distribution is log-normal. Weekly sampling for three years (n=156) allowed the estimation of the true mean with a 95% confidence interval of 0.3 $\log_{10}$ at DWTPs C1, C2, and D (Table 4-6). Four years of weekly sampling (n=208) would be required at DWTP A to reach 0.3 $\log_{10}$. These sample sizes should be doubled to reduce the uncertainty to 0.2 $\log_{10}$. Therefore, the lowest 95% confidence interval achievable with a reasonable number of samples would be 0.3 $\log_{10}$. These results are site-specific because they depend on the variance of the dataset. A conservative value of the variance could be assumed to determine the minimum sample size for a group of DWTPs. Other mathematical approaches should be considered to estimate the minimum sample size when observations follow Lomax or mixture distributions. The required minimum sample sizes to estimate the true mean with a 95% confidence interval will probably be higher than those determined for the log-normal distributions.

An estimation of the mean concentration with results from weekly sampling strategies for one year as regulated in Quebec for large DWTPs (n=52 samples) was sufficient to reach a confidence interval of around 0.4 $\log_{10}$ in urban rivers (DWTPs C1, C2, D), but not in the studied agricultural river (DWTP A) where the confidence interval was larger than 0.5 $\log_{10}$. Monthly sampling for two years (n=24 samples), as required by the US EPA in rivers where the arithmetic mean is lower than 50 *E. coli*/100 mL, would only predict the mean with a confidence interval lower than 0.5 $\log_{10}$ if the variance is small (value of the sigma parameter lower than 1.1, which is lower than observed at the sites in this study). The variance of the *E. coli* concentrations was higher for

DWTPs fed by the small rivers (DWTPs A and B) that are more subject to episodic changes in water quality. Therefore, robust methods for the design of sampling strategies should consider water quality variability, particularly in small agricultural catchments.

4.4.3 Integrating peak microbial contamination events

Accounting for hydrometeorological events is an important issue for the quantification of microbial treatment requirements (Petterson et al. 2015). Peak events need to be considered as they represent challenging periods for DWTPs as illustrated by major waterborne outbreaks in the past (Curriero et al. 2001, Hrudey et al. 2002, Thomas et al. 2006). The collection of event-based samples in addition to routine monitoring has been recently added to WHO guidance documents (WHO 2016b, a) and Australian drinking water guidelines (NHMRC 2018). In the Netherlands, incidental samples must be collected when peak concentrations in pathogen counts are assumed to occur (VROM-Inspectorate 2005).

As demonstrated in this study, new statistical approaches are needed to incorporate this information into risk assessment. Routine samples are quasi-independent and identically distributed (i.i.d.) random variables. This property implies that a given sample is independent of the previously collected sample. Alternatively, event-based samples are not i.i.d. random variables, and cannot be combined with routine samples for statistical inference. However, event-based samples can be used to 1) evaluate short-term exposure (e.g. maximum daily risk), and 2) evaluate whether peak concentrations are included or excluded from the tail of a parametric distribution inferred with routine monitoring data.

Short-term variations of *E. coli* were measured at DWTP C1 during and following two hydrometeorological events during the snowmelt period in 2017. Instead of relying on precipitation data, we used a microbial surrogate to time our event-based sampling. Online measurement of GLUC activity can be used as a reliable surrogate to identify periods of high *E. coli* concentrations (Burnet et al. 2019a, Burnet et al. 2019b) for the collection of samples. The maximum daily mean concentrations of 1,588 *E. coli*/100 mL in February and 2,567 *E. coli*/100 mL in April were higher than the 97th percentile and the 99th percentile retrieved from eight years of daily M-T (Monday to Thursday) sampling, respectively. Concentrations exceeding 1,000 *E. coli*/100 mL were continuously measured for about one day in February and during three days in April. As such, we demonstrated that online GLUC activity measurement-based sampling strategy is suitable for the

detection of critical periods of *E. coli* contamination in an urban river during the snowmelt period. This sampling strategy could be applied to target pathogen monitoring programs or study variations of pathogen concentrations in source water during hydrometeorological events. The CCDF plot for DWTP C1 showed that the gamma distribution could not predict the maximum daily mean concentrations during the April event (Figure 4-7). The maximum daily mean concentrations of these two events crossed the CCDF curves of the log-normal and the Lomax distributions. The log-normal distribution predicted a frequency of occurrence of these daily peaks between two to twenty days per year. Therefore, the log-normal distribution was a conservative bound for peak events if these maximum daily mean concentrations occurred less than 20 days a year. In this case, weekly sampling for two years estimated the true mean with a confidence interval of 0.3 $\log_{10}$ (Table 4-6) and included the influence of these peak events.

4.4.4 Identifying key contributors to peak events in agricultural and urban rivers

The protection of drinking water sources is a preventive approach to minimize the influence of peak events on the mean concentration and thereby ensure adequate health-based treatment requirements. We introduced generalized Lorenz curves as quantitative tools to determine how critical contamination periods influence the long-term mean *E. coli* concentrations for four DWTPs. The identification of these periods could guide the implementation of source water protection measures. The combined annual generalized Lorenz curves indicated that peak events had more influence on the mean concentration in small agricultural rivers (DWTPs A and B) than in large urban rivers (DWTP C1, C2, D) (Figure 4-4). Seasonal contributions to the long-term mean *E. coli* concentrations were different between urban and agricultural catchments. For agricultural rivers, the long-term mean was driven by samples collected during summer and fall. The conditions leading to the bimodal behavior of the distribution at DWTP B should be further investigated with hydrometeorological and land use data to identify potential factors triggering a different generative process for the distribution of tail events. Two primary sources of contamination could contribute to the observed pattern since four CSOs, and one WWTP are located upstream of the DWTP. During rainfall, the combined effect of these two sources could generate a different distribution.

In the urban rivers, critical periods of contamination at DWTPs were winter and spring. At DWTP C1, rapid snowmelt had more influence than rainfall on the variation of *E. coli* concentrations, and

recurrent peak events were observed at low flow rates in 2014 and 2015 (Figure 4-5). At DWTP C1 and C2, treated effluent discharges, but also sewage by-passes at WWTPs, and CSO discharges during snowmelt periods likely influence the behavior of the tail of the distribution (Burnet et al., 2019b). At DWTP D, Madoux-Humery et al. (2016) showed that approximately 80% of *E. coli* peak concentrations were linked to CSO discharges caused by daily precipitation exceeding ten millimeters or by spring snowmelt. Here, we show that these peaks could be predicted by a log-normal distribution (Figure 4-2) and that weekly sampling for two years (*n*=104 samples) at the DWTP enables to estimate the true mean concentration with a confidence interval of 0.3 $\log_{10}$ (Table 4-6).

4.5 Conclusions

We have shown that it is possible to use simple parametric models and graphical tools to consider different tail behaviors for the evaluation of the mean *E. coli* concentration in raw water. The application of this approach to large data sets collected with routine and event-based monitoring strategies at six drinking water treatment plants located in different types of catchments demonstrated that:

- Weekly sampling for three years in urban catchments and for four years in agricultural catchments produce reasonable estimates of the average raw water *E. coli* concentrations, and encompass peak event concentrations;
- Log-normal, Lomax, and a mixture of log-normal distributions better predict high *E. coli* concentrations in raw water;
- The kurtosis and the ratio of the standard deviation to the mean absolute deviation are useful indices for identifying sites vulnerable to peak *E. coli* concentrations;
- The log-normal distribution fit on extensive weekly monitoring data conservatively predicted peak *E. coli* concentrations as measured during two snowmelt events at a drinking water treatment plant under the influence of (un)treated sewage discharges.
- The generalized Lorenz curves show that a small proportion of samples predominantly contributes to the average *E. coli* concentrations in agricultural catchments.
- Critical seasons of high contamination levels were summer and fall in the agricultural catchment, and winter and spring in urban catchments.

- The characterization of site-specific variations can promote the effective implementation of mitigation measures to address contamination sources with the highest influence on the average *E. coli* concentrations at drinking water treatment plant intakes.

- The data collection and model validation methods described in this paper could be adapted for pathogens to explicitly consider hydrometeorological events in the quantification of microbial treatment targets

4.6 Acknowledgments

CHAPTER 5 ARTICLE 2 - IMPORTANCE OF DISTRIBUTIONAL FORMS FOR THE ASSESSMENT OF PROTOZOAN PATHOGENS CONCENTRATIONS IN DRINKING WATER SOURCES

It should be noted that Article 2 (Chapter 5) and Article 3 (Chapter 6) are companion articles. Both articles investigate temporal variations in source water protozoan pathogens concentrations. Article 2 is primarily focusing on model development and implementation. Article 3 adapted the model validation technique presented in Chapter 4 for the assessment of protozoan pathogens in source water.

This Chapter presents the development and implementation of Poisson and mixed Poisson models for the analysis of temporal variations in source water pathogen concentrations. Source water *Cryptosporidium* and *Giardia* data sets collected at 30 drinking water treatment plants are modeled. More specifically, this work investigates whether the choice of a parametric model can significantly influence the estimation of the mean pathogen concentration and its uncertainty. This article has been accepted in *Risk Analysis*. Supplementary information is presented in Appendix B.

Importance of distributional forms for the assessment of protozoan pathogens concentrations in drinking water sources

Émile Sylvestre [a,b], Michèle Prévost [a], Patrick Smeets [c], Gertjan Medema [c,d], Jean-Baptiste Burnet [a,b], Philippe Cantin [e], Manuela Villion [f], Caroline Robert [e], Sarah Dorner [b]

[a] NSERC Industrial Chair on Drinking Water, Department of Civil, Geological, and Mining Engineering, Polytechnique Montreal, Montreal, Quebec, H3C 3A7, Canada

[b] Canada Research Chair in Source Water Protection, Department of Civil, Geological, and Mining Engineering, Polytechnique Montreal, Montreal, Quebec, H3C 3A7, Canada

[c] KWR Water Research Institute, Groningenhaven 7, 3433 PE Nieuwegein, The Netherlands

[d] Sanitary Engineering, Department of Water Management, Faculty of Civil Engineering and Geosciences, Delft University of Technology, P.O. Box 5048, 2600GA, Delft, The Netherlands

[e] Ministère de l'Environnement et de la Lutte contre les changements climatiques, Québec, Canada

[f] Centre d'expertise en analyse environnementale du Québec, Ministère de l'Environnement et de la Lutte contre les changements climatiques, Québec, Canada

* Corresponding author e-mail: emile.sylvestre@polymtl.ca

Abstract

The identification of appropriately conservative statistical distributions is needed to predict microbial peak events in drinking water sources explicitly. In this study, Poisson and mixed Poisson distributions with different upper tail behaviors were used for modeling source water *Cryptosporidium* and *Giardia* data from 30 drinking water treatment plants. Small differences (< 0.5-log) were found between the "best" estimates of the mean *Cryptosporidium* and *Giardia* concentrations with the Poisson–gamma and Poisson–log-normal models. However, the upper bound of the 95% credibility interval on the mean *Cryptosporidium* concentrations of the Poisson–log-normal model was considerably higher (>0.5-log) than that of the Poisson–gamma model at four sites. The improper choice of a model may, therefore, mislead the assessment of treatment requirements and health risks associated with the water supply. Discrimination between models using the marginal deviance information criterion (mDIC) was unachievable because differences in upper tail behaviors were not well characterized with available datasets ($n < 30$). Therefore, the gamma and the log-normal distributions fit the data equally well but may predict different risk estimates when they are used as an input distribution in an exposure assessment. The collection of event-based monitoring data and the modeling of larger routine monitoring data sets are recommended to identify appropriately conservative distributions to predict microbial peak events.

5.1 Introduction

As part of a risk-based preventive approach, the World Health Organization (WHO) guidelines for drinking-water quality (WHO 2017b) promotes the use of quantitative microbial risk assessment (QMRA) to set health-based treatment targets at drinking water treatment plants (DWTPs). To undertake a QMRA for drinking water, the number of pathogens that correspond to a set of

exposures via drinking water is evaluated through an exposure assessment. The exposure pathway is defined in terms of source water pathogen quantification, treatment barriers, and tap water consumption. Reliable information on source water microbial quality is therefore needed to define treatment requirements and implement catchment protection measures. Multiple exposures to low doses of a pathogen in drinking water are typically characterized in terms of the mean pathogen concentration because conventional single-hit dose–response models rely on the assumption that microbial inoculum are characterized up to Poisson uncertainty (Haas 1996).

Reference pathogens for protozoan pathogens in surface drinking water sources are *Cryptosporidium spp.* and *Giardia lamblia* because they are highly prevalent in the population, and because they pose a treatment challenge as a result of their resistance to chlorination (WHO 2017b). When available, source water *Cryptosporidium* and *Giardia* data sets are typically of small size because of high analysis costs (e.g., USEPA Method 1623). Caution is needed when small data sets are modeled for risk assessment because the sample mean concentration may not be representative of the true mean concentration if high concentrations are not correctly characterized.

The Poisson distribution is commonly used to express the probability of a given number of microbial counts in a well-mixed water sample (Student 1907). However, in surface water, count data typically show more variation than implied by the Poisson distribution because of temporal covariate effects among sampling events (incidence of infections in the population, hydrometeorological conditions) and measurement errors (Emelko et al. 2010). To account for over-dispersion, a continuous probability distribution can be used to describing the underlying Poisson rate (i.e., population distribution). The Poisson–gamma mixture (negative-binomial) distribution is generally the default choice for the estimation of temporal concentration variations in surface water (Pipes et al. 1977, El-Shaarawi et al. 1981, Teunis et al. 1997, Medema et al. 2003, Pouillot et al. 2004, Teunis et al. 2009, Schijven et al. 2011, Petterson et al. 2015, Teunis and Schijven 2019). Other parametric distributions, such as the Poisson–log-normal distribution, have been used (Haas et al. 1999, Masago et al. 2004, Chik et al. 2018). The Poisson–log-normal is a more unusual but not less interesting alternative because the upper tail of the log-normal distribution is asymptotically heavier than the upper tail of the gamma distribution (Smeets et al.

2008), and this property is preserved under the formation of mixed Poisson models (Kaas and Hesselager 1995). The behaviors of mixed Poisson models were compared in a broad range of fields such as ecology (Millar 2009), actuarial science (Kaas and Hesselager 1995), transport safety (Aguero-Valverde 2013), and food safety (Gonzales-Barron and Butler 2011). However, this issue has not been extensively explored in drinking water safety management. The identification of appropriately conservative statistical distributions is needed as guidance documents recommend the explicit consideration of microbial peak events in exposure assessment (WHO 2009a, 2016b).

The main objective of this study is to determine whether the choice of a parametric distribution can significantly influence the estimation of the mean *Cryptosporidium* and *Giardia* concentrations using monitoring data from 30 drinking water treatment plants. Additional objectives included: (a) using the deviance information criterion (DIC) to compare the accuracy of the alternative models, (b) examining upper tail behaviors with complementary cumulative distribution functions, and (c) evaluating the influence of non-constant analytical recovery and sample-specific viability of *Cryptosporidium* oocysts on the statistical dispersion of the distributions.

5.2 Material and methods

5.2.1 Sample collection and analysis

Source waters of 30 drinking water treatment plants (DWTPs) in Quebec, Canada, were sampled. DWTPs were classified by types of drinking water sources (Table 5-1). Identification letters indicate if a DWTP is supplied by a river (A, B, C), a reservoir (D), or a lake (E). DWTPs supplied by rivers were classified based on the annual mean flow rate of the river: below 20 m^3/s (A), in between 20 and 100 m^3/s (B), and higher than 100 m^3/s (C). Monthly samples were collected for about four years between 2013 and 2016 at DWTPs C6, C10, C11. Monthly samples were collected for about two years between 2011 and 2019 at the other DWTPs. Volumes of raw water varying from 10 to 60 liters were filtered on-site with Envirochek HV, and samples were analyzed for the detection of *Cryptosporidium* oocysts and *Giardia* cysts following EPA method 1623 (USEPA 2005) from 2011 to 2013, and EPA method 1623.1 from 2013 to 2017 (USEPA 2012). All samples were analyzed at the Centre d'expertise en analyse environnementale du Québec (CEAEQ).

Matrix spike, ongoing precision, and recovery, and method blanks were performed following EPA method 1623 and EPA method 1623.1. A total of 43 *Cryptosporidium* and *Giardia* matrix spike recovery experiments (at least one per DWTP) were carried out in 10-liter raw water samples collected at the DWTP (Supplementary Table 5-1). Each sample was spiked with 98-100 ColorSeed^{TM} (oo)cysts (Colorseed^{TM}, BTF, Australia). The viability of *Cryptosporidium* oocysts was assessed based on the inclusion or exclusion of fluorogenic vital dyes. Oocysts that included the nuclear fluorochrome 4′, 6-diamidino-2-phenylindole (DAPI) were considered viable. DAPI-positive *Cryptosporidium* oocyst counts from nine sites (Supplementary Table 5-2) were evaluated to quantify the influence of the viability of *Cryptosporidium* oocysts on the statistical dispersion of the distributions.

The sample mean *Cryptosporidium* and *Giardia* concentrations were calculated by averaging all sample concentrations (count/volume). The sample maximum *Cryptosporidium* and *Giardia* concentration were also evaluated. The sample maximum represents the maximum of all concentrations (count/volume) measured at a site. The relative standard deviation (RSD), defined as the ratio of the sample standard deviation to the sample mean, was also calculated to estimate the importance of the difference between upper tail behavior among distributions (Haas 1997).

Table 5-1: Summary of *Cryptosporidium* and *Giardia* data and catchment information

DWTP	Main land cover type of the catchment	Catchment size (km²)	Mean discharge of river (m³/s)	*n*	Total volume analysed (L)	Sampling period		*Crypto.* oocysts detected	*Giardia* cysts detected
A01	Agricultural	100	<20	21	1026	2018/4/30	2019/3/28	12	283
A02	Agricultural	200	<20	21	1191	2018/4/30	2019/3/28	36	2182
A1	Forested	100	<20	20	1086	2016/5/17	2018/1/31	110	6153
A2	Mixed	<100	<20	20	710	2016/5/10	2018/1/31	79	6359
A3	Mixed	500	<20	21	830	2014/6/17	2016/3/21	37	1106
A4	Agricultural	<100	<20	24	936	2014/3/25	2016/3/15	125	1321
B1	Mixed	2500	23	22	848	2014/3/25	2016/3/15	129	1014
B2	Forested	4000	26	19	957	2016/5/10	2017/11/6	62	2306
B3	Mixed	2500	26	18	869	2016/05/9	2017/11/13	14	906
B4	Mixed	4200	27	15	276	2011/8/28	2013/8/13	16	736
B5	Mixed	1100	36	18	889	2016/5/17	2017/11/13	20	497
B6	Mixed	2500	70	18	458	2016/5/10	2017/11/6	16	448
B7	Agricultural	3400	74	16	428	2011/5/3	2013/9/23	14	232
C1	Mixed	10000	114	19	1077	2016/5/9	2017/11/7	186	1073
C2	Agricultural	10000	114	17	930	2016/5/9	2017/11/7	43	1068
C3	Mixed	7000	114	15	785	2014/3/25	2016/9/8	43	367
C4	Mixed	10000	190	22	606	2014/3/25	2016/3/15	49	587
C5	Agricultural	10000	190	15	145	2011/5/3	2013/9/23	8	86
C6	Urban	>50000	286	48	695	2013/1/1	2016/12/31	32	1016
C7	Urban	>50000	286	16	372	2011/8/22	2013/9/10	36	1030
C8	Mixed	23000	330	17	854	2014/3/25	2016/9/22	40	389
C9	Mixed	23000	330	15	169	2014/6/17	2015/9/22	4	63
C10	Urban	>50000	1,365	45	719	2013/1/1	2016/12/31	16	391
C11	Urban	>50000	1,365	46	659	2013/1/1	2016/12/31	15	255
C12	Urban	>50000	16000	16	147	2011/5/2	2013/9/10	17	539
C13	Mixed	>50000	16000	16	339	2011/8/22	2013/9/10	30	1016
C14	Mixed	>50000	16000	17	364	2011/5/2	2013/9/23	10	170
D1	Agricultural	200	Reserv.	22	707	2014/3/25	2016/3/21	57	1170
E1	Forested	100	Lake	20	1269	2018/4/30	2019/3/28	4	147
E2	Forested	3000	Lake	21	1003	2018/4/30	2019/3/28	12	2021

5.2.2 Model parametrization

The probabilistic framework of Nahrstedt and Gimbel (1996) and Emelko et al. (2010) were expanded to account for different temporal variability distributions. Within this framework, the distribution of one random variable is conditional on the distribution of another random variable from a higher level. Three levels of analysis were specified to account for temporal concentration variability. To consider a non-constant analytical recovery, i.e., the sample-to-sample variation of

the analytical recovery, the number of microorganisms y_i observed in sample i was modeled at the first level by a binomial distribution of x_i independent counts having a probability of recovery p_i.

$$y_i \sim \text{Binomial } (x_i, p_i) \tag{5.1}$$

The binomial process assumes independence for the detection of individual microorganisms. At the second level, the number of microorganisms x_i in the ith sampling event are treated as Poisson random variables with an observation-specific mean $\lambda_i = c_i V_i$ given as a product of the source water concentration (c_i) and the processed volume of the sample (V_i).

$$f(x) = \frac{\lambda^x e^{-\lambda}}{x!} = \frac{(cV)^x e^{-(cV)}}{x!} \tag{5.2}$$

At the third level, the unknown (unobserved) concentration c_i was described by a continuous *population* distribution. The gamma and log-normal distributions were selected to describe temporal variations in concentration c because their densities differ in their upper tail probabilities. The two-parameter gamma distribution has a density

$$f(c) = \frac{\lambda^\alpha c^{\alpha-1}}{\Gamma(\alpha)} e^{-\lambda c} \tag{5.3}$$

and an expectation (i.e., mean) $E(c) = \alpha\lambda$, where $\alpha > 0$ is the shape parameter and $\lambda > 0$ is a scale parameter. The two-parameter log-normal distribution has a density

$$f(c) = \frac{1}{\alpha c \sqrt{2\pi}} \exp\left[-\frac{1}{2} \frac{[\ln c - \lambda]^2}{\alpha^2}\right] \tag{5.4}$$

and an expectation $E(c) = \exp\left(\alpha + \frac{\lambda^2}{2}\right)$, where the shape parameter $\alpha > 0$ and the scale parameter λ may take each real value.

The density for high c decreases as $\exp[-\lambda c]$ and $\exp[-\frac{1}{2}[ln\, c - \lambda]^2/\alpha^2]$ for the gamma and the log-normal, respectively (Tijms 2003). The log-normal density always has a heavier tail than the gamma distributions for given values of the mean and the coefficient of variation. The Weibull distributions was also considered as a population distribution in preliminary work; however, its upper tail behavior was similar to that of the gamma distribution. Furthermore, convergence problems arose that limited its application.

The recovery rate p_i in Eq. 5.1 was assumed to be 100% for all samples because sample-specific recovery rates were not available. However, the influence of a non-constant analytical recovery was demonstrated using pooled recovery data from *Cryptosporidium* matrix spike recovery experiments (Supplementary Table 5-1). Pooled recovery data were assumed to be Beta distributed (Teunis et al. 1999). Parameters of the Beta distribution were estimated using a Beta-binomial model representing the variability in the number of seeded (oo)cysts that were observed n_i in matrix spike recovery experiment i.

$$n_i \sim \text{Binomial}\,(m_i, p_i) \tag{5.5}$$

$$p_i \sim \text{Beta}(\hat{\alpha}, \hat{\beta}) \tag{5.6}$$

The Beta-binomial model for analytical recovery assumes that the number of seeded (oo)cysts m_i is precisely known, the analytical recovery p_i is Beta distributed with mean values of parameters (α, β), and the analytical error is binomially distributed (Schmidt et al. 2010). The uncertainty of the Beta distribution parameters was not considered in the analysis.

5.2.3 Model implementation

Bayesian statistics were used rather than classical (frequentist) statistics because mixed Poisson models are easier to implement with Markov Chain Monte Carlo (MCMC) than with maximum likelihood estimation (MLE), which require high dimensional numerical integration. Furthermore, Bayesian methods are especially suited for relatively small data sets because Bayesian statistics are

not based on large samples (i.e., the central limit theorem) (van de Schoot and Miocević 2020). The Bayesian analysis was conducted via rjags (v4-6) (Plummer 2013) in R (v3.4.1). For each parameter, four Markov chains were run for 3×10^5 iterations after a burn-in phase of 10^4 iterations. The Brooks-Gelman-Rubin scale reduction factor was used to monitor the convergence of the four chains (Gelman and Shirley 2011). The effective sample size (ESS), the ratio of the sample size to the amount of autocorrelation in the Markov chains, was evaluated to ensure that the entire posterior distribution was explored (Kass et al. 1998). Estimates of the 95% credibility interval of the posterior distributions were considered reasonably accurate when an ESS higher than 10,000 was obtained (Kruschke 2014). The ESS was calculated using the diagMCMC function from Kruschke (2014). An illustration of these MCMC diagnostics for a specified parameter is presented in the Supplementary Material (Supplementary Figure 5-1). The mean (expected value) and the upper bound of the 95% credibility interval on the mean of the gamma and log-normal distributions were reported.

5.2.4 Prior distributions

In Bayesian analyses, the prior distribution needs to be chosen carefully when sample sizes are small because its parametrization can strongly impact the results. Prior knowledge on source water *Cryptosporidium* and *Giardia* concentration distributions was not available at these DWTPs; therefore, *uninformative* priors (priors with large variance) were adopted to have as little impact on the analysis as possible. Uninformative priors typically specify a wide range of probable parameter values and give similar results to a maximum likelihood estimation (MLE) analysis. In this study, the shape parameters α and β of the Beta distribution in the Beta-binomial model for analytical recovery were assigned uninformative uniform priors with hyperparameters set to Uniform (0.01, 100).

Conjugate priors can be chosen for the exponential family of distributions to minimize the influence of the data on the posterior and facilitate Gibbs sampling. A conjugate gamma prior with hyperparameters (i.e., parameters of the prior distribution) set to Gamma (0.01, 0.01) was selected to describe the concentration c of the Poisson model. This prior is practically flat to reflect no prior

knowledge. Bayesian estimations become more complicated for two-parameter distributions because they require two-dimensional prior distributions. The two-parameter gamma distribution does not have continuous joint prior distribution. Simulations results suggested that Bayesian estimation of a two-parameter gamma distribution using Lindley's approximation under the assumption of a gamma prior on the shape and rate (inverse scale) parameters behave like MLE (Pradhan and Kundu 2011). Gamma priors on the shape and rate parameters of the two-parameter Gamma distribution were thus selected. Hyperparameters were also set to Gamma (0.01, 0.01).

For the log-normal distribution, the shape parameter α was assigned a uniform prior. The prior was set to Uniform (-10, 10), given that the logarithm of the mean was not expected to be outside of this interval. A weakly informative prior was chosen to describe the variability of the scale (variance) parameter λ of the log-normal distribution. A commonly used prior for the variance parameter of a (log)normal distribution is the half-Cauchy distribution (Gelman 2006). JAGS does not have a built-in half-Cauchy distribution, and it employs the precision rather than the variance in its log-normal distribution. However, such a function can be approximated with an exponential prior on the standard deviation σ (McElreath 2020). The exponential distribution has a much thinner tail than the half-Cauchy and can help the convergence of the Markov chains. The exponential prior was set to $\exp(1)$ given that the logarithm of the standard deviation was expected to be well below five at all DWTPs.

5.2.5 Model comparison

5.2.5.1 Deviance Information Criterion

Poisson and mixed Poisson models were compared with an information criterion considering a constant recovery rate of 100%. Each model was fitted to the same set of observations to compare their out-of-sample predictions. The Deviance Information Criterion (Spiegelhalter et al. 2002) is commonly used to compare the accuracy of Bayesian models. This criterion allows to rank models by balancing goodness-of-fit and complexity using deviance and a penalty term weighted by the number of parameters. The DIC is given by:

$$\text{DIC} = \bar{D} - (\bar{D} - \hat{D}) = \bar{D} + p_D \tag{5.7}$$

where $\bar{D}$ is the mean of D, the deviance for each set of sampled parameter values in the posterior distribution, and $\hat{D}$ is the deviance of the posterior mean of the parameters. The difference $\bar{D} - \hat{D} = p_D$ can be interpreted as a penalty associated with the risk of overfitting. Smaller values of DIC suggest a better model. A proposed rule of thumb, appearing to work reasonably well for the comparison of DIC, is that a model with a difference of DIC within 1–2 of the "best" model deserves consideration, and 3–7 have considerably less support (Spiegelhalter et al. 2002).

In multilevel modeling, the DIC can be specified at different levels of model focus (Spiegelhalter et al. 2002, Celeux et al. 2006). The DIC can be expressed either as conditional upon latent variables (cDIC) or after marginalizing over latent variables (mDIC). In this study, the conditional-level likelihood is the Poisson distribution, and the marginal-level likelihood is the full Poisson mixture model. In the context of over-dispersed count data, Millar (2009) found evidence of the poor performance of the cDIC. Instead of reporting the cDIC, the author recommended calculating the mDIC using likelihood that is marginalized by integrating out the latent variables. A closed-form of the marginal distribution exists for the Poisson–gamma distribution, i.e., negative binomial distribution, but does not exist for the Poisson–log-normal distributions. Quintero and Lesaffre (2018) proposed a method to compute mDIC with Monte Carlo integration using the MCMC output of JAGS. This approach assumes that the marginalized likelihood components can be approximated by generating replicate samples from the density of the latent variables and taking the mean value of the conditional distribution evaluated in the sampled parameters. The method of Quintero and Lesaffre (2018) was adopted in this study to compute mDIC. The numbers of replicated samples to approximate the deviance D for each set of sampled parameter values in the posterior distribution and the deviance $\hat{D}$ on the posterior mean were set to 5,000. These numbers were adjusted to reduce the standard error on the mDIC to a value lower than 0.5. At this level, the variation in mDIC can be expected to be smaller than 1 (Quintero and Lesaffre 2018). The R code used to calculate mDIC with Monte Carlo integration is provided in the Supplementary Material.

5.2.5.2 Model checking

Observations were visually compared to simulated data under the fitted model with posterior predictive checks (Gelman et al. 2013, McElreath 2020). Selected data sets were represented with complementary cumulative distribution function (CCDF) curves to illustrate differences between upper tail probabilities of each distribution (Haas 1997, Smeets et al. 2010). CCDF curves were computed for probabilities of exceedance between 100% and 0.27% (1 day per year). Each distribution was generated using a point estimate (mean) of the posterior of the parameter (α, λ). The predictive interval about the best fit the distribution was created by simulating 1,000 CCDF curves parametrized by random values included in the 95% credibility interval of the posterior. The R code used to generate the figures is provided in the Supplementary Material.

5.3 Results

5.3.1 Characterization of the data sets

Cryptosporidium oocysts and *Giardia* cysts were detected in 55% and 95%, respectively, of the 553 raw water samples collected at 30 DWTPs. The sample mean *Cryptosporidium* concentration varied over 0.01 to 0.2 oocysts/L in rivers, and over 0.001 to 0.01 oocysts/L in lakes (Table 5-2). According to the WHO guidance on risk assessment of *Cryptosporidium* in drinking water (WHO 2009a), the microbial quality of water was "very pristine" (mean ~ 0.001 oocysts/L) at 1 DWTP, between "pristine" (mean ~ 0.01 oocysts/L) and "moderately polluted" (mean ~ 0.1 oocysts/L) at 19 DWTPs, and was between "moderately polluted" and "polluted" (mean ~ 1 oocysts/L) at 10 DWTPs. Moderately polluted sources were observed in small, midsize, and large rivers (Table 5-1). For *Giardia*, the sample mean concentration varied over 0.04 to 4 cysts/L (Table 5-2). The site-specific mean *Giardia* concentrations were 1 to 3-log higher than the site-specific mean *Cryptosporidium* concentrations. Sample mean concentrations higher than 1 cyst/L were estimated for small, midsize and large rivers, and for a lake. The RSD typically varied over 1.0 and 3.0 for *Cryptosporidium* and over 0.5 and 2.0 for *Giardia*. Higher RSD values were obtained for *Cryptosporidium* than for *Giardia* at 27 DWTPs.

Table 5-2: Sample size (number of positive samples), sample mean concentration, sample maximum concentration and relative standard deviation for raw water *Cryptosporidium* and *Giardia* concentrations at 30 drinking water treatment plants

| DWTP | *Cryptosporidium* | | | | *Giardia* | | | |
	Sample size (+ ve)	Sample mean (oocyst/L)	Sample maximum (oocyst/L)	Relative standard deviation	Sample size (+ ve)	Sample mean (cyst/L)	Sample maximum (cyst/L)	Relative standard deviation
A01	21 (7)	0.010	0.060	1.71	21 (21)	0.342	3.025	1.87
A02	21 (13)	0.028	0.139	1.24	21 (21)	1.840	7.869	0.97
A1	20 (20)	0.159	1.466	2.06	20 (20)	4.977	22.727	1.03
A2	20 (15)	0.127	0.588	1.32	20 (20)	9.110	22.250	0.61
A3	21 (12)	0.062	0.333	1.44	21 (21)	2.063	7.867	1.03
A4	24 (18)	0.181	1.387	1.63	24 (24)	1.543	7.179	1.01
B1	22 (19)	0.173	1.464	1.77	22 (22)	1.297	3.000	0.62
B2	19 (14)	0.080	0.625	1.77	19 (19)	2.268	5.245	0.63
B3	18 (7)	0.022	0.096	1.89	18 (18)	1.085	2.667	0.59
B4	15 (6)	0.076	0.363	1.49	15 (15)	3.290	7.231	0.64
B5	18 (13)	0.024	0.078	0.93	18 (17)	0.541	1.338	0.68
B6	18 (9)	0.048	0.250	1.47	18 (18)	1.044	3.571	0.90
B7	16 (9)	0.097	0.600	1.65	16 (16)	0.853	4.545	1.32
C1	18 (16)	0.179	0.809	1.42	18 (18)	1.419	14.693	2.34
C2	17 (14)	0.045	0.111	0.85	17 (17)	1.288	4.433	0.87
C3	15 (14)	0.055	0.333	1.41	15 (15)	0.534	2.179	1.10
C4	22 (8)	0.122	1.311	2.45	22 (22)	1.066	3.571	0.85
C5	15 (5)	0.062	0.428	1.90	15 (15)	1.364	8.750	1.73
C6	48 (20)	0.064	0.357	1.65	48 (43)	1.572	7.400	0.93
C7	16 (8)	0.105	0.500	1.42	16 (16)	4.624	21.875	1.35
C8	17 (10)	0.042	0.333	1.98	17 (17)	0.510	2.178	1.13
C9	15 (3)	0.023	0.181	2.26	15 (15)	0.423	1.400	0.90
C10	45 (13)	0.021	0.133	1.78	45 (39)	0.534	1.750	0.88
C11	46 (13)	0.021	0.133	1.72	46 (41)	0.416	1.667	1.02
C12	16 (10)	0.113	0.545	1.22	16 (16)	4.110	10.800	0.63
C13	16 (11)	0.100	0.529	1.33	16 (16)	3.143	8.174	0.73
C14	17 (6)	0.085	0.285	2.86	17 (17)	0.707	2.571	0.98
D1	22 (15)	0.079	0.406	1.42	22 (22)	1.927	7.826	0.93
E1	20 (3)	0.003	0.031	2.60	20 (20)	0.118	0.253	0.69
E2	21 (8)	0.011	0.076	1.72	21 (21)	1.799	7.272	1.13

5.3.2 Statistical inference

The mean of the posterior estimates of the parameter(s) of the Poisson, Poisson–gamma (PGA), and Poisson–log-normal (PLN) models are reported in Table 5-3. The MCMC chains of the Poisson model converged (ESS >10,000) for all *Cryptosporidium* and *Giardia* datasets. Convergence was also obtained with the PGA and PLN models for all *Giardia* datasets. However, ESSs >10,000 were not obtained for *Cryptosporidium* datasets from 12 DWTPs after 3×10^5 iterations with the PGA and PLN models. The total number of oocyst detected at these sites was 20 or lower and the number of positive samples (at least one oocyst detected) was generally lower than 10. The posterior estimates of the parameters of the gamma and log-normal distributions of *Cryptosporidium* concentrations were not reported for the sites. The collection of more samples would be needed for statistical analysis.

For all DWTPs, small differences (< 0.5-log) were found between the sample mean and the "best" estimates of the mean *Cryptosporidium* and *Giardia* concentrations with the PGA and PLN models (Figure 5-1). The upper bounds of the 95% credibility interval on the mean *Cryptosporidium* concentrations of the PLN were 0.5 to 1.2-log higher than those of the PGA for DWTPs B7, C1, C4, and C7. *Cryptosporidium* data sets from these four DWTPs are available in the Supplementary Material (Supplementary Table 5-3). For *Giardia*, only small differences (< 0.5-log) were observed between the upper bounds of the 95% credibility interval of the PGA and PLN models.

Table 5-3: Mean of the posterior estimates for parameters of the Poisson, Poisson–gamma (PGA), and Poisson–log-normal (PLN) models fit to source water *Cryptosporidium* and *Giardia* data at 30 drinking water treatment plants.

	Cryptosporidium					*Giardia*				
	Poisson	PGA		PLN		Poisson	PGA		PLN	
DWTP	$\hat{c}$	$\hat{\alpha}$	$\hat{\lambda}$	$\hat{\alpha}$	$\hat{\lambda}$	$\hat{c}$	$\hat{\alpha}$	$\hat{\lambda}$	$\hat{\alpha}$	$\hat{\lambda}$
A01	0.010					0.27	0.71	2.32	1.13	-1.74
A02	0.028	0.73	23.5	0.83	-3.82	1.83	0.97	0.51	1.32	-0.05
A1	0.106	0.36	2.17	1.44	-2.92	5.67	1.46	0.29	0.88	1.20
A2	0.112	0.53	3.80	1.26	-2.87	8.94	2.64	0.29	0.71	1.99
A3	0.045	0.41	6.04	1.35	-3.66	1.34	1.20	0.59	1.05	0.21
A4	0.136	0.49	2.79	1.34	-2.56	1.41	0.97	1.59	1.21	-0.08
B1	0.152	0.53	3.04	1.32	-2.58	1.20	2.43	2.01	0.71	0.05
B2	0.064	0.49	5.80	1.26	-3.24	2.42	1.99	0.88	0.86	0.55
B3	0.016					1.04	3.01	2.79	0.64	-0.09
B4	0.059					2.68	1.79	0.54	0.94	0.87
B5	0.022					0.55	2.66	5.13	0.65	-0.79
B6	0.035	0.35	7.52	1.09	-3.62	0.97	1.28	1.25	1.06	-0.40
B7	0.033	0.27	2.63	1.45	-3.73	0.54	0.61	0.30	1.40	-0.37
C1	0.174	0.40	2.08	1.57	-2.70	0.99	0.47	0.34	1.63	-1.03
C2	0.047	1.96	39.2	0.44	-3.16	1.15	1.27	1.02	1.09	-0.19
C3	0.054	1.04	17.6	0.85	-3.32	0.48	0.97	1.91	1.21	-1.19
C4	0.079	0.13	0.80	2.01	-3.93	0.97	1.36	1.27	1.02	-0.34
C5	0.057					0.60	0.79	0.77	1.25	-0.73
C6	0.049	0.55	11.4	0.96	-3.46	1.46	1.42	0.91	0.94	0.06
C7	0.096	0.26	1.90	1.45	-3.18	2.77	0.78	0.17	1.25	0.74
C8	0.046	0.32	5.86	1.35	-4.10	0.45	0.95	1.93	1.22	-1.25
C9	0.023					0.37	1.75	4.52	0.86	-1.19
C10	0.022					0.54	1.68	3.22	0.83	-0.93
C11	0.024					0.39	1.48	3.69	0.88	-1.26
C12	0.116					3.68	3.09	0.75	0.61	1.21
C13	0.089	0.60	5.62	0.98	-2.78	3.01	1.91	0.62	0.84	0.84
C14	0.028					0.47	1.11	1.75	1.11	-0.90
D1	0.080	0.50	5.62	1.18	-3.20	1.66	1.35	0.70	0.98	0.22
E1	0.002					0.11	1.99	17.9	0.75	-2.34
E2	0.010					2.01	0.80	0.42	1.49	-0.15
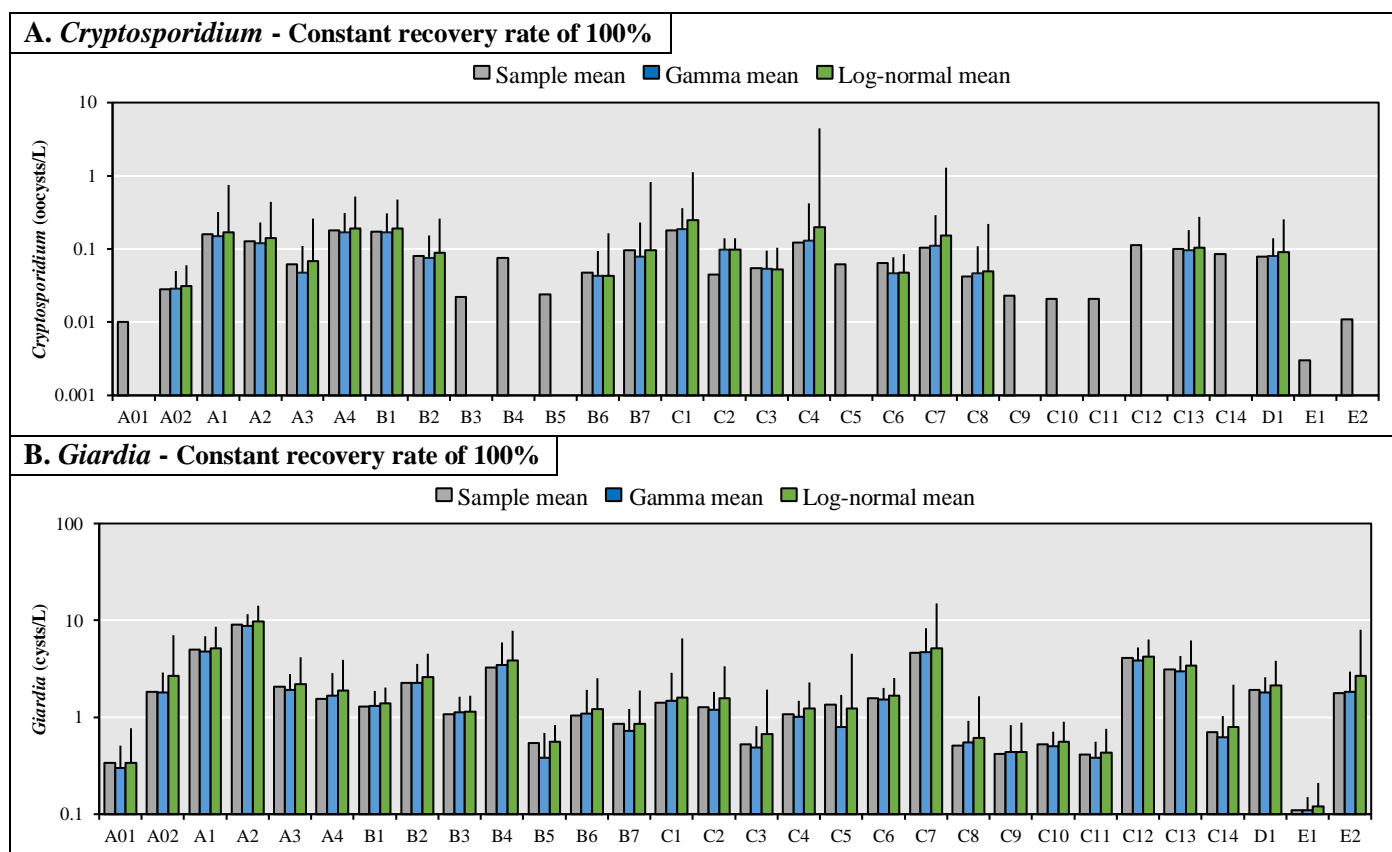
Figure 5-1: Sample mean concentration and expected mean concentrations of the gamma and log-normal distributions for *Cryptosporidium* and *Giardia* at 30 drinking water treatment plants. Grey columns represent sample means, blue columns represent Gamma means, and green columns represent log-normal means. Vertical error bars represent the upper bound of the 95% credibility intervals on the mean concentration. The expected mean concentrations of the gamma and log-normal distributions were not evaluated for *Cryptosporidium* at 12 drinking water treatment plants due to poor convergence of the Markov Chains.

5.3.3 Model comparison

The marginal deviance information criterion (mDIC) for the Poisson, PGA, and PLN models are listed in Table 5-4. The PGA and PLN models better fitted *Cryptosporidium* and *Giardia* data sets than the Poisson model at most DWTPs (difference in mDIC >7). Therefore, pathogen concentrations in raw water cannot be assumed to be stable at the sites. Negligible differences in

mDIC were generally observed between the mixed Poisson models. Differences in mDIC of 3-6 were obtained for 4 DWTPs for *Cryptosporidium* and 11 DWTPs for *Giardia*. The lowest mDIC support the PGA for 2 DWTPs for *Cryptosporidium* and 7 DWTPs for *Giardia*. The lowest mDIC support the PLN for 2 DWTPs for *Cryptosporidium* and 2 DWTPs for *Giardia*.

Table 5-4: The marginal deviance information criterion (DIC_m) indicates the relative accuracy of the Poisson, Poisson–Gamma (PGA) and Poisson–log-normal (PLN) models fit to *Cryptosporidium* and *Giardia* data at 30 drinking water treatment plants. Smaller values of DIC_m suggest a better model.

DWTP	*Cryptosporidium*			*Giardia*		
	Poisson	PGA	PLN	Poisson	PGA	PLN
A01				392.3	159.8	155.8
A02	86.1	75.7	77.7	2016	240.0	244.8
A1	254.0	112.3	110.3	4626	273.7	269.6
A2	161.2	97.4	97.5	2522	277.0	277.9
A3	104.9	81.2	83.5	975.2	222.3	221.2
A4	280.0	139.6	138.6	1332	243.8	246.4
B1	297.6	131.4	128.3	508.8	215.0	218.2
B2	143.4	95.7	94.2	1080	216.5	221.1
B3				403.5	179.4	182.2
B4				585.6	155.2	159.5
B5				297.0	157.4	158.3
B6	59.6	52.9	55.1	468.7	158.8	160.3
B7	66.2	53.6	56.1	310.0	120.1	117.0
C1	383.5	125.8	125.2	2388	197.3	191.1
C2	71.8	70.2	72.1	811.0	187.3	192.4
C3	96.9	70.4	67.4	435.9	139.1	139.5
C4	198.8	81.4	81.7	533.8	187.8	189.8
C5				169.8	95.1	91.7
C6	119.9	110.2	114.2	718.1	299.3	300.3
C7	101.2	63.3	64.7	1647	176.3	173.8
C8	120.4	67.1	65.2	463.7	145.9	146.6
C9				108.7	81.4	82.7
C10				217.8	148.3	148.5
C11				182.9	136.0	136.7
C12				290.1	142.1	143.2
C13	75.1	59.4	64.4	708.5	164.6	166.2
C14				245.9	118.8	119.4
D1	143.1	91.5	91.1	957.9	225.4	226.8
E1				155.5	123.3	127.4
E2				2090	230.8	234.5

Complementary cumulative distribution function (CCDF) curves were produced to illustrate the behavior of the upper tail of the gamma and log-normal distributions of *Cryptosporidium* concentrations for DWTPs B7, C1, C4, and C7 (Figure 5-2). Differences in upper tail behaviors were generally observed from a probability of exceedance of approximately 5 %. These CCDF curves show that the gamma distribution does not extrapolate to concentrations much higher the sample maximum concentration. In contrast, the log-normal distribution does extrapolate to concentrations approximatively 1.0-log than the sample maximum at a probability of exceedance of 0.2%. Furthermore, the size of the 95% predictive interval of the log-normal distribution increased with concentrations. In comparison, the 95% predictive interval of the gamma distribution stabilized at a probability of exceedance of around 20%.
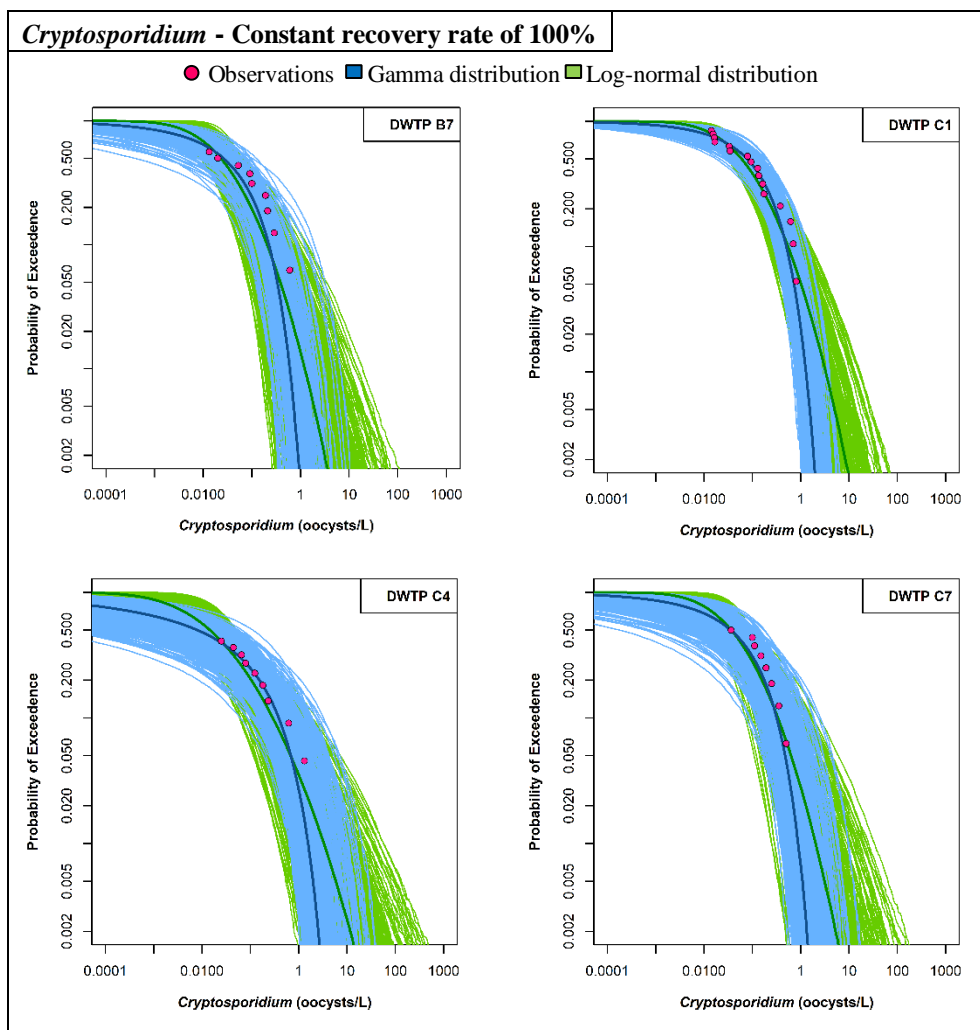
Figure 5-2: Complementary cumulative distribution function (CCDF) curves of the gamma and log-normal distributions of *Cryptosporidium* concentrations at four selected drinking water treatment plants. Dark blue lines and green lines represent the best-fit gamma and log-normal distributions, respectively. Blue and green surfaces represent the 95% predictive interval about the gamma and log-normal distributions, respectively. Pink points represent observed concentrations.

5.3.4 Influence of the non-constant analytical recovery and site-specific oocyst viability

Mean recovery rates were 0.46 (mean absolute deviation [MAD] = 0.11) for *Cryptosporidium* and 0.50 (MAD = 0.13) for *Giardia*. Mean values of the posterior distributions of the parameters of the Beta distribution were $(\hat{\alpha}, \hat{\beta}) = (6.48, 7.70)$ for *Cryptosporidium* and $(\hat{\alpha}, \hat{\beta}) = (3.80, 3.91)$ for *Giardia*. These quasi-symmetric Beta distribution (Figure 5-3A) shifts the location of the population distribution but does not change its dispersion (Figure 5-3B).
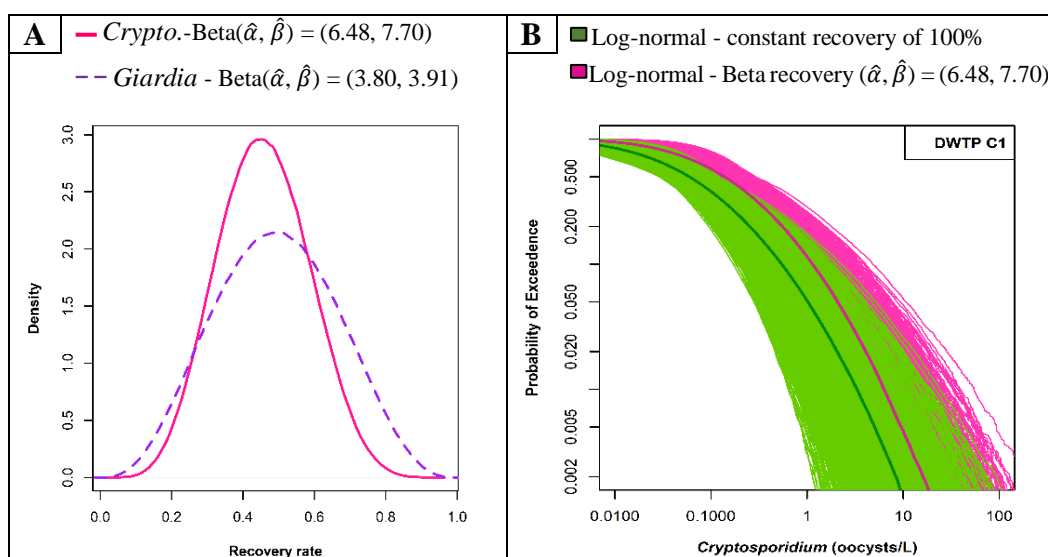
Figure 5-3: Impact of Beta distributed recovery rates on the statistical dispersion of the concentration distribution. A. Density plot of the Beta distributions of the pooled recovery data B. Complementary cumulative distribution function (CCDF) curves of log-normal distributions of *Cryptosporidium* concentrations considering a constant recovery rate of 100% (green) or a non-constant Beta distributed recovery rate (pink) for drinking water treatment plant C1.

Considering DAPI-positive oocysts rather than the IFA-positive oocysts reduces the mean *Cryptosporidium* concentration from less than 0.5-log for seven DWTPs and approximatively 0.6-log for two DWTPs (Figure 5-4). For DWTP A1, adjusting for viability increases the credibility interval on the mean concentration of the log-normal distribution of 0.6-log. Therefore, the

statistical dispersion of the log-normal distribution can, in some cases, increase with sample-specific viability data.
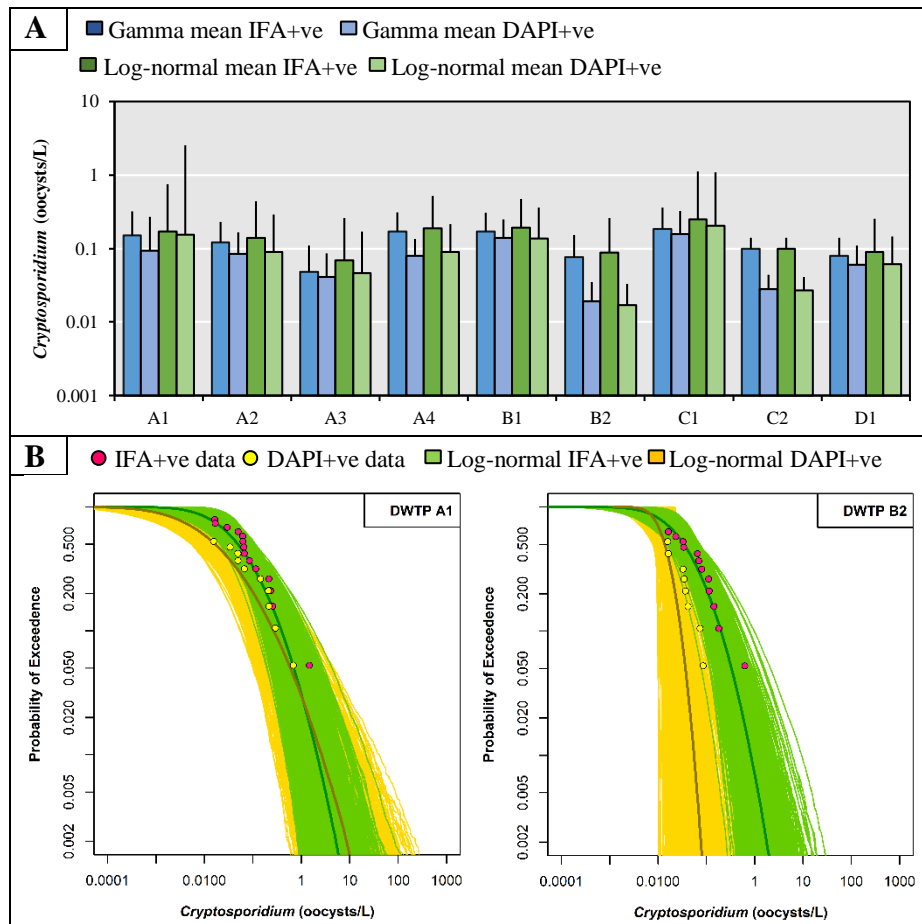
Figure 5-4: A. Impact of sample-specific viability of oocysts on the mean and the dispersion of *Cryptosporidium* concentrations: A. Mean *Cryptosporidium* concentrations calculated with IFA-positive oocysts versus DAPI-positive oocysts for nine drinking water treatment plants. Blue and green columns represent, respectively, gamma and log-normal means estimated with IFA-positive oocyst counts. Light blue and light green columns represent, respectively, gamma and log-normal means estimated with DAPI-positive oocyst counts.. B. Complementary cumulative distribution function (CCDF) curves of log-normal distributions of *Cryptosporidium* concentrations considering IFA-positive oocyst counts (green) or DAPI-positive oocyst counts (yellow) for drinking water treatment plants A1 and B2.

5.4 Discussion

5.4.1 Importance of the distributional form

The RSD was first considered as a heuristic to estimate the importance of the difference between upper tail probabilities of the *Cryptosporidium* and *Giardia* concentration distributions. RSD values higher than 1.0 were found for most of *Cryptosporidium* data sets and about half of the *Giardia* datasets. Haas (1997) demonstrated that considerable differences in the shape of the distributions might be observed at RSD values > 1.0. In our study, the selection of the log-normal distribution rather than the gamma distribution did not significantly influence the estimation of the arithmetic mean *Giardia* concentration and its uncertainty. In contrast, the choice of distribution considerably influenced the width of the 95% credibility interval on the mean *Cryptosporidium* concentration for four DWTPs (B7, C1, C4, and C7) supplied by midsized rivers (mean discharge: 75-286 m^3/s) located in urban, agricultural, and mixed catchments. For these DWTPs, the upper bound of the 95% credibility interval on the mean was more than 0.5-log higher with the log-normal distribution than with the gamma distribution.

Differences of more than 0.5-log higher are important for risk assessment because treatment performances are typically quantified in log-units; thus, health risk estimates are directly proportional to the pathogen concentration in source water. Direct proportionality is expected because the reduction performances of treatment processes are typically assumed to be independent and first-order with respect to the influent concentration of the microorganism (Haas et al. 1999). The first-order model considerably simplifies the exposure assessment because the same fraction of microorganisms is expected to be removed regardless of the influent concentration. If all treatment processes of a treatment train are first-order and independent, then the total average reduction performance of the treatment train is calculated by multiplying the average rate of passage (10^{-LR}) of each process (Haas and Trussell 1998, Teunis et al. 2009, Schmidt et al. 2020). Consequently, the improper choice of a model for source water concentrations may mislead the assessment of health risks associated with the water supply. Additionally, high-resolution data on

full-scale performance by treatment processes would be valuable to assess the validity of the first-order assumption under real-world dynamic conditions.

Health-based targets for drinking water safety are generally defined in terms of annual risk. There have been discussions about whether this appropriately protects against variable conditions, especially peaks (Signor and Ashbolt 2009, Smeets 2010). The adoption of a short-duration (e.g., daily) target has been suggested previously (Signor and Ashbolt 2009). In our study, the quantification of the uncertainty in the estimated parameter values of the distributions provides new insights for risk characterization. First, the CCDF curves of the gamma and the log-normal distributions are showing that, at an exceedance probability of 0.002 (~1 day per year), the width of the 95% predictive interval about the *Cryptosporidium* concentration is similar to the width of the 95% credibility interval on the expected value of the distribution. The uncertainty on the mean of the distribution is, therefore, highly sensitive to the uncertainty on the upper tail values. Second, the upper tail of the log-normal distribution continues to increase below an exceedance probability of 0.002. Hence, the annual mean concentration may vary from year to year, depending on the occurrence events with an exceedance probability below 0.002. This inter-year variability may considerably increase the width of the 95% credibility interval on the annual mean (see companion paper).

The consideration of short-duration targets would simplify the calculation performed during risk characterization and may reduce the uncertainty of risk estimates. The compliance with a short-duration target could be evaluated for a concentration (and its uncertainty) predicted at a given exceedance probability (e.g., 0.002) by an appropriately conservative distribution. Indeed, the probability of capacity exceedance is commonly used in civil engineering for the design of hydraulic structures (Plate and Duckstein 1988) and buildings (Moehle and Deierlein 2004). Nonetheless, it should be noted that a parametric model may not predict accidents or extreme weather events: a probability distribution is conditional on historical data. The identification of early signals and precursors is needed to manage these types of events. The development of early warning systems using meteorological data has been recently suggested to manage the risks of

waterborne diseases (Semenza 2020). Online monitoring of faecal indicators could also be useful for the development of early warning systems.

5.4.2 Methods to assist model selection

The mDIC were computed to compare the fit of Poisson and mixed Poisson models to *Cryptosporidium* and *Giardia* data. The mDIC values indicated that the PGA and PLN models better fitted *Cryptosporidium* and *Giardia* data sets than the Poisson model. However, the mDIC did not generally allow discrimination between the PGA and PLN models because sample sizes are too small to characterize the upper tail behaviors of the population distribution adequately. At an RSD of 1, Haas (1997) found that large sample sizes (over 200 in some cases) would be required to achieve a high level of reliability in distributional attribution. Indeed, the CCDF curves illustrated that upper tails behaviors were distinct from each other from a probability of exceedance of around 1%. Consequently, neither the gamma distribution nor the log-normal distribution should be selected as a default population distribution for modeling *Cryptosporidium* data. Additional information is therefore needed to assist model selection.

The statistical analysis of large data sets might help identifying how *Cryptosporidium* concentrations scale at large magnitudes. The investigation of how meteorological covariates influence temporal variations in microbial concentrations might also help address this issue. Several studies demonstrated short-term peak pathogen concentrations following rainfall events (Atherholt et al. 1998, Kistemann et al. 2002, Signor et al. 2005). Results from event-based monitoring and routine monitoring campaigns could be used to evaluate which distribution accurately predicts microbial peaks associated with these events. This methodology was recently implemented for the assessment of peak *E. coli* concentrations during snowmelt events at an urban DWTP (Sylvestre et al. 2020a). In our companion paper, we propose an adaptation of this method for protozoan pathogen data collected during snowmelt and rainfall events.

In the absence of empirical information, it might be helpful to read these probability distributions as statements about processes (Frank 2014). The gamma distribution scales linearly at large magnitudes because it expresses an additive process. The CCDF curves show that the upper tail of

the gamma distribution does not extrapolate to concentrations much larger than the sample maximum. The log-normal distribution also expresses an additive process but on the log scale. Consequently, the tail of the log-normal distribution extrapolates to concentrations approximatively 1.0-log higher than the sample maximum at a probability of exceedance of 0.2%. The log-normal distribution is, therefore, more conservative for the prediction of peak events than the gamma distribution, which might be a useful property to consider from a public health perspective. However, the selection of the log-normal distribution may result in the prediction of large uncertainties on the mean concentration, which could motivate unnecessary costs for water utilities. A potential option to reduce this uncertainty might be to collect sample volumes that would yield more positive counts rather than non-detects.

Other candidate distributions could be considered in future investigations of temporal variations in source water pathogen concentrations. Informative priors may however be required for modeling distributions with a heavier tail than the log-normal distribution. Prior knowledge could be obtained from the literature (meta-analyses, reviews, empirical studies) to increase the precision of posterior estimates (O'Hagan et al. 2006), but informative priors should be used carefully because variations in pathogen concentrations are catchment specific. We believe that the collection of more samples should be preferred to the use of more informative priors.

5.4.3 Limitations for the quantification of protozoan pathogen concentrations

The incorporation of the variation of the analytical recovery with Beta distributions did not influence the statistical dispersion of the population distribution of the PGA or PLN models because Beta distributions were close to symmetric ($\alpha \approx \beta$). Similar values of the parameters of the Beta distribution of the analytical recovery were obtained in other studies for *Cryptosporidium* (Connell et al. 2000, Pouillot et al. 2004) and *Giardia* (Connell et al. 2000, Jaidi et al. 2009). However, site-specific recovery data could produce skewed Beta distributions ($\alpha \neq \beta$), which may reduce ($\alpha > \beta$ for $\alpha > 1, \beta > 1$) or increase ($\alpha < \beta$ for $\alpha > 1, \beta > 1$) the statistical dispersion of the concentration distributions. The analytical recovery of *Cryptosporidium* oocysts may be correlated to temporal covariates, such as turbidity (DiGiorgio et al. 2002, Feng et al. 2003, Petterson et al. 2007). In our companion paper, we found a reduction of sample-specific recovery

rates of 0.9-log at agricultural DWTP A4 during a 24-hour period of peak source water *Cryptosporidium/Giardia* concentrations at moderately high turbidity levels (20-30 NTU).

Statistical methods to incorporate viability, infectivity and human specificity proportions in temporal concentration variability distributions have not yet been fully addressed in QMRA. In this study, the consideration of DAPI-positive oocyst counts rather than IFA-positive oocyst counts did not generally result in an important change in the scale of the distributions of *Cryptosporidium* concentrations. However, in some cases, adjusting for viability may increase the proportion of non-detects, which may result in increasing the uncertainty on the mean *Cryptosporidium* concentration. Lapen et al. (2016) applied Beta distributions to adjust for the human-pathogenic proportion of *Cryptosporidium* oocysts. In their study, the mean of the Beta distribution was estimated using the overall fraction of *C. hominis* and *C. parvum* detected at multiple sites located on the same river. The 99th percentile of the Beta distribution was approximated by the highest fraction of *C. hominis* and *C. parvum* observed among site/season combinations. The obtained Beta distributions were skewed to the right ($\alpha < \beta$), which is reducing the statistical dispersion of the concentration distribution. The validity of this assumption should be further investigated because, as discussed previously for the analytical recovery, the specificity and the infectivity of (oo)cysts could be correlated with concentrations because of temporal covariates (rainfall, snowmelt) influencing microbial transport mechanisms (Swaffer et al. 2014, Swaffer et al. 2018).

5.5 Conclusions

Bayesian analysis of mixed Poisson distributions with different upper tail behaviors offered a suitable framework to analyze source water *Cryptosporidium* and *Giardia* data obtained at 30 drinking water treatment plants. The following conclusions ensue from this work:

- The relative standard deviation (RSD) indicated that correct identification of the distribution was necessary (RSD > 1) for most of the DWTPs for *Cryptosporidium* and for about half of the DWTPs for *Giardia*. In these cases, the improper selection of a distribution may result in a biased estimate of the mean concentration;

- The convergence of Markov chains was obtained for the Poisson–gamma and Poisson–log-normal models for all *Giardia* datasets. However, convergence was only achieved for 18 of the 30 *Cryptosporidium* datasets. The convergence of the Markov chains should thus be examined thoroughly when distributions of concentration from pathogen data are modelled, especially when only small data sets are available.

- The gamma and log-normal distributions predicted similar mean concentrations for *Cryptosporidium* and *Giardia*. However, considerable differences (>0.5-log) in the upper bound of the 95% credibility interval on the mean *Cryptosporidium* concentrations were found at four sites. The application of methods to assist model selection is thus recommended to ensure that appropriately conservative distributions are selected in exposure assessment.

- Discrimination between candidate parametric distributions using the marginal deviance information criterion (mDIC) is unachievable because differences in the upper tail behaviors are not well characterized with small data sets ($n < 30$). Therefore, the gamma and the log-normal distributions fit the data equally well but may predict different risk outputs when they are used as an input distribution in an exposure assessment.

A possible approach to address this issue could be to compare the upper tail predictions of candidate distributions to field observations during critical periods of source water contamination. In the absence of empirical information, the log-normal distribution could be selected as a conservative model for the prediction of peak concentrations in source water. However, the selection of the log-normal distribution may result in the prediction of large uncertainties on the mean concentration. Source water monitoring strategies and risk management options should be investigated in further work to address this issue.

5.6 Acknowledgments

CHAPTER 6.   ARTICLE 3 - IMPACT OF HYDROMETEOROLOGICAL EVENTS FOR THE SELECTION OF PARAMETRIC MODELS FOR PROTOZOAN PATHOGENS IN DRINKING-WATER SOURCES

It should be noted that Article 2 (Chapter 5) and Article 3 (Chapter 6) are companion articles. Both articles investigate temporal variations in source water protozoan pathogens concentrations. Article 2 is primarily focusing on model development and implementation. Article 3 adapted the model validation technique presented in Chapter 4 for the assessment of protozoan pathogens in source water.

In this chapter, the potential of *in situ* β-D-glucuronidase activity measurements is evaluated for the identification of peak source water *Cryptosporidium* and *Giardia* concentrations during hydrometeorological events at drinking water treatment plants located in urban and agricultural catchments. Results from event-based monitoring campaigns are used to verify whether Poisson–gamma and Poisson–log-normal distributions (presented in Chapter 5) predicted *Cryptosporidium* and *Giardia* concentrations during these hydrometeorological events. This article has been accepted in *Risk Analysis*. Supplementary information is presented in Appendix C.

Impact of hydrometeorological events for the selection of parametric models for protozoan pathogens in drinking-water sources

Émile Sylvestre [a,b], Jean-Baptiste Burnet [a,b], Sarah Dorner [b], Patrick Smeets [c] Gertjan Medema [c,d], Manuela Villion [e], Mounia Hachad [a,b], Michèle Prévost [a]

[a] NSERC Industrial Chair on Drinking Water, Department of Civil, Geological, and Mining Engineering, Polytechnique Montreal, Montreal, Quebec, H3C 3A7, Canada

[b] Canada Research Chair in Source Water Protection, Department of Civil, Geological, and Mining Engineering, Polytechnique Montreal, Montreal, Quebec, H3C 3A7, Canada

[c] KWR Water Research Institute, Groningenhaven 7, 3433 PE Nieuwegein, The Netherlands

[d] Sanitary Engineering, Department of Water Management, Faculty of Civil Engineering and Geosciences, Delft University of Technology, P.O. Box 5048, 2600GA, Delft, The Netherlands

[e] Centre d'expertise en analyse environnementale du Québec, Ministère de l'Environnement et de la Lutte contre les changements climatiques, Québec, Canada

* Corresponding author e-mail: emile.sylvestre@polymtl.ca

Abstract Temporal variations in concentrations of pathogenic microorganisms in surface waters are well known to be influenced by hydrometeorological events. Reasonable methods for accounting for microbial peaks in the quantification of drinking water treatment requirements need to be addressed. Here, we applied a novel method for data collection and model validation to explicitly account for weather events (rainfall, snowmelt) when concentrations of pathogens are estimated in source water. Online *in situ* β-D-glucuronidase activity measurements were used to trigger sequential grab sampling of source water to quantify *Cryptosporidium* and *Giardia* concentrations during rainfall and snowmelt events at an urban and an agricultural drinking water treatment plant in Quebec, Canada. We then evaluate whether mixed Poisson distributions fitted to monthly sampling data (n~30 samples) could accurately predict daily mean concentrations during these events. We found that using the gamma distribution underestimated high *Cryptosporidium* and *Giardia* concentrations measured with routine or event-based monitoring. However, the log-normal distribution accurately predicted these high concentrations. The selection of a log-normal distribution in preference to a gamma distribution increased the annual mean concentration by less than 0.1-log but increased the upper bound of the 95% credibility interval on the annual mean by about 0.5-log. Considering parametric uncertainty in an exposure assessment is essential to account for microbial peaks in risk assessment.

6.1 Introduction

Hydrometeorological events such as heavy rainfall and snowmelt can lead to short-term deterioration of source water quality and may pose a challenge for drinking water treatment. Peak concentrations of pathogens in source water have been recognized as causes of waterborne

outbreaks associated with drinking water when synchronous with sub-optimal or inadequate treatment performance (Hrudey and Hrudey 2004). Over the last 20 years, event-based sampling strategies have been developed to assess variations of protozoan pathogens concentrations during rainfall-induced runoff conditions in tributaries of drinking water sources (Kistemann et al. 2002, Dorner et al. 2007, Swaffer et al. 2014, Swaffer et al. 2018), in reservoirs used as a drinking water source (Burnet et al. 2014), and in raw water from surface drinking water systems (Atherholt et al. 1998, Signor et al. 2005, Astrom et al. 2007, Dechesne and Soyeux 2007). In these studies, the association between target pathogens, fecal indicator bacteria (FIB), and physical parameters (flow rate, water level, turbidity) were investigated. Although progress has been made to accelerate culture-based methods for the detection of FIB, these methods cannot be used as a trigger for event-based sampling because culture typically requires 6- to 24-hours incubation periods. Advances in rapid detection of enzyme activity that is associated with fecal contamination (George et al. 2000, Farnleitner et al. 2001) and its recent automation (Ryzinska-Paier et al. 2014, Koschelnik et al. 2015) allows for rapid detection of peak fecal contamination events and trigger for simultaneous collection of sample for pathogens. Commercially available prototypes for β-D-glucuronidase (GLUC) activity *in situ* monitoring in near real-time are now available to characterize faecal pollution temporal dynamics in environmental waters (Ryzinska-Paier et al. 2014, Stadler et al. 2016, Burnet et al. 2019a, Burnet et al. 2019b). These automated measurement systems could further be used to design new sampling strategies targeting short-term fluctuations in microbial pathogen concentrations during hydrometeorological events.

Upon characterization of a critical contamination event, risk assessors need to integrate this information into a probabilistic risk assessment. Basic principles of probability theory need to be considered to adequately use results from event-based sampling to inform microbial risk assessment. Results from routine sampling (also known as systematic sampling) are independent and identically distributed (i.i.d.) random variables because routine samples are collected at a fixed periodic interval (e.g., monthly sampling). Mixed Poisson distributions, such as the Poisson–Gamma (negative binomial) distribution and the Poisson–log-normal distribution, have been used to infer microbiological data (Teunis et al. 1997, Haas et al. 1999, Masago et al. 2004, Westrell et

al. 2006), but these distributions have not yet been validated for the prediction of microbial peak events. Results from event-based sampling can also be considered as i.i.d. random variables if event-based samples are collected at a fixed periodic interval (e.g., hourly) during the event. However, routine and event-based samples cannot be combined for statistical inference because their periodic intervals differ. A potential solution to this problem could be to use results from event-based sampling campaigns to evaluate whether mixed Poisson models fitted to routine monitoring data can accurately predict pathogen concentrations during peak events. The identification of the most appropriate distribution to predict these peak events would improve the assessment of health risk associated with the finished water and the selection of treatment requirements.

The first objective of this study is therefore to determine if online GLUC activity and turbidity measurements can indicate periods of high concentrations of protozoan pathogens in source water. The second objective is to determine whether mixed Poisson distributions fitted to routine monitoring data accurately predict *Cryptosporidium* and *Giardia* concentrations during hydrometeorological events (snowmelt and rainfall episodes).

6.2 Material and methods

6.2.1 Sample site

Two drinking water treatment plants (DWTPs) introduced in the companion paper (DWTPs C6, A4) were selected for case studies.

6.2.1.1 Urban site

DWTP C6 is supplied by surface water from a river in the Greater Montreal Area in Quebec, Canada (Table 6-1). Raw and settled water were sampled during event-based campaigns. From February to April 2017, the raw water was processed by a sludge blanket clarifier dosed with aluminum sulfate hydrate "alum" ($Al_2(SO_4)_3$; dosing rate: 50 mg L^{-1}) and silica (SiO_2; dosing rate: 2 mg L^{-1}) in 1°C raw water at pH 6.0. The land use in this area is dominated by low to medium intensity urban residential areas. The air temperature during winter (January to March) averages -

10°C. The flow rate of the river is measured continuously at a gauging station 5 kilometers downstream of the drinking water intake. Between 1970 and 2012, the average flow rate of the river during winter was around 200 m^3/s. During the local snowmelt period, generally in March and April, the average flow rate peaks at approximately 600 m^3/s. The flow rate typically peaks 1 week following the local snowmelt because of the large size of the catchment (146,334 km^2). Up to 10 kilometers upstream from DWTP C6, the river receives treated effluent discharges from four municipal wastewater treatment plants (WTTPs), as well as untreated sewage discharges from 37 combined sewer overflow (CSO) outfalls, and two tributaries draining agricultural lands of approximately 70 km^2. Limited catchment management practices are implemented to control the volume and the duration of CSO discharges during snowmelt periods (Gouvernement du Québec 2015).

6.2.1.2 Agricultural site

DWTP A4 is supplied by a small agricultural river in southern Quebec. The annual average flow rate of the river is 16 m^3/s. A municipal WWTP and four CSO outfalls are located 10 km upstream from the drinking water intake. At the WWTP, wastewater is treated through aerated ponds, and around 10,000 m^3/day of treated water is discharged into the river. The regional watershed protection plan indicates that intensive pig and cattle farming (>1500 animal units) occurs in this area and that 30 to 60% of the land is dedicated to agriculture. Cattle and swine manure is applied to agricultural lands from April to October, and a maximum of 35% of manure produced on-site can be used for agricultural spraying. Buffer strips of at least 3 meters from the river are required for source water protection (Gouverment du Québec 2018).

Table 6-1: Summary of catchment information for drinking water treatment plants (DWTPs) C6 and A4

DWTP	Mean river flow rate (m^3/s) [min-max]	Catchment size (km^2)	Main land cover type in the intake protection zone [A]	WWTPs /CSOs in the intake protection zone [A]
C6	300 [20-1000]	>50,000	Urban	4/26
A4	15 [3-100]	<100	Agricultural	1/4

[A] 10 km upstream and 100 m downstream from the withdrawal site. The distances include surface water, portions of tributaries and a 120 m strip of land measured from the high-water mark.

6.2.2 Monitoring strategies

Raw water samples were collected monthly (from 2014 to 2017 at DWTP C6 and from 2014 to 2015 at DWTP A4) for the enumeration of *Cryptosporidium* and *Giardia*. No samples were collected between June and September from 2015 to 2017 at DWTP C6. A statistical characterization of these data sets is presented in Table 6-2. An automated rapid on-site monitoring system (ColiMinder™, VWMS GmbH, Vienna, Austria) was installed at each DWTP intake around 30 days before snowmelt or rainfall events for a preliminary investigation of the β-D-glucuronidase (GLUC) activity fluctuation ranges in each source water. Detailed technical information about the device can be found in Koschelnik et al. (2015). Analytical validation of the technology for source waters and challenging against established culture- and molecular-based assays has been recently performed by Burnet et al. (2019a). The GLUC activity was measured every 1 to 3 hours during dry weather conditions and every 30 to 60 minutes during hydrometeorological events. Fifteen minutes after sample collection, results are reported online and expressed in modified Fishman units (MFU/100 mL) based on the enzyme unit definition for GLUC activity (Koschelnik et al. 2015).

Table 6-2: Sample size, sample mean concentration, and relative standard deviation for *Cryptosporidium* and *Giardia* concentrations (uncorrected for recovery) for drinking water treatment plants (DWTPs) C6 and A4

DWTP	*Cryptosporidium*			*Giardia*		
	Sample size	Sample mean (oocysts/L)	Relative standard deviation	Sample size	Sample mean (cysts/L)	Relative standard deviation
C6	27	0.064	1.65	27	1.57	0.93
A4	24	0.181	1.63	24	1.54	1.01

Event-based samples were collected when two conditions were met: 1) cumulative rainfall exceeding 20 mm or air temperature higher than 5 degrees Celsius (causing rapid snowmelt) were measured in 24 hours, and 2) an increase in GLUC activity of 5 mMFU/100 mL was observed within an hour. A trigger of 5 mMFU/100 mL was selected based on short-term increases in GLUC activity measured during previous hydrometeorological events at these DWTPs (Figure 6-1). For sample collection, 1-liter grab samples of raw water were collected in autoclaved polypropylene

bottles at a frequency of 4 to 6 hours for around 24 hours for the enumeration of *E. coli*. Additionally, 10 to 40 liter-samples were simultaneously filtered on-site for the enumeration of *Cryptosporidium* and *Giardia* using Envirochek HV sampling capsules (Pall Gelman Laboratory, Ann Arbor, MI, USA) at DWTP C6, and Hemoflow F80A hollow-fiber ultrafilters (Fresenius Medical Care, Lexington, MA) at DWTP A4. Ten liter-samples are not typical for surface water sampling, but the filtration of small volumes was necessary to avoid filter clogging due to high raw water turbidities during the rainfall event at DWTP A4. Sequential grab samples were collected for 24 hours to estimate the daily mean concentration. At DWTP C6, 50 liter-samples of settled water were also filtered during the first event-based sampling campaigns. Settled water samples were collected 3 hours after raw water samples to match the theoretical hydraulic residence time throughout coagulation/flocculation/sedimentation (C. Durivage, *personal communication*). The sampling capsules (Envirochek HV filtration) or concentrates (Hemoflow ultrafiltration) were shipped overnight in coolers at 4 °C to the Centre d'expertise en analyse environnementale du Québec (CEAEQ) in Quebec City, QC, and eluted (Envirochek filters) and processed within 48 hours of sampling.
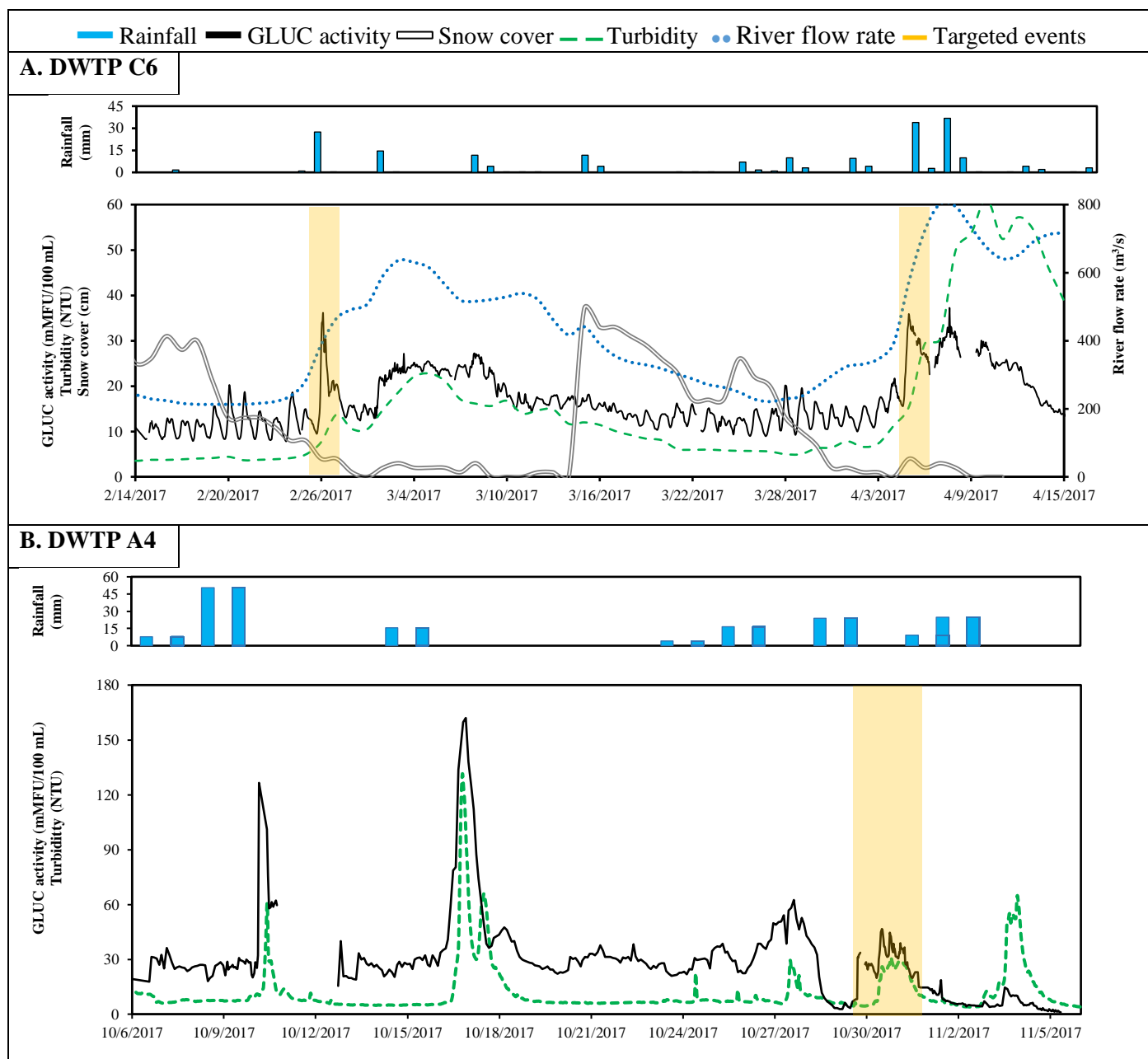
Figure 6-1: Time series of daily rainfall, GLUC activity, snow cover, turbidity, and river flow rate during sampling periods at drinking water treatment plants C6 and A4. Yellow rectangles indicate targeted events.

6.2.3 Microbial enumeration methods

Escherichia coli was enumerated using the defined substrate technology (IDEXX Quanti-Tray/2000) with Colilert reagents (Method 9223B, American Public Health Association, 2005). The enumeration of oocysts of *Cryptosporidium* and cysts of *Giardia* filtered with Envirochek HV sampling capsules was carried out following the USEPA method 1623.1 (USEPA, 2012). The elution procedure was adapted for the enumeration of (oo)cysts filtered with Hemoflow ultrafilters. Following Hemoflow-based concentration, volumes of filter eluates were approximately 500-700 mL. Post-concentration was done by centrifugation to obtain a final volume between 20 and 50 mL and a packed pellet volume between 2 and 5 ml. Between 20 and 50% of the packed pellet volume was then processed by immunomagnetic separation (IMS), before sample staining and examination following USEPA method 1623.1.

Sample-specific analytical recoveries were not measured for routine monitoring samples, but ongoing precision recovery (OPR) samples prepared in tap water were done regularly, following standard method recommendations (USEPA, 2012). Mean analytical recovery rates of 0.46 (Standard Deviation [SD] = 0.14) and 0.50 (SD = 0.17) were measured for *Cryptosporidium* and *Giardia*, respectively, based on 43 *Cryptosporidium* and *Giardia* matrix spike recovery experiments. These experiments were carried out with flow-cytometry sorted fluorescently labeled (oo)cysts (Colorseed™, BTF, Australia) by spiking a target dose of 98-100 (oo)cysts in ten liter-samples of raw water collected at 30 DWTPs in Quebec over 9 years. Additional recovery rates were measured for each sample collected during the event-based campaign at DWTP A4. The same fluorescently labeled controls (Colorseed™) were spiked at a target dose of 98-100 (oo)cysts in the raw water sample before careful manual mixing and on-site concentration using hollow-fiber ultrafiltration. Seeded oocysts and naturally occurring oocysts were enumerated in each event-based sample. At DWTP A4, some samples were partially analyzed because of the high turbidity of the raw water. For these samples, the distribution of seeded (oo)cysts was assumed to be homogenous at the time of sub-sampling and directly proportional to the analyzed volume. Sample-specific analytical recovery rates were not measured for samples collected during both

events at DWTP C6. We conservatively assumed that all detected *Cryptosporidium* oocysts and *Giardia* cysts were human infectious.

6.2.4 Statistical analysis

6.2.4.1 Model parametrization and implementation

The temporal variations in protozoan pathogen concentrations were evaluated with the three-level hierarchical Bayesian model presented in detail in the companion paper. Briefly, at the first level, the analytical error of the enumeration method is binomially distributed:

$$y_i \sim \text{Binomial }(x_i, p_i) \tag{6.1}$$

where y_i is the number of (oo)cysts observed in each sample i; x_i is the true number of (oo)cysts in the sample; and p_i is the probability of detection of each organism x_i. The nonconstant analytical recovery p_i (i.e., the sample-to-sample variability in recovery rate) was assumed to vary randomly according to a beta distribution with shape parameters α and β. Posterior means of the parameters were $(\hat{\alpha}, \hat{\beta}) = (6.48, 7.70)$ for *Cryptosporidium* and $(\hat{\alpha}, \hat{\beta}) = (3.80, 3.91)$ for *Giardia*. The second level of the hierarchical structure takes into consideration the sampling error. The true number of (oo)cysts x_i is Poisson distributed with mean $\lambda_i = c_i V_i$, the product of the concentration (c_i) and the analyzed volume (V_i).

$$f(x) = \frac{\lambda^x e^{-\lambda}}{x!} = \frac{(cV)^x e^{-(cV)}}{x!} \tag{6.2}$$

At the third level, temporal variations of the concentration c_i are described by a continuous distribution. In this study, concentrations predicted by these models are assumed to be daily mean concentrations. The gamma and log-normal distributions were selected and compared because they have different upper tail behaviors at large coefficients of variation (Haas 1997), and this property is preserved under mixed Poisson models (Kaas and Hesselager 1995). The gamma distribution has a density

$$f(c) = \frac{\lambda^\alpha c^{\alpha-1}}{\Gamma(\alpha)} e^{-\lambda c} \tag{6.3}$$

and an expectation (i.e., mean) $E(c) = \alpha/\lambda$, where $\alpha > 0$ is the shape parameter and $\lambda > 0$ is a scale parameter. The log-normal distribution has a density

$$f(c) = \frac{1}{\alpha c \sqrt{2\pi}} \exp\left[-\frac{1}{2}\frac{[ln\ c - \lambda]^2}{\alpha^2}\right] \tag{6.4}$$

and an expectation $E(c) = \exp\left(\alpha + \frac{\lambda^2}{2}\right)$, where the shape parameter $\alpha > 0$ and the scale parameter λ may take each real value.

Estimations and inferences were carried out in a Bayesian framework using Markov Chain Monte Carlo (MCMC). Gamma priors with hyperparameters set to Gamma (0.01, 0.01) were selected for the shape parameter α and the scale parameter λ of the gamma distribution. For the log-normal distribution, the shape parameter α was assigned a uniform prior with hyperparameters set to Uniform (-10, 10), and the scale parameter λ was assigned a weakly informative exponential prior with hyperparameters set to exp (1). The hyperparameter in the weakly informative prior was set to a conservative value based on evidence regarding the logarithm of the empirical standard deviation of *Cryptosporidium* and *Giardia* measured at 30 DWTPs (see companion paper). The rationale for the selection of the other priors is presented in the companion paper. A sensitivity analysis was conducted in this study to investigate the influence of the hyperparameter value in the exponential prior of the scale parameter λ of the log-normal distribution. The hyperparameter value was adjusted upward (exp (0.1)) and downward (exp (3)), and the log-normal distribution was re-estimated with these varied priors.

Models were fitted using the MCMC technique with rjags (v4-6) (Plummer 2013) in R (v3.4.1). Four Markov chains were run for 10^4 iterations after a burn-in phase of 10^3 iterations. The convergence of the four chains was monitored with the Brooks-Gelman-Rubin scale reduction factor (Gelman and Shirley 2011).

6.2.5 Estimation of daily mean concentrations during events

The daily mean concentration was considered in this study because: 1) the exposure is usually characterized in terms of the arithmetic mean number of organisms in the dose (Haas 1996), and 2) a 24-hour period is typically used to account for short-term exposures in microbial risk assessment (WHO 2016b). *Cryptosporidium* and *Giardia* concentrations in each event-based sample were estimated with a Poisson model (eq. 6.2). Counts were corrected with sample-specific recovery rates when available (DWTP A4). The daily mean concentration $\bar{C}_{Event}$ was estimated by averaging concentrations C_i collected at regular intervals over 24 hours.

$$\bar{C}_{Event} = \frac{1}{n}\sum_{i=1}^{n} C_i \qquad (6.5)$$

The uncertainty of the daily mean concentrations was evaluated with Monte Carlo simulations. A random sample was drawn from the 95% credibility interval on the mean concentration c_i (eq. 6.2) of each sample i. The draws were summed and divided by the number of event-based samples N collected in 24 hours. The procedure was repeated 10000 times to estimate the 95% predictive interval for the daily mean concentration. The R code used to calculate these daily mean concentrations is provided in the Supplementary Material.

6.2.6 Model validation

Distributions were illustrated with complementary cumulative distribution function (CCDF) curves. Each best fit distribution was generated for probabilities of exceedance between 100% and 0.27% (1 day per year) using the posterior mean of the parameters (α, λ). The predictive interval about each best fit distribution was created by simulating 1000 CCDF curves parametrized by random values included in the 95% credibility interval for the parameters. To visually assess the capacity of the distributions to predict high concentration observations, two vertical lines were juxtaposed with CCDF curves. These two lines represent 1) the sample maximum concentration measured with routine monitoring, and 2) the daily mean concentration during the hydrometeorological event. Only the highest event mean *Cryptosporidium* and *Giardia*

concentrations (Event 1) were illustrated for DWTP C6. We assumed that these daily mean concentrations have probabilities of exceedance higher than one day per year.

6.2.7 Estimation of annual mean concentrations

It is important to note that there may be a difference between the uncertainty on the *mean* of the distribution and the uncertainty on the *annual mean* predicted by a skewed distribution. A difference will be observed if the upper tail of the distribution does not have an asymptotic behavior from a probability of exceedance smaller than one day per year. In other words, the occurrence of daily concentrations predicted to occur less than once a year may generate variations in the annual mean estimates. To investigate the importance of this difference, the upper bound of the 95% credibility interval on the mean of the distribution was compared to the upper bound of the 95% credibility interval on the annual mean of the distribution. The upper bound of the 95% credibility interval on the annual mean of the distribution was evaluated as follows:

1. the 95% credibility interval was calculated for the shape parameter α and the scale parameter λ of the distribution;
2. the pair of parameters contained in the 95% credibility interval that maximize the mean of the distribution was determined;
3. 365 samples were drawn randomly from the distribution generated with the pair of parameters determined in step (2). The average of these 365 samples (annual mean) was calculated;
4. Step 3 was repeated 10,000 times to produce a distribution of these annual means. The 97.5^{th} percentile of the distribution of these annual means was determined.

This model was implemented using R (v3.4.1). The R code is provided in the Supplementary Material.

6.3 Results and discussion

6.3.1 Short-term fluctuations in microbial contaminants

Short-term fluctuations in microbial contaminants were studied during two snowmelt events in an urban catchment and one rainfall event in an agricultural catchment. The collection of event-based samples was triggered by meteorological conditions (cumulative rainfall, change in air temperature) and rapid increases in the GLUC activity level. This sampling strategy allowed us to characterize short-term variations in *Cryptosporidium* and *Giardia* concentrations in raw water.

At the urban DWTP C6, the amplitudes of *E. coli*, *Cryptosporidium*, and *Giardia* concentration peaks were 1.1 $\log_{10}$-units, 0.7 $\log_{10}$-units, and 1.4 $\log_{10}$-units, respectively, during Event 1 (Figure 6-2). Sample-specific recovery rates were not measured at DWTP C6; therefore, the intra-event variation in protozoan pathogen concentrations could be influenced by the difference in recovery rates among samples. The impact of source water turbidity on recovery rates could be small during Event 1 because turbidity was low and only ranged from 6 to 13 NTU (mean absolute deviation (MAD)=1.5 NTU). However, other short-term changes in the composition of the water matrix could have influenced the recovery performance. At the agricultural DWTP A4, the amplitudes of the protozoan pathogen concentration peaks were higher (0.8-1.1 $\log_{10}$-units) than the amplitude of the *E. coli* concentration peaks (0.5 $\log_{10}$-units) (Figure 6-3). In 24 hours, sample-specific recovery rates varied between 22 and 70% for *Cryptosporidium* and between 8 and 70% for *Giardia* (Table 6-3). Sample-specific recovery rates decreased through the contamination event, especially for *Giardia*. These results show the importance of measuring sample-specific recovery rates to estimate concentrations of *Cryptosporidium* and *Giardia* during hydrometeorological events in agricultural catchments. Negative correlations between turbidity and recovery rates were obtained for *Cryptosporidium* ($r = -0.50$) and *Giardia* ($r = -0.87$) at DWTP A4; however, these results should be interpreted with caution because the sample size was small (n=6) and turbidity only ranged from 18 to 28 NTU (MAD=2.8 NTU). Low recovery rates during peak events could be associated with the nature of the turbidity and the background matrix of the water (DiGiorgio et al. 2002). Positive correlations between measured concentrations (i.e., uncorrected for the

analytical recovery) and recovery rates were obtained for *Cryptosporidium* ($r = 0.83$) and *Giardia* ($r = 0.57$). Theoretical recovery rates of 30% were assumed for all event-based samples collected at urban DWTP C6 based on average recovery rates measured during the rainfall event at DWTP A4.

During these three hydrometeorological events, the GLUC activity level rapidly increased for about 12 hours and then slowly decreased over several days to return to the baseline level (Figure 6-1). *Cryptosporidium* and *Giardia* concentrations also increased during the first 12 hours but did not decrease in the 12 hours following the GLUC activity peak. Therefore, a decrease in GLUC activity level may not indicate a decrease in protozoan pathogen concentrations during snowmelt/rainfall episodes. The 24-hour sampling strategy did not allow us to determine the full duration of protozoan pathogen peaks. Consequently, measured 24-hour mean *Cryptosporidium* and *Giardia* concentrations could be lower than the maximum 24-hour mean concentrations for these events. Nevertheless, at the two DWTPs, the 24-hour event mean *Giardia* concentration was higher than the sample maximum measured with routine monitoring (corrected for recovery) at DWTP C6 (Event 1; +0.3-log) and DWTP A4 (+0.7-log) (Table 6-3).

During the two events at DWTP C6, the turbidity did not increase simultaneously with protozoan pathogen concentrations (Figure 6-4A, Figure 6-4B). The lack of systematic association between protozoan pathogen concentrations and turbidity has been reported for large datasets (USEPA, 2005). Differences in protozoan pathogens and turbidity dynamics may be associated with the varying contributions of multiple sources, including watershed-scale nonpoint source pollution during snowmelt- and rainfall-runoff and local point source discharges of faecal contamination. Local sewer discharges can increase faecal contamination loads in the river without increasing total suspended solids (TSS) because correlations between these parameters are not expected during the snowmelt period (Madoux-Humery et al. 2013). At agricultural DWTP A4, GLUC activity, *Cryptosporidium*, and *Giardia* concentrations increased with turbidity, suggesting that turbidity could be a valid surrogate to trigger the sampling of peak protozoan pathogen concentrations in agricultural catchments. Additional event-based sampling campaigns could be designed to assess whether the magnitude of turbidity and microbial peaks are associated.

However, recovery rates for protozoan pathogens may be very low at the high raw water turbidities (>100 NTU) that can be measured at the drinking water intake.
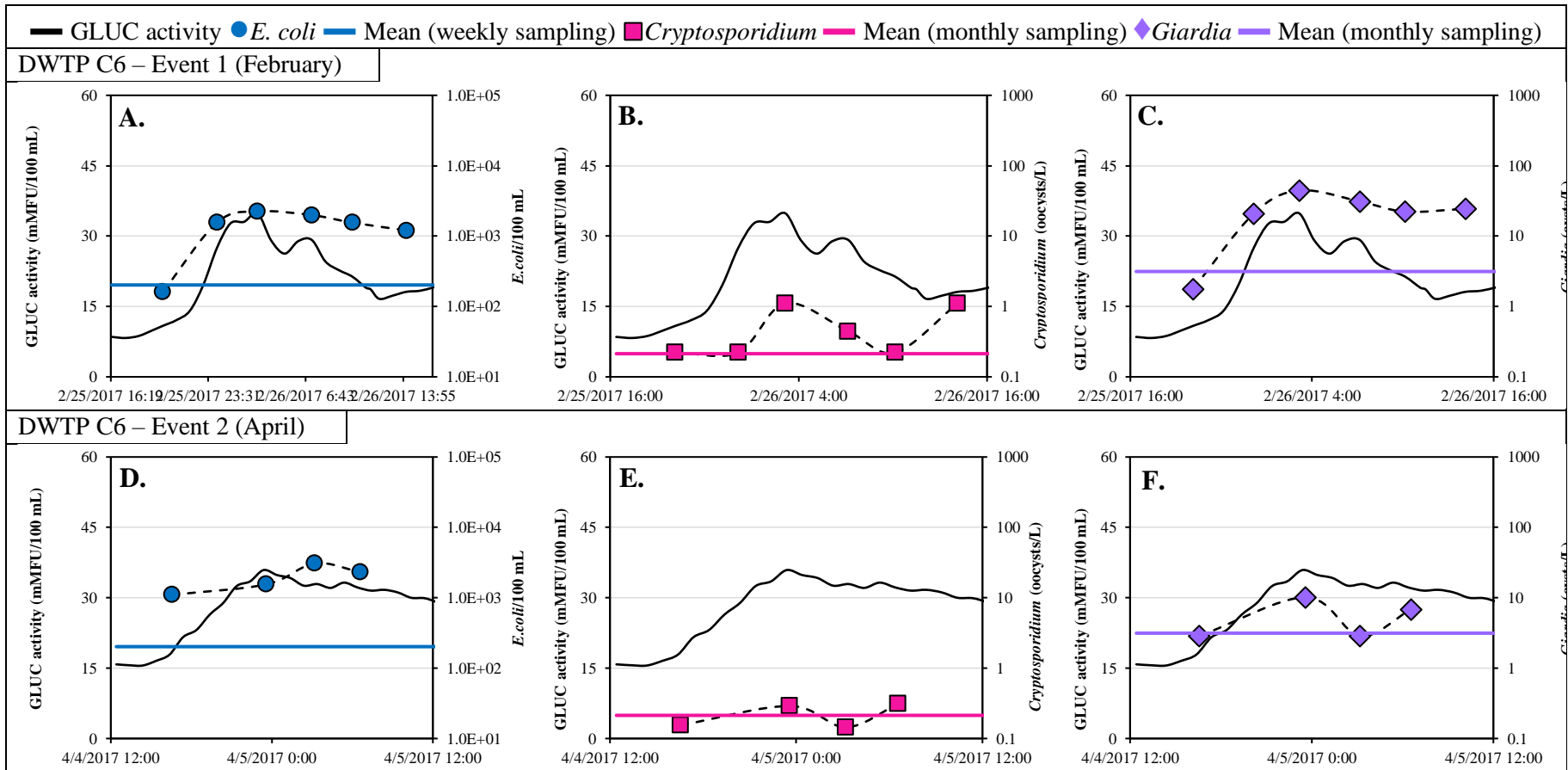
Figure 6-2: Short-term variations of *E. coli*, *Cryptosporidium*, and *Giardia* concentrations for the first 24 hours of two hydrometeorological events (snowmelt and rainfall) in February (Event 1) and April (Event 2) 2017 at drinking water treatment plant (DWTP) C6.
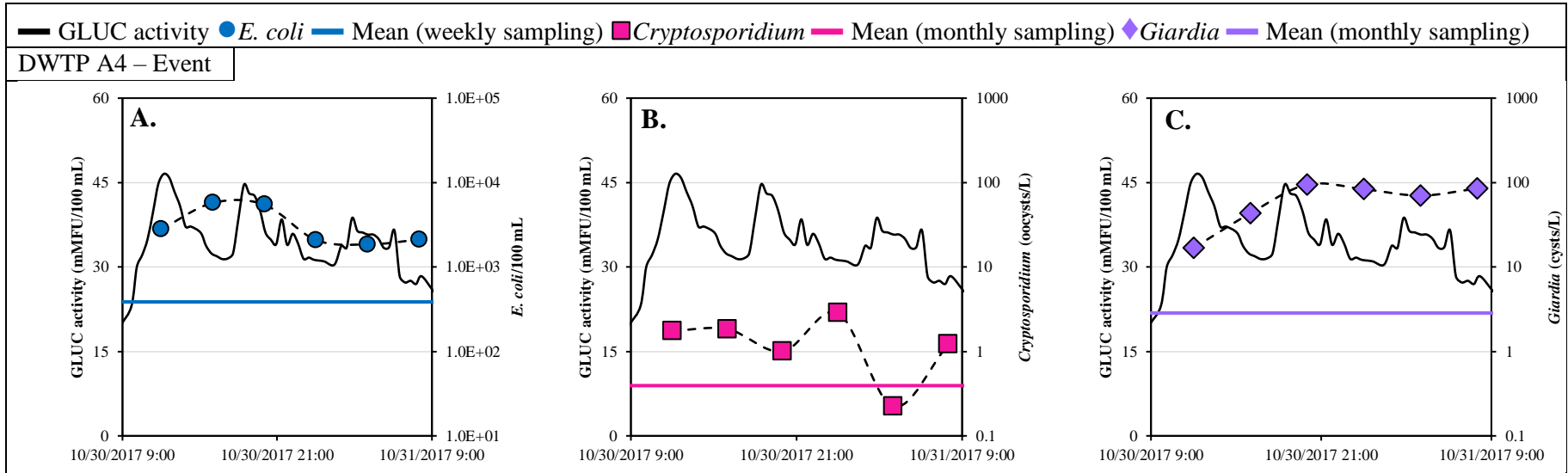
Figure 6-3: Short-term variations of *E. coli* (A), *Cryptosporidium* (B), and *Giardia* (C) concentrations for the first 24 hours of an hydrometeorological event (rainfall) in October 2017 at drinking water treatment plant (DWTP) A4

Table 6-3: Characterization of raw water samples collected with event-based sampling at drinking water treatment plants C6 and A4

DWTP	Event	Date/hour	Raw water turbidity (NTU)	Count Oocysts	Cysts	Vol. sampled (L)	Vol. analyzed (L)	Colorseed count Oocysts	Cysts	Recovery rate [A] Crypto.	Giardia	Concentration (oo)cysts/L [B] Crypto.	Giardia
C6	February	25/20:11	6.1	1	8	15	15	-	-	0.30	0.30	0.22	1.8
		26/00:04	7.8	1	94	15	15	-	-	0.30	0.30	0.22	20.8
		26/3:11	8.4	5	200	15	15	-	-	0.30	0.30	1.11	44.4
		26/7:11	10.4	2	138	15	15	-	-	0.30	0.30	0.44	31.1
		26/10:18	10.7	0	102	15	15	-	-	0.30	0.30	0.00	22.2
		26/14:13	12.9	5	110	15	15	-	-	0.30	0.30	1.11	24.4
										24-hour event mean		0.52	24.1
	April	4/16:49	14.0	1	40	14	14	-	-	0.30	0.30	0.15	2.9
		4/23:52	17.2	2	152	15	15	-	-	0.30	0.30	0.28	10.1
		5/3:47	20.7	1	43	15	15	-	-	0.30	0.30	0.15	2.9
		5/6:35	27.3	2	96	14	14	-	-	0.30	0.30	0.31	6.9
										24-hour event mean		0.22	5.7
A4	October	30/12:00	18.4	7	94	40	8	10	14	0.50	0.70	1.80	16.8
		30/16:00	23.4	9	121	35	7	14	8	0.70	0.40	1.80	43.2
		30/20:00	28.0	6	142	30	15	20	5	0.40	0.10	1.00	94.7
		31/00:00	24.0	12	117	35	17.5	12	0	0.24	<0.08	2.90	83.6
		31/4:00	28.0	1	202	32	16	14	9	0.28	0.18	0.20	70.1
		31/8:00	27.0	4	102	30	15	11	4	0.22	0.08	1.20	85.0
										24-hour event mean		1.48	65.5

[A] Theoretical recovery rates at DWTP C6 and sample-specific recovery rates at DWTP A4
[B] Concentrations corrected for the analytical recovery
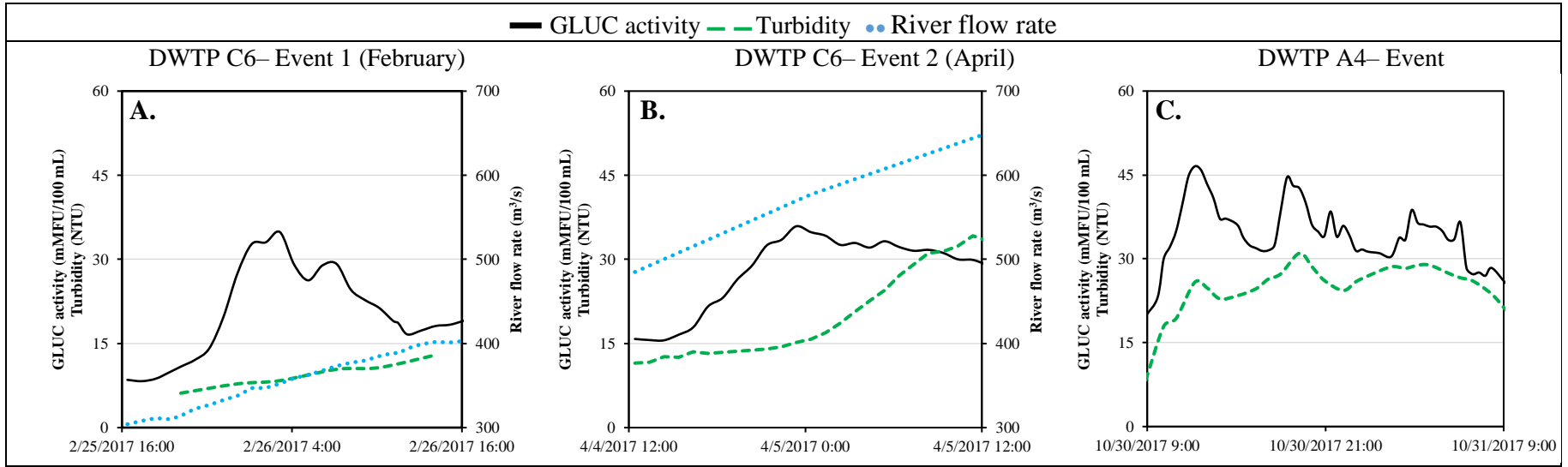
Figure 6-4: Short-term fluctuations of GLUC activity, raw water turbidity, and river flow rate during event conditions (first 24 hours) at drinking water treatment plant (DWTP) C6 in February 2017 (A), April 2017 (B) and DWTP A4 in October 2018 (C). River flow rate measurements were not available at DWTP A4.

6.3.2 Model validation

It was demonstrated in the companion paper that, as only a few samples informed on the behavior of the upper tail, the differences in marginalized deviance information criterion (mDIC) between candidate parametric distributions (gamma, Weibull, log-normal) were too small (less than 4 points) for model selection based on mDIC alone. Results from the sensitivity analysis of the influence of hyperparameter values in the exponential prior of the scale parameter λ of the log-normal distribution are shown in the Supplementary Material (Supplementary Figure 6-1). Changes in hyperparameter values had a small effect on the behavior of the upper tail of the distribution for *Cryptosporidium* and a negligible effect for *Giardia* (Supplementary Figure 6-1).

The present study allowed investigating whether results from event-based sampling of protozoan pathogens can be predicted by a parametric distribution fitted to routine monitoring data. The CCDF curves of the gamma and the log-normal distributions fitted to routine monitoring *Cryptosporidium* and *Giardia* data are presented in Figure 6-5. The capacity of each distribution to predict a fixed concentration (e.g., event mean concentration) can be visually assessed for probabilities of exceedance varying between 1.0 (all the time) and 0.002 (about 1 day per year). For the agricultural DWTP A4, the gamma and the log-normal distribution predicted the 24-hour event mean *Cryptosporidium* concentration at a probability of exceedance of 0.002 (Figure 6-5A). However, only the log-normal distribution predicted the 24-hour event mean *Giardia* concentration; the upper tail of the gamma distribution did not predict high enough concentrations (Figure 6-5B). For DWTP C6, at a probability of exceedance of 0.002, only the log-normal distribution conservatively predicted the sample maximum *Cryptosporidium* concentration measured with routine monitoring (Figure 6-5C) and the 24-hour event mean *Giardia* concentration (Figure 6-5D). Sylvestre et al. (2020a) recently demonstrated, using raw water *E. coli* concentration data collected at DWTP C6, that the log-normal distribution better predicted peak *E. coli* concentrations than the gamma distribution during snowmelt events. Hence, care needs to be taken when a distribution is selected to describe temporal variations in source water concentrations because its upper tail may be too light to account for peak contamination levels. Quantifying the maximum concentration of a distribution might also be of interest to evaluate worst-case scenarios in a quantitative risk assessment. If so, extreme value theory may be used to

evaluate the expected maximum concentration of a distribution based on observations (Embrechts et al. 2013).
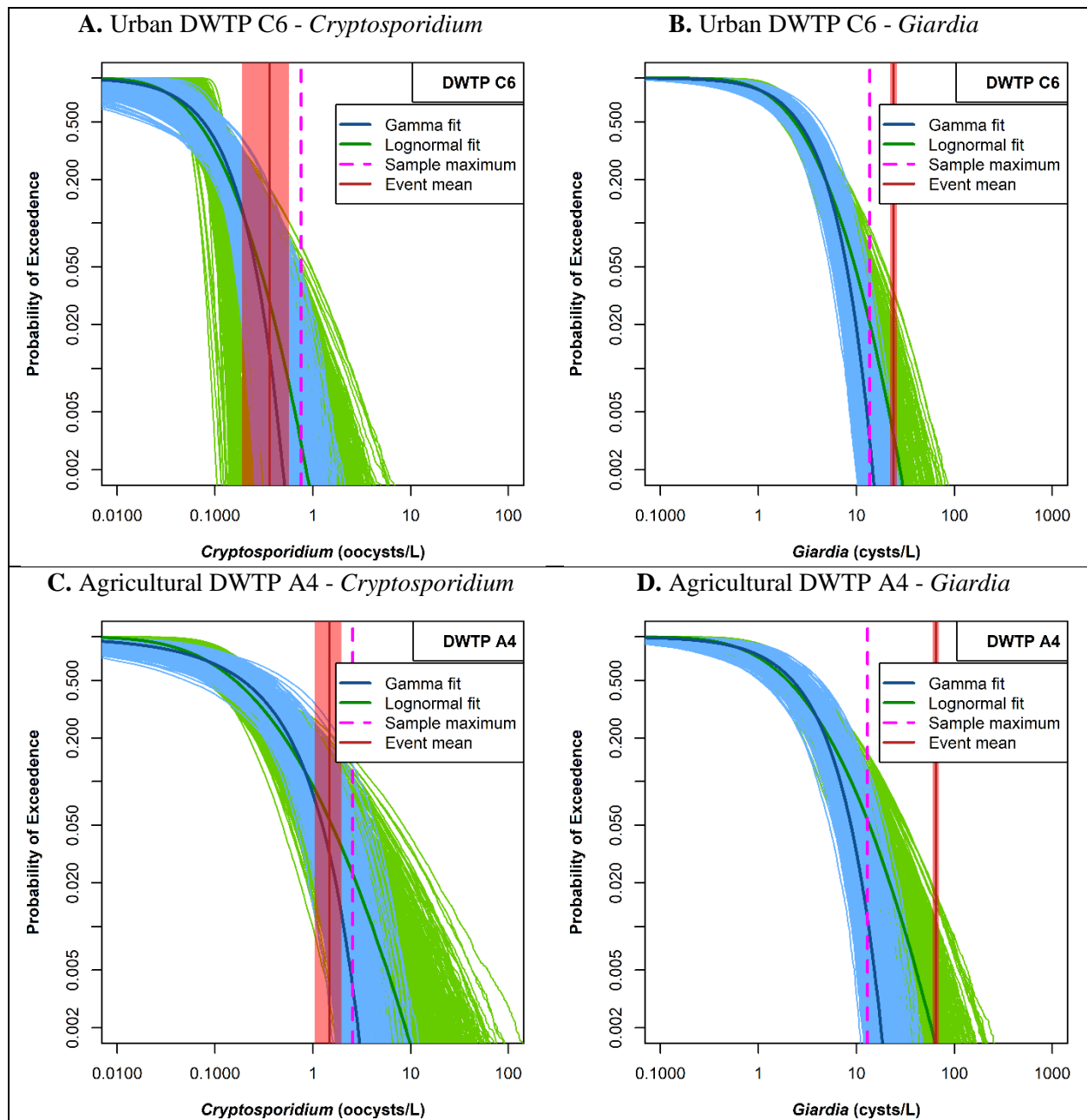
Figure 6-5: Complementary cumulative distribution functions (CCDF) of *Cryptosporidium* and *Giardia* concentrations in raw water at drinking water treatment plants (DWTPs) C6 and A4. Implications for risk assessment

The selection of a log-normal distribution in preference to a gamma distribution had a minor effect on the estimate of the annual mean concentration but increases the upper bound of the 95% credibility interval on the annual mean from 0.5-log for *Cryptosporidium* and 0.3-log for *Giarda* at DWTP C6, and from 0.6-log for *Cryptosporidium* and 0.4-log for *Giarda* at DWTP A4 (Figure 6-6). Treatment requirements for the reduction of microbial pathogens at DWTPs are commonly scaled to log_{10}-reduction; therefore, the choice of parametric distribution for source water characterization could result in different treatment requirements. It should be noted that the upper bound of the 95% credibility interval on the *annual mean* is higher than the upper bound of the 95% credibility interval on the *mean* of the distribution for the log-normal but not for the gamma (Figure 6-6). This difference indicates that, for the log-normal distribution, daily mean concentrations having a very small probability of exceedance (e.g., once every 10 years) can have a significant impact on the annual mean concentration. Improved knowledge of the dependencies between source water concentrations and removal/inactivation efficiencies of treatment processes could also reduce uncertainties on exposure estimates. In this study, stable *Giardia* concentrations (0.08 ± 0.02 cyst/L) were measured in settled water at DWTP C6 during Event 1 regardless of an increase in source water concentrations of 1.4-log (Figure 6-7). These results must be interpreted with care because the sample size is small, and recovery rates in raw and settled water matrices were not measured. It is worth noting that, according to the Smoluchowski theory of flocculation, a higher flocculation rate should be observed at higher particle concentrations (Benjamin and Lawler 2013). Basic research on the mechanisms of aggregation of microorganisms during coagulation/flocculation and the evaluation of full-scale performances of treatment processes during periods of microbial challenge in raw water could be valuable to improve the assessment and management of microbial peaks at DWTPs.
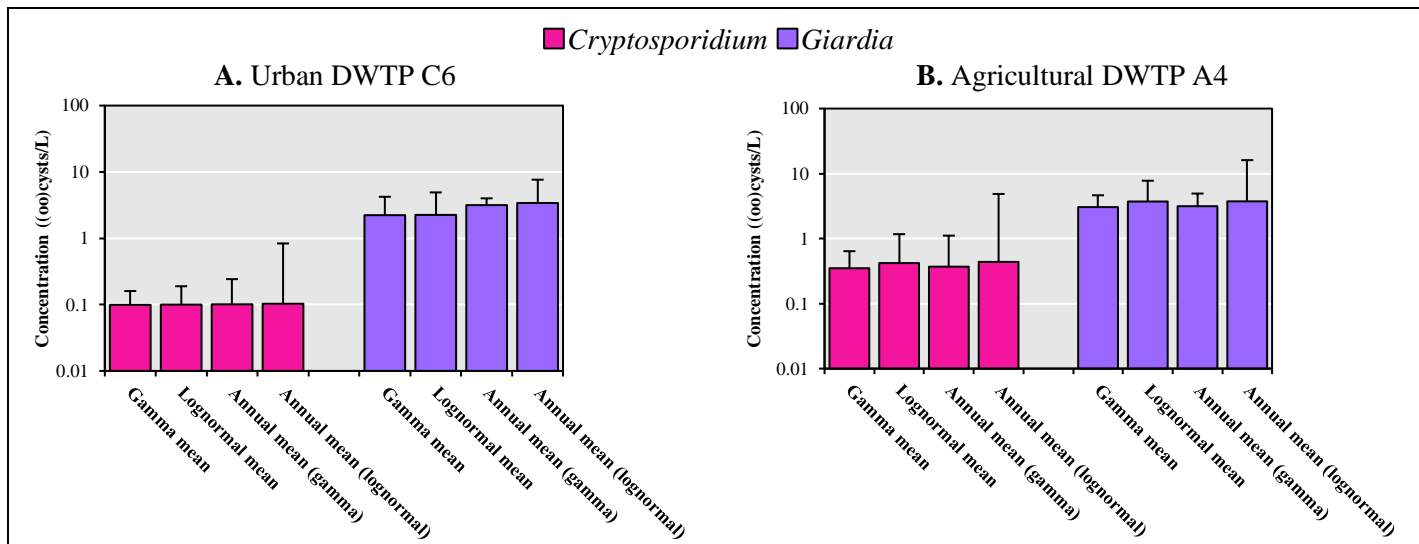
Figure 6-6: Mean and annual mean of the gamma and log-normal distributions at drinking water treatment plants (DWTPs) C6 (A) and A4 (B). Whiskers indicate the upper bound on the 95% credibility interval. For the annual mean, the 95% credibility interval represents the year-to-year variation (365 daily mean concentrations per year) of the upper bounds of the 95% predictive interval about the best fit distribution.
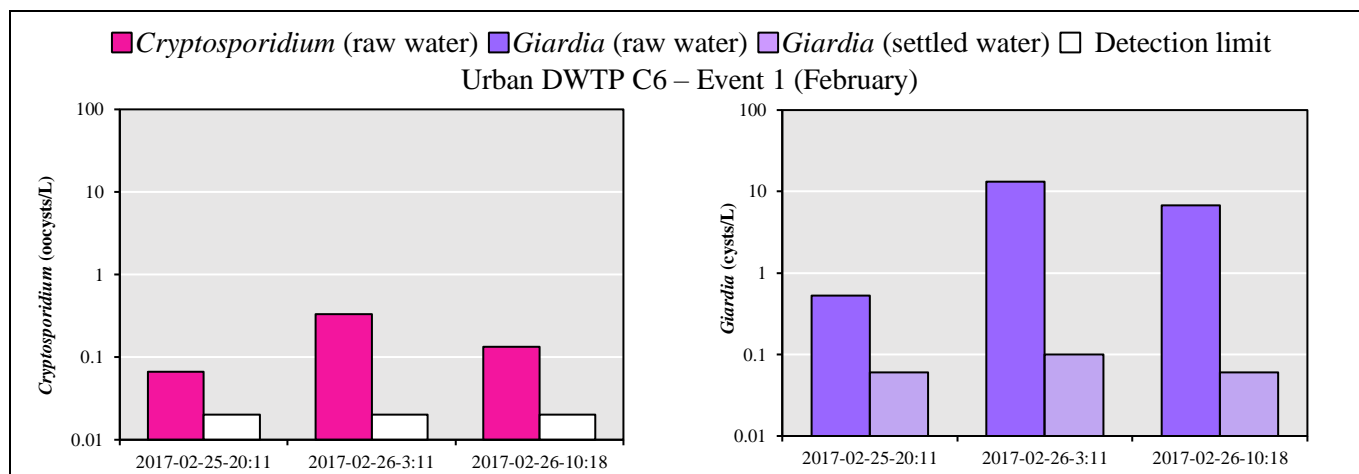
Figure 6-7: Short-term variations of *Cryptosporidium* (A) and *Giardia* (B) concentrations in raw water and settled water for the first 24 hours of an hydrometeorological event (snowmelt and rainfall) in February (Event 1) at drinking water treatment plant (DWTP) C6.

6.4 Conclusions

This article describes a methodology for data collection and model validation to explicitly account for hydrometeorological events when source water pathogen concentrations are characterized. An event-based sampling strategy triggered by meteorological conditions and rapid increases in β-D-glucuronidase (GLUC) activity was implemented at two drinking water treatment plants to investigate the impact of snowmelt and rainfall events on source water contamination. These event-based campaigns allowed us to find that:

- Increase in GLUC activity was indicative of an increase in *Cryptosporidium* and *Giardia* concentrations in source water, which varied over about 1.0-log over 24 hours;
- At the urban site, GLUC activity level was a better surrogate than turbidity to identify transient peak contaminations by protozoan pathogens in source water during two snowmelt events.

The use of a model validation approach using mixed Poisson distributions and results from event-based sampling demonstrated that:

- The gamma distribution underestimated high protozoan pathogen concentrations collected with routine and event-based monitoring, but the log-normal distribution accurately predicted these high protozoan pathogen concentrations;

- The selection of a log-normal distribution rather than a gamma distribution increased the uncertainty of the annual mean concentration by about 0.5-log, which can result in additional treatment requirements. Appropriately conservative parametric models should be carefully chosen to manage human health risks adequately but also to avoid unnecessary costs for water utilities.

Additional studies confirming these findings in other catchments and for other hydrometeorological events would be relevant. Improved knowledge of full-scale reduction of protozoan pathogens and microbial surrogates during hydrometeorological events would be valuable to quantify the risk of microbial peaks at drinking water treatment plants.

6.5 Acknowledgments

CHAPTER 7.   ARTICLE 4 - DEMONSTRATING THE REDUCTION OF ENTERIC VIRUSES BY DRINKING WATER TREATMENT DURING SNOWMELT EPISODES IN URBAN AREAS

In this Chapter, the event-based monitoring strategy presented in Chapter 4 and Chapter 6 is adapted for the assessment of virus concentrations in source water and treated water throughout the treatment train of two urban drinking water treatment plants. The collected data sets are used to quantify the extent of virus removal achieved by individual and combined treatment processes during challenging periods of source water microbial contamination. This article was submitted to *Water Research*.

Demonstrating the reduction of enteric viruses by drinking water treatment during snowmelt episodes in urban areas

Émile Sylvestre [a,b], Michèle Prévost [a], Jean-Baptiste Burnet [a,b], Xiaoli Pang [c,d], Yuanyuan Qiu [c], Patrick Smeets [e], Gertjan Medema [e,f], Mounia Hachad [a,b], Sarah Dorner [b]

[a] NSERC Industrial Chair on Drinking Water, Department of Civil, Geological, and Mining Engineering, Polytechnique Montreal, Montreal, Quebec, H3C 3A7, Canada

[b] Canada Research Chair in Source Water Protection, Department of Civil, Geological, and Mining Engineering, Polytechnique Montreal, Montreal, Quebec, H3C 3A7, Canada

[c] Department of Laboratory Medicine and Pathology, University of Alberta, 116st & 85 Ave, Edmonton, AB, T6G 2R3, Canada

[d] Public Health Laboratory, Alberta Precision Laboratoires, 8440-112st, Edmonton, AB, T6G 2J2, Canada

[e] KWR Water Research Institute, Groningenhaven 7, 3433 PE Nieuwegein, The Netherlands

[f] Sanitary Engineering, Department of Water Management, Faculty of Civil Engineering and Geosciences, Delft University of Technology, P.O. Box 5048, 2600GA, Delft, The Netherlands

* Corresponding author e-mail: emile.sylvestre@polymtl.ca

Abstract This study proposes a method to quantify the extent of virus removal achieved by full-scale drinking water treatment processes during challenging periods of microbial contamination. Critical periods were identified at two urban drinking water treatment plants during snowmelt freshet using online *in situ* β-D-glucuronidase activity measurements. Concentrations of norovirus, rotavirus, enterovirus, adenovirus, and JC virus in these periods were evaluated by reverse transcription and real-time quantitative PCR after concentrating large volumes of water at the source and throughout the treatment train. Virus infectivity was assessed through viral culture by measurement of cytopathic effect and integrated cell culture qPCR. Event-based sampling indicated that concentrations of viruses in raw water during snowmelt freshet were about 1.0-log higher than concentrations under baseline conditions. Virus removal performances were similar or higher during snowmelt episodes than in baseline conditions and were, to some extent, associated with raw water virus concentration and turbidity. Enterovirus, noroviruses GI and GII, and JC virus were primarily removed by coagulation/flocculation. Rotavirus and adenovirus were detected after ozonation, filtration, and UV disinfection, and infectious adenoviruses were detected after UV disinfection. β-D-glucuronidase guided virus monitoring can be used to assess virus reduction during peak faecal contamination events in urban water sources.

7.1 Introduction

Accurate data on the physical removal and inactivation of enteric viruses by engineered water treatment processes is essential to the implementation of risk-based preventive approaches to ensure drinking water safety (WHO 2017b). Virus removal performances are commonly assessed by spiking cultured or isolated virus stocks. These performances have been estimated at bench- or pilot plant-scale by plaque assays (Guy et al. 1977, Rao et al. 1988, Nasser et al. 1995, Hijnen et al. 2010) or quantitative PCR (qPCR) assays (Shin and Sobsey 2015, Shirasaki et al. 2017, Kato et al. 2018). A limited number of studies also investigated the removal of viruses under full-scale operating conditions in drinking water treatment plants (DWTPs) (Stetler et al. 1984, Payment et al. 1985, Payment and Franco 1993, Havelaar et al. 1995, Albinana-Gimenez et al. 2009, Teunis et al. 2009, Asami et al. 2016). However, these removal performances are usually measured under random raw water quality conditions, and little is known about specific removal performances during hydrometeorological events.

Flocculation is a critical step during intermittent changes in raw water quality. Inadequate floc formation, floc breakdown, and filter overloading could lead to increased amounts of particles in finished water, which can render virus disinfection ineffective (Hejkal et al. 1979). An increase of natural organic matter (NOM) concentration in raw water can occur following rainfall events (Hurst et al. 2004), which can interfere with virus flocculation performance (Nasser et al. 1995). Furthermore, coagulation with hydrolyzing metal salts can perform less well at low water temperature due to lower solubility of the metal hydroxides (Driscoll and Letterman 1988, Kang and Cleasby 1995) and poor floc formation (Morris and Knocke 1984, Hanson and Cleasby 1990). Snowmelt episodes associated with high virus concentrations in river water during cold months could, thus, represent periods of higher viral risks for drinking water consumers (Sokolova et al. 2015). However, the identification and characterization of virus concentration peaks during hydrometeorological events remain challenging at DWTPs. The automatization of rapid methods for the detection of indicators of faecal contamination in surface water (Ryzinska-Paier et al. 2014, Koschelnik et al. 2015) could stimulate the development of new sampling strategies to characterize viral removal performances at full-scale during microbial peak events.

The main objective of this work was to investigate the virus removal performance of full-scale drinking water processes during periods of microbial challenge in raw water. Online β-D-glucuronidase (GLUC) activity measurements were used to trigger sequential sampling of large volumes of raw water (50-2200 L) and treated water throughout the treatment train. The concentrations of multiple enteric viruses, including norovirus, rotavirus, reovirus, sapovirus, astrovirus, enterovirus, adenovirus, and a non-enteric virus JC virus were quantified by reverse transcription (where needed) and real-time quantitative PCR, and virus infectivity of cultivable viruses was assessed using the cytopathic effect in cell culture and integrated cell culture with qPCR (ICC-qPCR).

7.2 Material and methods

7.2.1 Catchment description

Sampling campaigns were carried out at two drinking water treatment plants (DWTPs) treating water from the Milles Iles River in the greater Montreal area in Quebec, Canada. The river has a length of 40 km, an average water discharge of 286 m^3 s^{-1}. It is one of the major rivers of the

Montreal Archipelago, where the Ottawa River meets the Saint Lawrence River. Locally, it is under the direct influence of a series of smaller watersheds totalling 1,190 km^2. Drinking water intakes A and B are located at the middle point and the end of the river, respectively. One hundred and eighty-four combined sewer overflows (CSOs) and 14 municipal wastewater treatment plants (WWTPs) using mostly aerated ponds or combined biological and physicochemical treatment discharge to the river and its tributaries. Diffuse pollution sources may also contribute to viral contamination of animal origin in drinking water supplies because river tributaries are draining agricultural lands. Spring snowmelt freshet usually occurs between February and April in Southern Quebec, and it is the critical period for microbial peaks at drinking water intakes located in this river (Burnet et al. 2019b).

7.2.2 Drinking water treatment description

An overview of unit processes involved in the treatment train of each DWTP and the location of sampling points is illustrated in Figure 7-1. At both DWTPs, Supervisory Control and Data Acquisition (SCADA) data (flow rate, turbidity, pH, coagulant dosage, disinfectant residual) were collected to relate these parameters with the observed removal of viruses.

DWTP A was operated at a capacity of 1.1×10^5 m^3 d^{-1}. The raw water was coagulated with aluminum sulfate "alum" (Al$_2$(SO$_4$)$_3$·18 H$_2$O; dosing rate: 50 mg L^{-1}) and silica sand (SiO$_2$; dosing rate: 2 mg L^{-1}) at pH 6.0 and processed by a floc blanket clarifier. A first-stage dual sand-anthracite filtration then processed the settled water (10 m h^{-1}; 30 cm sand-bottom and 60 cm anthracite-top). The filtered water then passed through inter-ozonation (dose rate: 1.2 mg L^{-1} O$_3$), second-stage granular activated carbon (GAC) filtration (5-10 m h^{-1}; 200 cm of activated carbon), and chemical disinfection with chlorine dioxide (2.3 mg L^{-1} ClO$_2$).

DWTP B was operated at a capacity of 1.0×10^5 m^3 d^{-1}. The raw water was processed by an ACTIFLO® microsand ballasted clarifier (Veolia Water Technologies, QC, Canada). During the sampling period, alum (Al$_2$(SO$_4$)$_3$; dosing rate:15 mg L^{-1}), polyaluminosilicate-sulfate (PASS-10; dosing rate: 50 mg L^{-1}), cationic polyacrylamide (CPAM; dosing rate: 0.25 mg L^{-1}) and silica sand (SiO$_2$; dosing rate: 4 g L^{-1}) were added in 1°C raw water at pH 6.7. The settled water then passed through inter-ozonation (dosing rate:1.0 mg L^{-1} O$_3$; Ct$_{10}$: 0.6 mg L^{-1} min^{-1}) for 20-22 minutes and is processed by dual sand and granular activated carbon (GAC) filters (10 m h^{-1}, 15 cm sand-bottom

and 140 cm activated carbon-top). The filtered water then went through low pressure (LP, $\lambda = 254$ nm) UV disinfection (dose: 40 mJ cm^{-2}, Wedeco BX 3200; Xylem Water Solutions, Herford, Germany) and chemical disinfection with sodium hypochlorite (dosing rate: 2.1 mg L^{-1} NaOCl).
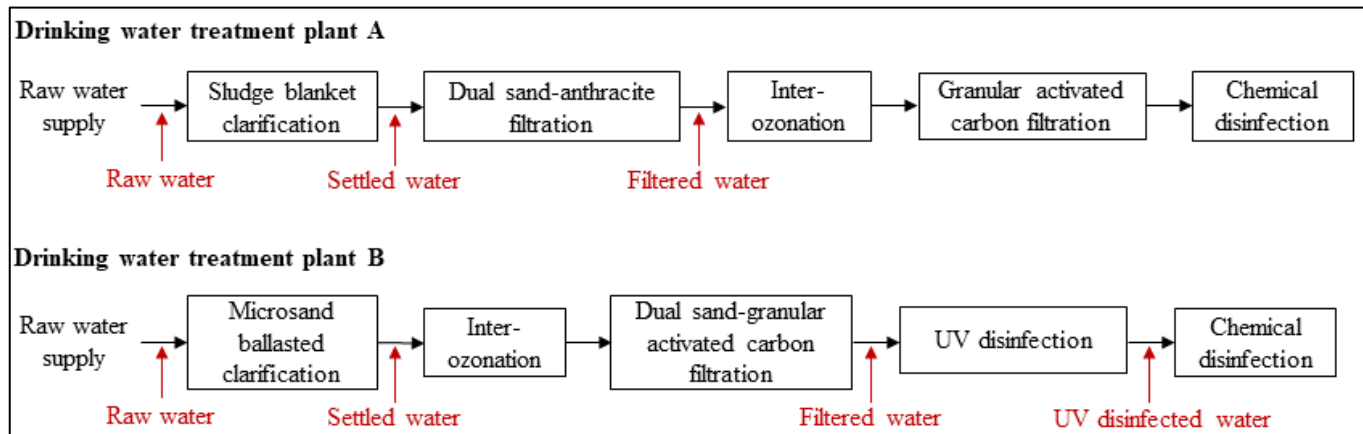
Figure 7-1:Unit processes involved in the treatment train of drinking water treatment plants A and B and location of sampling points (red).

7.2.3 Sampling strategy

An automated rapid monitoring system (ColiMinder^{TM} VWMS GmbH, Vienna, Austria) was installed at each DWTP in February (1-2 months before significant snowmelt episodes) to monitor variations of β-D-glucuronidase (GLUC) activity in raw water. GLUC activity was measured every 1-3 hours and was reported online in modified Fishman units (mMFU 100 mL^{-1}). GLUC activity was used as a surrogate for faecal contamination levels in raw water. Turbidity levels were measured continuously in raw water, and every 4 hours in settled water, individual filter effluents, as well as in combined effluent from all filters.

At DWTP A, the event-based sampling strategy was based on meteorological conditions (daily rainfall > 20 mm or air temperature > 5°C over 24 hours) and GLUC activity levels (variation > +5 mMFU 100 mL^{-1} over 1 hour). Two events (Event A1 in February and Event A2 in April) were captured with this sampling strategy. Sequential grab raw water samples (110-500 L) were collected at a frequency of 4 to 6 hours for around 24 hours to obtain a virus concentration profile over time. Sequential grab samples of settled and filtered waters (300-600 L) were collected to match theoretical mean hydraulic residence times through clarification (3 hours) and filtration (2 hours) (C. Durivage, *personal communication*).

The event-based sampling strategy was modified at DWTP B because a rapid increase in the level of the GLUC activity (+20 mMFU/100 mL) in raw water was observed during dry weather conditions. Two event-based sampling campaigns were carried out when the GLUC activity level was above 40 mMFU 100 mL^{-1}, and three baseline sampling campaigns were conducted when the GLUC activity level was below 40 mMFU 100 mL^{-1} sampling campaigns were conducted. On February 7, 2018, a planned discharge of raw sewage (4 hours) was undertaken for maintenance on the main sewer system at a municipal wastewater treatment plant (WWTP) located 5 kilometers upstream of DWTP B. The WWTP serves a population of 37,000 residents and treats, on average, 28,000 m^3 of raw sewage per day. In normal conditions, the wastewater is treated using aerated lagoons. The impact of this discharge on raw water quality at DWTP B was evaluated using the GLUC activity to trigger grab sampling (Event B1). A second event-based sampling campaign was conducted in March 2018 (Event B2). Sequential grab samples of raw water (50-200 L), settled (350-520 L), filtered (1000-2000 L), and UV disinfected (1200-2700 L) waters were collected over 4 days during Event B2. Grab samples of settled, filtered, and UV disinfected waters were also collected during baseline sampling campaigns. Theoretical mean hydraulic residence times throughout clarification (1.5 hours), filtration, and UV disinfection (1.5 hours) were matched for each raw water sample (M. Marchand, *personal communication*).

7.2.4 Virus concentration method

An adsorption-elution method was applied to concentrate viruses from water samples using electropositive filters NanoCeram VS2.5-5 (Argonide Corp, Sanford, FL, USA). Samples were filtered on-site at the DWTPs under a constant flow rate of 5-15 L min^{-1}according to the turbidity of the water sample. Pre-filters were not used in this study. A decontamination protocol was applied to prevent cross-contamination during repeat use of the filtration system. Before each use, the intake and cartridge housing modules were sterilized with 6% NaOCl for 30 minutes, rinsed with sterile ddH$_2$O, and then dechlorinated with a sodium thiosulfate solution. After filtration, cartridges were stored and kept cool (between 1-10 °C) in a transport cooler and shipped to the University Alberta Hospital in Edmonton, AB, Canada, for processing within 48 hours after the start of the field sample collection. Eight samples collected at DWTP B on February 28, 2018, could only be processed 96 hours after the collection due to shipment delay. The elution and flocculation steps after filtration were performed to concentrate the viruses in the samples as previously described

(Pang et al. 2012). In brief, viruses retained by the positively charged filter were eluted with 1 liter of 1.5% beef extract (BE) buffer (pH 9.75). The eluate was further flocculated with $FeCl_3$ and pH adjustment to 3.5 followed by centrifugation. The water concentrate was suspended in glycine buffer (0.5 mol/L glycine, pH 9.0) with a final volume of 15 mL. The pH of the suspension was adjusted to 7.2 ± 0.2. The concentrate was stored at $-70\,^{\circ}C$ until assayed.

7.2.5 Nucleic acid extraction and quantification of enteric viruses by qPCR

Total nucleic acids were extracted from 200 μL of concentrated water samples and eluted in 50 μL RNase-free water using the MagaZorb® total RNA Prep kit (Promega, WI, USA). Nucleic acid extracts were tested for norovirus genogroup I and GII (GI/GII), rotavirus, sapovirus, astrovirus, generic adenovirus, enterovirus, JC polyomavirus, and reovirus. Quantification of virus was performed by a two-step reaction (reverse transcription (RT) real-time quantitative PCR (qPCR)) with the ABI PRISM 7500 Sequence Detection System (ABI) as previously described (Qiu et al. 2015, Qiu et al. 2016). The primer and probes used for qPCR were published previously (Pang et al. 2012, Qiu et al. 2015, Qiu et al. 2018). RT and qPCR were carried out as described previously (Pang et al. 2012). Salmon DNA was included as internal control to monitor inhibition. An external standard curve was established for quantification of all seven viruses using the 875 bp DNA fragment of norovirus GII by 10-fold dilution from 10 to 1×10^6 genome-copies (Qiu et al. 2016). Optimization of the panel qPCR assay for the eight viruses was performed by adjusting thermal cycler conditions and concentration of primers and probes to achieve similar qPCR efficiencies. Based on the standard curves and the Ct values, the virus concentration (free or encapsidated genomes) was expressed as genome-copies per liter. Sample-specific recovery rates were not measured, but the recovery rates of qPCR-based assays were described in a previous study (Pang et al. 2012). The limit of detection (LOD) of qPCR-based assays was one genome copy per PCR reaction, which was equal to 2–140 genome-copies per 100 mL based on each sample's volume and their concentrate volume.

7.2.6 Virus cell culture

Viral replication in cultures was determined by monitoring cytopathic effects (CPE). Infectivity of rotavirus, enterovirus, adenovirus, and reovirus was assessed in each sample using Buffalo green monkey kidney cells (BGM) and African rhesus monkey kidney cells (MA104) grown separately

on Eagle's MEM medium (Sigma, ON, Canada) as previously described (Qiu et al. 2015). Integrated cell culture (ICC)-qPCR assay was used to evaluate the presence of infectious virions in the sample, as detailed by Qiu et al. (2015).

7.2.7 Quantification of virus concentrations

A hierarchical Bayesian framework was adopted to evaluate virus concentrations. Two levels of analysis were specified to describe uncertainties related to the random error in sample collection and the analytical recovery due to losses during sample processing. The number of viral genome-copies detected by PCR (N_p) in a sample was assumed to be randomly distributed according to a Poisson distribution with a mean λ_p. This model assumes that viruses are randomly dispersed in the water (i.e., homogeneous concentration) within the time and space from which the sample was collected. The expected analytical recovery of the detection method was assumed to vary randomly among samples according to a beta distribution (Wu et al. 2014). The model can be written as:

$$N_p[i] \sim \text{Poisson}(\lambda_p[i]) \tag{7.1}$$

$$\lambda_p[i] = \left[v[i] * V_S[i] * \frac{V_{PCR}[i]}{V_P[i]} \right] * r[i] \tag{7.2}$$

$$r[i] \sim \text{Beta}(\alpha, \beta) \tag{7.3}$$

where v is the virus concentration, V_S is the volume of raw of treated water filtered with the NanoCeram ® filter, V_{PCR} is the volume for the PCR reaction, V_P is the volume of the pellet (i.e., concentrated sample for the nucleic acid extraction), and r is the expected analytical recovery. Shape parameters (α, β) of the Beta distribution were estimated from recovery rates previously published for adenovirus 41 (n=3; mean=0.18, standard deviation (STD)=0.03) and norovirus GII.4 (n=3; mean=0.19, STD=0.03) spiked and concentrated from 10 L of river water by NanoCeram® filtration and assayed by real-time quantitative RT-PCR and PCR (Pang et al. 2012). Beta distributions for adenovirus 41 and norovirus GII.4 were used to describe the recovery rates of other DNA and RNA viruses, respectively.

The Bayesian analysis was conducted in R (v3.4.1) via rjags (v4-6) (Plummer 2013). The uncertainty in parameter values was explored using a Markov Chain Monte Carlo procedure. Four Markov chains were run for 10^4 iterations after a burn-in phase of 10^3 iterations. The Brooks-Gelman-Rubin scale reduction factor was considered to monitor the convergence of the four chains (Gelman and Shirley 2011). A conjugate gamma prior with hyperparameters set to Gamma (0.001, 0.001) was selected to describe the virus concentration v of the Poisson model. This prior reflects practically no prior knowledge. The best estimate virus concentration and a 95% credibility interval on this mean were reported. The R code used to quantify virus concentrations is provided in the Supplementary Material.

7.2.8 Quantification of virus removal

Treatment removal performances were quantified using an empirical approach. Point estimates of the log-removal (LR) across a treatment unit (paired sample) were calculated as follows:

$$\text{LR} = \log_{10}\left(\frac{C_{in}}{C_{out}}\right) \tag{7.4}$$

where C_{in} and C_{out} are the best estimate virus concentration per sample (genome-copies L^{-1}) before and after treatment, respectively. The uncertainty in virus concentrations was not considered in the quantification of LR. The limit of detection was considered in the calculation when C_{out} was not quantified. The effective log-removal ($\text{LR}_{\text{effective}}$) was obtained as follows:

$$\text{LR}_{\text{effective}} = \log_{10}\left(\frac{\bar{C}_{in}}{\bar{C}_{out}}\right) \tag{7.5}$$

Each treatment step of the DWTP was assumed to behave as a plug flow reactor operated hydraulically at a steady state. The theoretical hydraulic residence time was assumed to be a valid approximation of the retention time of the viruses.

7.3 Results

7.3.1 Raw water fluctuations at DWTP A

Time series of the GLUC activity, turbidity and hydrometeorological variables (flow rate of the river, snow cover on the ground) represent raw water during the 2017 snowmelt period at DWTP A (Figure 7-2A). Relationship between times series for GLUC activity, turbidity, and river flow rates during the 2017 snowmelt period at DWTP A, and identification of the dominant upstream fecal pollution sources were described elsewhere (Burnet et al. 2019b).

Rotavirus, adenovirus, norovirus GII, and JC virus were detected in most samples during the two snowmelt events (Table 7-1). Raw water concentrations peaked at around 10^4 genome-copies L^{-1} for adenovirus and rotavirus and 10^3 genome-copies L^{-1} for norovirus GII and JC virus (Figure 7-3A). Rotavirus and adenovirus concentrations varied from 0.6 to 0.9 log during these 24-hour periods. Reovirus was positive in viral culture with ICC-qPCR for all raw water samples (Table 7-2). Rotavirus, adenovirus, and enterovirus in raw water samples were predominantly negative in viral culture. The uncertainties related to the random error in sample collection and the analytical error are shown with credibility intervals in Figure 7-4 and Figure 7-5. These 95% credibility intervals indicate that the uncertainty on the mean virus concentration per sample is approximately 0.5-log for each virus.

7.3.2 Raw water fluctuations at DWTP B

Two different types of peak events were observed at DWTP B. On February 7, raw water GLUC activity increased from 20 to 40 mMFU 100 mL^{-1} about 10 hours following the planned wastewater discharge. This peak had a duration of approximately 24 hours (Figure 7-2B). In March, the raw water GLUC activity gradually increased from 20 to 50 mMFU 100 mL^{-1} over 5 days without major cumulative rainfall (<10 mm) and cumulative snowmelt (<10 cm) over the ten days preceding the GLUC activity peak. Concentrations of rotavirus, adenovirus, norovirus GII, and JC virus were about 1.0-log higher during peak event conditions than during baseline conditions (Figure 7-3B). Enterovirus, astrovirus, and sapovirus, were sporadically measured in event-based samples. Infectious adenovirus and reovirus were detected in viral culture in raw water samples (Table 7-2). Raw water concentrations peaked at around 10^5 genome-copies L^{-1} for adenovirus and

rotavirus and 10^4 genome-copies L^{-1} for norovirus GII and JC virus. These concentrations were approximately 1.0-log lower than treated wastewater effluent concentrations and approximately 2.0-log lower than raw sewage concentrations as measured at the upstream WWTP (Supplementary Figure 7-1).
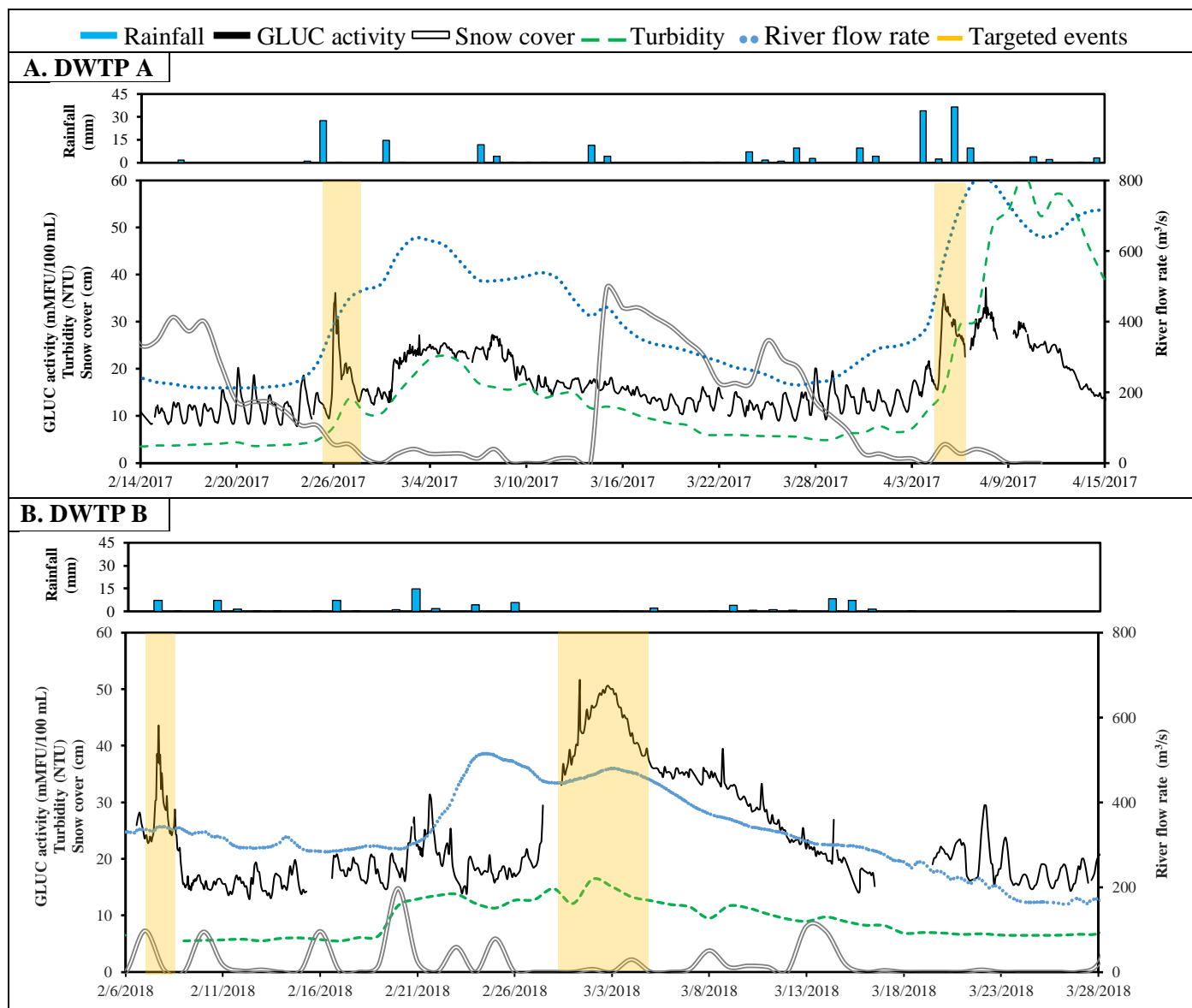
Figure 7-2: Time series of daily rainfall, GLUC activity, snow cover, raw water turbidity, and river flow rate during snowmelt freshet at drinking water treatment plants (DWTPs) A and B. Yellow rectangles indicate targeted events.

Table 7-1: Number of positive samples by qPCR for each virus at each treatment step at drinking water treatment plants A and B

| | DWTP A | | | DWTP B | | | |
	Raw water	Floc blanket clarif.	Rapid sand filtration	Raw water	Ballasted clarif.	Ozonation + GAC filtration	UV disinf.
n	8 (%)	6 (%)	6 (%)	8 (%)	6 (%)	6 (%)	6 (%)
Rotavirus	8 (100)	6 (100)	1(17)	8 (100)	6 (100)	3 (50)	3 (50)
Adenovirus	8 (100)	6 (100)	0	8 (100)	6 (100)	2 (33)	0
Norovirus GI	1 (13)	0 (0)	0	8 (100)	0	0	0
Norovirus GII	6 (75)	3 (50)	0	8 (100)	0	0	0
JC virus	6 (75)	4 (66)	0	8 (100)	3 (50)	0	0
Enterovirus	0	0	0	3 (38)	0	0	0
Reovirus	0	0	0	0	0	0	0
Astrovirus	0	0	0	2 (25)	0	0	0
Sapovirus	1 (13)	0	0	1 (13)	0	0	0

Table 7-2: Detection of infectious viruses in water samples by cell culture and integrated cell culture (ICC) qPCR

| | | DWTP A | | | DWTP B | | | |
		Raw water	Floc blanket clarif.	Rapid sand filtration	Raw water	Ballasted clarif.	Ozonation + GAC filtration	UV disinf.
CPE	Positive viral culture, n (%)	8 (100)	3 (50)	2 (33)	8 (100)	1 (16)	0 (0)	0 (0)
ICC-qPCR (positive samples)	Rotavirus	0	0	0	0	0	0	0
	Adenovirus	0	1	0	4	0	0	2
	Enterovirus	1	0	0	0	0	0	0
	Reovirus	8	1	2	7	0	0	0
	Unknown[1]	0	1	0	0	1	0	0

[1] Unknown : Samples showed CPE in the cell culture but could not be identified for a specific virus by ICC-qPCR
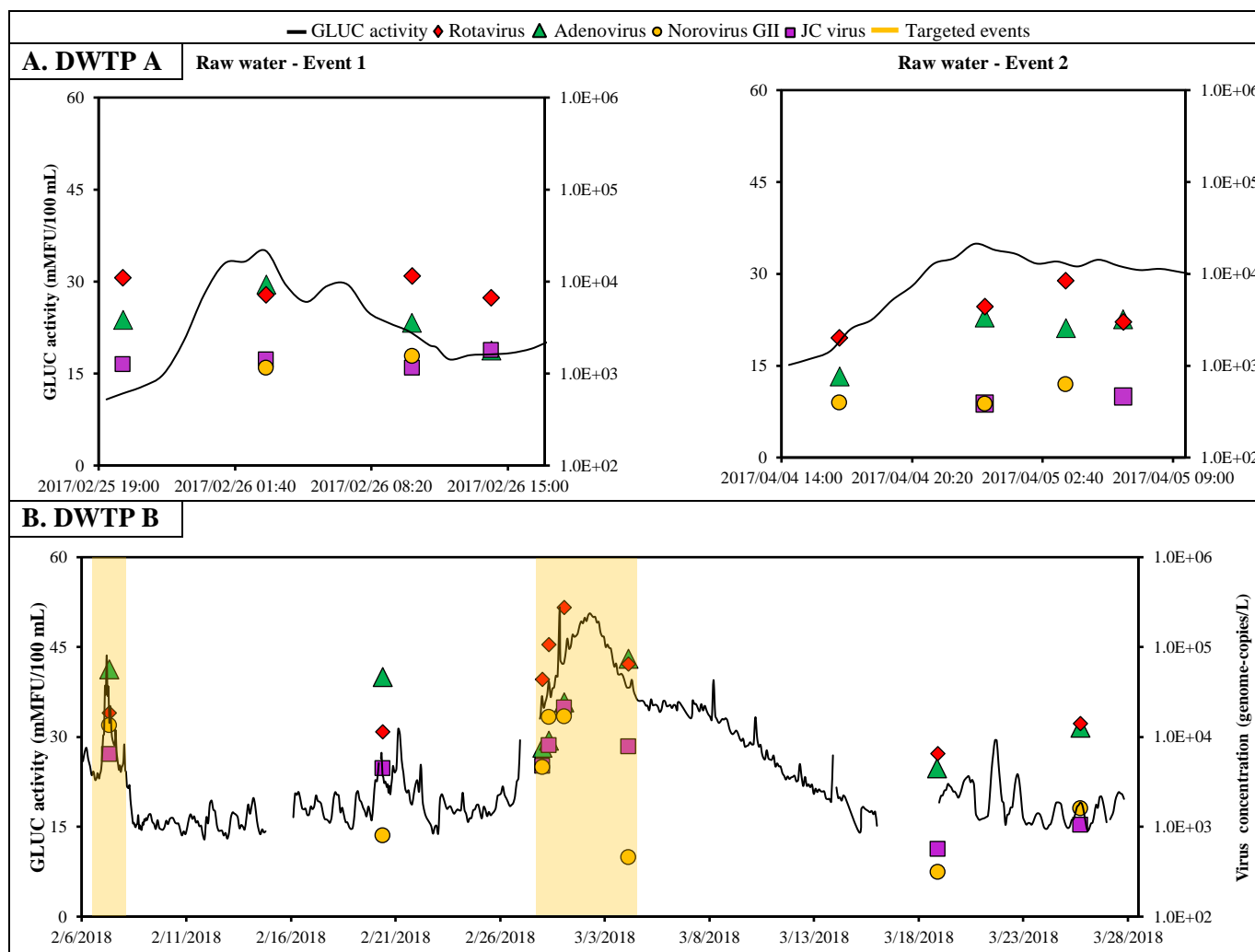
Figure 7-3: Time series of GLUC activity measurements and rotavirus, adenovirus, norovirus GII, and JC virus concentrations during snowmelt episodes at drinking water treatment plants (DWTPs) A and B. Yellow rectangles indicate targeted events.

7.3.3 Removal by coagulation/flocculation

Time series of removal of viruses throughout the treatment trains are presented in Figure 7-4 and Figure 7-5. Error bars represent the 95% credibility interval on the mean concentration as a result of the analytical error and the random distribution of the genome-copies in the sample. At both DWTPs, the concentration of 300 to 520 liters of settled water allowed the quantification of rotavirus and adenovirus (>300 genome-copies/L) in all samples. Norovirus GII was sporadically detected in settled water at DWTP A but not at DWTP B. At both DWTPs, reovirus, sapovirus,

astrovirus, and enteroviruses were not detected in any samples collected throughout the treatment train.

Large variations in removal performance for rotavirus, adenovirus, norovirus GI and GII, and JC virus are presented in Table 7-3. For adenovirus, log-removal varied from 0.3 to 1.3 log at DWTP A (floc blanket clarification), and from 1.2 to 1.7-log at DWTP B (ballasted clarification) (Table 7-3). For rotavirus and norovirus GII, removal performances were also higher at DWTP B than at DWTP A. At DWTP A, the removal of rotavirus and norovirus GII were negligible. Conversely, removals up to 2.6-log were measured for norovirus GII during the peak event at DWTP B (Figure 7-3).

Results from sequential grab samples show that the coagulation/flocculation of viruses did not deteriorate during these snowmelt episodes (Figure 7-6); peak concentrations of adenovirus were buffered by coagulation/flocculation at both DWTPs. A buffering effect was also observed for rotavirus and JC virus at DWTP B.
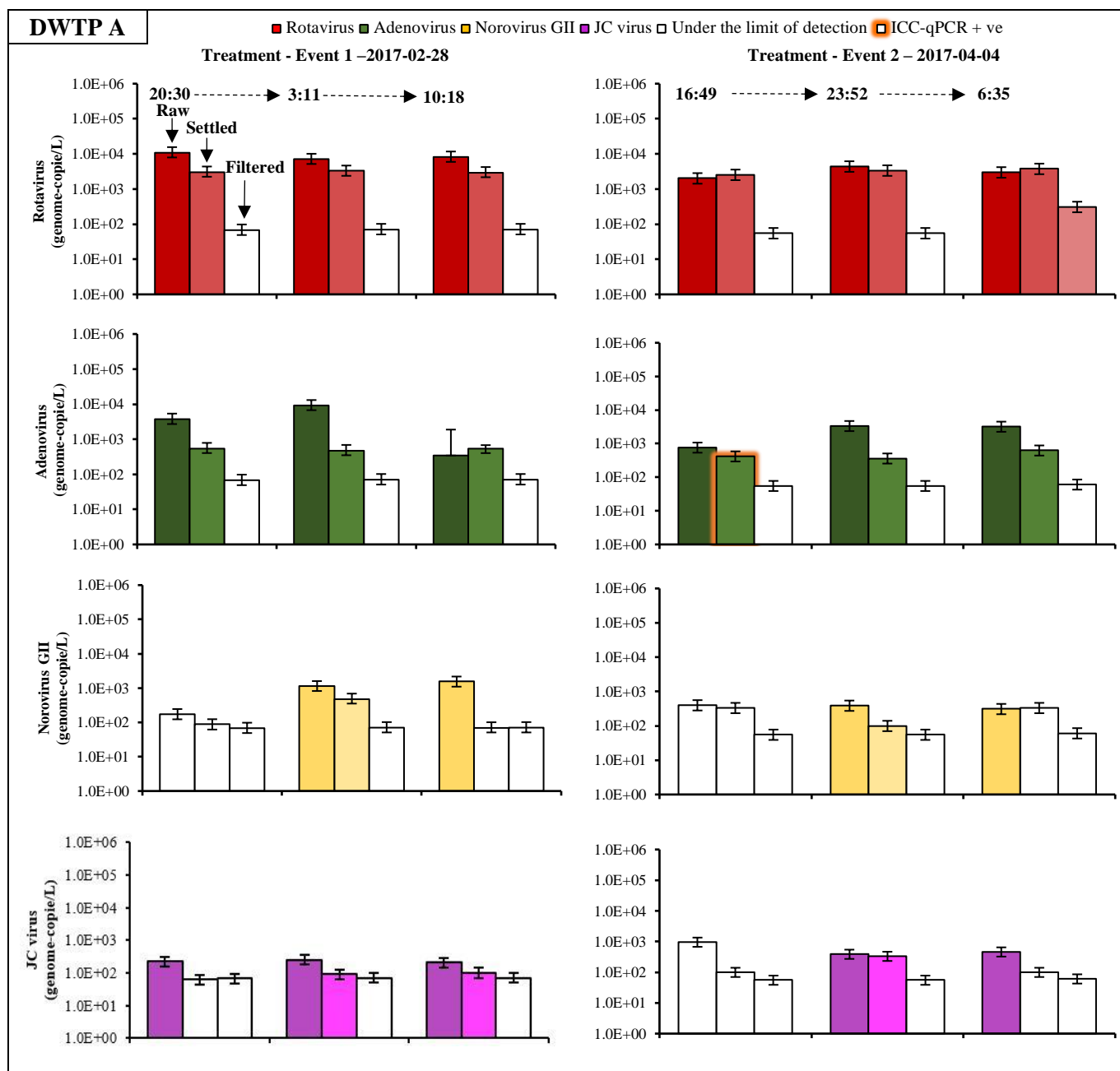
Figure 7-4: Histograms for rotavirus, adenovirus, norovirus, and JC virus concentrations in raw water, settled water, and filtered water during hydrometeorological events 1 and 2 at drinking water treatment plant A. Error bars represent the 95% credibility interval on the mean virus concentration. Columns with no colour represent the limit of detection. Orange glowing bars represent samples positive by ICC-qPCR.
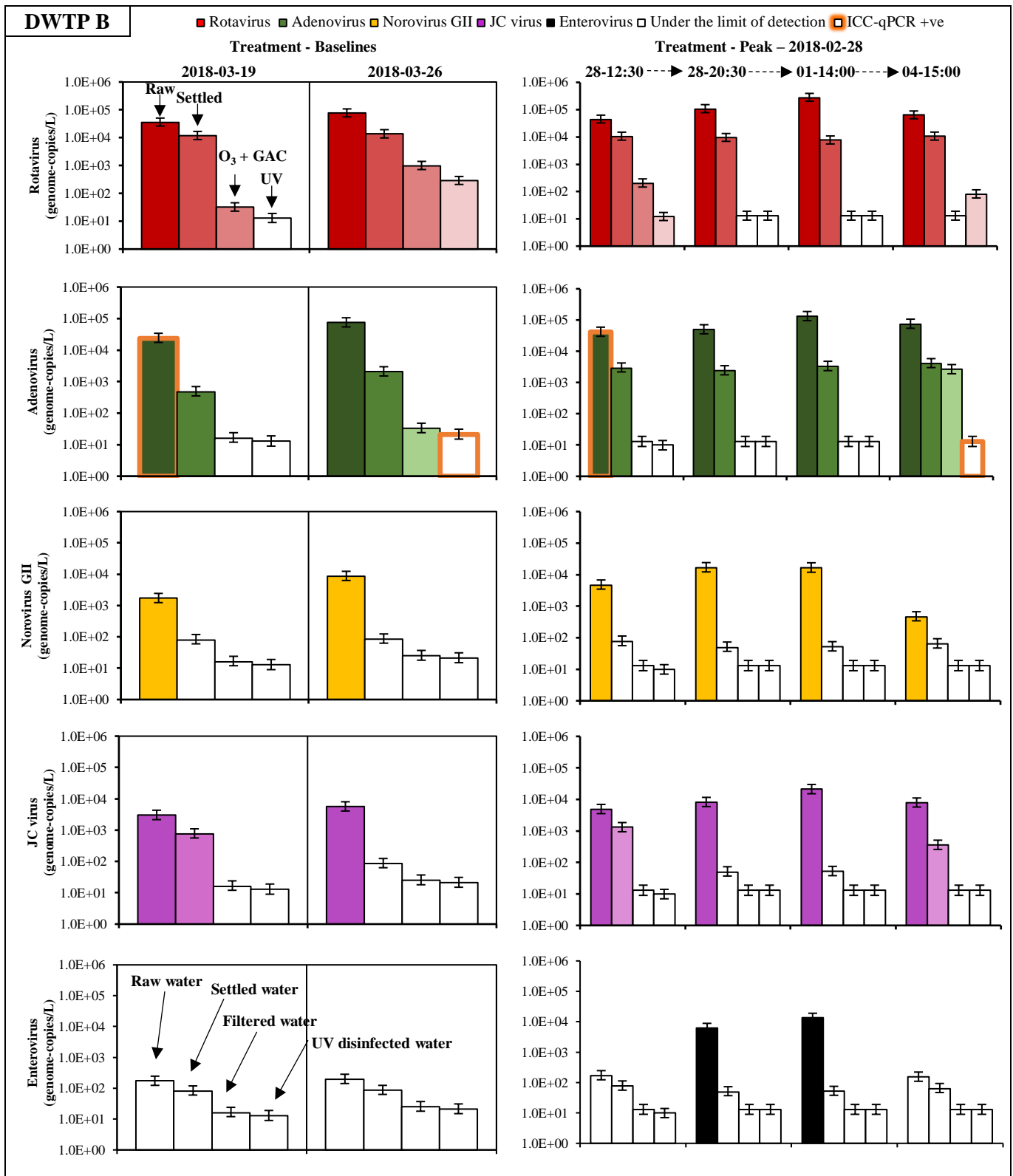
Figure 7-5: Histograms for virus concentrations in raw water, settled water, filtered water and UV disinfected water under baseline and event conditions at drinking water treatment plant B

Table 7-3: Log-removal for rotavirus, adenovirus, noroviruses, and JC virus via floc blanket clarification and filtration at drinking water treatment plant (DWTP) A and via microsand ballasted clarification, biological activated carbon filtration, and UV disinfection at DWTP B. $LR_{effective}$ is the effective log-reduction during event conditions. The log-removal has a greater-than sign (>) when the removal was quantified using the limit of detection of the effluent sample.

DWTP A		
Sample id.	FBC[A]	RGF$_{sand}$[B]
Rotavirus		
Event 1-01	0.5	>1.6
Event 1-02	0.3	>1.7
Event 1-03	0.4	>1.6
$LR_{eff.}$ Event 1	0.4	1.6
Event 2-01	0.0	>1.7
Event 2-02	0.1	>1.8
Event 2-03	0.0	1.1
$LR_{eff.}$ Event 2	0.0	1.4
Adenovirus		
Event 1-01	0.8	>0.9
Event 1-02	1.3	>0.8
Event 1-03	0.8	>0.9
$LR_{eff.}$ Event 1	1.0	0.9
Event 2-01	0.3	>0.9
Event 2-02	1.0	>0.8
Event 2-03	0.7	>1.0
$LR_{eff.}$ Event 2	0.7	0.9
Norovirus GII		
Event 1-01	-	-
Event 1-02	0.4	>0.8
Event 1-03	>1.3	-
$LR_{eff.}$ Event 1	-	-
Event 2-01	0.1	>0.8
Event 2-02	>0.6	-
Event 2-03	-	>0.7
$LR_{eff.}$ Event 2	-	-
JC virus		
Event 1-01	>0.6	-
Event 1-02	0.5	0.1
Event 1-03	0.3	0.2
$LR_{eff.}$ Event 1	0.4	-
Event 2-01	-	-
Event 2-02	0.1	>0.8
Event 2-03	>0.7	-
$LR_{eff.}$ Event 2	-	-

DWTP B			
Sample id.	BC[C]	O$_3$+RGF$_{GAC}$[D]	UV
Rotavirus			
Baseline 1	0.5	2.6	>0.4
Baseline 2	0.7	1.1	0.5
Event-01	0.6	1.7	0.6
Event-02	1.1	>2.9	-
Event-03	1.6	>2.8	-
Event-04	0.8	2.9	0.0
$LR_{eff.}$ Event	1.1	2.2	-
Adenovirus			
Baseline 1	1.7	>1.5	-
Baseline 2	1.6	1.8	>0.2
Event-01	1.2	>2.3	-
Event-02	1.3	>2.3	-
Event-03	1.6	>2.4	-
Event-04	1.2	0.2	>2.3
$LR_{eff.}$ Event	1.4	0.67	-
Norovirus GI			
Baseline 1	>1.2	-	-
Baseline 2	>1.3	-	-
Event-01	>1.2	-	-
Event-02	>1.8	-	-
Event-03	>2.0	-	-
Event-04	>1.1	-	-
$LR_{eff.}$ Event	1.5	-	-
Norovirus GII			
Baseline 1	>1.3	-	-
Baseline 2	>2.0	-	-
Event-01	>1.8	-	-
Event-02	>2.5	-	-
Event-03	>2.5	-	-
Event-04	>0.9	-	-
$LR_{eff.}$ Event	2.2	-	-
JC virus			
Baseline 1	0.6	>1.6	-
Baseline 2	1.8	-	-
Event-01	0.6	>2.0	-
Event-02	>2.2	-	-
Event-03	>2.6	-	-
Event-04	1.3	>1.4	-
$LR_{eff.}$ Event	1.4	-	-

Table 7-4: Raw and settled water turbidity in baseline and event conditions at drinking water treatment plants (DWTPs) A and B

	Sample id.	Turbidity (NTU)		
		Raw water	Settled water	Log-removal
DWTP A	Event 1-01	6.14	0.65	1.0
	Event 1-02	7.80	0.65	1.1
	Event 1-03	8.37	0.66	1.1
	Event 2-01	13.5	0.72	1.3
	Event 2-02	15.8	0.78	1.3
	Event 2-03	27.1	0.78	1.5
DWTP B	Baseline-01	6.99	0.66	1.0
	Baseline-02	6.51	0.74	1.0
	Event-01	14.74	0.97	1.2
	Event-02	12.12	0.82	1.2
	Event-03	16.42	0.80	1.3
	Event-04	15.09	0.69	1.3
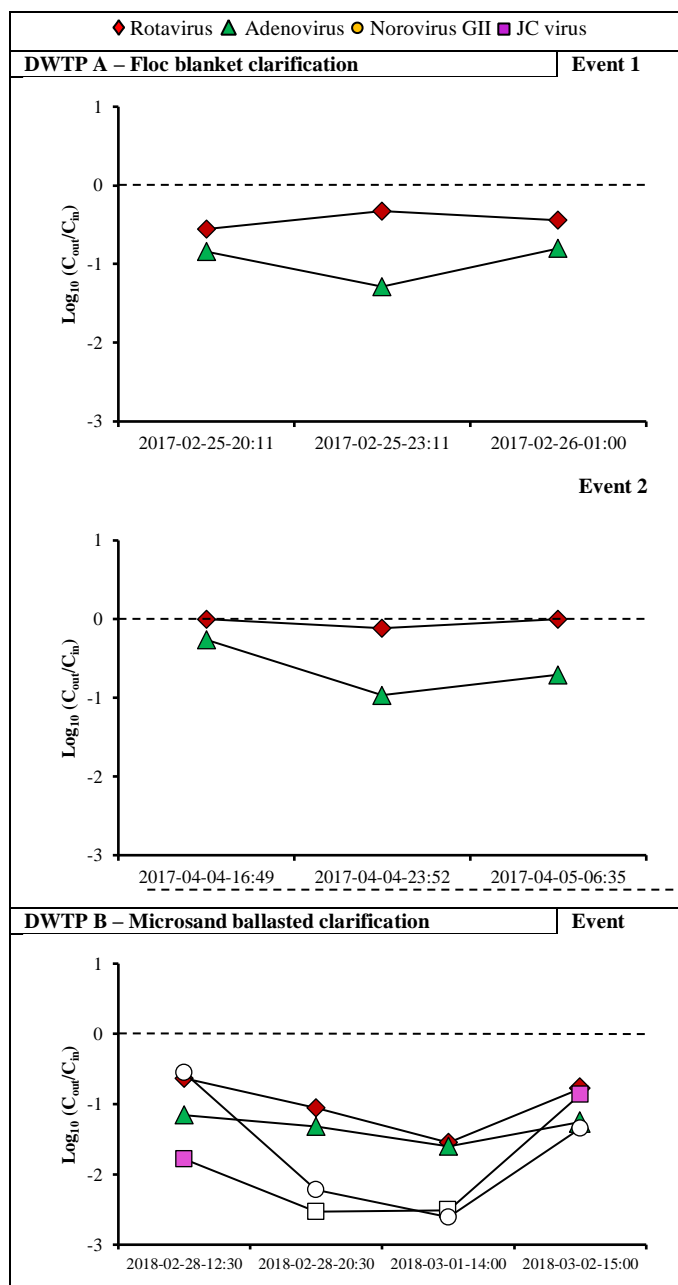
Figure 7-6: Change in virus removal performances of coagulation/flocculation in response to enteric virus peak concentrations in raw water during snowmelt episodes at drinking water treatment plants (DWTPs) A and B. White circles and squares represent minimum removal performance values due to the inability to quantify the virus in settled water (below the detection limit).

7.3.4 Removal by filtration and inactivation by UV disinfection

The concentration of 500 to 2,200 liters did not allow us to quantify the log-removal of enteric viruses by filtration accurately. However, virus concentrations were sporadically quantified at DWTP A after filtration (rotavirus) (Figure 6-4), and at DWTP B after GAC filtration (adenovirus and rotavirus) and UV disinfection (rotavirus) (Figure 7-5). In two instances, adenovirus was quantified after GAC filtration (with inter-ozonation) and positive with ICC-qPCR after UV disinfection (Table 7-2).

7.4 Discussion

7.4.1 Magnitude and variability of virus concentrations in raw water

Event-based sampling triggered by GLUC activity measurements indicated that concentrations of enteric viruses during snowmelt freshet could be expected to be about 1.0-log higher than concentrations under baseline conditions. Short-term variations of around 1.0-log in virus concentrations were previously reported in surface water with daily sampling (Westrell et al. 2006), and with event-based sampling during autumn rainfall episodes (Hata et al. 2014). At DWTP B, peak concentrations in raw water were around 2.0 log lower than virus concentrations in raw sewage and around 1.0-log lower than virus concentrations in treated wastewater effluent (aerated lagoons) of an upstream WWTP. Payment (2003) also estimated that the cumulative effect of wastewater effluent discharges in the Mille Îles River accounted for approximately 1.0% of the flow rate at DWTP B under average streamflow conditions. Although virus concentrations were not quantified during the same year at DWTP A (2017) and DWTP B (2018), findings from the current study suggest that the magnitude and variability of virus concentrations increased along the urban river that is influenced by numerous wastewater discharges. Increases in detection frequency and virus concentrations along rivers were also reported for major urban centers in France (Prevost et al. 2015) and in Alberta, Canada (Pang et al. 2019).

Several factors may influence fluctuations of enteric virus concentrations in urban water sources for a short period of time. Winter and spring peaks in sporadic viral gastroenteritis were previously observed for norovirus GII and rotavirus, respectively, in a 1-year study in Alberta, Canada (Pang et al. 2014). Winter may also be a period of higher enteric virus concentration in environmental

waters because of their persistence in cold water (Skraber et al. 2009). On a day-to-day basis, CSO discharges and WWTP by-passes can contribute to short-term increases in microbial loads at DWTPs during winter and spring (Burnet et al. 2019b, Taghipour et al. 2019); this is especially the case during the early snowmelt freshet when the dilution of untreated sewage discharges is likely limited (Madoux-Humery et al. 2013). Our results indicated that short-term raw sewage discharges (over 4 hours) in winter conditions have a measurable effect on viral concentrations at a downstream DWTP intake.

7.4.2 Virus-type specific removal

Viral removal performances of specific types of enteric viruses by coagulation/flocculation were observed at two DWTPs. At DWTP B, higher mean log-removals were observed for enterovirus, norovirus, and JC virus in comparison to those of rotavirus and adenovirus. At DWTP A, higher mean log-removals were seen for adenovirus than for rotavirus. Streaming current, electrophoretic mobility or zeta potential measurements were not available, which limits the interpretation of these results in terms of surface charge. In theory, nearly all viral particles in natural water carry a negative surface charge because the water pH is above their isoelectric point (i.e., pH value at which the net surface charge switches its sign) (Michen and Graule 2010). Hence, viral particles are stable as a result of electrical repulsion. Destabilization of the virus can be achieved during coagulation by adding metal salts that, under the right conditions of dosage and pH, interact specifically with negative viral particles to neutralize their charge (Shirasaki et al. 2016)hi. Proposed destabilization mechanisms for viral particles include charge neutralization (i.e., positively charged precipitate particles deposit on viral particles) and sweep coagulation (i.e., viral particles are enmeshed in the growing hydroxide precipitate) (Heffron and Mayer 2016). In the current study, adenovirus and norovirus would be negatively charged during treatment at pH 6.0-7.0 because of their low isoelectric point (Michen and Graule 2010). Conversely, rotavirus has a higher isoelectric point (8.0) and would be positively charged, which may inhibit its destabilization (the isoelectric point of alum is 8–9). Hence, for coagulation/flocculation processes, the removal of rotavirus is expected to be lower than the removal of adenovirus and norovirus, as observed in this study for both DWTPs.

Even if large volumes of water (300-2700 liters) were concentrated, the quantification of virus removal performances by chemically assisted filtration and disinfection remained a challenge

because of detection limits. Nevertheless, rotavirus and adenovirus genomes were sporadically detected after filtration, ozonation, and UV disinfection, and infectious adenoviruses were detected after UV disinfection at DWTP B. Previous studies reported low removal of viruses and bacteriophages by GAC filtration at pilot plant scale (0.0–0.7 log; Guy et al. (1977); Hijnen et al. (2010)) and high UV-resistance of adenovirus at a dose of 40 mJ cm^{-2} (Meng and Gerba 1996, Thurston-Enriquez et al. 2003). However, a viral ozonation study demonstrated that a Ct value of 0.6 mg L^{-1} min^{-1} (calculated Ct value at DWTP B) should be sufficient to inactivate adenovirus type 40 by at least 4.0-logs in treated water (Thurston-Enriquez et al. 2005). The disparity between our results and those of Thurston-Enriquez et al. (2005) makes it difficult to conclude on the extent to which full-scale ozonation processes may inactivate naturally occurring adenovirus. Poor mixing and hydraulic conditions have been found to reduce the inactivation of *E. coli* by full-scale ozonation processes (Smeets et al. 2006). The hydraulics of the full-scale ozonation system assessed in our study may also limit the reduction of adenovirus.

7.4.3 Kinetics aspects of flocculation for the removal of viruses

Short-term increases in removal performances by coagulation/flocculation were observed during raw water peak events for adenovirus at DWTP A, and for adenovirus, rotavirus, and JC virus at DWTP B. These results indicate that the performance of coagulation/flocculation is, to some extent, dependent on the raw water quality. Higher removal of rotavirus and JC virus by ballasted clarification was observed at raw water turbidity levels of 12-16 nephelometric turbidity units (NTU) (peak event) than at levels of 6-7 NTU (baselines conditions) (Tables 3, Table 4). However, adenovirus removal performances increased with the same trend as turbidity levels increased in the raw water. A hypothesis based on the Smoluchowski theory for particle coagulation can be advanced to explain these differences in performance.

According to Smoluchowski, the prediction of flocculation rates is a two-step process. First, a mathematical expression (size distribution function) is derived to keep particle count as a function of their size. Second, a collision rate coefficient based on a physical model (Brownian motion, fluid shear, differential sedimentation) is introduced into the expression that keeps counts of collisions (Han and Lawler 1992, Youn and Lawler 2019). The rate of irreversible heteroaggregation of a free virus particle can be calculated as following:

$$\frac{dn_i}{dt} = -\alpha_{ij}\beta_{ij}n_in_j \qquad (7.7)$$

where n_i is the concentration of i-sized free virus particles in raw water, n_j is the concentration of j-sized abiotic particles in raw water; α_{ij} is a collision efficiency coefficient; and β_{ij} is a collision rate coefficient. In natural aquatic environments, abiotic particles are typically present at much higher concentrations than viruses; thus, it can be assumed that $n_j \approx n_{j,0}$, where $n_{j,0}$ is the number of abiotic particle at $t = 0$. In this case, eq. 7.7 can be approximate by as a *pseudo-first-order* process:

$$\frac{dn_i}{dt} \approx -\alpha_{ij}\beta_{ij}n_{j,0}n_i \qquad (7.8)$$

Integrating once yields

$$n_i = n_{i,0}\exp\left(-n_{j,0}\alpha_{ij}\beta_{ij}t\right) \qquad (7.9)$$

where $n_{i,0}$ is the number of virus at $t = 0$. Even without knowing any details of α_{ij} and β_{ij}, it can be anticipated that the initial raw water abiotic particle concentration $n_{j,0}$ influence the aggregation rate of viruses during flocculation.

Kinetics equations accounting for the influence of a ballasted medium on the aggregation rate of particles have not been developed for ballasted clarification. However, it can be hypothesized that the initial raw water abiotic particle and the silica sand particles (ballasted medium) are both contributing to the aggregation of viruses. Higher removal performances by ballasted clarifiers have been reported at higher influent suspended solids concentrations at pilot-scale (Plum et al. 1998), and at higher influent turbidity levels at bench-scale (Lapointe et al. 2017). For conventional treatment, it has been demonstrated with population balance models using Smoluchowski coagulation equations that changes in raw water particle concentrations and size distributions can substantially influence the removal of submicron particles (Lawler et al. 1978, Lawler and Nason 2005). The characterization of particles in raw water using multiple parameters (turbidity, particle count, suspended solids) is therefore recommended for the assessment of virus removal performances by coagulation/flocculation processes.

Performances by floc blanket clarification (DWTP A) during two snowmelt episodes were lower than those observed with ballasted clarification (DWTP B) during baseline and event conditions. Virus removal performances by floc blanket clarification did not increase with raw water turbidity, but according to kinetic equations describing this process, such a relationship should not be expected. During floc blanket clarification, the microflocs produced during rapid mixing encounter a fluidized bed (quasi-stationary distribution of large flocs [10–100 µm]) maintained in suspension by the upward flow of the water. A single collector model based on colloid filtration theory was proposed to predict particles/flocs aggregation in the fluidized bed (Bache and Gregory 2007). The loss of i-incoming particles passing through a layer of j-collector is also given by eq. 7-8 with $\alpha \equiv \alpha_{pc} \times \eta_{pc}$, where α_{pc} is the particle-collector collision efficiency, and η_{pc} is the single collector collision efficiency. In contrast with kinetic equations for conventional flocculator, the concentration of flocs forming the fluidized bed (n_j) is not expected to vary temporarily. However, adenovirus removal performances increased proportionally to raw water adenovirus concentrations during the two events at DWTP A. The reason for this trend is unclear. Alum was dosed at a constant concentration of 44 mg L^{-1} throughout the first event (February 2017), but the dosage was increased from 49 to 53 mg L^{-1} during the second event (April 2017), which may have enhanced adenovirus removal. During both events, the capacity of the DWTP was stable at approximately 4.1×10^4 m^3 d^{-1}.

Dependence observed between source water virus concentrations and removal performances by high-rate clarifiers may have important implications for viral risk assessment at some DWTPs, especially if post disinfection is not present. The removal performance of a physical treatment process (log-removal) is commonly assumed to be a first-order process with respect to the influent concentration of the virus (i.e., the same fraction of viruses is removed regardless of the influent concentration) (Haas and Trussell 1998). The traditional approach might be inadequate if the flocculation performance is correlated with the concentration of particles in raw water. Nonetheless, these findings are site-specific and only represent conditions observed during three hydrometeorological events. Larger data sets would be needed to conduct statistical analysis. Basic research on the impact of water quality parameters and floc densification on the aggregation of viruses could be valuable to enable site-specific and potentially dynamic assessments.

7.4.4 Limitations for the quantification of virus concentrations

Spatial heterogeneity of viruses may have an impact on the quantification log-removal during full-scale treatment. In this study, viral genome-copies were assumed to be Poisson distributed in all samples. Overdispersion was not evaluated because sample replicates were not collected, but large-volume samples were used for concentrating the viruses in the samples (>300 L), which should minimize this source of uncertainty. Samples were all collected under stable operation conditions (turbidity < 0.1 NTU at individual filter effluents). Nevertheless, the removal of viruses through a filter cycle may be more dynamic than the filter effluent turbidity. Nilsen et al. (2019) recently showed at pilot-scale that, even if the filter effluent turbidity was <0.1 NTU, the removal performance of phages MS2 and 28B by dual-media contact filtration varied by about 1.5-log during the ripening and the breakthrough phase. The occasional high concentrations of adenovirus and rotavirus in the combined effluent from all the filters and in the UV disinfected water at DWTP B may originate from sampling during such phases.

Owing to the limitations in analytical viral recovery data in the full-scale treatment, the uncertainty in method recovery performance was incorporated in virus concentration estimates using a beta distribution of recovery rates reported by Pang et al. (2012). The same laboratory recently reported slightly lower recovery rates (human adenovirus 2/4, n=28; mean=0.14, STD=0.14; norovirus GII, n=10, mean=0.10, STD=0.06) for wastewater samples subjected to secondary treatment (Li et al. 2019). Monitoring the efficiency of the virus concentration step with a process control could increase the accuracy of virus concentration estimates in raw water during hydrometeorological events (Hata et al. 2014). Recovery rates for samples collected after treatment processes may also differ from those measured in raw water because of changes in matrix composition, although Pang et al. (2012) did not observe significant differences in recovery rates among pure, tap and raw water samples for two RNA viruses (norovirus and echovirus) and one DNA virus (adenovirus 41). Nevertheless, the presence of alum and silica sand in settled water may influence analytical recovery efficiencies.

The presence of viral genomes after ozonation and UV disinfection is challenging to interpret because encapsidated genomes and free nucleic acids can be detected. Infectious rotaviruses in raw water were usually not detected by ICC-qPCR unless high concentrations of those viruses were present in raw water (>10^4 genome-copies L^{-1}). One of the reasons is that human rotavirus does not

propagate efficiently in the continuous in vitro cell lines we used (MA104 and BGM) (Ward et al. 1984, Arnold et al. 2009). ICC-qPCR has limited value to assess the inactivation of viruses in water samples because this method only indicates the absence/presence of an infectious virus. Serial dilutions of wastewater and source water samples have recently been carried out to quantify human infectious virus concentrations by ICC-qPCR with the most probable number (MPN) method (Qiu et al. 2018, Schijven et al. 2019); however, concentrations of naturally occurring viruses throughout full-scale drinking water treatment train may be too low for quantification using dilutions. Considering these limitations, the fact that positive infectious adenoviruses were found in treated water after a combination of advanced treatment processes point to the need to develop improved infectious virus detection methods.

7.5 Conclusion

Two full-scale drinking water treatment plants in Quebec, Canada, were selected to assess the extent of virus removal during periods of high viral contamination in raw water during three hydrometeorological snowmelt events. The following conclusions are drawn:

- Event-based sampling using GLUC activity measurements as a guide indicated that concentrations of enteric viruses during snowmelt freshet were about 1.0-log higher than concentrations under baseline conditions. Maximum virus concentrations in raw water during these periods were approximately 10^5 genome-copies L^{-1} for rotavirus and adenovirus, and 10^4 genome-copies L^{-1} for norovirus GII and JC virus, which was approximately 2.0-log lower than virus concentrations in raw sewage;

- Removal performances by coagulation/flocculation processes under these conditions were virus-type specific;

- Increases in full-scale removal performance of adenovirus by floc blanket clarification and of adenovirus and rotavirus by ballasted clarification were observed during peak virus concentrations in raw water;

- Limited effectiveness of UV disinfection against naturally occurring adenovirus was observed at current operative doses of 40 mJ cm^{-2} after a combination of ballasted clarification, ozonation, GAC filtration.

The observed dependency between influent concentrations and process removals has important ramifications for viral risk assessment. Typically, the reduction performance is assumed to be a first-order process with respect to the influent concentration of the virus (i.e., the same fraction of viruses is removed regardless of the influent concentration). This common assumption might be inadequate if flocculation mechanisms allow for higher removal performances during transient peaks in raw water contamination. As our results may be site-specific, larger data sets would be needed to validate these observations. Basic research on the impact of water quality parameters and floc densification on the aggregation of viruses could be valuable to enable site-specific and potentially dynamic assessments.

Finally, results from this study support the use of adenovirus as a reference viral pathogen for risk assessment in urban rivers. More performance demonstrations over a wide range of raw water virus concentrations are needed to quantitatively and reproducibly evaluate full-scale virus removal achieved by drinking water treatment processes.

7.6 Acknowledgments

CHAPTER 8. USING SURROGATE DATA TO ASSESS MICROBIAL RISKS ASSOCIATED WITH HYDROMETEOROLOGICAL EVENTS FOR DRINKING WATER SAFETY

This Chapter presents an adaptation of the event-based monitoring strategy presented in Chapter 7. The reduction of surrogate microorganisms by full-scale treatment processes is evaluated during baseline and event (rainfall, snowmelt freshet) raw water conditions at two drinking water treatment plants. Site-specific source water pathogen data and full-scale surrogate organism reduction data are then inputted into a quantitative microbial risk assessment (QMRA) model to assess daily risks of infection for different source water conditions. This article will be submitted to *Water Research*.

Abstract

Microbial reduction performances of full-scale drinking water treatment processes were evaluated at an urban and an agricultural site during baseline and event (rainfall, snowmelt) conditions. Online monitoring of β-D-glucuronidase activity was used to identify peak faecal contamination events at the source. Sequential high volume (50-1500 L) grab samples were collected to evaluate the reduction performance of coagulation/flocculation, filtration, ozonation, and UV disinfection processes, and analyzed for two surrogate organisms: *Escherichia coli* and *Clostridium perfringens*. Site-specific source water *Cryptosporidium* and *C. perfringens* reduction data were entered into a quantitative microbial risk assessment (QMRA) model to estimate daily infection risks by *Cryptosporidium* via the consumption of drinking water. This sampling strategy enabled the detection of daily mean source water *E. coli* concentrations in the top 15% of what occurs through the year based on historical routine monitoring data. Full-scale reduction performances of up to 6.0-log for *E. coli* and 5.6-log for *C. perfringens* were measured. Increased reduction of *E. coli* and *C. perfringens* by ballasted clarification and rapid sand filtration compensated for the augmented concentrations in raw water during events. As a result, daily infection risks by *Cryptosporidium* were not higher during events than during baseline conditions based on *C. perfringens* reduction data. Our findings suggest that that physical treatment processes optimized for turbidity reduction can effectively manage short-term increases in raw water microbial quality.

8.1 Introduction

Recent developments in drinking water quality management in Canada and abroad resulted in a shift from the traditional focus on end-product by faecal indicator bacteria (FIB) monitoring to a preventive, risk-based approach covering source to exposure (WHO 2004). To implement a risk-based approach, quantitative information is needed on reduction by water treatment processes during normal operating conditions but also during period of poor source water quality (Bartram et al. 2001). Hydrometeorological events, such as heavy rainfall, are known to be detrimental to surface water quality by increasing microbial concentrations as well as natural organic matter (NOM) concentrations and turbidity (Atherholt et al. 1998, Kistemann et al. 2002, Hurst et al. 2004, Dorner et al. 2007). However, identifying transient peaks in faecal contamination in raw water has proven to be difficult because of a lack of rapid detection methods. Recently, on-site β-D-glucuronidase (GLUC) activity *in situ* monitoring was used to successfully characterize microbial

peaks in surface water (Burnet et al. 2019b, Cazals et al. 2020, Sylvestre et al. 2020a). Yet, this technology has not been employed to guide the assessment of full-scale reduction of surrogate microorganisms by drinking water treatment processes.

To evaluate full-scale treatment performances, surrogate microorganisms are typically selected for each pathogen class. An ideal surrogate should be similar in size, surface properties and persistence to the pathogen being targeted (WHO 2016b). Furthermore, the surrogate should be present in environmental waters at relatively high concentrations for its detection through treatment barriers (Ashbolt et al. 2001). Pre-concentration methods of large volumes of water for on-site isolation are usually required to quantify the progressive removal of surrogates and pathogens through full-scale treatment trains (Payment et al. 2002, Hijnen et al. 2007). Spores of sulfite-reducing clostridia (including *Clostridium perfringens*) have been shown to be a conservative surrogate for index protozoan pathogens (*Cryptosporidium* and *Giardia*) removal through conventional treatment (Payment and Franco 1993, Hijnen et al. 2000). *Clostridium perfringens* (*C. perfringens*) is currently recommended as a surrogate organism for protozoan pathogens in World Health Organization (WHO) guideline and guidance documents (WHO 2016b, 2017b). Thermotolerant coliforms (including *Escherichia coli*) were found to be a proper surrogate for an index bacterial pathogen (*Campylobacter*) removal by rapid sand filtration (Hijnen et al. 1998) and inactivation by ozonation (Smeets and Medema 2006).

The objective of this study was to undertake a high-resolution investigation of the reduction performance of surrogate microorganisms by full-scale treatment processes at two drinking water treatment plants during baseline and event (rainfall, snowmelt freshet) raw water conditions. An approach was developed that involved: (i) using online GLUC activity measurements to identified critical periods of microbial contamination in raw water; (ii) concentrating large water volumes to quantify the reduction of surrogate organisms throughout the treatment train; (iii) inputting site-specific source water pathogen data and full-scale surrogate organism reduction data into a quantitative microbial risk assessment (QMRA) model to assess daily risks of infection for different source water conditions.

8.2 Material and methods

8.2.1 Catchment and drinking water treatment description

Unit processes present in the treatment trains of drinking water treatment plants (DWTPs) A and B and the location of sampling points are illustrated in Figure 8-1. Supervisory Control and Data Acquisition (SCADA) data (flow rate, coagulant dosage, turbidity, pH, disinfectant residual, and temperature measurements) were obtained to relate these parameters with the observed reduction of microorganisms.
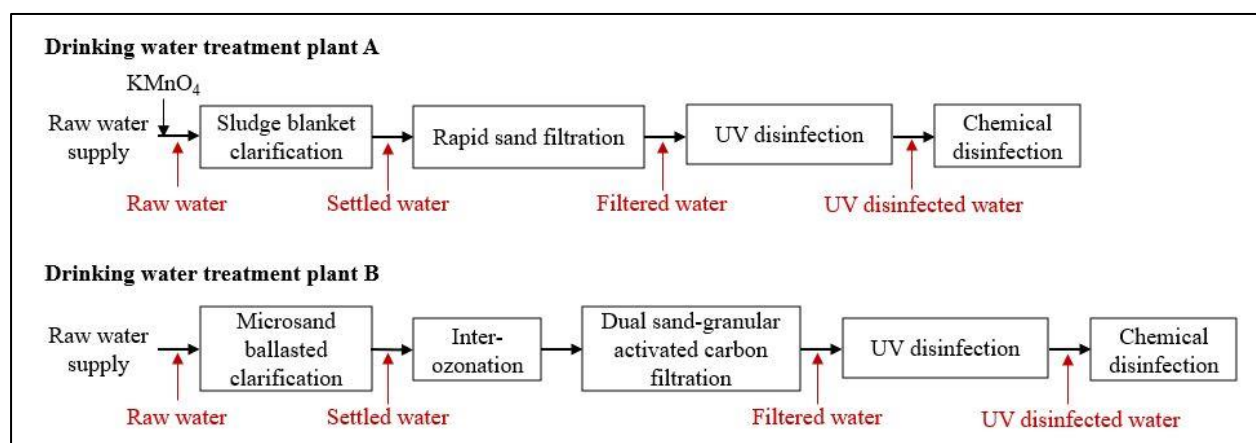
Figure 8-1:Unit processes involved in the treatment chain of drinking water treatment plants A and B and the location of sampling points (red)

8.2.1.1 Agricultural drinking water treatment plant A

DWTP A abstracts raw water from a small agricultural river (annual average flow rate of the river is 16 m^3/s) situated in southern Quebec. The microbial water quality of raw water at DWTP A can be influenced by four combined sewer overflows (CSOs) and a municipal wastewater treatment plant (WWTP) discharging 10 kilometers upstream of the drinking water intake. At the WWTP, human sewage is treated through an aerated pond and discharged in the river at an average rate of 10,000 m^3/day. Cattle and swine manures are applied for agriculture in the catchment area, with buffer strips of at least 3 meters from the river being required (Gouvernement du Québec, 2018). During the sampling campaigns, DWTP A was operated at a capacity of approximately 3,500 m^3 d^{-1}, about 20% of the design rate (18,000 m^3 d^{-1}). During water treatment, potassium permanganate (KMnO$_4$; 0.6 mg L^{-1}) was first added to the raw water. After permanganate oxidation,

polyaluminum chloride (PACl; PAX-XL8: 110 mg L^{-1}) and cationic polyacrylamide (C-492; dosing rate: 0.11 mg L^{-1}) were added in water at pH 6.2 and temperature of approximately 10°C and processed by Ultrapulsator® floc blanket clarification (Suez, Quebec, Canada). The settled water was then filtered by four single-media sand filters (0.8 m h^{-1}; 140 cm sand) and disinfected by a medium pressure UV system (fluence: 40 mJ cm^{-2}; Trojan UV Swift; Trojan Technologies, Schöllkrippen, Germany) and chlorine dioxide (ClO$_2$).

8.2.1.2   Urban drinking water treatment plant B

Located in the greater Montreal area, DWTP B is supplied by the Mille Îles river, an urban river with an annual average flow rate of the river of 286 m^3/s. The Mille Îles river is a channel of the Ottawa river, which drains an area of about 146,300 km^2. The river is also under the direct influence of a series of small local dense urban watersheds totalling 1,190 km^2. Around 180 combined sewer overflows (CSOs) and 14 municipal WWTPs (mostly aerated ponds or combined biological and physicochemical treatment) can discharge in the river and its tributaries during the snowmelt freshet (typically from February to April). Tributaries of the river also drain agricultural lands, which potentially contribute to microbial contamination from livestock.

DWTP B was operated at a capacity of 46,800 m^3 d^{-1}, about 40% of the design rate (120,000 m^3 d^{-1}). During the sampling period, alum (Al$_2$(SO$_4$)$_3$; dosing rate:15 mg L^{-1}), polyaluminosilicate-sulfate (PASS-10; dosing rate: 50 mg L^{-1}), cationic polyacrylamide (dosing rate: 0.25 mg L^{-1}) and silica sand (SiO$_2$; dosing rate: 4 g L^{-1}) were dosed in 1°C raw water at pH 6.7 and processed by ACTIFLO® microsand ballasted clarification (Veolia Water Technologies, Quebec, Canada) operated at a superficial velocity of 40 m/h. The settled water was then disinfected by inter-ozonation (dosing rate:1.0 mg L^{-1} O$_3$; Ct$_{10}$: 0.6 mg L^{-1} min^{-1}) for 20-22 minutes and filtered by ten dual sand and granular activated carbon (GAC) filters (10 m h^{-1}, 15 cm sand-bottom and 140 cm activated carbon-top). Filtered water was then disinfected with a low pressure (LP, λ = 254 nm) UV system (fluence: 40 mJ cm^{-2}; Wedeco BX 3200; Xylem Water Solutions, Herford, Germany) and sodium hypochlorite (NaOCl).

8.2.2 Sampling campaigns

8.2.2.1 Routine monitoring

Weekly monitoring raw water *E. coli* data collected between 2013 and 2017 were analyzed to identify periods of high faecal contamination at the selected DWTPs. The statistical modeling of these datasets is presented elsewhere (Sylvestre et al. 2020a). Statistical characterization of empirical distributions of *E. coli* concentrations is shown in Table 8-1.

Table 8-1: Statistical characterization of empirical distribution of *E. coli* concentration in raw water (*E. coli*/100 mL) at drinking water treatment plants A and B

Site	n	Arithmetic mean	Median	Standard deviation (SD)	Mean absolute deviation (MAD)	Ratio SD/MAD	Skewness	Excess kurtosis
A	245	386	64	1168	523	2.23	4.89	25.56
B	437	318	170	668	272	2.46	10.70	155.88

8.2.2.2 Baseline and event-based monitoring

An automated rapid on-site monitoring system (ColiMinder^{TM} VWM GmbH, Vienna, Austria) was installed at each DWTP around one month before carrying out the sampling campaigns to measure usual background variations in raw water β-D-glucuronidase (GLUC) activity. Automated sampling was set to frequencies varying between 1 and 3 hours to ensure the characterization of short-term fluctuations reflecting hydrometeorological events.

At DWTP A, three baseline sampling campaigns were carried out during dry weather conditions (no rainfall in the last 48 hours), and one event-based sampling campaign was triggered by the combination of rainfall (48-hour total rainfall >40 mm) and a short-term increase in GLUC activity concentrations (variation > +5 mMFU 100 mL^{-1} over 1 hour). A trigger of 5 mMFU mL^{-1} was set based on short-term increases in GLUC activity measured during previous hydrometeorological events at this DWTP. Single grab sample (baseline condition) or sequential grab samples (event condition; n=3) of raw, settled (200 L), filtered (1000 L), and UV disinfected (1500 L) waters were collected to match theoretical mean hydraulic residence times through clarification (3 hours), filtration and UV disinfection (2 hours) (A. Verroneau, *personal communication*). Additionally, during event conditions, six 30 to 40 liter-samples of raw water were filtered on-site over 24 hours

to estimate the daily mean *Cryptosporidium* concentration. A detailed description of this *Cryptosporidium* dataset is presented elsewhere (Sylvestre et al. 2020b).

The sampling strategy was adjusted at DWTP B because a short-term increase in the GLUC activity level (+20 mMFU mL^{-1} over 48 hours) was measured in dry weather conditions (no rainfall or snowmelt in the last 48 hours) in late February 2018. Baseline and event conditions were thereby defined based on a fixed trigger of 40 mMFU mL^{-1}. Three baseline sampling campaigns (GLUC activity < 40 mMFU mL^{-1}) and one event-based sampling campaign (GLUC activity > 40 mMFU mL^{-1}) were carried out. Single grab sample (baseline condition) and sequential grab samples (event condition; n=4) of raw, settled (200 L), filtered (1000 L), and UV disinfected (1500 L) waters were collected to match theoretical mean hydraulic residence times through clarification (0.5 hours), ozonation, filtration, and UV disinfection (1.5 hours) (M. Marchand, *personal communication*). Additionally, three grab 25 to 30 liter-samples were filtered on-site over 4 days to estimate the mean *Cryptosporidium* concentration in raw water during the targeted event. Single grab 25 liter-samples were also collected during baseline campaigns to estimate *Cryptosporidium* concentration in raw water.

Mean *E. coli* concentrations evaluated during baseline and event conditions were compared to the median *E. coli* concentrations calculated with routine monitoring data. The median was selected as a summary statistic to represent faecal contamination level during typical source water conditions.

8.2.3 Sample concentration

Raw water samples were concentrated with Hemoflow HF80S filters (Fresenius, Ontario, Canada) for the enumeration of *Cryptosporidium*. Concentrates were shipped overnight in coolers at 4 °C to the Centre d'expertise en analyse environnementale du Québec (CEAEQ) in Quebec City, QC, and processed within 48 hours of sampling. The Hemoflow concentration method was also used to simultaneously concentrate *E. coli* and *C. perfringens* spores in raw, settled, filtered and UV-disinfected raw water samples. One tank was filled with 50 L of settled water and multiple tanks of 1000 L were filled with 1000-1500 L of filtered or UV disinfected water. From these tanks, the water was pumped through the Hemoflow HF80S filter (Fresenius, Ontario, Canada) at a minimum speed of 4 liters per minute. The overpressure over the filter was increased to a maximum of 0.7 bar until the water filtrate was pressed through the walls of the straws with a speed of around 0.9

L/min (Veenendaal and Brouwer-Hanzens 2007). Installations with four Hemoflow-filters in parallel were built to concentrate large water volumes more rapidly (<6.5 hours) (Figure 8-2). The concentration process was stopped when the concentrate volume only filled the hoses. Filtrate water was pumped through the hoses once and then collected in a sterile bottle. The total end volume was approximately 600 mL. Samples were kept at 4 °C and analyzed within 24 hours. The recovery rate of the Hemoflow concentration method was evaluated for raw water samples collected at each DWTP. The recovery rate was calculated as the ratio of the concentration of the surrogate in an un-concentrated (grab) sample to its concentration in a Hemoflow concentrated sample (100 L at DWTP A and 20 L at DWTP B). At DWTP A, recovery rates of 103% for *E. coli* and 125% for *C. perfringens* were measured for raw water samples. At DWTP B, a recovery rate of 124% was measured for *C. perfringens* in raw water. No recovery rate was determined for *E. coli* at DWTP B. Recovery rates from settled, filtered, and UV disinfected water samples were not measured. Recovery rates of 100% were assumed for the calculations of all *E. coli* and *C. perfringens* concentrations.

Figure 8-2: Installations with four Hemoflow-filters in parallel for the rapid concentration of microorganisms in large volumes of water

8.2.4 Sample processing and analysis

Volumes of Hemoflow-filter eluates for the enumeration of oocysts of *Cryptosporidium* were approximately 500-700 mL. Post-concentration was carried out by centrifugation to obtain a final volume between 20 and 50 mL and a packed pellet volume between 2 and 5 ml. Between 20 and

50% of the packed pellet volume was then processed by immunomagnetic separation (IMS), before sample staining and examination following USEPA method 1623.1. Sample-specific recovery rates were measured for each sample collected during baseline and event-based campaigns. Fluorescently labeled controls (Colorseed[TM]) were spiked at a target dose of 98-100 (oo)cysts in the raw water sample before careful manual mixing and on-site concentration using the Hemoflow method.

Volumes of Hemoflow-filter eluates for the enumeration of surrogate organisms were approximately 500-700 mL. From these volumes, two aliquots of 100-200 mL were taken for the detection of *E. coli* and *C. perfringens* spores. *E. coli* was enumerated by membrane filtration using modified membrane-thermotolerant *E. coli* agar (modified mTEC) (EPA method 1603), with plate counts on EC-MUG medium (APHA 2005), or by the defined substrate technology using the IDEXX Quanti-Tray/2000 System with Colilert reagent (APHA 2005). Three tenfold serial dilutions (0.1, 0.01, 0.001) were applied with the modified mTEC method to obtain countable ranges of 20-80 CFUs per plate, and two tenfold serial dilutions (0.1, 0.01) with countable ranges of 1-2419 MPN/100 mL were carried out with Colilert. Spores of *C. perfringens* were enumerated on m-CP medium as described previously (Armon and Payment 1988).

8.2.5 Quantification of reduction by treatment processes

The reduction performance of each treatment process was evaluated by comparing the inflow concentration (C_{in}) and the outflow concentration (C_{out}) of the surrogate organism. Point estimates of reduction (i.e., removal or inactivation) representing the log-reduction (LR) across a treatment unit (paired sample) were calculated by the following equation:

$$\text{LR} = \log_{10}\left(\frac{C_{in}}{C_{out}}\right) \qquad (8.1)$$

The average percent reduction, expressed as effective log-reduction ($\text{LR}_{\text{effective}}$), during event conditions was calculated as follows:

$$\text{LR}_{\text{effective}} = \log_{10}\left(\frac{\bar{C}_{in}}{\bar{C}_{out}}\right) \qquad (8.2)$$

The standard error of the mean log-reduction ($\sigma_{\overline{\text{LR}}}$) was evaluated to provide a simple measure of uncertainty in the LR. It can be regarded as the dispersion of the LR across a treatment unit (paired sample) around the mean LR. The standard error was calculated as follows:

$$\sigma_{\overline{\text{LR}}} = \frac{S_{\text{LR}}}{\sqrt{n}} \tag{8.3}$$

where S_{LR} is the standard deviation of all LRs evaluated across a treatment unit (paired sample) and n is the sample size. For simplicity's sake, each treatment step of the DWTP was assumed to behave as a plug-low reactor operated hydraulically at a steady state during the sampling period.

8.2.6 Quantitative microbial risk analysis for *Cryptosporidium*

Site-specific raw water *Cryptosporidium* data and *C. perfringens* reduction data were entered in a QMRA model to quantify daily risks of infection by *Cryptosporidium* via consumption of municipally treated drinking water. A linear low-dose approximation to the single-hit dose–response relationship was adopted to simplify calculations (WHO 2016b, 2017b). The risk of infection associated with an exposure to more than one oocyst was assumed to be negligible. The daily probability of infection during baseline conditions was calculated as follows:

$$\text{P}_{\text{inf.baseline}} = C_{\text{baseline}} \cdot 10^{-\text{LR}_{\text{baseline}}} \cdot \text{V} \cdot \text{r} \tag{8.4}$$

where C_{baseline} is the *Cryptosporidium* concentration in raw water during baseline conditions, $\text{LR}_{\text{baseline}}$ is the total reduction of *C. perfringens* by treatment processes during baseline conditions, V is the ingested volume of drinking water per person per day, and r is the probability that any single ingested *Cryptosporidium* oocyst succeeds in infecting the host. C_{baseline} were not measured at DWTP A, thereby it was assumed that C_{baseline} was the sample arithmetic mean *Cryptosporidium* concentration in raw water evaluated with monthly sampling for two years. The daily probability of infection during event conditions was evaluated as follows:

$$\text{P}_{\text{inf.event}} = \bar{C}_{\text{event}} \cdot 10^{-\overline{\text{LR}}_{event}} \cdot \text{V} \cdot \text{r} \tag{8.5}$$

where $\bar{C}_{\text{event}}$ is the mean *Cryptosporidium* concentration in raw water during event conditions and $\overline{\text{LR}}_{event}$ is the reduction of *C. perfringens* by treatment processes during event conditions. It was

conservatively assumed that: 1) all detected *Cryptosporidium* oocysts in raw water were human infectious, 2) the reduction of bacterial spores was equivalent to the reduction of oocysts (Teunis et al. 1997, Barbeau et al. 2000), and 3) free chlorine did not inactivate *Cryptosporidium parvum* oocysts (Venczel et al. 1997). The ingested volume V was set to 1 liter per person per day (WHO 2017b). The single oocyst infectivity r was set to 0.2 as recommended in WHO (2017b). A r of 0.2 represents the mode of the predictive distribution of the expected value of the single *Cryptosporidium parvum* oocyst infectivity obtained by fitting a two-level hierarchical hypergeometric dose-response model (variation within and between isolates) to data from four isolates (Iowa, TAMU, UCP and Moredun) (WHO 2009a).

E. coli reduction data were not entered in a QMRA model because concentrations of bacterial pathogens in source water were not available and *E. coli* reductions by chlorine disinfection processes were not measured. However, the risk of infection by bacterial pathogens should be very low at these sites because, in general, bacteria are very sensitive to chlorine (Petterson and Stenström 2015).

8.3 Results

8.3.1 Agricultural drinking water treatment plant A

The GLUC activity in raw water during dry weather conditions (no rainfall in the last 48 hours) decreased from 30 mMFU/100 mL in mid-October to around 5 mMFU/100 mL at the beginning of November (Figure 8-3A). Four peaks in GLUC activity of similar duration (approximately 24 hours) but of different amplitudes (40-160 mMFU/100 mL) were measured after rainfall events. The amplitudes of these peaks decreased over the evaluated period. Mean *E. coli* concentrations in raw water measured during baseline conditions (781 *E. coli*/100 mL, $n=3$) and event conditions (3,543 *E. coli*/100 mL, $n=6$) were 1.0-log and 1.7-log higher, respectively, than the median *E. coli* concentration evaluated with weekly monitoring (64 *E. coli*/100 mL, $n=245$) (Table 8-1, Figure 8-4A). Mean *C. perfringens* concentrations in raw water were 0.5-log higher during event conditions (109 CFU/100 mL, $n=6$) than during baseline conditions (39 CFU/100 mL, $n=3$).
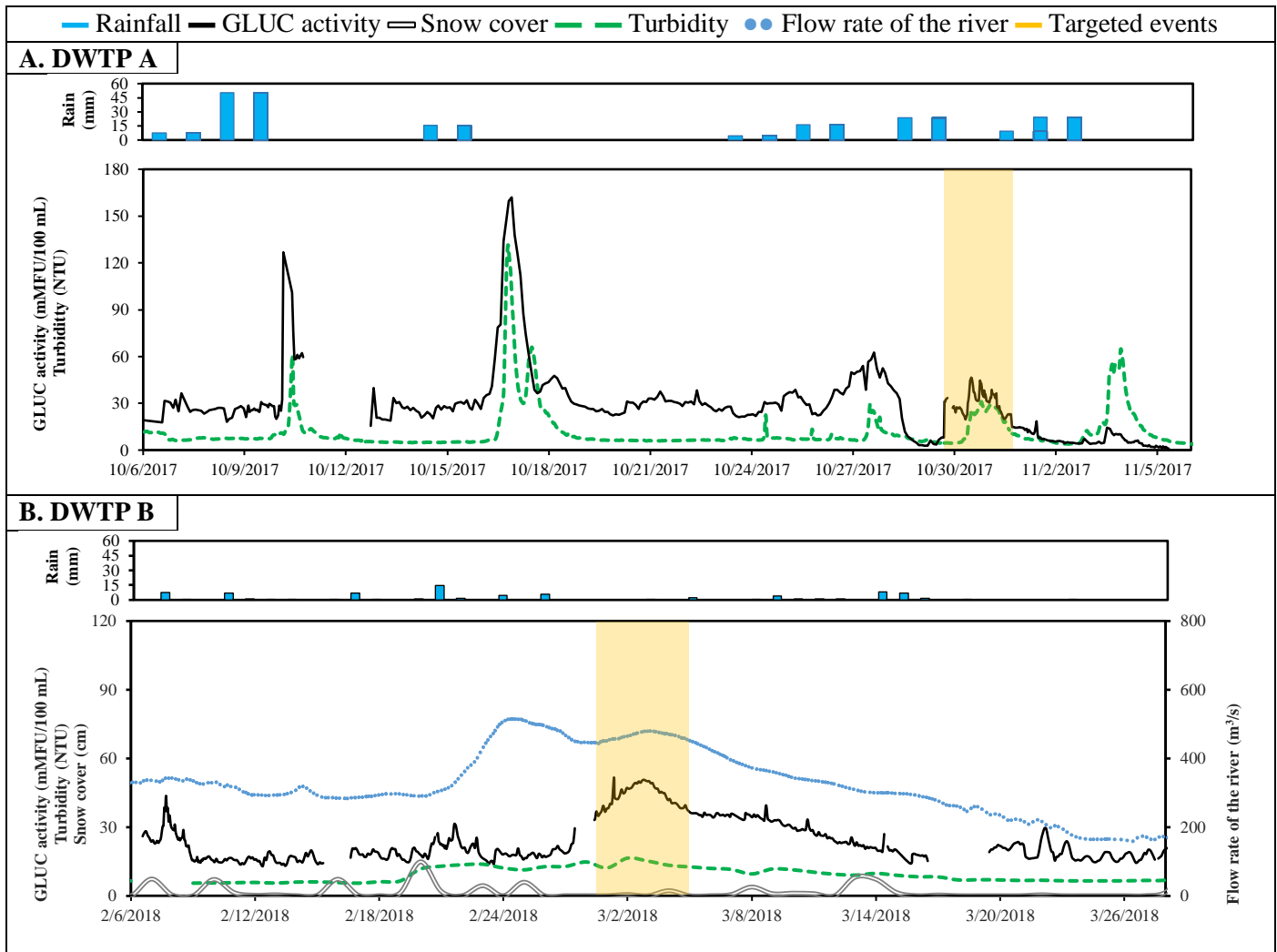
Figure 8-3: Time series of daily rainfall, GLUC activity, snow cover on the ground, raw water turbidity, and flow rate of the river during snowmelt freshet at intakes of drinking water treatment plants A and B. Yellow rectangles indicate targeted events.
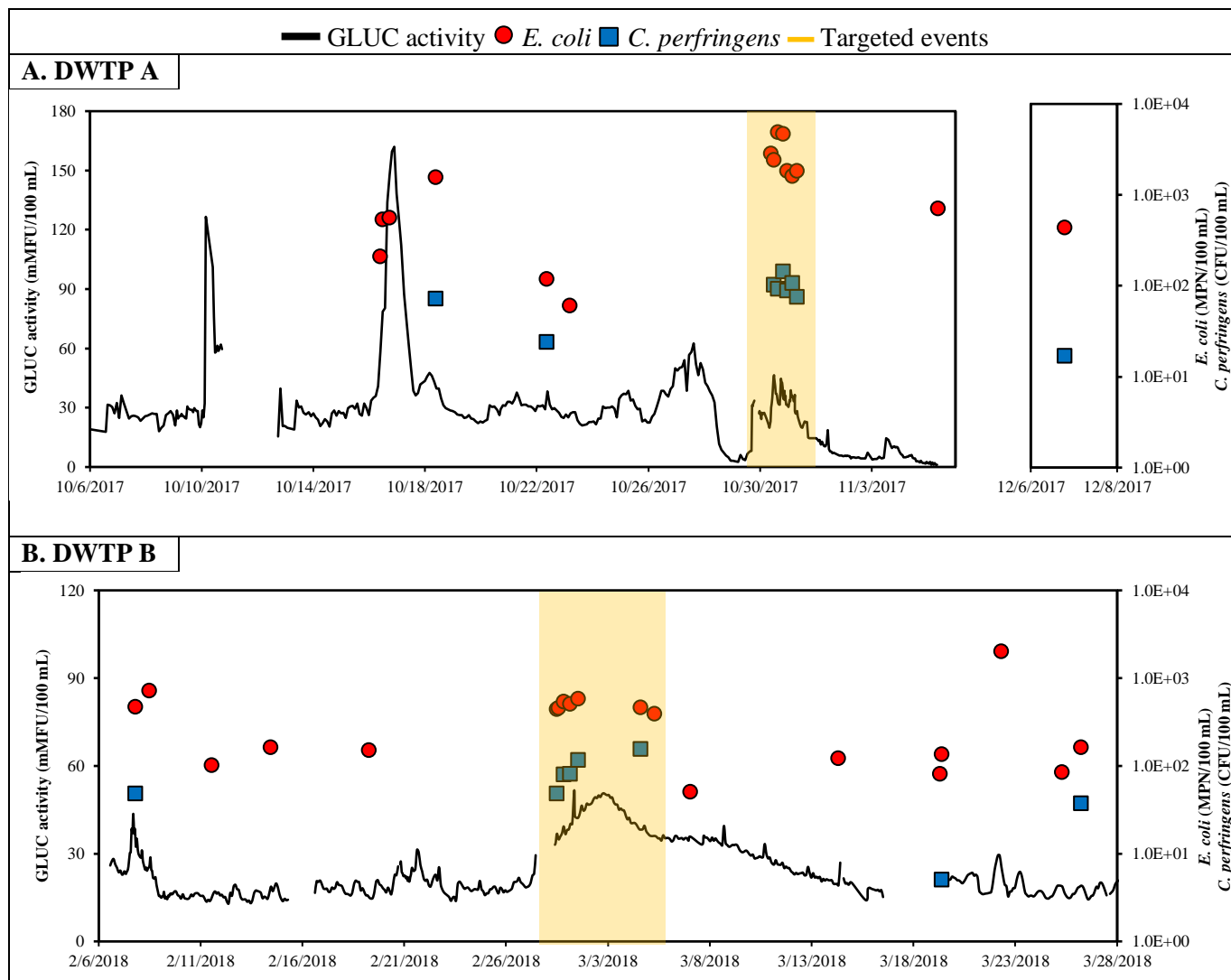
Figure 8-4: Time series of the GLUC activity and surrogate microorganism concentrations in raw water at intakes of drinking water treatment plants A and B. Yellow rectangles indicate targeted events.

E. coli was detected in all filtered water samples (*n*=6) and *C. perfringens* was detected in all filtered and UV-disinfected water samples (*n*=6) (Figure 8-5). *E. coli* concentrations after UV-disinfection were not considered because autofluorescence in these samples potentially led to false-positive results. Maximum reduction performances of 4.7-log and 5.5-log were quantified for *E. coli* and *C. perfringens*, respectively (Table 8-2). Effective log-reductions by floc blanket clarification were around 3.0-log for both surrogate organisms during baseline and event conditions. The hourly abstraction flow rate and the turbidity of settled water were similar during baseline and event conditions (Table 8-3). The water temperature was around 10°C lower during one baseline campaign (baseline-03) than during the other baseline and event-based campaigns.

The standard errors of the mean log-removal ($\sigma_{\overline{LR}}$) were higher for rapid sand filtration than for floc blanket clarification. Overall, UV disinfection had a negligible effect on the inactivation of *C. perfringens*. The total effective log-reduction of *C. perfringens* by treatment processes were similar in baseline (4.3-log) and event conditions (4.5-log), but the standard error on the log-removal was higher for baseline conditions ($\sigma_{\overline{LR}}$=0.4-log) than for event conditions ($\sigma_{\overline{LR}}$=0.1-log).

Short-term variations in the log-removal of surrogate organisms and turbidity by floc blanket clarifiers and rapid sand filters during the event are illustrated in Fig. 8-6A. Removal performances did not deteriorate.

The daily infection risks for *Cryptosporidium*, calculated using the *C. perfringens* reduction performance results, are shown in Table 8-4. The daily infection risk during event conditions was 0.3-log lower than during the second baseline campaign, even if the mean *Cryptosporidium* concentration was 0.6-log higher during event conditions than during routine monitoring conditions.
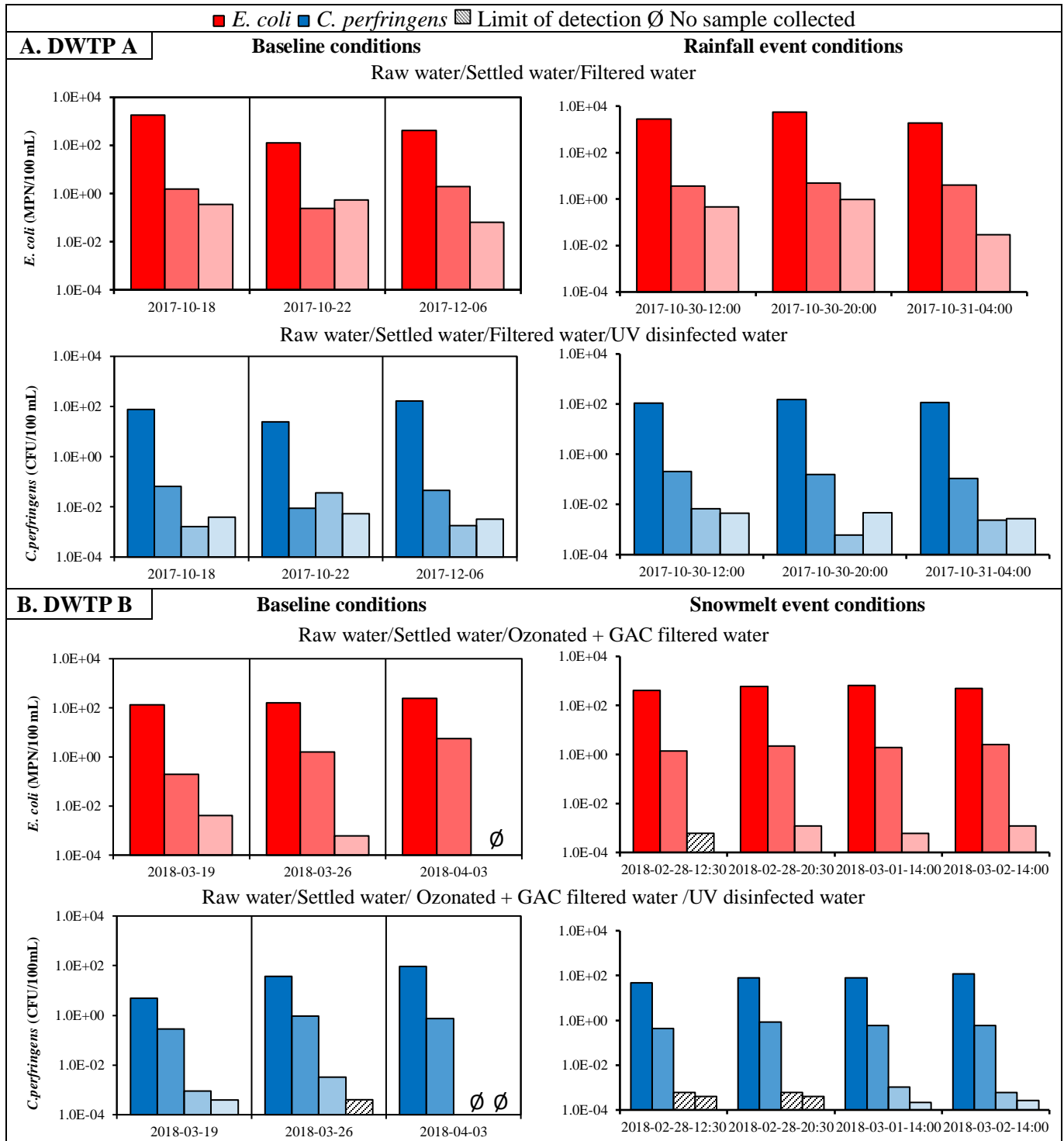
Figure 8-5: Reduction of surrogate microorganisms by subsequent treatment processes during baseline and event conditions at drinking water treatment plants A and B

Table 8-2: Log-reduction of *E. coli* and *C. perfringens* by treatment processes during baseline and event conditions at drinking water treatment plants A and B. $LR_{effective}$ is the effective log-reduction during event condition. $\sigma_{\overline{LRV}}$ is the standard error on the mean log-reduction.

DWTP A				
Sample id.	**FBC[A]**	**RGF[B]**	**UV**	**Total**
C. perfringens				
Baseline-01	3.0	1.6	-0.4	4.2
Baseline-02	3.4	-0.6	0.8	3.6
Baseline-03	3.5	1.4	-0.2	4.9
Baseline-$LR_{eff.}$	3.3	0.5	0.5	4.3
Baseline-$\sigma_{\overline{LR}}$	0.2	0.7	0.4	0.4
Event-01	2.7	1.5	0.2	4.4
Event-02	3.0	2.4	-0.9	4.5
Event-03	3.0	1.6	0.0	4.6
Event-$LR_{eff.}$	2.9	1.7	-0.3	4.5
Event-$\sigma_{\overline{LR}}$	0.1	0.3	0.3	0.1
E. coli				
Baseline-01	3.0	0.6	-	-
Baseline-02	2.7	-0.3	-	-
Baseline-03	2.3	1.5	-	-
Baseline-$LR_{eff.}$	2.8	0.6	-	-
Baseline-$\sigma_{\overline{LR}}$	0.2	0.5	-	-
Event-01	2.8	0.9	-	-
Event-02	3.0	0.7	-	-
Event-03	2.6	2.1	-	-
Event-$LR_{eff.}$	2.9	1.2	-	-
Event-$\sigma_{\overline{LR}}$	0.1	0.4	-	-

DWTP B				
Sample id.	**BC[C]**	**O_3+RGF$_{GAC}$[D]**	**UV**	**Total**
C. perfringens				
Baseline-01	1.2	2.5	0.3	4.0
Baseline-02	1.6	2.4	1.2	5.2
Baseline-03	2.1	-	-	-
Baseline-$LR_{eff.}$	1.8	2.4	0.8	4.7
Baseline-$\sigma_{\overline{LR}}$	0.3	0.1	0.5	0.6
Event-01	2.0	2.8	0.2	5.0
Event-02	2.0	3.1	0.2	5.3
Event-03	2.1	2.8	0.7	5.6
Event-04	2.3	3.0	0.3	5.6
Event-$LR_{eff.}$	2.1	2.9	0.3	5.4
Event-$\sigma_{\overline{LR}}$	0.0	0.1	0.1	0.1
E. coli				
Baseline-01	2.8	1.7	-	-
Baseline-02	2.0	3.4	-	-
Baseline-03	1.6	-	-	-
Baseline-$LR_{eff.}$	1.9	2.5	-	-
Baseline-$\sigma_{\overline{LR}}$	0.2	0.8	-	-
Event-01	2.4	3.3	-	-
Event-02	2.4	3.2	-	-
Event-03	2.5	3.5	-	-
Event-04	2.3	3.3	-	-
Event-$LR_{eff.}$	2.4	3.4	-	-
Event-$\sigma_{\overline{LR}}$	0.0	0.1	-	-

[A] Floc blanket clarification
[B] Rapid sand filtration
[C] Ballasted clarification
[D] Ozone and granular activated carbon filtration

Table 8-3: Hourly flow rate, water temperature and turbidity of raw water and settled water during baseline and event conditions at DWTPs A and B

| | Sample id. | Hourly flow rate (m³/h) | Water temp. (°C) | Turbidity (NTU) | |
				Raw water	Settled water
DWTP A	Baseline-01	190	11	6.92	0.06
	Baseline-02	116	12	6.28	0.08
	Baseline-03	117	3	43.86	0.16
	Event-01	124	12	25.80	0.20
	Event-02	126	11	28.60	0.10
	Event-03	112	10	28.85	0.08
DWTP B	Baseline-01	1967	2	6.99	0.66
	Baseline-02	1950	2	6.51	0.74
	Baseline-03	2083	2	24.14	1.06
	Event-01	1950	2	14.74	0.97
	Event-02	1917	2	12.12	0.82
	Event-03	1883	1	16.42	0.80
	Event-04	1967	2	15.09	0.69
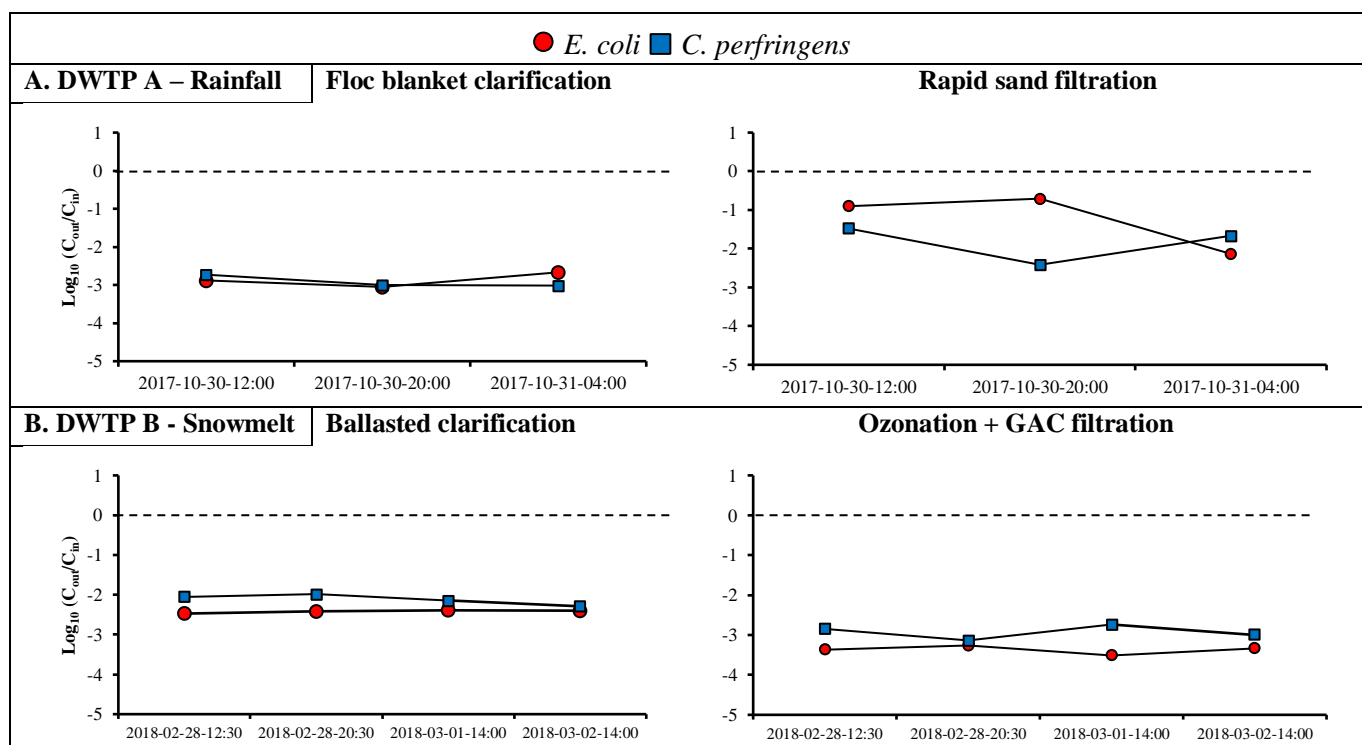
Figure 8-6: Short-term variations in the log-reduction of *E. coli* and *C. perfringens* by coagulation/flocculation and filtration during event conditions at drinking water treatment plants A and B.

Table 8-4: Daily risk of infection/person/day for *Cryptosporidium* during baseline and event conditions at drinking water treatment plants A and B

	Sample id.	Raw water *Cryptosporidium* (oocyst/L)	Reduction *C. perfringens* ($\log_{10}$-units)	Daily risk (inf./per/day)
DWTP A	Baseline-01	0.39	4.2	4.92 E-06
	Baseline-02	0.39	3.6	1.95 E-05
	Baseline-03	0.39	4.9	9.81 E-07
	Event-LR$_{eff.}$	1.48	4.5	9.36 E-06
DWTP B	Baseline-01	0.08	4.0	1.60 E-06
	Baseline-02	0.11	5.2	1.38 E-07
	Event-LR$_{eff.}$	0.40	5.4	3.18 E-07

8.3.2 Urban drinking water treatment plant B

At DWTP B, the baseline GLUC activity level was stable at a level of about 15 mMFU/100 mL (Figure 8-3B). The GLUC activity peaked at 44 mMFU/100 mL in early February following a planned discharge of raw sewage at a wastewater treatment plant around 5 kilometers upstream of the drinking water intake. At the beginning of March, the GLUC activity peaked at 49 mMFU/100 mL and then slowly decreased for around two weeks before returning to a baseline level.

Mean *E. coli* concentrations in raw water during baseline conditions (177 *E. coli*/100 mL, $n=3$) were similar to median *E. coli* concentration evaluated with weekly monitoring (170 *E. coli*/100 mL, $n=437$) but increased to 468 *E. coli*/100 mL ($n=6$) during event conditions (Table 8-1, Figure 8-4B). Mean *C. perfringens* concentrations during event conditions (95 CFU/100 mL, $n=6$) were 0.5-log higher than during baseline conditions (30 CFU/100 mL, $n=3$).

E. coli was detected in 83% of the filtered water samples ($n=6$) and *C. perfringens* was detected in 66% of the UV-disinfected water samples ($n=6$) (Figure 8-5). Maximum reduction performance of 6.0-log and 5.6-log were quantified for *E. coli* and *C. perfringens*, respectively (Table 8-2). Effective log-reductions by ballasted clarification were approximatively 2.0-log for both surrogate organisms. Log-reductions by a combination of ozone and GAC filtration ranged from 1.7 to 3.5-log for *E. coli* and from 2.4 to 3.1-log for *C. perfringens*. UV disinfection had a small effect on *C. perfringens* inactivation (effective log-inactivation <1.0-log) during baseline and event conditions. The total effective log-reduction of *C. perfringens* by treatment processes increased during event conditions (5.4-log) as compared to baseline conditions (4.7-log); however, the standard error of the effective log-reduction was large ($\sigma_{\overline{LR}}$ = 0.6-log) during baseline conditions.

Short-term deterioration of the removal performance of both surrogate organisms was not observed during event conditions (Fig. 8-6B). *C. perfringens* and *E. coli* were better removed than the turbidity by ballasted clarification and by the combination of ozone and GAC filtration. The abstraction flow rate, the water temperature, and the turbidity of settled water were similar during baseline and event conditions (Table 8-3).

The daily infection risk, computed using *C. perfringens* reduction data, was 1.3-log lower during event conditions than during the first baseline sampling campaign, even if the mean *Cryptosporidium* concentration during event conditions was approximately 0.7-log higher than during baseline conditions (Table 8-4).

8.4 Discussion

8.4.1 Identification of periods of microbial challenge

8.4.1.1 Agricultural catchment

Temporal variations in faecal contamination were evaluated following a rainfall episode at agricultural DWTP A using a locally derived rate of increased GLUC activity as the trigger for sampling. Trends in GLUC activity show large and rapid increases suggesting the contribution of local sources to faecal contamination at the water intake. To establish whether the event so targeted represents a rare contamination event, results obtained during baseline and event-based sampling campaigns can be compared to existing data from routine monitoring at the intake of this plant.

According to a recent analysis of *E. coli* monitoring in raw water over 5 years at DWTP A, the daily *E. coli* concentration measured during the event has an exceedance probability of approximatively 1% (Sylvestre *et al.*, 2020a). Routine *C. perfringens* montitoring data were not available to estimate an exceedance probability. However, previous modeling results of routine monitoring protozoan pathogens at the intake of DWTP A indicate that the exceedance probability of protozoan pathogen concentrations measured during this event was approximatively 5% for *Cryptosporidium* and approximatively 2% for *Giardia* (Sylvestre et al. 2020b). Hence, these observations support the hypothesis that this study investigated the performances of treatment processes during a low-frequency faecal contamination event. In this small agricultural catchment,

GLUC activity, *E. coli*, and *C. perfringens* concentrations increased with the turbidity of raw water, suggesting that turbidity could be a useful indicator to trigger event-based sampling.

8.4.1.2 Urban catchment

At DWTP B, event-based sampling was triggered on February 28, 2018, using the locally derived GLUC activity threshold (40 mMFU/100 mL). Periods of high GLUC activity levels are less pronounced and sudden than those observed in the smaller agricultural catchment. This relatively low reactivity most probably reflects the cumulation of multiple discharges from upstream wastewater facilities and CSOs in this large urban catchment. Short-term trends in GLUC activity could reflect contamination transported over long distances, which would explain why the GLUC activity significantly increased in dry weather conditions during the spring snowmelt period. It has been established that that viable but non-culturable (VBNC) *E. coli* can contribute to the GLUC activity signal (Garcia-Armisen et al. 2005, Stadler et al. 2016, Ender et al. 2017, Burnet et al. 2019a, Stadler et al. 2019), and that viable but non-culturable (VBNC) *E. coli* decreased much more slowly than culturable *E. coli* (Servais et al. 2009). Moreover, Burnet et al. (2019b) reported snowmelt runoff is likely to carry a higher proportion of VBNC, yet GLUC active *E. coli* cells. Therefore, a large amount of non-culturable *E. coli* may have contributed to the GLUC activity signal during the studied peak event.

Nonetheless, the maximum daily mean *E. coli* concentrations detected during peaks correspond to an *E. coli* contamination level with a relatively low exceedance probability (10-15%) when considering the long-term data set of *E. coli* at the intake (Sylvestre et al. 2020a). Previous modeling results of routine monitoring protozoan pathogens at the intake of DWTP B indicate that that the exceedance probability of protozoan pathogen concentrations measured during this event was approximatively 5% for *Cryptosporidium* and approximatively 20% for *Giardia*. However, samples collected for the enumeration of protozoan pathogens in this case could only be collected at the beginning and the end of the GLUC activity peak, which may underestimate the maximum daily *Cryptosporidium* and *Giardia* concentrations during this event. Additional studies investigating the validity of GLUC activity monitoring for the detection of rare contamination events in urban catchments are needed. A better understanding of the relationship between the GLUC activity and microbial pathogens/indicators in source water may allow detecting contamination events with lower exceedance probabilities.

8.4.2 Reduction performance of physical-chemical processes

8.4.2.1 Floc blanket clarification and rapid sand filtration

Results from this study provide full-scale observations of the reduction performance of conventional treatment processes facing high microbial loads during hydrometeorological events. High reduction performances observed at DWTP A may, in part, be attributed to the presence of pre-oxidation with potassium permanganate ($KMnO_4$) before coagulation, and in part to the type of clarifier. Previous investigations have shown that permanganate pre-oxidation inactivates *E. coli* (Cleasby et al. 1964) and improves the removal of particles by coagulation/flocculation/sedimentation (Liu et al. 2013). A mean removal performance of 3.7-log for *C. perfringens* by floc blanket clarification with pre-ozonation was also previously reported for a DWTP supplied by an agricultural river in Quebec (Payment and Franco 1993). It should also be emphasized that treatment processes of DWTP A were optimized for turbidity reduction and operated at approximately 20% of their nominal design capacity during studied baseline and event conditions.

The effective log-removals of *E. coli* by floc blanket clarification were similar in baseline and event conditions; however, the log-removal of *C. perfringens* was 0.4-log lower during event conditions than during baseline conditions. The removal performance of a floc blanket clarifier as used in DWTP A should not theoretically be influenced by the particle concentration in raw water. The aggregation of micro-sized particles in a fluidized bed (floc blanket) is typically approximated by a first-order process by assuming that the size of the flocs in the fluidized bed is independent of the incoming primary particles (Bache and Gregory 2007). However, changes in temperature and turbidity can cause preferential currents in the sludge blanket resulting in lower performances. These results and flocculation theory suggest that the floc blanket clarifiers as operated were not capable of buffering a short-term increase in microbial concentration in raw water caused by a rainfall event.

Removal performances by rapid sand filtration at DWTP A were higher in event conditions than in baseline conditions. Still, they are somewhat difficult to ascertain because of a high standard error on the log-removal of both surrogate organisms during baseline conditions. The standard error is driven by a negative removal for both *E. coli* and *C. perfringens* by filtration during one baseline

campaign (baseline-02). A potential cause for this breakthrough was not determined. The collection of sequential grab samples during event conditions but also during baseline conditions is recommended in future work to capture temporal changes in sedimentation and filter effluent quality adequately.

8.4.2.2 Ballasted clarification

Removal performances by ballasted clarification as used in DWTP B are at the high end of the range of full-scale coagulation/flocculation removal performances reported for bacteria and bacterial spores (Hijnen and Medema 2010). A mean removal performance of 2.0-log of aerobic bacterial endospores by ballasted clarification was previously reported at pilot-scale (Huertas et al. 2001). The incorporation of a ballasted media (typically silica sand) within the incoming stream of flocs makes ballasted clarification more robust for the removal of turbidity regardless of rapid changes of water quality (Kumar et al. 2016). In our study, higher removal performances of *C. perfringens* by ballasted clarification were observed at turbidity levels of 12-24 nephelometric turbidity units (NTU) (event, baseline 3) than at slightly lower levels of 6-7 NTU (baselines 1, 2).

According to the Smoluchowski coagulation theory of particles, the removal of suspended bacteria during flocculation is likely to be governed by heteroaggregation between bacteria and abiotic particles. Bacteria and bacterial spores concentrations in natural aquatic environments are typically very low in comparison to abiotic particle concentrations (e.g., inorganic and organic materials). If the initial concentration of a i-sized bacteria $n_{i,0}$ is assumed to be much smaller than the initial concentration of a j-sized abiotic particle $n_{j,0}$, then the rate of loss of the concentration of the bacteria can be approximated by a pseudo-first-order process given by:

$$\frac{dn_i}{dt} \approx -\alpha_{ij}\beta_{ij}n_{j,0}n_i \tag{8.7}$$

where α_{ij} is a collision efficiency coefficient; β_{ij} is a collision rate coefficient; and t is the detention time in the flocculator. Integrating Equation (8.7) once yields:

$$n_i = n_{i,0}\exp(-n_{j,0}\alpha_{ij}\beta_{ij}t) \tag{8.8}$$

Therefore, it can be anticipated that the initial particle concentration $n_{j,0}$ has an impact on the aggregation of the bacteria at the beginning of flocculation. Further research on the aggregation of microorganisms during flocculation would be relevant to quantify the buffering capacity of ballasted systems.

Finally, the mechanisms described in Equation 8.8 call for caution in considering any results from pathogen spiking flocculation experiments during which the spiked dose of the pathogen was similar or higher than the initial particle concentration. In these conditions, the spiked dose may self-aggregate, which could lead to an overestimation of the removal performance of the flocculation process.

8.4.3 Reduction performance by disinfection processes

At DWTP B, the combination of inter-ozonation and GAC filtration, referred to as biological activated carbon (BAC) filtration, considerably reduced *E. coli* concentrations (1.7 to 3.5-log) and *C. perfringens* concentrations (2.4 to 3.1-log). It is likely that most *C. perfringens* was mainly removed by GAC filtration because inactivation of environmental *C. perfringens* under full-scale conditions is expected to be small (<0.5-log) at a Ct_{10}-value of around 0.6 mg L^{-1} min^{-1} (Hijnen et al. 2002). Conversely, the inactivation of *E. coli* was most likely driven by ozonation. Between 2.0- and 3.0-log inactivation of *E. coli* were previously reported in full-scale conditions at Ct_{10}-values between 0.5 and 1.0 mg L^{-1} min^{-1} and water temperature below 10°C (Smeets et al. 2006). Slightly higher *C. perfringens* reduction performances were measured during event conditions (2.8 to 3.1-log) than during baseline conditions (2.4 to 2.5-log). The variations do not appear to be related to the *C. perfringens* concentration or the turbidity level in settled water. Low inactivation (<1.0-log) of *C. perfringens* were found for UV medium pressure lamps (DWTP A) and UV low pressure lamps (DWTP B) operated at a fluence of 40 mJ cm^{-2}. These inactivation performances were lower than those previously reported at a fluence of 40 mJ cm^{-2}. Inactivation of *C. perfringens* of approximately 1.0-log were observed at a full-scale municipal wastewater treatment plant with low pressure lamps (Gehr et al. 2003). Inactivation of environmental spores of sulfite-reducing clostridia (SSRC) of approximately 2.4-log were obtained at pilot-scale with medium pressure lamps (Hijnen et al. 2004)

8.4.4 Implications for risk assessment and management

At the two DWTPs, daily infection risks by *Cryptosporidium* via consumption of treated drinking water were not higher during hydrometeorological events than during baseline conditions (Table 8-4). The relative impact of short-term contamination events on risks of infection by *Cryptosporidium* has been investigated by modeling *Cryptosporidium* concentrations in source water and assuming treatment performances from literature data. Signor et al. (2007) demonstrated with a QMRA model combined to a hydrograph filtering algorithm that the majority of the annual risk at a DWTP abstracting raw water from a small agricultural river was attributable to runoff event periods. In contrast, Taghipour et al. (2019) showed with a discharge-based QMRA combined with hydrodynamic modeling that the number of combined sewer overflow events per year had a negligible impact on the annual risk at two DWTPs abstracting raw water from a large urban river. Smeets et al. (2007) evaluated *Cryptosporidium* data measured routinely in the treated water of eight DWTPs with similar physical treatment processes. They found that average treated water concentrations were similar at sites, independently of their average *Cryptosporidium* concentration in source water. The authors hypothesized that "well operated" conventional treatment may be more effective in removing high concentrations of microorganisms than low concentrations. Indeed, results from the current study also suggest that that physical treatment processes optimized for turbidity reduction can effectively manage short-term increases in raw water microbial quality.

Our findings should be interpreted within their context. During the studied events, turbidity levels in raw water were moderate (DWTP A: $\bar{x} = 28$ NTU; DWTP B: $\bar{x} = 15$ NTU) and treatment processes at the plants investigated were optimized for turbidity reduction (turbidity <1.0 NTU in settled water; turbidity < 0.1 NTU at individual filter effluents). Although turbidity reduction after filtration is not a direct indicator of pathogen control, it is an effective indicator of process control. For example, the Long Term 2 Enhanced Surface Water Treatment Rule (LT2ESWTR) award 0.5 or 1.0-log additional *Cryptosporidium* credit for achieving filter effluent turbidity < 0.1 NTU (USEPA 2010). Sedimentation effluent turbidity targets (typically < 1 NTU) are also recommended by industry optimization programs (USEPA 2010); these targets could also be useful to manage short-term fluctuations in microbial contamination in raw water.

Nonetheless, in some catchments, pathogens can peak before turbidity (Dorner et al. 2007, St-Pierre et al. 2009, Sylvestre et al. 2020b). In these situations, achieving sedimentation or filter effluent turbidity targets may not be indicative of adequate pathogen removal. Floc blanket and ballasted clarifiers may be well suited to manage low-turbidity microbial peaks because particle concentrations are intentionally kept high during flocculation/sedimentation. An online zeta potential analyzer may also be a useful tool to dynamically manage coagulation dosing rates to optimize microbial reduction performance (Lee 2019).

8.4.5 Limitations of the quantification of reduction performance at full-scale

E. coli and *C. perfringens* counts were assumed to be Poisson distributed in all samples. However, previous studies suggested that treatment processes could increase variance in microbial counts to a higher value than what can be accommodated by the Poisson distribution (Gale et al. 2002). Overdispersion was not evaluated in this study because sample replicates were not available, but large-volume samples were concentrated after treatment (50-1500 L), which should minimize this potential sampling bias.

Another limitation of the present study is that the log-reduction performances were evaluated by pairing inflow concentration (C_{in}) and the outflow concentration (C_{out}) by assuming that the hydraulic mean retention time of water was a valid approximation of the actual detention time of the microorganisms. It has been pointed out that microorganisms entering in a treatment train following a microbial peak in raw water may be retained in physical processes and remobilized over time (Smeets et al. 2007, Hijnen 2009). Higher loads of microorganisms removed by ballasted clarification during the peak event are not likely to be remobilized through treatment because settled sludges are continuously pumped from the bottom of the clarifier and recycled via hydro-cyclone to separate the silica sand from the sludge. However, remobilization could occur in floc blanket clarifiers. To maintain a steady volume fluidized bed, excess material (so-called sludge bleed) is withdrawn from the fluidized bed at a flow rate of approximately 1% of the inflow at an alum dose of 50 mg L^{-1} (Ives 2001); thus, remobilization of microorganisms in settled water could occur during a period equivalent to the mean residence time of the flocs. Remobilization of pathogens from filtration processes could also happen by the end of the filter cycle before turbidity increases. The collection of composite filtered water samples for an extended period following

critical periods of raw water microbial quality may be valuable to improve process control strategies for filter operations.

Overall, high-resolution investigations of the full-scale treatment performances during hydrometeorological events were logistically challenging and costly; thus, only a small number of samples were collected. High variations in microbial concentrations, such as those observed after rapid sand filtration at DWTP A, limited the comparison between treatment performances in baseline and event conditions. The development of automated sampling devices and faster concentration methods would be needed to increase the sampling frequency throughout the full-scale treatment train.

8.5 Conclusions

A sampling strategy was implemented at two drinking water treatment plants in Quebec, Canada, to quantify the full-scale removal performance of surrogate microorganisms by treatment processes under varying source water conditions. The following conclusions are drawn:

- Online measurements of β-D-glucuronidase activity can be used for characterization sampling of full-scale treatment performances during baseline conditions and periods of poor source water quality. Daily mean *E. coli* concentrations evaluated during hydrometeorological peak events had low exceedance probabilities (1% at the agricultural site, 10-15% at the urban site) when compared to long-term raw water monitoring data (5 years).

- Full-scale reduction performances of up to 6.0-log for *E. coli* and 5.6-log for *C. perfringens* were measured by concentrating large volumes of water (50-1500 L) throughout the treatment train. Removal performances by coagulation/flocculation processes could be estimated under baseline and peak event conditions. However, removal performances by rapid sand filtration were highly variable based on paired samples, which we suspect are caused by processes of retention and release rather than actual performances of the filters.

- Increased reduction of *E. coli* and *C. perfringens* by ballasted clarification and rapid sand filtration compensated for the augmented concentrations in source water. At the two sites, daily infection risks by *Cryptosporidium* via consumption of drinking water were not higher during peak contamination events than during baseline conditions based on *C. perfringens*

reduction data. Thus, daily risks during transient peaks in raw water contamination unlikely dominate the annual risk at these sites.

Additional studies investigating the reduction of pathogens and surrogate microorganisms by full-scale treatment processes under variable source water conditions would be desirable to validate our findings, especially in drinking water treatment plants subjected to severe water quality changes at the source.

8.6 Acknowledgments

CHAPTER 9. GENERAL DISCUSSION

The findings of this research project are discussed in this chapter to integrate the various aspects of the investigations conducted and to help identify their regulatory implications. The general objective of this thesis was to develop a methodology to systematically assess microbial risks associated with hydrometeorological events for drinking water safety. The first step of this project was to expand the stochastic modeling framework for source water characterization by proposing candidate probability distributions and using them to model routine monitoring pathogens/indicators data sets. Event-based monitoring campaigns were then implemented to collect data on short-term fluctuations in source water microbial concentrations at three drinking water treatment plants. The last step was to incorporate results from event-based monitoring campaigns into a quantitative microbial risk analysis (QMRA) to estimate the relative contribution of short-term contamination events to the overall risk. The specific objectives and the research hypotheses are presented once again in Figure 9-1 and Table 9-1, respectively.
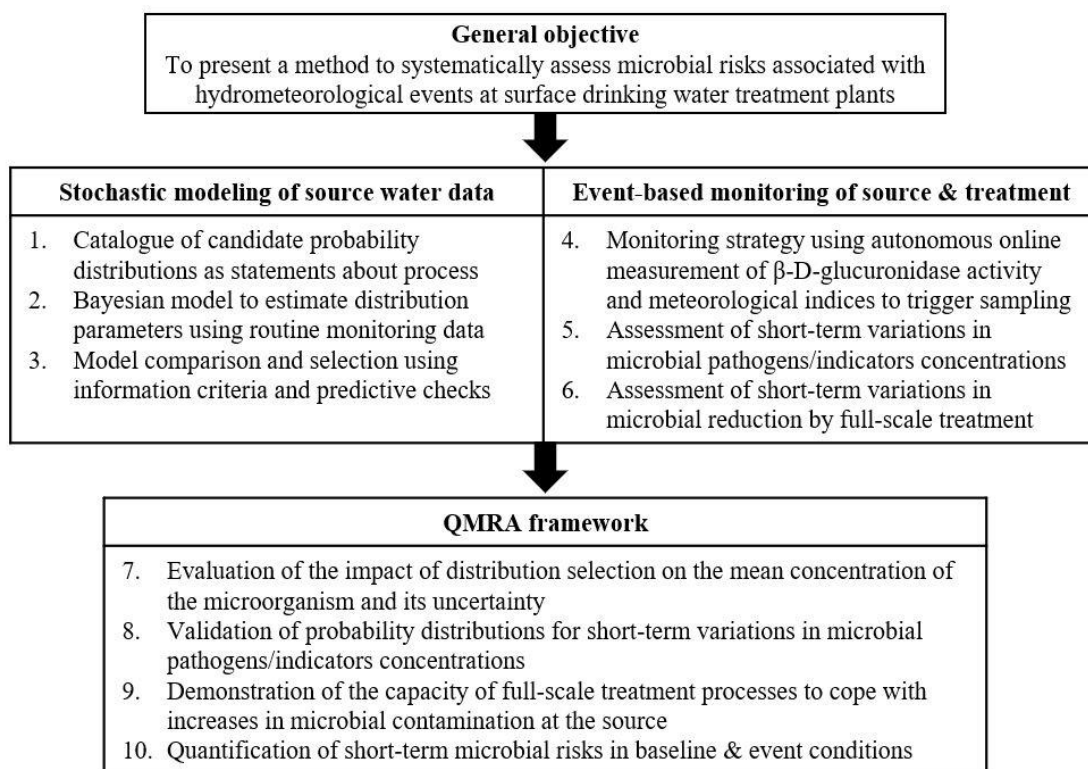
Figure 9-1: Flowchart representing the objectives of the thesis

Table 9-1: Research hypotheses, criteria for their validation, and corresponding articles

	Statement	Hypothesis	Validation	Article
1	A precise estimate of the mean source water microbial concentration and its uncertainty is required for defining site-specific drinking water treatment requirements.	Correct identification of the tail behavior of a probability distribution fitted to monitoring data is necessary to estimate the mean source water microbial concentration and its uncertainty.	The upper bound of the 95% uncertainty interval on the mean source water microbial concentration varies from >0.5-log among distributions fitted to the same data.	1,2,3
2	The characterization of low-frequency events of source water microbial contamination is needed to validate the tail behavior of a probability distribution fitted to small monitoring data sets.	Online β-D-glucuronidase monitoring captures events necessary for characterizing low-frequency events in source water microbial concentrations.	The exceedance probability of the daily mean microbial concentration during captured events is <5% based on a gamma distribution fitted to historical monitoring data.	1,3,5
3	Transient peaks in source water microbial contamination should be explicitly considered in source water characterization.	The gamma distribution does not reasonably predict source water microbial concentrations during snowmelt and rainfall events.	The gamma distribution predicts daily mean concentrations at an exceedance probability < 0.1% during snowmelt and rainfall events.	1,3
4	The reduction of a microorganism by each treatment process is assumed to be a first-order process with respect to its influent concentration.	The concentration of a microorganism in treated drinking water increases proportionally to its source water concentration.	An increase in the daily mean microbial concentration > 1.0-log is measured in settled water or filtered water during a source water event.	3,4,5

9.1 Stochastic modeling of routine monitoring data

Candidate continuous probability distributions were proposed to expand the stochastic modeling framework for source water characterization (Chapter 2). Distributions representing statements about additive and multiplicative processes were selected because these processes are commonly observed in nature (Frank 2014). These candidate probability distributions were then used to assess temporal variations in source water microbial concentrations at 30 surface drinking water treatment plants in Quebec, Canada. The first hypothesis is confirmed for *Cryptosporidium* but not for *E. coli* and *Giardia*. The upper bound of the 95% uncertainty interval on the mean source water *Cryptosporidium* concentration can vary from more than 0.5-log among candidate distributions. The implications of these findings will be discussed for the assessment of faecal indicator concentrations in section 9.1.1 and for the assessment of protozoan pathogen concentrations in section 9.1.2.

9.1.1 Temporal variations in faecal indicator concentrations

The first article (Chapter 4) presented a statistical analysis of source water *E. coli* data collected with routine monitoring at six DWTPs over extended periods (5-8 years). The first hypothesis was invalidated for *E. coli* because the upper bound of the 95% credibility interval on the mean *E. coli* concentration varied from less than 0.5-log among selected candidate distributions (gamma, log-normal, Lomax, bimodal log-normal distribution). Therefore, the upper tail behavior of these distributions did not produce significant changes in the predicted mean *E. coli* concentration and its uncertainty. Nonetheless, this assessment provided useful information on the magnitude of peak *E. coli* concentrations. High *E. coli* concentrations were better predicted by log-normal, Lomax or bimodal log-normal distributions than the gamma distribution (Figure 4-2). Moreover, the observation of a bimodal log-normal distribution at an agricultural site suggested that two different underlying generative processes may influence variations in microbial concentrations (Figure 4-3). Nevertheless, the quantitative relationship between *E. coli* concentrations and pathogen concentrations is site-specific (Lalancette et al. 2014, Sylvestre et al. 2018). The covariance between pathogen concentrations and *E. coli* concentrations during hydrometeorological events is highly uncertain and should be investigated in future work.

In this study, non-detects were replaced by a detection limit of 1 *E. coli*/100 mL to fit concentration distributions. It must be noted that this practice could result in substantial estimation biases if the proportion of non-detects is high. Alternatively, mixed Poisson distributions could be used in further work to model *E. coli* counts and volumes reported in colony-forming unit (CFU) assays. A mixture distribution could also be obtained by combining the statistical model of a most probable number (MPN) assay[5] and a density distribution (Haas et al. 1999)[6]. It should also be emphasized that the reporting of "too numerous to count" (TNTC) results should be avoided. The consideration of "too numerous to count" (TNTC) in the statistical analysis may result in a biased estimate of the variability of the system. A conservative number of serial dilutions should be prepared to ensure that high *E. coli* concentrations are accurately quantified.

9.1.2 Temporal variations in protozoan pathogens concentrations

The statistical analysis of temporal variations in source water *Cryptosporidium* and *Giardia* concentrations from 30 DWTPs was presented in Chapter 5. The gamma and log-normal distributions predicted similar mean concentrations for *Cryptosporidium* and *Giardia*. However, important differences (> 0.5-log) between the upper bound of the 95% credibility interval on the mean concentration of the two distributions were found at some sites for *Cryptosporidium* (Figure 5-1). As discussed in Chapter 2, these differences may have an important influence on risk estimates because microbial reduction by treatment processes are typically assumed to be first-order with respect to the influent concentration. The application of model selection techniques is thus recommended for the characterization of temporal variations in source water *Cryptosporidium* concentrations.

---

[5] This model can be describe as a binomial distribution with a success probability for each trial given by the zero term of the Poisson distribution (Haas and Heller 1988).

[6] Statistical inference with this mixture model would require the number of positive wells (and their associated volumes) per sample rather than reported concentrations from standard MPN tables.

However, it was demonstrated in Chapter 5 that differences in marginal deviance information criterion (mDIC) values between mixed Poisson models are generally too small for discrimination as only a few samples informed on the behavior of the upper tail (Table 5-4). Consequently, the gamma and the log-normal distributions fit the data equally well but may predict different risk estimates when they are used as input distributions in stochastic QMRA. A possible approach to address this issue could be to compare the upper tail predictions of candidate distributions to field observations during critical periods of source water contamination, as demonstrated in Chapters 4 and 6 (see section 9.2.2). In the absence of empirical information, one possible solution could be to choose the log-normal distribution as a reasonably conservative model for the prediction of peak concentrations. As shown in Chapter 5, the selection of the log-normal distribution may result in the prediction of large uncertainties on the mean concentration. However, alternative risk management options could be considered to deal with this uncertainty.

9.2 Impact of hydrometeorological events on microbial concentrations in source water

Online GLUC activity measurements were used to evaluate short-term variations in concentrations of *E. coli* (Chapter 4, Chapter 8), *Cryptosporidium* and *Giardia* (Chapter 6), and enteric viruses (Chapter 7) during hydrometeorological events. The second hypothesis is partially validated: the exceedance probabilities of daily mean *E. coli*, *Cryptosporidium*, and *Giardia* concentrations during captured events were generally below 5%. The third hypothesis is validated: the gamma distribution did not predict daily mean concentrations at a reasonable exceedance probability (<0.1%) for some snowmelt and rainfall events. The significance of the increases in source water microbial concentrations during GLUC activity peaks will be discussed in section 9.2.1. The relevance of a model validation approach using event-based monitoring data will be discussed in section 9.2.2.

9.2.1 Identification of critical periods of microbial contamination

The exceedance probabilities of daily mean *E. coli*, *Cryptosporidium* and *Giardia* concentrations evaluated during hydrometeorological events are listed in Table 9-2. The criterion of 5% was generally met for events captured at DWTPs C6 and A4 but was not met for events captured at DWTP C7. The potential of GLUC activity for characterizing low-frequency events of *E. coli*, *Cryptosporidium* and *Giardia* contamination may therefore be site-specific. At DWTPs C6 and A4, the GLUC activity peaks could indicate local contamination originating from combined sewer overflow (CSO) discharges and agricultural runoff. The GLUC activity peaks at DWTP C7 could, in contrast, reflect contamination transported over long periods (Chapter 8). Additional studies confirming these findings in other catchments and for other hydrometeorological events would be relevant.

Table 9-2: Exceedance probabilities of daily mean *E. coli*, *Cryptosporidium* and *Giardia* concentrations sampled during hydrometeorological events predicted by the gamma distribution or the log-normal distribution fitted to routine monitoring data. Green shaded cells represent exceedance probabilities below 5%. Yellow shaded cells represent exceedance probabilities between 5% and 20%. Red shaded cells represent exceedance probabilities above 20%.

DWTP id. - Event	Gamma			Log-normal		
	E. coli	*Crypto.*	*Giardia*	*E. coli*	*Crypto.*	*Giardia*
DWTP C6 - Snowmelt event 1	< 0.001	0.017	< 0.001	0.012	0.039	0.026
DWTP C6 - Snowmelt event 2	< 0.001	0.127	< 0.001	0.004	0.119	0.042
DWTP A4 – Rainfall event	0.014	0.063	< 0.001	0.012	0.054	0.016
DWTP C7 - Snowmelt event 1	0.112	0.350	0.070	0.102	0.330	0.085
DWTP C7 - Snowmelt event 2	0.155	0.085	0.308	0.147	0.051	0.220

It was not possible to evaluate the importance of peak virus concentrations with exceedance probabilities. Concentrations of adenovirus, rotavirus, norovirus, and JC virus at DWTP C7 were about 1.0-log higher during GLUC activity peaks than during baseline conditions (Figure 7-3B). However, virus concentrations were quantified using a quantitative real-time polymerase chain reaction (qPCR) method, which detects the DNA/RNA from viable and nonviable viruses.

Qualitative results (presence or absence of infectious viruses) obtained with integrated cell culture (ICC) qPCR indicated that adenovirus, rotavirus, and enterovirus found in samples of source water were mostly not infectious.

Turbidity was not a useful indicator to trigger pathogen sampling during snowmelt events at urban DWTP C6 (Chapter 6) and DWTP C7 (Chapter 7). At DWTP C6, *Cryptosporidium* and *Giardia* concentrations increased before turbidity during two snowmelt events (Figure 6-2, Figure 6-4). Weak correlations between turbidity and bacterial pathogens during hydrometeorological events were previously reported (Dorner et al. 2007, St-Pierre et al. 2009). At agricultural DWTP A4, the turbidity did peak with *Cryptosporidium* and *Giardia* concentrations during a rainfall event (Figure 6-3, Figure 6-4). Different pollution sources may govern short-term fluctuations in source water microbial contamination during hydrometeorological events. Pollution in the urban catchment (DWTPs C6, C7) may be dominated by point sources (CSO discharges), whereas pollution in the agricultural catchment (DWTP A4) may be dominated by non-point sources (agricultural runoff). Pathogen and turbidity are more likely to be correlated in a catchment in which diffuse sources dominate because they have the same sources. In contrast, in the urban watershed, pathogens may come from point sources, but turbidity comes from the whole watershed.

9.2.2 Model validation using event-based monitoring data

Results from this research suggest that the log-normal distribution conservatively predicts *E. coli, Cryptosporidium* and *Giardia* concentrations during hydrometeorological events (Chapter 4, Chapter 6). In contrast, the gamma distribution did not reasonably predict (exceedance probability < 0.1%) *E. coli* concentrations during two snowmelt events at urban DWTP C6 (Figure 4-7), *Giardia* concentrations during a snowmelt event at urban DWTP C6, and *Giardia* concentrations during a rainfall event at agricultural DWTP A4 (Figure 6-5). The gamma distribution reasonably predicted the daily mean *Cryptosporidium* concentrations for snowmelt events at urban DWTPs C6 and C7 and a rainfall event at agricultural DWTP A4. However, the gamma distribution did not predict the sample maximum *Cryptosporidium* concentration (obtained from routine monitoring) at DWTP C6 (Figure 8-5).

The selection of the log-normal distribution as an input distribution in a stochastic QMRA may thus be a reasonable method to account for hydrometeorological events in the quantification of treatment targets. However, the log-normal distributions may require special considerations because: 1) the uncertainty on its expected value is highly sensitive to the uncertainty on its upper tail values, and 2) its annual mean can vary from year to year depending on the occurrence of rare events (exceedance probability < 1 day per year) (Chapter 6). Whether a short-term or a long-term risk target is more appropriate in drinking water safety management has been discussed previously (Signor and Ashbolt 2009, Smeets 2010). The uncertainty analysis presented in our research project provided new insights to ponder the advantages and limitations of these targets. As discussed in Chapter 5, the consideration of a short-duration target rather than an annual target may simplify mathematical calculations and reduce the uncertainty of risk estimates.

Finally, it should be noted that a parametric distribution fitted to historical monitoring data may not predict accidents or extreme weather events. Resilience analysis might be used as a supplement to the traditional microbial risk assessment approach for the assessment of such events. The development of early warning systems using meteorological data has been recently suggested to manage the risks of waterborne diseases (Semenza 2020). Online monitoring of faecal indicators could also be useful for the development of early warning systems.

9.3 Impact of hydrometeorological events on microbial reduction by treatment barriers

The reduction performance of full-scale treatment processes was evaluated during hydrometeorological events for *Cryptosporidium* and *Giardia* (Chapter 6), enteric viruses (Chapter 7), *E. coli* and *C. perfringens* (Chapter 8). Results from these campaigns invalidated the fourth hypothesis: the pathogen concentration in drinking water is *not* expected to increase proportionally to its concentration in source water. Microbial peaks in source water were buffered by high-rate clarifiers (ballasted or floc blanket) for *Giardia* (Figure 6-7), adenovirus (Figure 7-4, Figure 7-5), rotavirus (Figure 7-5), *E. coli* and *C. perfringens* (Figure 8-4B), and by rapid sand filtration for *E. coli* and *C. perfringens* (Figure 8-4A). The implications of these results for the assessment of the

performance of coagulation/flocculation and filtration/disinfection processes will be discussed in section 9.3.1 and 9.3.2. The implications of these findings for QMRA will be discussed in section 9.3.3.

9.3.1 Coagulation/flocculation processes

Increases in turbidity/particle concentrations in raw water are known to increase the reduction of protozoan parasites by conventional treatment (LeChevallier et al. 1991, LeChevallier and Norton 1992, Nieminski and Ongerth 1995, McTigue et al. 1998, Dugan et al. 2001). As detailed in Chapters 1, 7, and 8, heteroaggregation between microorganisms and abiotic particles should occur during flocculation. Heteroaggregation is a pseudo-first-order process because it depends on the initial particle concentration. At an optimal coagulation dosage, a positive correlation between particle and microbial concentrations in raw water should therefore increase the reduction performance of the flocculator. As predicted by the Smoluchowski theory of coagulation, removals of *E. coli*, *C. perfringens*, rotavirus, adenovirus by ballasted clarification (urban DWTP C7) improved with raw water turbidity (Chapter 7, Chapter 8). These findings represent the behavior of this system during a single snowmelt event; however, other studies reported higher removal performances by ballasted clarifiers at higher influent turbidity/suspended solids concentrations (Plum et al. 1998, Lapointe et al. 2017). The characterization of particles in raw water using multiple parameters (turbidity, particle count, suspended solids) is recommended in future work evaluating the microbial removal performances of coagulation/flocculation processes. Investigating the effect of the ballasted medium on the heteroaggregation of microorganisms could be relevant for the design and operation of ballasted clarifiers.

Mixed results were obtained for floc blanket clarifiers during hydrometeorological events. In contrast with conventional flocculator, the concentration of flocs forming the fluidized bed is not expected to vary at the short-term because of the temporary increase of incoming particle concentrations (Bache and Gregory 2007). Therefore, the removal of microorganisms by floc blanket clarifiers is expected to be a first-order process with respect to the influent microorganism concentration. Indeed, removals of *E. coli* and *C. perfringens* by floc blanket clarification at agricultural DWTP A4 were similar or slightly lower during a rainfall event than in dry weather

conditions. However, during snowmelt events, the removal performance of the floc blanket clarifier at urban DWTP C6 increased proportionally to the concentration of *Giardia* and adenovirus in raw water (Figure 6-7, Figure 7-4). A small increase in the coagulation dosage may have increased the performance during one of the two snowmelt events assessed at DWTP C6. Future studies could characterize the flocs forming the fluidized bed during hydrometeorological events to validate whether these systems are first-order.

9.3.2 Filtration and disinfection processes

The concentration of volumes of about 300 L per microorganism using Hemoflow method allowed to quantify *E. coli* and *C. perfringens* concentrations in all samples after rapid sand filtration (Figure 8-4A) and first stage dual media biological filtration (combination of ozonation and GAC filtration) (Figure 8-4B). Removals of *E. coli* and *C. perfringens* by rapid sand filtration at DWTP A4 were higher in event conditions than in baseline conditions. The signification of this difference is uncertain because a breakthrough highly influenced the mean log-removal in baseline conditions (Table 8-2). The collection of sequential grab samples in baseline conditions could improve the comparison between baseline and event conditions. According to the single spherical collector model, particle removal in filters are expected to be first-order with respect to the influent particle concentrations (Benjamin and Lawler 2013). Nevertheless, the single collector transport efficiency depends on the particle diameter; thus, a change in the floc size following a turbidity peak in source water may influence the filter performance (Lawler et al. 1978).

Adenovirus and rotavirus were sporadically detected in samples after rapid sand filtration (Figure 7-4) and first stage dual media biological filtration (Figure 7-5) by concentrating large water volumes (1000-2000 L) with electropositive filters. However, sample sizes were too small to determine whether breakthroughs were more likely under event conditions than baseline conditions. The concentration of multiple large volumes simultaneously could reduce the detection limit low enough to adequality characterize the removal performance of these filters.

The performance of disinfection processes was not directly influenced by variations in source water microbial concentrations because ballasted clarifier buffered these fluctuations (Figure 7-5, Figure

8-4). However, our results suggest than full-scale inactivation performances may be much lower than those obtained in lab-scale inactivation studies of *E. coli* (Zhou and Smith 1994, Hunt and Marinas 1997) and adenovirus (Thurston-Enriquez et al. 2005). The hydraulics of the full-scale ozonation system investigated in our work may be the cause of this lower inactivation. Finally, infectious adenoviruses were detected after UV disinfection at a dose of 40 mJ cm^{-2} under baseline and event conditions. High UV-resistance of adenovirus has also been found in lab-scale inactivation studies (Meng and Gerba 1996, Thurston-Enriquez et al. 2003). However, the fact that positive infectious adenoviruses were observed in treated water after a combination of advanced treatment processes points to the need to develop improved concentration and detection methods for the assessment of infectious viruses in full-scale systems with unperfect hydraulics.

9.4 Impact of snowmelt and rainfall events on daily infection risks

Daily risks of infection with *Cryptosporidium* were evaluated at two sites assuming daily exposure from either drinking water treated under baseline or event conditions (Chapter 8). These daily risks were calculated using source water *Cryptosporidium* data and full-scale *C. perfringens* reduction data. Daily risks under event conditions were not higher than daily risks under baseline conditions (Table 8-4). These results suggest that the annual infection risk is not likely to be dominated by variations in pathogen concentrations in source water. As discussed in Chapter 8, our results are in accordance with those of Smeets et al. (2007). During our campaigns, conventional treatment processes were optimized for turbidity reduction (settled water <1.0 NTU; individual filters effluents < 0.1 NTU). Therefore, as hypothesized by Smeets et al. (2007), "well operated" conventional treatment may be more effective in removing high concentrations of microorganisms than low concentrations. Achieving sedimentation effluent turbidity targets and filter effluent turbidity targets may be beneficial for the management of microbial associated with hydrometeorological events. Additional studies assessing the full-scale performance of conventional treatment under variable source water conditions, particularly at low turbidity, would be relevant.

The statistical independence between source water pathogen concentrations and microbial reduction performances is typically assumed for risk characterization with Monte Carlo methods (Teunis et al. 1997, Schijven et al. 2011). The assumption of statistical independence could be highly conservative if reduction performances are positively correlated with source water concentrations. Further work is needed to determine how these correlations could be assessed and incorporated into QMRA.

CONCLUSIONS AND RECOMMANDATIONS

The general objective of this research project was to develop a systematic methodology to assess microbial risks associated with hydrometeorological events for drinking water safety management. Fundamental questions were initially raised in Chapter 3: Which probability distributions adequately describe temporal variations in source water microbial concentrations? Can automated rapid microbiological measurements facilitate the identification of microbial peaks in source water? Does the microbial reduction performance of treatment processes deteriorate/improve during hydrometeorological events? What is the magnitude of short-term microbial risks during hydrometeorological events and how important are these risks?

The main conclusions of this research are formulated to address these questions. Recommendations are then made to support the development and implementation of site-specific microbial risk assessments. Finally, ideas for future research are suggested.

Candidate continuous probability distributions were proposed to expand the stochastic modeling framework for source water characterization. The following conclusions can be drawn from this work:

- The Bayesian analysis of microbial data with mixed Poisson models produces reasonable results for small data sets and allow incorporating different sources of uncertainty into the analysis. The convergence of the Markov chains should however be examined thoroughly with these models.

- Correct identification of the mixture distribution is needed to model temporal variations in source water *Cryptosporidium* concentrations when available data sets are small ($n < 30$ samples per site). The selection of a log-normal distribution rather than the gamma distribution can considerably increase (>0.5-log) the upper 95% credibility interval on the mean concentration. Peak concentrations may thus play a substantial role in defining the uncertainty on the mean *Cryptosporidium* concentration.

- Differences in marginal deviance information criterion (mDIC) values are generally too small for discrimination between candidate distributions. Consequently, candidate

distributions fit the data equally well but may predict different risk estimates when they are used as input distributions in stochastic QMRA.

- For *E. coli* and *Giardia*, differences in upper tail behaviors among candidate distributions do not significantly impact the mean concentration estimate and its uncertainty. Nonetheless, the gamma distribution does not reasonably predict *E. coli* concentrations at large magnitudes.

- At large sample sizes ($n>156$ in urban catchments, $n>208$ in agricultural catchments), the 95% credibility interval on the mean source water *E. coli* concentration is small (<0.3-log).

An event-based sampling strategy triggered by online β-D-glucuronidase (GLUC) activity measurements was proposed to capture microbial peaks during hydrometeorological events. This strategy was implemented at three drinking water treatment plants to assess variations during four hydrometeorological events. The following conclusions ensue from this work:

- Low-frequency events can be detected using this event-based monitoring strategy. The exceedance probabilities of daily mean *E. coli*, *Cryptosporidium* and *Giardia* concentrations evaluated during targeted events were generally below 5% based on historical monitoring data at two sites. Higher exceedance probabilities (10-35%) were obtained at the third site. The potential of GLUC activity for characterizing low-frequency events is, therefore, site-specific.

- The log-normal distribution conservatively predicted daily mean concentrations of *E. coli, Cryptosporidium* and *Giardia* evaluated during two snowmelt episodes and one rainfall event. For these events, the gamma distribution did predict daily mean *Cryptosporidium* concentrations but did not reasonably predict daily mean *E. coli* and *Giardia* concentrations. The tail of the gamma distribution may thus be to thin do predict source water microbial concentrations during hydrometeorological events adequately.

- At an urban site, source water concentrations of adenovirus, rotavirus, norovirus, and JC virus were about 1.0-log higher during GLUC activity peaks than during baseline

conditions. Therefore, online GLUC activity monitoring could also be used to capture short-term fluctuations in viral contamination in urban rivers.

- Turbidity was not a useful indicator to trigger pathogen sampling during snowmelt events at urban sites. In contrast, the turbidity did peak with protozoan pathogen concentrations during a rainfall event at the agricultural site. The potential of turbidity for characterizing low-frequency events is, therefore, site-specific.

The full-scale reduction performance of treatment processes was evaluated during: 1) snowmelt episodes at two drinking water treatment plants located in a large urban catchment, and 2) a rainfall event at one drinking water treatment plant located in a small agricultural catchment. This work led to the following conclusions:

- During snowmelt events, the reduction performance of high-rate clarifiers (ballasted or floc blanket) increased proportionally to source water concentrations of *Giardia*, adenovirus, rotavirus, *E. coli* and *C. perfringens*. During a rainfall event, the reduction performance of *E. coli* and *C. perfringens* by floc blanket clarification did not increase. Still, the reduction performance of *E. coli* and *C. perfringens* by rapid sand filtration did increase proportionally to their source water concentrations. Conventional treatment processes optimized for turbidity reduction (settled water <1.0 NTU; individual filters effluents < 0.1 NTU) were thus more effective in removing high concentrations of microorganisms than low concentrations.

- Full-scale inactivation performances of *E. coli* and adenovirus by ozonation systems can be lower than those obtained in lab-scale inactivation studies, potentially because of poor mixing and hydraulic conditions. Furthermore, limited effectiveness of UV disinfection against naturally occurring adenovirus can be observed at operative doses of 40 mJ cm^{-2}, even after a combination of ballasted clarification, ozonation, GAC filtration.

Site-specific raw water *Cryptosporidium* data and *C. perfringens* reduction data were entered into a QMRA model to estimate daily infection risks by *Cryptosporidium* oocysts via the consumption of drinking water. Results from these two site-specific risk assessments indicated that daily infection risks following snowmelt and rainfall episodes are not higher than the daily risks under

baseline conditions. It should be emphasized that conventional treatment processes were optimized for turbidity reduction and operated at 20-40% of their nominal capacity during baseline and event conditions at these sites. Optimizing the removal performance of coagulation/flocculation and filtration processes may therefore be valuable treatment options for the control of short-term risks associated with transient peaks in source water microbial contamination.

Based on these conclusions, we can formulate a number of recommendations supported by our findings:

- ➢ Assessment of source water concentrations
  - Candidate probability distributions with different upper tail behaviors should be used to evaluate temporal variations in source water microbial concentrations. The application of methods to assist model selection is recommended to ensure that appropriately conservative distributions are selected for source water characterization.
  - Online GLUC activity monitoring is recommended for the assessment of source water microbial peak events at drinking water treatment plants during hydrometeorological events. Additional studies are needed on the potential of this sampling strategy in other catchments and for other hydrometeorological events.
  - In the absence of empirical information, we recommend the selection of the log-normal distribution as a reasonably conservative model for the prediction of daily mean microbial concentrations during hydrometeorological events. The choice of the log-normal distribution may result in the prediction of large uncertainties on the mean *Cryptosporidium* concentration. A potential option to reduce this uncertainty might be to collect sample volumes that would yield more positive counts rather than non-detects.
  - Turbidity should *not* be used to trigger event-based sampling of protozoan pathogens. Online monitoring of faecal indicators is more reliable for the detection of short-term fluctuations in pathogen concentrations, especially in catchments in which faecal contamination likely originates from point source pollution.

➢ Assessment of pathogen reduction across treatment processes

- The assessment of full-scale reduction performances of treatment processes is recommended to ensure that treatment is fully maintained during challenging source water conditions.

- Additional studies investigating the reduction of pathogens and surrogate microorganisms by full-scale treatment processes under variable source water conditions are needed to validate our findings. The development of rapid and automated methods for the detection of microorganisms in large water volumes is recommended to increase sample sizes. Large sample sizes could give greater power to detect changes in performance under different source water conditions.

- Without site-specific information on full-scale reduction performances, statistical independence should be assumed between the distribution of source water microbial concentrations and the distribution of microbial reduction performances by treatment processes. Based on our findings, this assumption would be conservative in a stochastic QMRA.

- The characterization of particles in source water using multiple parameters (turbidity, particle count, suspended solids) is recommended to evaluate their influence on the microbial removal performances of coagulation/flocculation processes.

Several research topics could advance risk assessment and management of short-term fluctuations in microbial water quality. It would be interesting to:

- Identify pollution sources that substantially contribute to increases in pathogen concentrations at drinking water intakes during hydrometeorological events. Tracking theses sources would be valuable for the implementation of risk-based source water protection measures.

- Evaluate the covariation between microbial pathogens and faecal indicators in source water during hydrometeorological events.

- Understand the impact of water quality parameters and ballasted medium on the aggregation of microorganisms during coagulation/flocculation.

- Characterize short-term fluctuations in faecal indicator concentrations after full-scale treatment processes using online monitoring technologies. Barrier efficiency could be dynamically regulated using online data. Furthermore, the development and implementation of new methods for the enumeration of pathogens and surrogate microorganisms in treated drinking water could substantially improve risk assessment procedures.

- Develop resilience analysis approaches to complement the traditional risk assessment framework. Strengthen resilience would be relevant to the management of accidents and extreme weather events.

REFERENCES

Aguero-Valverde, J. 2013. Full Bayes Poisson gamma, Poisson lognormal, and zero inflated random effects models: Comparing the precision of crash frequency estimates. Accident Analysis & Prevention **50**:289-297.

Albinana-Gimenez, N., M. P. Miagostovich, B. Calgua, J. M. Huguet, L. Matia, and R. Girones. 2009. Analysis of adenoviruses and polyomaviruses quantified by qPCR as indicators of water quality in source and drinking-water treatment plants. Water Research **43**:2011-2019.

APHA. 2005. Standard methods for the examination of water and wastewater (21th Edition), Washington, DC, USA.

APHA. 2012. Standard methods for the examination of water and wastewater. American Public Health Association, Washington, D.C.

Arias, C., M. Sala, A. Domínguez, R. Bartolome, A. Benavente, P. Veciana, A. Pedrol, and G. Hoyo. 2006. Waterborne epidemic outbreak of Shigella sonnei gastroenteritis in Santa Maria de Palautordera, Catalonia, Spain. Epidemiology & Infection **134**:598-604.

Armon, R., and P. Payment. 1988. A modified m-CP medium for enumerating Clostridium perfringens from water samples. Canadian Journal of Microbiology **34**:78-79.

Arnold, M., J. T. Patton, and S. M. McDonald. 2009. Culturing, storage, and quantification of rotaviruses. Current protocols in microbiology **15**:15C. 13.11-15C. 13.24.

Asami, T., H. Katayama, J. R. Torrey, C. Visvanathan, and H. Furumai. 2016. Evaluation of virus removal efficiency of coagulation-sedimentation and rapid sand filtration processes in a drinking water treatment plant in Bangkok, Thailand. Water Research **101**:84-94.

Ashbolt, N., W. O. K. Grabow, and M. Snozzi. 2001. Indicators of microbial water quality.*in* W. H. O. (WHO), editor. Water Quality: Guidelines, Standards and Health. IWA Publishing, London.

Astrom, J., S. Petterson, O. Bergstedt, T. J. Pettersson, and T. A. Stenstrom. 2007. Evaluation of the microbial risk reduction due to selective closure of the raw water intake before drinking water treatment. Journal of Water and Health **5**:81-97.

Atherholt, T. B., M. W. LeChevallier, W. D. Norton, and J. S. Rosen. 1998. Effect of rainfall of *Giardia* and *Crypto*. Journal American Water Works Association **90**:66-80.

Bache, D. H., and R. Gregory. 2007. Flocs in water treatment. IWA publishing.

Barbeau, B., P. Payment, J. Coallier, B. Clément, and M. Prévost. 2000. Evaluating the risk of infection from the presence of Giardia and Cryptosporidium in drinking water. Quantitative Microbiology **2**:37-54.

Bartram, J. 2009. Water safety plan manual: step-by-step risk management for drinking-water suppliers. World Health Organization.

Bartram, J., L. Fewtrell, and T.-A. Stenström. 2001. Harmonised assessment of risk and risk management for water-related infectious disease: an overview (Chapter 1). Pages 1-16 *in* L. F. a. J. Bartram, editor. Water Quality: Guidelines, Standards and Health. World Health Organization and International Water Association Publishing, London, United Kingdom.

Benjamin, M. M., and D. F. Lawler. 2013. Water quality engineering : Physical/chemical treatment processes. John Wiley & Sons, Inc.

Bolstad, W. M. 2009. Understanding computational Bayesian statistics. John Wiley & Sons.

Burnet, J.-B., Q. T. Dinh, S. Imbeault, P. Servais, S. Dorner, and M. Prévost. 2019a. Autonomous online measurement of β-D-glucuronidase activity in surface water: is it suitable for rapid E. coli monitoring? Water Research **152**:241-250.

Burnet, J.-B., C. Penny, L. Ogorzaly, and H.-M. Cauchie. 2014. Spatial and temporal distribution of Cryptosporidium and Giardia in a drinking water resource: implications for monitoring and risk assessment. Science of the Total Environment **472**:1023-1035.

Burnet, J.-B., É. Sylvestre, J. Jalbert, S. Imbeault, P. Servais, M. Prévost, and S. Dorner. 2019b. Tracking the contribution of multiple raw and treated wastewater discharges at an urban drinking water supply using near real-time monitoring of β-d-glucuronidase activity. Water Research **164**:114869.

Burnham, K. P., and D. R. Anderson. 2004. Multimodel inference: understanding AIC and BIC in model selection. Sociological methods & research **33**:261-304.

Cazals, M., R. Stott, C. Fleury, F. Proulx, M. Prévost, P. Servais, S. Dorner, and J.-B. Burnet. 2020. Near-real time notification of water quality impairments in recreational freshwaters using rapid online detection of β-D-glucuronidase activity as a surrogate for *Escherichia coli* monitoring. Science of the Total Environment **720**:137303.

CCME. 2009. Canada-wide strategy for the management of municipal wastewater effluent.

Celeux, G., F. Forbes, C. P. Robert, and D. M. Titterington. 2006. Deviance information criteria for missing data models. Bayesian analysis **1**:651-673.

Chik, A. H. S., P. J. Schmidt, and M. B. Emelko. 2018. Learning something from nothing: the critical importance of rethinking microbial non-detects. Frontiers in Microbiology **9**:2304.

Clancy, J. L., Z. Bukhari, T. M. Hargy, J. R. Bolton, B. W. Dussert, and M. M. Marshall. 2000. Using UV to inactivate Cryptosporidium. Journal American Water Works Association **92**:97-104.

Clancy, J. L., T. M. Hargy, M. M. Marshall, and J. E. Dyksen. 1998. UV light inactivation of Cryptosporidium oocysts. Journal American Water Works Association **90**:92-102.

Cleasby, J. L., E. R. Baumann, and C. D. Black. 1964. Effectiveness of potassium permanganate for disinfection. Journal American Water Works Association **56**:466-474.

Connell, K., C. C. Rodgers, H. L. Shank-Givens, J. Scheller, M. L. Pope, and K. Miller. 2000. Building a better protozoa data set. Journal American Water Works Association **92**:30-43.

Craik, S. A., D. Weldon, G. R. Finch, J. R. Bolton, and M. Belosevic. 2001. Inactivation of Cryptosporidium parvum oocysts using medium- and low-pressure ultraviolet radiation. Water Research **35**:1387-1398.

Curriero, F. C., J. A. Patz, J. B. Rose, and S. Lele. 2001. The association between extreme precipitation and waterborne disease outbreaks in the United States, 1948-1994. American Journal of Public Health **91**:1194-1199.

Dechesne, M., and E. Soyeux. 2007. Assessment of source water pathogen contamination. Journal of Water and Health **5**:39-50.

DeSilva, M. B., S. Schafer, M. Kendall Scott, B. Robinson, A. Hills, G. L. Buser, K. Salis, J. Gargano, J. Yoder, V. Hill, L. Xiao, D. Roellig, and K. Hedberg. 2015. Communitywide cryptosporidiosis outbreak associated with a surface water-supplied municipal water system--Baker City, Oregon, 2013. Epidemiol and Infection **144**:274-284.

DiGiorgio, C. L., D. A. Gonzalez, and C. C. Huitt. 2002. Cryptosporidium and Giardia recoveries in natural waters by using environmental protection agency Method 1623. Applied and Environmental Microbiology **68**:5952-5955.

Dorner, S., W. B. Anderson, T. Gaulin, H. L. Candon, R. M. Slawson, P. Payment, and P. M. Huck. 2007. Pathogen and indicator variability in a heavily impacted watershed. Journal of Water and Health **5**:241-257.

Dorner, S. M., W. B. Anderson, R. M. Slawson, N. Kouwen, and P. M. Huck. 2006. Hydrologic modeling of pathogen fate and transport. Environmental Science and Technology **40**:4746-4753.

Driscoll, C. T., and R. D. Letterman. 1988. Chemistry and fate of Al (III) in treated drinking water. Journal of Environmental Engineering **114**:21-37.

Dugan, N. R., K. R. Fox, J. H. Owens, and R. J. Miltner. 2001. Controlling Cryptosporidium oocysts using conventional treatment. Journal American Water Works Association **93**:64-76.

El-Shaarawi, A. H., S. R. Esterby, and B. J. Dutka. 1981. Bacterial density in water determined by poisson or negative binomial distributions. Applied and Environmental Microbiology **41**:107-116.

Embrechts, P., C. Klüppelberg, and T. Mikosch. 2013. Modelling extremal events: for insurance and finance. Springer Science & Business Media.

Emelko, M. B., P. J. Schmidt, and P. M. Reilly. 2010. Particle and microorganism enumeration data: enabling quantitative rigor and judicious interpretation. Environmental Science and Technology **44**:1720-1727.

Ender, A., N. Goeppert, F. Grimmeisen, and N. Goldscheider. 2017. Evaluation of β-d-glucuronidase and particle-size distribution for microbiological water quality monitoring in Northern Vietnam. Science of the Total Environment **580**:996-1006.

Farnleitner, A. H., L. Hocke, and C. Beiwl. 2001. Rapid enzymatic detection of *Escherichia coli* contamination in polluted river water. Letters in Applied Microbiology **33**:246-250.

Feng, Y. Y., S. L. Ong, J. Y. Hu, L. F. Song, X. L. Tan, and W. J. Ng. 2003. Effect of particles on the recovery of Cryptosporidium oocysts from source water samples of various turbidities. Applied and Environmental Microbiology **69**:1898-1903.

Fewtrell, L., and J. Bartram. 2001. Water quality. Guidelines, standards and health: assessment of risk and risk management for water-related infectious disease. World Health Organization (WHO) and International Water Association (IWA), London, United Kingdom.

Frank, S. A. 2009. The common patterns of nature. Journal of evolutionary biology **22**:1563-1585.

Frank, S. A. 2014. How to read probability distributions as statements about process. Entropy **16**:6059-6098.

Frank, S. A., and D. E. Smith. 2010. Measurement invariance, entropy, and probability. Entropy **12**:289-303.

Gale, P., R. Pitchers, and P. Gray. 2002. The effect of drinking water treatment on the spatial heterogeneity of micro-organisms: implications for assessment of treatment efficiency and health risk. Water Research **36**:1640-1648.

Garcia-Armisen, T., P. Lebaron, and P. Servais. 2005. Beta-D-glucuronidase activity assay to assess viable *Escherichia coli* abundance in freshwaters. Journal of Applied Microbiology **40**:278-282.

Gehr, R., M. Wagner, P. Veerasubramanian, and P. Payment. 2003. Disinfection efficiency of peracetic acid, UV and ozone after enhanced primary treatment of municipal wastewater. Water Research **37**:4573-4586.

Gelman, A. 2006. Prior distributions for variance parameters in hierarchical models (comment on article by Browne and Draper). Bayesian analysis **1**:515-534.

Gelman, A., J. B. Carlin, H. S. Stern, D. B. Dunson, A. Vehtari, and D. B. Rubin. 2013. Bayesian data analysis. CRC press.

Gelman, A., and J. Hill. 2006. Data analysis using regression and multilevel/hierarchical models. Cambridge university press.

Gelman, A., and K. Shirley. 2011. Inference from simulations and monitoring convergence. Handbook of markov chain monte carlo **6**:163-174.

George, I., M. Petit, and P. Servais. 2000. Use of enzymatic methods for rapid enumeration of coliforms in freshwaters. Journal of Applied Microbiology **88**:404-413.

Gonzales-Barron, U., and F. Butler. 2011. A comparison between the discrete Poisson-gamma and Poisson-lognormal distributions to characterise microbial counts in foods. Food Control **22**:1279-1286.

Gouverment du Québec. 2018. Chapitre Q-2, r. 26. Règlement sur les exploitations agricoles. Loi sur la qualité de l'environnement (chapitre Q-2, a. 31, 53.30, 70, 115.27, 115.34 et 124.1).

Gouvernement du Québec. 2015. Règlement sur les ouvrages municipaux d'assainissement des eaux usées. Page 17, Québec, Canada.

Government of New Zealand. 2007. Drinking-water standards for New Zealand (Legislation). Ministry of Health.

Gregory, J. 2005. Particles in water: properties and processes. CRC Press.

Gregory, J., and C. R. O'Melia. 1989. Fundamentals of flocculation. Critical Reviews in Environmental Control **19**:185-230.

Guy, M., J. McIver, and M. Lewis. 1977. The removal of virus by a pilot treatment plant. Water Research **11**:421-428.

Gyürék, L. L., and G. R. Finch. 1998. Modeling water treatment chemical disinfection kinetics. Journal of Environmental Engineering **124**:783-793.

Haas, C. N. 1983. Estimation of risk due to low doses of microorganisms: a comparison of alternative methodologies. American Journal of Epidemiology **118**:573-582.

Haas, C. N. 1996. How to average microbial densities to characterize risk. Water Research **30**:1036-1038.

Haas, C. N. 1997. Importance of distributional form in characterizing inputs to Monte Carlo risk assessments. Risk Analysis **17**:107-113.

Haas, C. N. 1999. On modeling correlated random variables in risk assessment. Risk Analysis **19**:1205-1214.

Haas, C. N. 2002. Conditional dose-response relationships for microorganisms: development and application. Risk Analysis **22**:455-463.

Haas, C. N., C. S. Crockett, J. B. Rose, C. P. Gerba, and A. M. Fazil. 1996. Assessing the risk posed by oocysts in drinking water. Journal American Water Works Association **88**:131-136.

Haas, C. N., and B. Heller. 1988. Test of the validity of the Poisson assumption for analysis of most-probable-number results. Applied and Environmental Microbiology **54**:2996-3002.

Haas, C. N., and B. Kaymak. 2003. Effect of initial microbial density on inactivation of Giardia muris by ozone. Water Research **37**:2980-2988.

Haas, C. N., J. B. Rose, C. Gerba, and S. Regli. 1993. Risk assessment of virus in drinking water. Risk Analysis **13**:545-552.

Haas, C. N., J. B. Rose, and C. P. Gerba. 1999. Quantitative microbial risk assessment. John Wiley and Sons, Inc., New York, USA.

Haas, C. N., and R. R. Trussell. 1998. Frameworks for assessing reliability of multiple, independent barriers in potable water reuse. Water Science and Technology **38**:1-8.

Han, M., and D. F. Lawler. 1992. The (relative) insignificance of G in flocculation. Journal American Water Works Association **84**:79-91.

Hanson, A. T., and J. L. Cleasby. 1990. Effects of temperature on turbulent flocculation: fluid dynamics and chemistry. Journal American Water Works Association **82**:56-73.

Harremoës, P. 1988. Stochastic models for estimation of extreme pollution from urban runoff. Water Research **22**:1017-1026.

Hata, A., H. Katayama, K. Kojima, S. Sano, I. Kasuga, M. Kitajima, and H. Furumai. 2014. Effects of rainfall events on the occurrence and detection efficiency of viruses in river water impacted by combined sewer overflows. Science of the Total Environment **468–469**:757-763.

Havelaar, A., M. Van Olphen, and J. Schijven. 1995. Removal and inactivation of viruses by drinking water treatment processes under full scale conditions. Water Science and Technology **31**:55-62.

Health Canada. 2019. Guidance on the Use of Quantitative Microbial Risk Assessment in Drinking Water. Water and Air Quality Bureau, Healthy Environments and Consumer Safety Branch, Health Canada, Ottawa, Ontario.

Heffron, J., and B. K. Mayer. 2016. Emerging investigators series: virus mitigation by coagulation: recent discoveries and future directions. Environmental Science: Water Research & Technology **2**:443-459.

Hejkal, T. W., F. M. Wellings, P. A. Larock, and A. L. Lewis. 1979. Survival of poliovirus within organic solids during chlorination. Applied and Environmental Microbiology **38**:114-116.

Hijnen, W., G. Wübbels, A. Soppe, H. Wolters, P. Nobel, D. van der Kooij, and G. Medema. 1998. Removal of indicator bacteria during drinking water production at location De Punt, Water Company Groningen. Kiwa report.

Hijnen, W. A. M. 2009. Elimination of micro-organisms in water treament. University of Utrecht, Utrecht, The Netherlands, The Netherlands.

Hijnen, W. A. M., Y. J. Dullemont, J. F. Schijven, A. J. Hanzens-Brouwer, M. Rosielle, and G. Medema. 2007. Removal and fate of Cryptosporidium parvum, Clostridium perfringens and small-sized centric diatoms (Stephanodiscus hantzschii) in slow sand filters. Water Research **41**:2151-2162.

Hijnen, W. A. M., and G. J. Medema. 2010. Elimination of micro-organisms by drinking water treatment processes. IWA publishing London.

Hijnen, W. A. M., G. M. H. Suylen, J. A. Bahlman, A. Brouwer-Hanzens, and G. J. Medema. 2010. GAC adsorption filters as barriers for viruses, bacteria and protozoan (oo)cysts in water treatment. Water Research **44**:1224-1234.

Hijnen, W. A. M., A. J. Van Der Veer, E. F. Beerendonk, and G. J. Medema. 2004. Increased resistance of environmental anaerobic spores to inactivation by UV. Water Science and Technology: Water Supply **4**:55-61.

Hijnen, W. A. M., A. J. Van der Veer, J. Van Beveren, and G. J. Medema. 2002. Spores of sulphite-reducing clostridia (SSRC) as surrogate for verification of the inactivation capacity of full-scale ozonation for Cryptosporidium. Water Science and Technology: Water Supply **2**:163-170.

Hijnen, W. A. M., J. Willemsen-Zwaagstra, P. Hiemstra, G. J. Medema, and D. van der Kooij. 2000. Removal of sulphite-reducing clostridia spores by full-scale water treatment processes as a surrogate for protozoan (oo)cysts removal. Water Science and Technology **41**:165-171.

Howard, G., R. Calow, A. Macdonald, and J. Bartram. 2016. Climate change and water and sanitation: likely impacts and emerging trends for action. Annual Review of Environment and Resources **41**:253-276.

Hrudey, S., and E. Hrudey. 2019. Common themes contributing to recent drinking water disease outbreaks in affluent nations. Water Supply **19**:1767-1777.

Hrudey, S. E., and E. J. Hrudey. 2004. Safe drinking water. Lessons from recent outbreaks in affluent nations. International Water Association Publishing, London, United Kingdom.

Hrudey, S. E., P. M. Huck, P. Payment, R. W. Gillham, and E. J. Hrudey. 2002. Walkerton: Lessons learned in comparison with waterborne outbreaks in the developed world. Environmental Engineering and Science **1**:397-407.

Huertas, A., B. Barbeau, C. Desjardins, and G. A. Toranzos. 2001. The use of alternate microbiological indicators of water treatment plant performance. Proceedings of the Water Environment Federation **2001**:394-402.

Hunt, N. K., and B. J. Marinas. 1997. Kinetics of *Escherichia coli* inactivation with ozone. Water Research **31**:1355-1362.

Hurst, A. M., M. J. Edwards, M. Chipps, B. Jefferson, and S. A. Parsons. 2004. The impact of rainstorm events on coagulation and clarifier performance in potable water treatment. Science of the Total Environment **321**:219-230.

IPCC. 2014. Climate Change 2014 – Impacts, adaptation and vulnerability: Part A: Global and sectoral aspects. Cambridge University Press, Cambridge.

Ives, K. J. 2001. Coagulation and flocculation: Part II—orthokinetic flocculation. Pages 130-165 Solid-Liquid Separation. Elsevier.

Jaidi, K., B. Barbeau, A. Carrière, R. Desjardins, and M. Prévost. 2009. Including operational data in QMRA model: Development and of model inputs impact Journal of Water and Health **7**:77-95.

Jalliffier-Verne, I., M. Heniche, A.-S. Madoux-Humery, M. Galarneau, P. Servais, M. Prévost, and S. Dorner. 2016. Cumulative effects of fecal contamination from combined sewer overflows: Management for source water protection. Journal of Environmental Management **174**:62-70.

Jennings, P., and A. Rhatigan. 2002. Cryptosporidiosis outbreak in Ireland linked to public water supply. Weekly releases (1997–2007) **6**:2089.

Kaas, R., and O. Hesselager. 1995. Ordering claim size distributions and mixed Poisson probabilities. Insurance: Mathematics and Economics **17**:193-201.

Kang, L. S., and J. L. Cleasby. 1995. Temperature effects on flocculation kinetics using Fe(III) coagulant. Journal of Environmental Engineering **121**:893-901.

Kass, R. E., B. P. Carlin, A. Gelman, and R. M. Neal. 1998. Markov chain Monte Carlo in practice: a roundtable discussion. The American Statistician **52**:93-100.

Kato, R., T. Asami, E. Utagawa, H. Furumai, and H. Katayama. 2018. Pepper mild mottle virus as a process indicator at drinking water treatment plants employing coagulation-sedimentation, rapid sand filtration, ozonation, and biological activated carbon treatments in Japan. Water Research **132**:61-70.

Katz, R. W., M. B. Parlange, and P. Naveau. 2002. Statistics of extremes in hydrology. Advances in Water Resources **25**:1287-1304.

Kaymak, B., and C. N. Haas. 2008. Effect of initial microbial density on inactivation of Escherichia coli by monochloramine. Journal of Environmental Engineering and Science **7**:237-245.

Khan, S. J., D. Deere, F. D. Leusch, A. Humpage, M. Jenkins, and D. Cunliffe. 2015. Extreme weather events: Should drinking water quality management systems adapt to changing risk profiles? Water Research **85**:124-136.

Kistemann, T., T. Classen, C. Koch, F. Dangendorf, R. Fischeder, J. Gebel, V. Vacata, and M. Exner. 2002. Microbial load of drinking water reservoir tributaries during extreme rainfall and runoff. Applied and Environmental Microbiology **68**:2188-2197.

Koponen, I. 1995. Analytic approach to the problem of convergence of truncated Lévy flights towards the Gaussian stochastic process. Physical Review E **52**:1197.

Koschelnik, J., W. Vogl, M. Epp, and M. Lackner. 2015. Rapid analysis of β-D-glucuronidase activity in water using fully automated technology. Pages 471 - 481 *in* WIT Transactions on Ecology and the Environment.

Kruschke, J. K. 2014. Doing Bayesian data analysis : A tutorial with R, JAGS, and Stan. 2nd edition edition. Amsterdam Academic Press.

Kumar, S., N. C. Ghosh, and A. Kazmi. 2016. Ballasted sand flocculation for water, wastewater and CSO treatment. Environmental Technology Reviews **5**:57-67.

Lalancette, C., I. Papineau, P. Payment, S. Dorner, P. Servais, B. Barbeau, G. Di Giovanni, and M. Prévost. 2014. Changes in *E. coli to Cryptosporidium* ratio from various fecal pollution sources and drinking water intakes. Water Research **55**:150–161.

Lapen, D. R., P. J. Schmidt, J. L. Thomas, T. A. Edge, C. Flemming, J. Keithlin, N. Neumann, F. Pollari, N. Ruecker, A. Simhon, E. Topp, G. Wilkes, and K. D. M. Pintar. 2016. Towards a more accurate quantitative assessment of seasonal *Cryptosporidium* infection risks in surface waters using species and genotype information. Water Research **105**:625-637.

Lapointe, M., C. Brosseau, Y. Comeau, and B. Barbeau. 2017. Assessing alternative media for ballasted flocculation. Journal of Environmental Engineering **143**:04017071.

Larsson, C., Y. Andersson, G. Allestam, A. Lindqvist, N. Nenonen, and O. Bergstedt. 2014. Epidemiology and estimated costs of a large waterborne outbreak of norovirus infection in Sweden. Epidemiology & Infection **142**:592-600.

Lawler, D. F., and J. A. Nason. 2005. Integral water treatment plant modeling: improvements for particle processes. Environmental Science & Technology **39**:6337-6342.

Lawler, D. F., C. R. O'Melia, and J. E. Tobiason. 1978. Integral water treament plant design: particle size and plant performance. American Chemical Society, Division of Environmental Chemistry, Preprints **18**:243-245.

LeChevallier, M. W., and W. D. Norton. 1992. Examining relationships between particle counts and Giardia, Cryptosporidium, and turbidity. Journal American Water Works Association **84**:54-60.

LeChevallier, M. W., W. D. Norton, and R. G. Lee. 1991. Occurrence of Giardia and Cryptosporidium spp. in surface water supplies. Applied and Environmental Microbiology **57**:2610-2616.

Lee, K. M. 2019. The Critical Role of Chemical Pre-Treatment in Ensuring Cryptosporidium Removal by Filtration of High Quality Source Water. University of Waterloo.

Li, Q., Y. Qiu, X. L. Pang, and N. J. Ashbolt. 2019. Spiked virus level needed to correctly assess enteric virus recovery in water matrices. Applied and Environmental Microbiology **85**.

Liu, R., L. Sun, R. Ju, H. Liu, J. Gu, and G. Li. 2013. Treatment of low-turbidity source water by permanganate pre-oxidation: In situ formed hydrous manganese dioxide as filter aid. Separation and Purification Technology **117**:69-74.

Mac Kenzie, W. R., N. J. Hoxie, M. E. Proctor, M. S. Gradus, K. A. Blair, D. E. Peterson, J. J. Kazmierczak, D. G. Addiss, K. R. Fox, J. B. Rose, and J. P. Davis. 1994. A massive outbreak in Milwaukee of *Cryptosporidium* infection transmitted through the public water supply. The New England Journal of Medicine **331**:161-167.

Madoux-Humery, A.-S., S. Dorner, S. Sauvé, K. Aboulfadl, M. Galarneau, P. Servais, and M. Prévost. 2013. Temporal variability of combined sewer overflow contaminants: Evaluation of wastewater micropollutants as tracers of fecal contamination. Water Research **47**:4370-4382.

Madoux-Humery, A.-S., S. Dorner, S. Sauvé, K. Aboulfadl, M. Galarneau, P. Servais, and M. Prévost. 2016. The effects of combined sewer overflow events on riverine sources of drinking water. Water Research **92**:218-227.

Mantegna, R. N., and H. E. Stanley. 1995. Scaling behaviour in the dynamics of an economic index. Nature **376**:46-49.

Mariani, M. C., and Y. Liu. 2007. Normalized truncated Levy walks applied to the study of financial indices. Physica A: Statistical Mechanics and its Applications **377**:590-598.

Masago, Y., K. Oguma, H. Katayama, T. Hirata, and S. Ohgaki. 2004. *Cryptosporidium* monitoring system at a water treatment plant, based on waterborne risk assessment. Water Science and Technology **50**:293-299.

McElreath, R. 2020. Statistical rethinking: A Bayesian course with examples in R and Stan. CRC press.

McTigue, N. E., M. LeChevallier, H. Arora, and J. Clancy. 1998. National assessment of particle removal by filtration. 90757, American Water Works Association Research Foundation and American Water Works Association, Denver, Colorado, USA.

Medema, G., and N. Ashbolt. 2006. QMRA: its value for risk management. Microrisk.

Medema, G., and P. Smeets. 2009. Quantitative risk assessment in the water safety plan: case studies from drinking water practice. Water Science and Technology: Water Supply **9**:127-132.

Medema, G. J., W. Hoogenboezem, A. J. van der Veer, H. A. M. Ketelaars, W. A. M. Hijnen, and P. J. Nobel. 2003. Quantitative risk assessment of Cryptosporidium in surface water treatment. Water Science and Technology **47**:241-247.

Meng, Q. S., and C. P. Gerba. 1996. Comparative inactivation of enteric adenoviruses, poliovirus and coliphages by ultraviolet irradiation. Water Research **30**:2665-2668.

Michen, B., and T. Graule. 2010. Isoelectric points of viruses. Journal of Applied Microbiology **109**:388-397.

Millar, R. B. 2009. Comparison of hierarchical Bayesian models for overdispersed count data using DIC and Bayes' factors. Biometrics **65**:962-969.

Milly, P. C. D., J. Betancourt, M. Falkenmark, R. M. Hirsch, Z. W. Kundzewicz, D. P. Lettenmaier, and R. J. Stouffer. 2008. Stationarity is dead: Whither water management? Science **319**:573-574.

Ministry of Health. 2008. Drinking-water standards for New Zealand 2005 (revised 2008). Wellington, New Zealand.

Mitzenmacher, M. 2004. A brief history of generative models for power law and lognormal distributions. Internet mathematics **1**:226-251.

Moehle, J., and G. G. Deierlein. 2004. A framework methodology for performance-based earthquake engineering.*in* 13th world conference on earthquake engineering.

Moreira, N. A., and M. Bondelind. 2017. Safe drinking water and waterborne outbreaks. Journal of Water and Health **15**:83-96.

Morris, J. K., and W. R. Knocke. 1984. Temperature effects on the use of metal-ion coagulants for water treatment. Journal American Water Works Association **76**:74-79.

Nahrstedt, A., and R. Gimbel. 1996. A statistical method for determining the reliability of the analytical results in the detection of Cryptosporidium and Giardia in water. Aqua- Journal of Water Supply: Research and Technology **45**:101-111.

Nasser, A., D. Weinberg, N. Dinoor, B. Fattal, and A. Adin. 1995. Removal of hepatitis A virus (HAV), poliovirus and MS2 coliphage by coagulation and high rate filtration. Water Science and Technology **31**:63-68.

Newman, M. E. 2005. Power laws, Pareto distributions and Zipf's law. Contemporary physics **46**:323-351.

NHMRC. 2018. Australian drinking water guidelines: Revised chapter 5 microbial quality of drinking water incorporating a microbial health based target. Australian Government.

Nieminski, E. C., and J. E. Ongerth. 1995. Removing Giardia and Cryptosporidium by conventional treatment and direct filtration. Journal ot the American Water Works Association **87**:96-106.

Nilsen, V., E. Christensen, M. Myrmel, and A. Heistad. 2019. Spatio-temporal dynamics of virus and bacteria removal in dual-media contact-filtration for drinking water. Water Research **156**:9-22.

Nilsen, V., and J. Wyller. 2016. QMRA for drinking water: 2. The effect of pathogen clustering in single-hit dose-response models. Risk Analysis **36**:163-181.

Nygard, K., B. Schimmer, O. Sobstad, A. Walde, I. Tveit, N. Langeland, T. Hausken, and P. Aavitsland. 2006. A large community outbreak of waterborne giardiasis- delayed detection in a non-endemic urban area. BMC Public Health **6**:141.

O'Hagan, A., C. E. Buck, A. Daneshkhah, J. R. Eiser, P. H. Garthwaite, D. J. Jenkinson, J. E. Oakley, and T. Rakow. 2006. Uncertain judgements: eliciting experts' probabilities. John Wiley & Sons.

Olsson, U. 2005. Confidence intervals for the mean of a log-normal distribution. Journal of Statistics Education **13**.

Ott, W. R. 1994. Environmental statistics and data analysis. CRC Press.

Pang, X., Y. Qiu, T. Gao, R. Zurawell, N. F. Neumann, S. Craik, and B. E. Lee. 2019. Prevalence, levels and seasonal variations of human enteric viruses in six major rivers in Alberta, Canada. Water Research **153**:349-356.

Pang, X. L., B. E. Lee, K. Pabbaraju, S. Gabos, S. Craik, P. Payment, and N. Neumann. 2012. Pre-analytical and analytical procedures for the detection of enteric viruses and enterovirus in water samples. Journal of virological methods **184**:77-83.

Pang, X. L., J. K. Preiksaitis, and B. E. Lee. 2014. Enhanced enteric virus detection in sporadic gastroenteritis using a multi-target real-time PCR panel: a one-year study. Journal of Medical Virology **86**:1594-1601.

Payment, P. 2003. Enlèvement des microorganismes pathogènes et des bactéries indicatrices par les stations de traitement des eaux usées municipales situées sur la rivière des Mille îles. 3336.11.00.01, Ministère de l'Environnement du Québec. Programme d'aide à la recherche et au développement en environnement (PARDE).

Payment, P., and E. Franco. 1993. Clostridium perfringens and somatic coliphages as indicators of the efficiency of drinking water treatment for viruses and protozoan cysts. Applied and Environmental Microbiology **59**:2418-2424.

Payment, P., A. Godfree, and D. Sartory. 2002. Clostridium. Bitton, G. John Wiley & Sons.

Payment, P., M. Trudel, and R. Plante. 1985. Elimination of viruses and indicator bacteria at each step of treatment during preparation of drinking water at seven water treatment plants. Applied and Environmental Microbiology **49**:1418-1428.

Pelly, H., M. Cormican, D. O'Donovan, R. Chalmers, B. Hanahoe, R. Cloughley, P. McKeown, and G. Corbett-Feeney. 2007. A large outbreak of cryptosporidiosis in western Ireland linked to public water supply: a preliminary report. Weekly releases (1997–2007) **12**:3187.

Petterson, S., D. Roser, and D. Deere. 2015. Characterizing the concentration of *Cryptosporidium* in Australian surface waters for setting health-based targets for drinking water treatment. J Water Health **13**:879-896.

Petterson, S., R. Signor, N. Ashbolt, and D. Roser 2006. QMRA methodology. Microrisk.

Petterson, S., and T.-A. Stenström. 2015. Quantification of pathogen inactivation efficacy by free chlorine disinfection of drinking water for QMRA. Journal of Water and Health **13**:625-644.

Petterson, S. R., and N. J. Ashbolt. 2016. QMRA and water safety management: Review of application in drinking water systems. Journal of Water and Health **14**:571-589.

Petterson, S. R., R. S. Signor, and N. J. Ashbolt. 2007. Incorporating method recovery uncertainties in stochastic estimates of raw water protozoan concentrations for QMRA. Journal of Water and Health **5**:51-65.

Pipes, W. O., P. Ward, and S. H. Ahn. 1977. Frequency distributions for coliform bacteria in water. Journal American Water Works Association **69**:664-668.

Plate, E. J., and L. Duckstein. 1988. RELIABILITY-BASED DESIGN CONCEPTS IN HYDRAULIC ENGINEERING 1. JAWRA Journal of the American Water Resources Association **24**:235-245.

Plum, V., C. P. Dahl, L. Bentsen, C. R. Petersen, L. Napstjert, and N. B. Thomsen. 1998. The Actiflo method. Water Science and Technology **37**:269-275.

Plummer, M. 2013. JAGS: Just Another Gibbs Sampler (Version 3.4. 0)[Computer software].

Pollard, S. J., R. Yearsley, N. Reynard, I. C. Meadowcroft, R. Duarte-Davidson, and S. L. Duerden. 2002. Current directions in the practice of environmental risk assessment in the United Kingdom. ACS Publications.

Pouillot, R., P. Beaudeau, J. B. Denis, and F. Derouin. 2004. A quantitative risk assessment of waterborne cryptospridiosis in France using second-order Monte Carlo simulation. Risk Analysis **24**:17.

Pradhan, B., and D. Kundu. 2011. Bayes estimation and prediction of the two-parameter gamma distribution. Journal of Statistical Computation and Simulation **81**:1187-1198.

Prevost, B., F. Lucas, A. Goncalves, F. Richard, L. Moulin, and S. Wurtzer. 2015. Large scale survey of enteric viruses in river and waste water underlines the health status of the local population. Environment International **79**:42-50.

Qiu, Y., B. E. Lee, N. Neumann, N. Ashbolt, S. Craik, R. Maal-Bared, and X. L. Pang. 2015. Assessment of human virus removal during municipal wastewater treatment in Edmonton, Canada. Journal of Applied Microbiology **119**:1729-1739.

Qiu, Y., B. E. Lee, N. J. Ruecker, N. Neumann, N. Ashbolt, and X. Pang. 2016. A one-step centrifugal ultrafiltration method to concentrate enteric viruses from wastewater. Journal of virological methods **237**:150-153.

Qiu, Y., Q. Li, B. E. Lee, N. J. Ruecker, N. F. Neumann, N. J. Ashbolt, and X. Pang. 2018. UV inactivation of human infectious viruses at two full-scale wastewater treatment plants in Canada. Water Research **147**:73-81.

Quintero, A., and E. Lesaffre. 2018. Comparing hierarchical models via the marginalized deviance information criterion. Stat Med **37**:2440-2454.

Rao, V. C., J. M. Symons, A. Ling, P. Wang, T. G. Metcalf, J. C. Hoff, and J. L. Melnick. 1988. Removal of hepatitis A virus and rotavirus by drinking water treatment. Journal-American Water Works Association **80**:59-67.

Regli, S., J. B. Rose, C. N. Haas, and C. P. Gerba. 1991. Modeling the risk from Giardia and viruses in drinking water. Journal American Water Works Association **83**:76-84.

Ryzinska-Paier, G., T. Lendenfeld, K. Correa, P. Stadler, A. P. Blaschke, R. L. Mach, H. Stadler, A. K. Kirschner, and A. H. Farnleitner. 2014. A sensitive and robust method for automated on-line monitoring of enzymatic activities in water and water resources. Water Science & Technology **69**:1349-1358.

Schijven, J., P. Teunis, T. Suylen, H. Ketelaars, L. Hornstra, and S. Rutjes. 2019. QMRA of adenovirus in drinking water at a drinking water treatment plant using UV and chlorine dioxide disinfection. Water Research **158**:34-45.

Schijven, J. F., P. F. M. Teunis, S. A. Rutjes, M. Bouwknegt, and A. M. de Roda Husman. 2011. QMRAspot: a tool for quantitative microbial risk assessment from surface water to potable water. Water Research **45**:5564-5576.

Schmidt, P. J., W. B. Anderson, and M. B. Emelko. 2020. Describing water treatment process performance: Why average log-reduction can be a misleading statistic. Water Research:115702.

Schmidt, P. J., M. B. Emelko, and P. M. Reilly. 2010. Quantification of analytical recovery in particle and microorganism enumeration methods. Environmental Science & Technology **44**:1705-1712.

Semenza, J. C. 2020. Cascading risks of waterborne diseases from climate change. Nature Immunology **21**:484-487.

Servais, P., J. Prats, J. Passerat, and T. Garcia-Armisen. 2009. Abundance of culturable versus viable *Escherichia coli* in freshwater. Canadian Journal of Microbiology **55**:905-909.

Shin, G.-A., K. G. Linden, M. J. Arrowood, G. Faubert, and M. D. Sobsey. 2001. DNA repair of UV-irradiated Cryptosporidium parvum oocysts and Giardia lamblia cysts. Page 8 *in* First International Congress on UV Technologies. IUVA, Washington, DC, USA.

Shin, G.-A., and M. D. Sobsey. 2015. Removal of norovirus from water by coagulation, flocculation and sedimentation processes. Water Science and Technology: Water Supply **15**:158-163.

Shirasaki, N., T. Matsushita, Y. Matsui, and T. Marubayashi. 2016. Effect of aluminum hydrolyte species on human enterovirus removal from water during the coagulation process. Chemical Engineering Journal **284**:786-793.

Shirasaki, N., T. Matsushita, Y. Matsui, K. Murai, and A. Aochi. 2017. Elimination of representative contaminant candidate list viruses, coxsackievirus, echovirus, hepatitis A virus, and norovirus, from water by coagulation processes. Journal of Hazardous Materials **326**:110-119.

Shorrocks, A. F. 1983. Ranking income distributions. Economica **50**:3-17.

Signor, R. S., and N. J. Ashbolt. 2009. Comparing probabilistic microbial risk assessments for drinking water against daily rather than annualised infection probability targets. Journal of Water and Health **7**:535-543.

Signor, R. S., N. J. Ashbolt, and D. J. Roser. 2007. Microbial risk implications of rainfall-induced runoff events entering a reservoir used as a drinking-water source. Water Supply: Research and Technology-Aqua **56**:515-531.

Signor, R. S., D. J. Roser, N. J. Ashbolt, and J. E. Ball. 2005. Quantifying the impact of runoff events on microbiological contaminant concentrations entering surface drinking source waters. Journal of Water and Health **3**:453-468.

Sinclair, M., J. O'Toole, K. Gibney, and K. Leder. 2015. Evolution of regulatory targets for drinking water quality. Journal of Water and Health **13**:413-426.

Skraber, S., L. Ogorzaly, K. Helmi, A. Maul, L. Hoffmann, H.-M. Cauchie, and C. Gantzer. 2009. Occurrence and persistence of enteroviruses, noroviruses and F-specific RNA phages in natural wastewater biofilms. Water Research **43**:4780-4789.

Smeets, P. W. M. H. 2010. Stochastic modelling of drinking water treatment in quantitative microbial risk assessment. International Water Association Publishing, London, United Kingdom.

Smeets, P. W. M. H., Y. J. Dullemont, P. H. A. M. Van Gelder, J. C. van Dijk, and G. J. Medema. 2008. Improved methods for modelling drinking water treatment in quantitative microbial risk assessment; a case study of Campylobacter reduction by filtration and ozonation. Journal of Water and Health **6**:301-314.

Smeets, P. W. M. H., L. C. Rietveld, J. C. van Dijk, and G. J. Medema. 2010. Practical applications of quantitative microbial risk assessment (QMRA) for water safety plans. Water Science and Technology **61**:1561-1568.

Smeets, P. W. M. H., A. W. C. van der Helm, Y. J. Dullemont, L. C. Rietveld, J. C. van Dijk, and G. J. Medema. 2006. Inactivation of *Escherichia coli* by ozone under bench-scale plug flow and full-scale hydraulic conditions. Water Research **40**:3239-3248.

Smeets, P. W. M. H., J. C. van Dijk, G. Stanfield, L. C. Rietveld, and G. J. Medema. 2007. How can the UK statutory Cryptosporidium monitoring be used for quantitative risk assessment of Cryptosporidium in drinking water? Journal of Water and Health **5**:107-118.

Smeets, W. M., and G. J. Medema. 2006. Combined use of microbiological and non-microbiological data to assess treatment efficacy. Water Science and Technology **54**:35-40.

Smith, A. E., P. B. Ryan, and J. S. Evans. 1992. The effect of neglecting correlations when propagating uncertainty and estimating the population distribution of risk. Risk Analysis **12**:467-474.

Sokolova, E., S. R. Petterson, O. Dienus, F. Nyström, P.-E. Lindgren, and T. J. Pettersson. 2015. Microbial risk assessment of drinking water based on hydrodynamic modelling of pathogen concentrations in source water. Science of the Total Environment **526**:177-186.

Sornette, D. 2006. Critical phenomena in natural sciences: chaos, fractals, selforganization and disorder: concepts and tools. Springer Science & Business Media.

Sornette, D., and R. Cont. 1997. Convergent multiplicative processes repelled from zero: power laws and truncated power laws. Journal de Physique I **7**:431-444.

Spiegelhalter, D. J., N. G. Best, B. R. Carlin, and A. van der Linde. 2002. Bayesian measures of model complexity and fit. Journal of the Royal Statistical Society Series B-Statistical Methodology **64**:583-616.

St-Pierre, K., S. Levesque, E. Frost, N. Carrier, R. D. Arbeit, and S. Michaud. 2009. Thermotolerant coliforms are not a good surrogate for Campylobacter spp. in environmental water. Applied and Environmental Microbiology **75**:6736-6744.

Stadler, P., G. Blöschl, L. Nemeth, M. Oismüller, M. Kumpan, J. Krampe, A. H. Farnleitner, and M. Zessner. 2019. Event-transport of beta-d-glucuronidase in an agricultural headwater stream: Assessment of seasonal patterns by on-line enzymatic activity measurements and environmental isotopes. Science of the Total Environment **662**:236-245.

Stadler, P., G. Blöschl, W. Vogl, J. Koschelnik, M. Epp, M. Lackner, M. Oismüller, M. Kumpan, L. Nemeth, P. Strauss, R. Sommer, G. Ryzinska-Paier, A. H. Farnleitner, and M. Zessner. 2016. Real-time monitoring of beta-d-glucuronidase activity in sediment laden streams: A comparison of prototypes. Water Research **101**:252-261.

Stetler, R., R. Ward, and S. Waltrip. 1984. Enteric virus and indicator bacteria levels in a water treatment system modified to reduce trihalomethane production. Applied and Environmental Microbiology **47**:319-324.

Stirling, R., J. Aramini, A. Ellis, G. Lim, R. Meyers, M. Fleury, and D. Werker. 2001. Waterborne cryptosporidiosis outbreak, North Battleford, Saskatchewan, Spring 2001. Canada Communicable Disease Report (CCDR) **27**:185-192.

Student. 1907. On the error of counting with a haemacytometer. Biometrika:351-360.

Swaffer, B., H. Abbott, B. King, L. van der Linden, and P. Monis. 2018. Understanding human infectious *Cryptosporidium* risk in drinking water supply catchments. Water Research **138**:282-292.

Swaffer, B. A., H. M. Vial, B. J. King, R. Daly, J. Frizenschaf, and P. T. Monis. 2014. Investigating source water *Cryptosporidium* concentration, species and infectivity rates during rainfall-runoff in a multi-use catchment. Water Res **67**:310-320.

Sylvestre, E., J.-B. Burnet, M. Prévost, P. Cantin, C. Robert, M. Villion, P. Smeets, G. Medema, and S. Dorner. 2018. Can *E. coli* reliably inform on the magnitude and fluctuations in waterborne pathogens for microbial risk assessment? A study of 26 drinking water treatment plants. Page 22 *in* American Water Works Association-Water Quality Technology Conference (WQTC), Toronto, ON, Canada.

Sylvestre, E., J.-B. Burnet, P. Smeets, G. Medma, M. Prévost, and S. Dorner. 2020a. Can routine monitoring of *E. coli* fully account for peak event concentrations at drinking water intakes in agricultural and urban rivers? Water Research **170**:115369.

Sylvestre, É., J. B. Burnet, S. Dorner, P. Smeets, G. Medema, and M. Prévost. 2020b. Impact of hydrometeorological events for the selection of parametric models for protozoan pathogens in drinking-water sources (in press). Risk Analysis.

Taghipour, M., A. Shakibaeinia, É. Sylvestre, S. Tolouei, and S. Dorner. 2019. Microbial risk associated with CSOs upstream of drinking water sources in a transboundary river using hydrodynamic and water quality modeling. Science of the Total Environment **683**:547-558.

Taleb, N. N. 2015. Silent risk. Preliminary Book Draft.

Teunis, P., A. Davidson, and D. Deere. 2004. Short term fluctuations in drinking water quality and their significance for public health.

Teunis, P., and J. Schijven. 2019. Generic Guidance to Quantitative Microbial Risk Assessment for Food and Water.

Teunis, P. F., and A. H. Havelaar. 2000. The beta poisson dose-response model is not a single-hit model. Risk Analysis **20**:513-520.

Teunis, P. F. M., E. G. Evers, and W. Slob. 1999. Analysis of variable fractrions resulting from microbial counts. Quantitative Microbiology **1**:63-88.

Teunis, P. F. M., G. J. Medema, L. Kruidenier, and A. H. Havelaar. 1997. Assessment of the risk of infection by Cryptosporidium or Giardia in drinking water from a surface water source. Water Research **31**:1333-1346.

Teunis, P. F. M., S. A. Rutjes, T. Westrell, and A. M. de Roda Husman. 2009. Characterization of drinking water treatment for virus risk assessment. Water Research **43**:395-404.

Thomas, H. A. 1955. Statistical analysis of coliform data. Sewage and Industrial Wastes:212-222.

Thomas, K. M., D. F. Charron, D. Waltner-Toews, C. Schuster, A. R. Maarouf, and J. D. Holt. 2006. A role of high impact weather events in waterborne disease outbreaks in Canada, 1975-2001. International Journal of Environmental Health Research **16**:167-180.

Thurston-Enriquez, J. A., C. N. Haas, J. Jacangelo, and C. P. Gerba. 2005. Inactivation of enteric adenovirus and feline calicivirus by ozone. Water Research **39**:3650-3656.

Thurston-Enriquez, J. A., C. N. Haas, J. Jacangelo, K. Riley, and C. P. Gerba. 2003. Inactivation of feline calicivirus and adenovirus type 40 by UV radiation. Applied and Environmental Microbiology **69**:577-582.

Tijms, H. C. 2003. A first course in stochastic models. John Wiley and sons.

USEPA. 2005. Method 1623: Cryptosporidium and Giardia in water by filtration/IMS/FA. EPA 815-R-05-002, Office of Water (4607), Washington, DC, USA.

USEPA. 2006. Long term 2 - Enhanced surface water treatment rule (Final rule). Office of Water, Washington, DC, USA.

USEPA. 2010. Long term 2 enhanced surface water treatment rule toolbox guidance manual. EPA 815-D-09-001, Office of Water, Washington, DC, USA.

USEPA. 2012. Method 1623.1: Cryptosporidium and Giardia in Water by Filtration/IMS/FA.

van de Schoot, R., and M. Miocević. 2020. Small sample size solutions: A guide for applied researchers and practitioners. Taylor & Francis.

Veenendaal, H., and A. Brouwer-Hanzens. 2007. A method for the concentration of microbes in large volumes of water. D **3**:1-30.

Venczel, L. V., M. Arrowood, M. Hurd, and M. D. Sobsey. 1997. Inactivation of Cryptosporidium parvum oocysts and Clostridium perfringens spores by a mixed-oxidant

disinfectant and by free chlorine. Applied and Environmental Microbiology **63**:1598-1601.

VROM-Inspectorate. 2005. Inspectorate Guideline. Assessment of the microbial safety of drinking water. Netherlands.

Ward, R. L., D. R. Knowlton, and M. J. Pierce. 1984. Efficiency of human rotavirus propagation in cell culture. Journal of Clinical Microbiology **19**:748-753.

Westrell, T., P. Teunis, H. van den Berg, W. Lodder, H. Ketelaars, T. A. Stenstrom, and A. M. de Roda Husman. 2006. Short- and long-term variations of norovirus concentrations in the Meuse river during a 2-year study period. Water Research **40**:2613-2620.

WHO. 2004. Guidelines for drinking water-quality. Third Edition (Volume 1). Recommendations. Geneva, Switzerland.

WHO. 2009a. Risk assessment of Cryptosporidium in drinking water. WHO/HSE/WSH/09.04, Public Health and Environment, Water, Sanitation, Hygiene and Health, Geneva, Switzerland.

WHO. 2009b. Water safety plan manual: step-by-step risk management for drinking-water suppliers. International Water Association (IWA), Geneva, Switzerland.

WHO. 2011. Guidelines for drinking-water quality (Fourth Edition). Geneva, Switzerland.

WHO. 2016a. Protecting surface water for health. Identifying, assessing and managing drinking-water quality risks in surface-water catchments. Geneva, Switzerland.

WHO. 2016b. Quantitative microbial risk assessment: Application for water safety management. Geneva, Switzerland.

WHO. 2017a. Climate-resilient water safety plans: Managing health risks associated with climate variability and change.

WHO. 2017b. Guidelines for drinking-water quality: Fourth edition incorporating the first addendum.

WHO, I. 2017c. Global Status Report on Water Safety Plans: A review of proactive risk assessment and risk management practices to ensure the safety of drinking-water. World Health Organization, International Water Association.

Wu, F.-C., and Y.-P. Tsang. 2004. Second-order Monte Carlo uncertainty/variability analysis using correlated model parameters: application to salmonid embryo survival risk assessment. Ecological Modelling **177**:393-414.

Wu, J., A. D. Gronewold, R. A. Rodriguez, J. R. Stewart, and M. D. Sobsey. 2014. Integrating quantitative PCR and Bayesian statistics in quantifying human adenoviruses in small volumes of source water. Science of the Total Environment **470**:255-262.

Youn, S., and D. F. Lawler. 2019. The (relative) insignificance of G revisited to include nanoparticles. AWWA Water Science **1**:e1138.

Yu, Y. 2018. mixR: Finite Mixture Modeling for Raw and Binned Data.

Zeileis, A., and C. Kleiber. 2014. Ineq: measuring inequality, concentration, and poverty. R package version 0.2-13, URL http://CRAN. R-project. org/package= ineq. Affiliation: Sebastián Cano-Berlanga Department d'Economia Facultat d'Economia i Empresa Universitat Rovira i Virgili/GRODE **43204**.

Zhou, H., and D. W. Smith. 1994. Kinetics of ozone disinfection in completely mixed system. Journal of Environmental Engineering **120**:841-858.

APPENDIX A SUPPLEMENTAL MATERIAL, ARTICLE 1: CAN ROUTINE MONITORING OF *E. COLI* FULLY ACCOUNT FOR PEAK EVENT CONCENTRATIONS AT DRINKING WATER INTAKES IN AGRICULTURAL AND URBAN RIVERS?

Journal: Water Research

Title: Can routine monitoring of *E. coli* fully account for peak event concentrations at drinking water intakes in agricultural and urban rivers?

Authors: Émile Sylvestre, Jean-Baptiste Burnet, Patrick Smeets, Gertjan Medema, Michèle Prévost, Sarah Dorner

Number of pages: 3

Number of tables: 2

Supplementary Table 4-1

Supplementary Table 4-2

Supplementary Table 4-1: *E. coli*-based classification systems to set minimum treatment targets

for surface DWTPs

Current document	Reassessment period	Sampling frequency - samples (n)	Statistical measure for bin classification	Number per 100ml	Minimum log reduction requirements			
					Protozoa (*Crypto.*)	Protozoa (*Giardia*)	Viruses	Bacteria
Guidelines for Drinking-Water Quality, 2nd edition. Volume 2. (WHO, 1996)	Not mentioned	Not mentioned	Not mentioned	< 20	Disinfection			
				20 to 2000	Filtration and disinfection			
				> 2000	Filtration, disinfection, and at least one other process capable of producing additional reduction of viruses of >99%			
USEPA LT2 (USEPA, 2010)	9 years	Monthly for 24 months or bimonthly for 12 months (n=24)	Arithmetic mean	< 10 (lake or reservoir)	3	3	4	-
				< 50 (flowing stream source)	3	3	4	-
Regulation respecting the quality of drinking water (Gouvernement du Québec, 2016)	Continuously	Weekly for 36 months (n=156)	Maximum value of the 12-months moving arithmetic mean	< 15	3	3	4	-
				15 to 150	3	4	5	-
				150 to 1500	4	5	6	-
				> 1500	5	6	7	-
Australian Drinking Water Guidelines (Draft framework on microbial HBT) (NHRMC, 2016)	Not mentioned	Weekly for 24 months (n=104) including event-based in the dataset	Maximum value	< 20 (protected)	0	-	0	4
				< 20 (unprotected)	2.5	-	3	5
				20 to 2000 (protected)	2.5	-	3	5
				20 to 2000 (unprotected)	3.5	-	4	5
				> 2000	5.5	-	6	6

Supplementary Table 4-2: *Cryptosporidium*-based classification systems to set minimum treatment targets for surface DWTPs

Current document	Reassessment period	Sampling frequency – samples (n)	Descriptive statistic for bin classification	Number of organisms per liter	Minimum log reduction requirements			
					Protozoa (*Crypto.*)	Protozoa (*Giardia*)	Viruses	Bacteria
USEPA LT2 (System serving at least 10,000 persons) (USEPA, 2010)	9 years	Monthly for 24 months or bimonthly for 12 months (n=24)	Arithmetic mean	< 0.075 0.075 to 1 < 1 to 3 > 3	3 4 5 5.5	3	4	-
New Zealand Drinking water Standards (System serving at least 10,000 persons) (Ministry of Health, 2005)	5 years	At least 26 samples collected over a 12-month period at approximately equal time intervals	Arithmetic mean	< 0.075 0.075 to 1 > 1	3 4 5	-	-	-
Australian Drinking Water Guidelines (Draft framework on microbial HBT) (NHRMC, 2016)	Not mentioned	Not mentioned	Arithmetic mean	< 0.01 0.01 to 0.1 < 0.1 to 1 < 1 to 10 > 10	3 4 5 6 6.5	-	3 3.5 4.5 5.5 6	3 3.5 4.5 5.5 6

APPENDIX B   SUPPLEMENTAL MATERIAL, ARTICLE 2: IMPORTANCE OF DISTRIBUTIONAL FORMS FOR THE ASSESSMENT OF PROTOZOAN PATHOGENS CONCENTRATIONS IN DRINKING WATER SOURCES

Journal: Risk Analysis

Title: Importance of distributional forms for the assessment of protozoan pathogens concentrations in drinking water sources

Number of pages: 6

Number of tables: 3

Supplementary Table 5-1

Supplementary Table 5-2

Supplementary Table 5-3

Number of figures: 1

Supplementary Figure 5-1

Supplementary Table 5-1: Calculated recovery rate for 43 *Cryptosporidium* and *Giardia* matrix spike recovery experiments carried out in 10-liter raw water samples collected at the drinking water intake of 30 drinking water treatment plants (at least one experiments per site)

Cryptosporidium			*Giardia*		
Target oocyst dose	Number of recovered oocysts	Recovery rate	Target cyst dose	Number of recovered cysts	Recovery rate
100	37	0.37	100	14	0.14
100	20	0.20	100	10	0.10
100	36	0.36	100	76	0.76
100	36	0.36	100	60	0.60
100	27	0.27	100	39	0.39
100	63	0.63	100	58	0.58
100	50	0.50	100	66	0.66
100	45	0.45	100	47	0.47
100	37	0.37	100	42	0.42
100	70	0.70	100	51	0.51
100	65	0.65	100	52	0.52
100	57	0.57	100	58	0.58
100	51	0.51	100	56	0.56
100	17	0.17	100	37	0.37
100	31	0.31	100	50	0.50
100	36	0.36	100	57	0.57
100	57	0.57	100	78	0.78
100	64	0.64	100	80	0.80
100	46	0.46	100	66	0.66
100	35	0.35	100	68	0.68
100	57	0.57	100	68	0.68
100	35	0.35	100	54	0.54
100	41	0.41	100	29	0.29
100	34	0.34	100	28	0.28
100	58	0.58	100	57	0.57
100	40	0.40	100	48	0.48
100	41	0.41	100	42	0.42
100	57	0.57	100	62	0.62
100	41	0.41	100	53	0.53
100	44	0.44	100	72	0.72
100	43	0.43	100	69	0.69
100	53	0.53	100	62	0.62
100	65	0.65	100	62	0.62
100	50	0.50	100	53	0.53
100	75	0.75	100	75	0.75
100	69	0.69	100	35	0.35
100	55	0.55	100	19	0.19
100	53	0.53	100	17	0.17
100	70	0.70	100	37	0.37
100	34	0.34	100	45	0.45
100	46	0.46	100	38	0.38
100	28	0.28	100	41	0.41
100	33	0.33	100	28	0.28

Supplementary Table 5-2: Count, sample mean concentration and sample maximum concentration for IFA-positive *Cryptosporidium* oocyst and DAPI-positive *Cryptosporidium* oocyst measured in raw water at eight drinking water treatment plants.

DWTP	Main land cover type of the catchment	*n*	Total volume analysed (L)	IFA +ve *Crypto.* oocysts	DAPI +ve *Crypto.* oocysts	Sample mean (IFA+ve oocyst/L)	Sample mean (DAPI +ve oocyst/L)	Sample maximum (IFA +ve oocyst/L)	Sample maximum (DAPI +ve oocyst/L)
A1	Forested	20	1086	110	61	0.159	0.092	1.466	0.684
A2	Mixed	20	710	79	48	0.127	0.086	0.588	0.558
A3	Mixed	21	830	37	26	0.062	0.047	0.333	0.250
A4	Agricultural	24	936	125	69	0.181	0.080	1.387	0.358
B1	Mixed	22	848	129	100	0.173	0.136	1.464	1.393
B2	Forested	19	957	62	16	0.630	0.020	0.625	0.086
C1	Mixed	18	1077	186	157	0.179	0.150	0.809	0.714
C2	Agricultural	17	930	43	25	0.045	0.027	0.111	0.088
D1	Agricultural	22	707	57	44	0.079	0.059	0.406	0.356
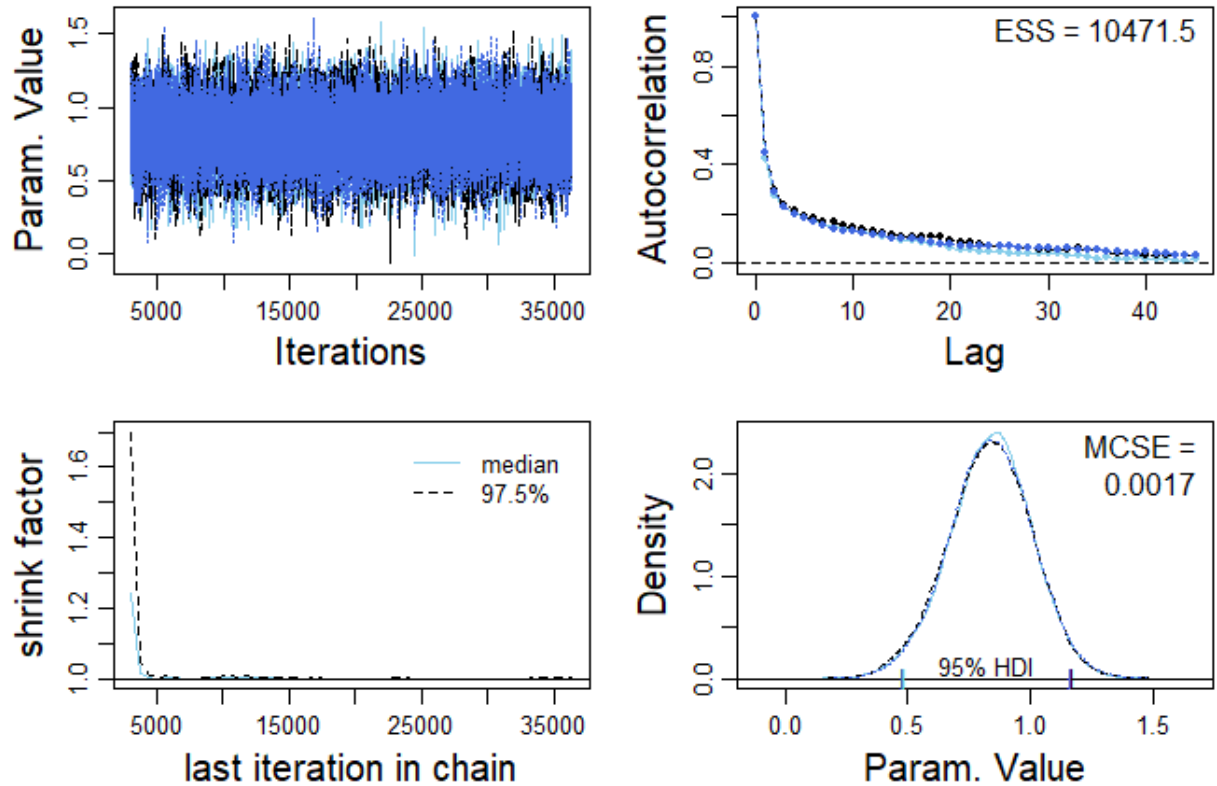
Supplementary Figure 5-1: Illustration from MCMC diagnostics for a specified parameter. *Upper-left:* Evolution of parameter values of three chains as the number of iterations increases (trace plot). A burn-in period of 2000 steps was applied. *Upper-right:* Autocorrelation diagnostic for lags from 1 to 35. *Lower-left:* Evolution of Gelman and Rubin's shrink factor as the number of iterations increases. *Lower-right:* Density plots of the parameter values sampled in three MCMC chains. Generated in R using the diagMCMC function from Kruschke (2014).

Supplementary Table 5-3: *Cryptosporidium* oocyst counts and analyzed water volumes from four drinking water treatment plants.

DWTP B7		DWTP C1		DWTP C4		DWTP C7	
Oocyst count	Volume	Oocyst count	Volume	Oocyst count	Volume	Oocyst count	Volume
0	33	0	62	2	11	0	1.9
0	41	51	63	0	11	0	16
0	25	31	44.22	0	10.5	0	22
1	4.75	39	63	0	49	5	26
0	42.5	23	61	0	12	2	20
1	10	6	64	0	30	15	30
3	5	5	63	0	25	6	17
1	11	1	61	3	37.52	3	20
1	19	0	60	0	57	1	9
0	60	2	60	0	12.5	2	8
1	75.5	1	65	0	12.75	0	12.4
1	50.5	4	29.5	0	12	0	15
2	10.5	1	60	2	16.17	0	25
0	27.5	0	66	0	40.87	0	25
0	2.2	7	40.5	0	13.6	0	70
3	10.4	1	70.5	2	30.5	2	55
		8	62.5	20	15.25		
		4	24.5	13	21		
		2	57.5	1	40		
				0	68		
				3	67		
				3	12.87		

APPENDIX C   SUPPLEMENTAL MATERIAL, ARTICLE 3: IMPACT OF HYDROMETEOROLOGICAL EVENTS FOR THE SELECTION OF PARAMETRIC MODELS FOR PROTOZOAN PATHOGENS IN DRINKING-WATER SOURCES
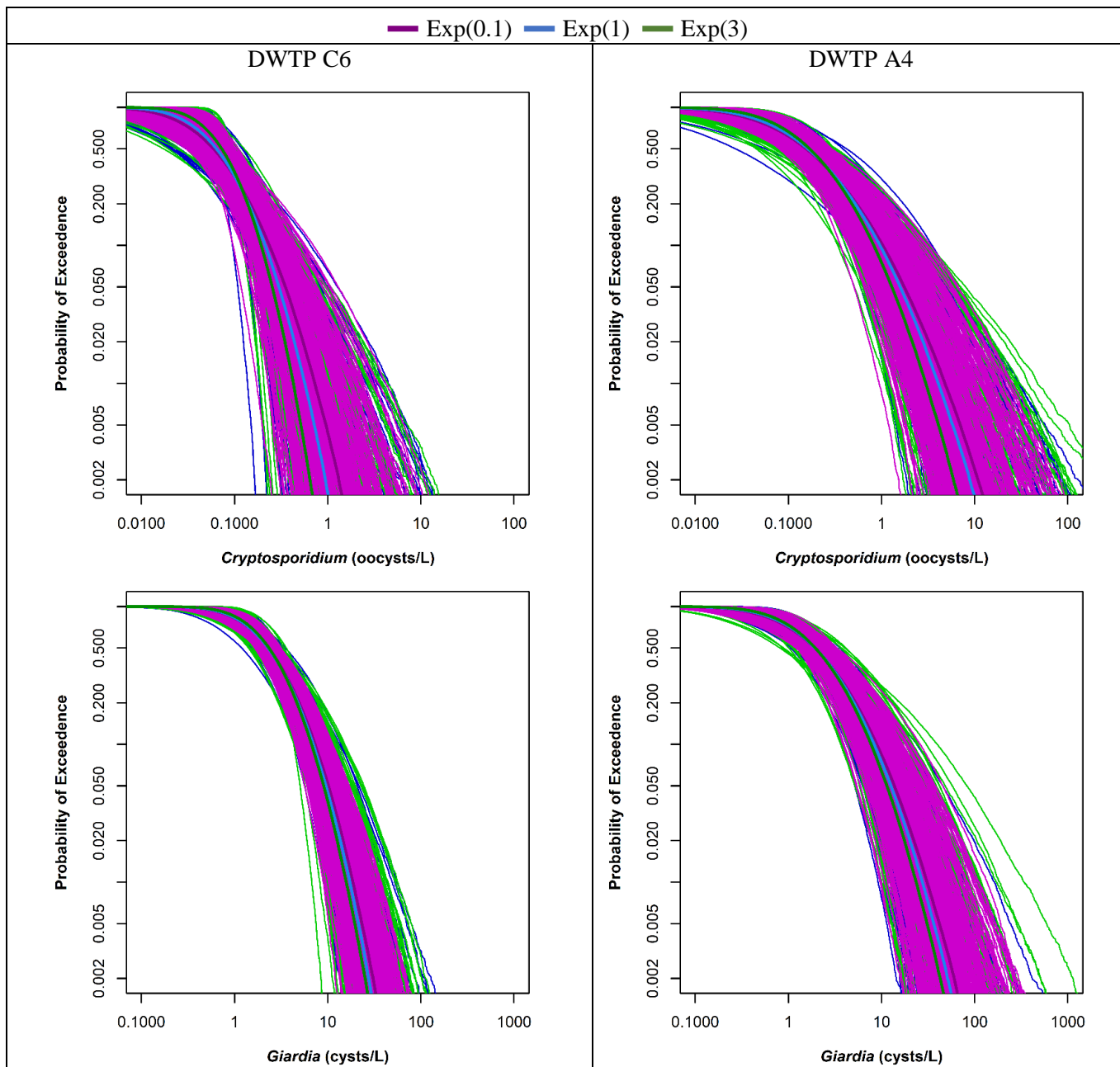
Journal: Risk Analysis

Title: Impact of hydrometeorological events for the selection of parametric models for protozoan pathogens in drinking-water sources

Authors: Émile Sylvestre, Jean-Baptiste Burnet, Sarah Dorner, Patrick Smeets, Gertjan Medema, Manuela Villion, Mounia Hachad, Michèle Prévost

Number of pages: 2

Number of figures: 1

Supplementary Figure 6-1

Supplementary Figure 6-1: Complementary cumulative distribution function (CCDF) curves for the log-normal distribution of *Cryptosporidium* and *Giardia* concentrations using different values of the hyperparameter on the prior its the scale parameter λ at drinking water treatment plants A and B. Surfaces represent the 95% predictive interval for each log-normal distribution.

APPENDIX D   SUPPLEMENTAL MATERIAL, ARTICLE 4: DEMONSTRATING THE REDUCTION OF ENTERIC VIRUSES BY DRINKING WATER TREATMENT DURING SNOWMELT EPISODES IN URBAN AREAS
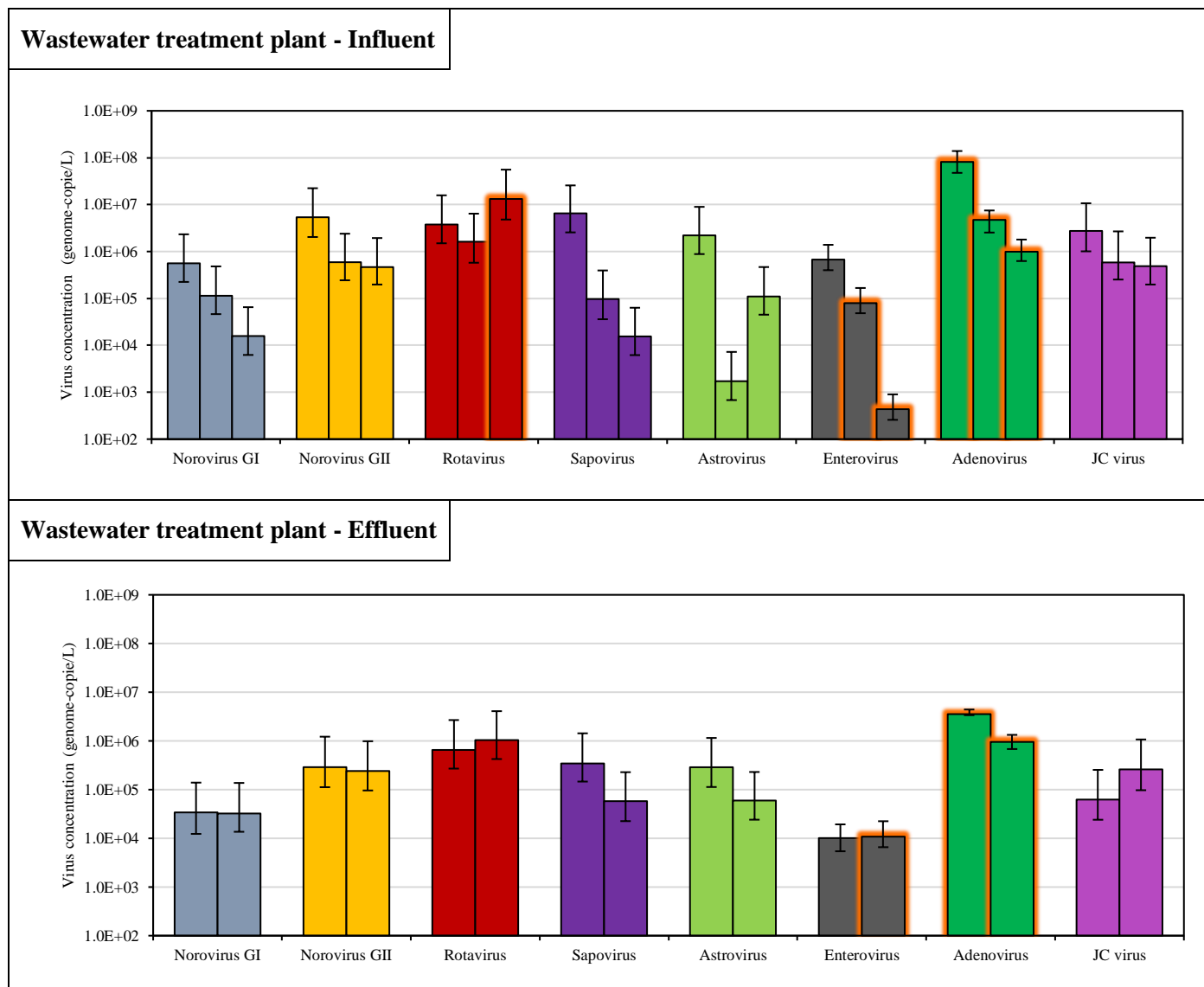
Journal: Water Research

Title: Demonstrating the reduction of enteric viruses by drinking water treatment during snowmelt episodes in urban areas

Authors: Émile Sylvestre, Michèle Prévost, Jean-Baptiste Burnet, Xiaoli Pang, Yuanyuan Qiu, Patrick Smeets, Gertjan Medema, Mounia Hachad, Sarah Dorner

Number of pages: 2

Number of figures: 1

Supplementary Figure 7-1

Supplementary Figure 7-1: Histograms for the concentrations of 8 enteric viruses at the influent and effluent of a wastewater treatment plant located 5 kilometers upstream from drinking water treatment plant (DWTP) B. Error bars represent the uncertainty in virus concentrations due to the analytical error and the random error in sample collection. Influent samples were collected on three occasions in 2018 on February 28, March 19, and March 26. Effluent samples were collected on February 28 and March 26. Orange glowing bars represent samples positive for ICC-qPCR.